PolyPublie
Polytechnique Montréal

POLYTECHNIQUE MONTRÉAL
UNIVERSITÉ D'INGÉNIERIE

Titre: Title:	The seismic behaviour of steel braces with large sections
Auteur: Author:	Carmen Izvernari Bara
Date:	2007
Type:	Mémoire ou thèse / Dissertation or Thesis
Référence: Citation:	Izvernari Bara, C. (2007). The seismic behaviour of steel braces with large sections [Mémoire de maîtrise, École Polytechnique de Montréal]. PolyPublie. https://publications.polymtl.ca/7957/

Document en libre accès dans PolyPublie
Open Access document in PolyPublie

URL de PolyPublie: PolyPublie URL:	https://publications.polymtl.ca/7957/
Directeurs de recherche: Advisors:	
Programme: Program:	Non spécifié

Ce fichier a été téléchargé à partir de PolyPublie, le dépôt institutionnel de Polytechnique Montréal
This file has been downloaded from PolyPublie, the institutional repository of Polytechnique Montréal

https://publications.polymtl.ca

UNIVERSITÉ DE MONTRÉAL

THE SEISMIC BEHAVIOUR OF STEEL BRACES WITH LARGE SECTIONS

CARMEN IZVERNARI BARA

DÉPARTEMENT DES GÉNIES CIVIL, GÉOLOGIQUE ET DES MINES
ÉCOLE POLYTECHNIQUE DE MONTRÉAL

MÉMOIRE PRÉSENTÉ EN VUE DE L'OBTENTION
DU DIPLÔME DE MAÎTRISE ÈS SCIENCES APPLIQUÉES
(GÉNIE CIVIL)
AVRIL 2007

©Carmen Izvernari Bara, 2007.

Library and Archives Canada

Published Heritage Branch

395 Wellington Street
Ottawa ON K1A 0N4
Canada

Bibliothèque et Archives Canada

Direction du Patrimoine de l'édition

395, rue Wellington
Ottawa ON K1A 0N4
Canada

Your file Votre référence
ISBN: 978-0-494-29212-9
Our file Notre référence
ISBN: 978-0-494-29212-9

NOTICE:
The author has granted a non-exclusive license allowing Library and Archives Canada to reproduce, publish, archive, preserve, conserve, communicate to the public by telecommunication or on the Internet, loan, distribute and sell theses worldwide, for commercial or non-commercial purposes, in microform, paper, electronic and/or any other formats.

The author retains copyright ownership and moral rights in this thesis. Neither the thesis nor substantial extracts from it may be printed or otherwise reproduced without the author's permission.

AVIS:
L'auteur a accordé une licence non exclusive permettant à la Bibliothèque et Archives Canada de reproduire, publier, archiver, sauvegarder, conserver, transmettre au public par télécommunication ou par l'Internet, prêter, distribuer et vendre des thèses partout dans le monde, à des fins commerciales ou autres, sur support microforme, papier, électronique et/ou autres formats.

L'auteur conserve la propriété du droit d'auteur et des droits moraux qui protège cette thèse. Ni la thèse ni des extraits substantiels de celle-ci ne doivent être imprimés ou autrement reproduits sans son autorisation.

In compliance with the Canadian Privacy Act some supporting forms may have been removed from this thesis.

While these forms may be included in the document page count, their removal does not represent any loss of content from the thesis.

Conformément à la loi canadienne sur la protection de la vie privée, quelques formulaires secondaires ont été enlevés de cette thèse.

Bien que ces formulaires aient inclus dans la pagination, il n'y aura aucun contenu manquant.

Canada

UNIVERSITÉ DE MONTRÉAL

ÉCOLE POLYTECHNIQUE DE MONTRÉAL

Ce mémoire intitulé:

THE SEISMIC BEHAVIOUR OF STEEL BRACES WITH LARGE SECTIONS

présenté par : IZVERNARI BARA Carmen

en vue de l'obtention du diplôme de : Maîtrise ès sciences appliquées

a été dûment accepté par le jury d'examen constitué de :

M. BOUAANANI Najib, Ph.D., président

M. TREMBLAY Robert, Ph.D., membre et directeur de recherche

M. MASSICOTTE Bruno, Ph.D., membre

To my husband, Adrian

To my parents and grandparents

AKNOWLEDGEMENTS

First of all, I would like to express my gratefulness to my research supervisor, Prof. Robert Tremblay, for his moral and financial support during my research, for his knowledge and experience, his time and efforts invested in this project.

My thanks to all professors from the Group for Research in Structural Engineering, for their professionalism and passion transmitted to us, the students, and especially to Prof. Najib Bouaanani and Prof. Bruno Massicotte for the time took to read and evaluate this project.

I would like to give special thanks to Prof. Antonio Aguero from Spain, for teaching me and guiding me during my work with OpenSees program and for his precious collaboration on our article. Special thanks, also, to Martin Lacerte and Charles-Philippe Lamarche for their help during my research work.

I will always remember with pleasure the time spent at school with my colleagues, the classes took together, and the fun we had together. Thank you, Camelia Nedisan, Emre Yildiz and Sina Merzouq for your help and advices, and also thanks to the whole group for their help and the friendly atmosphere that they made and maintain at school.

I would also like to thank M. Ciro Martoni for his support and understanding and to my colleagues from Martoni, Cyr & Associés, especially to Mélanie Chamarre.

Last but not least, I wouldn't make this project without the help, support and love of my family. Thank you.

RESUMÉ

Depuis le séisme de Northridge (1994), les structures contreventées en acier ont gagné en popularité comme systèmes de résistance contre les charges latérales. La dissipation d'énergie dans ces systèmes est réalisée par le flambement inélastique et la plastification en tension des diagonales de contreventement. La fracture de diagonales sous les charges cyclique inélastique est toujours possible et elle peut limiter la ductilité permise par le système. Même si les contreventements concentriques sont très utilisés en pratique, il y a peu d'essais à grande échelle qui ont été réalisée jusqu'à présent et les modèles analytiques détaillés pour les diagonales et les connections sont aussi limités. Il existe un besoin pour des modèles analytiques qui sont validés avec des tests réalisés sur des diagonales de contreventement ayant une grande section, comme celles utilisés couramment dans les structures multi-étagées en acier, ceci pour pouvoir prédire correctement leur performance sous des séismes de grande intensité.

Les principaux objectifs de ce projet étaient d'étudier la performance séismique globale, de même que la stabilité de structures multi-étagées construites avec des contreventements en acier de type Split-X et conçues selon les dispositions séismiques du Code National du Bâtiment Canada (CNBC) 2005 et la norme CSA-S16S1-05. On voulait aussi développer une base de données numérique pouvant être employée pour le développement de protocoles de chargement pour des essais séismiques des diagonales de contreventements en acier.

Des études paramétriques ont d'abord été effectuées pour évaluer l'influence des hypothèses de modélisation pour le comportement hystérétique des diagonales de contreventements en acier avec le logiciel Opensees. Les comparaisons entre les résultats d'essais et des analyses de même que l'analyse dynamique non linéaire d'une structure

simple ont confirmé la validité des hypothèses faites pour des structures en acier de faible hauteur.

Par la suite, on a réalisé des études analytiques sur des structures en acier avec des diagonales de contreventements disposés en Split-X. Cinq hauteurs de bâtiments ont été choisies pour l'étude : 2, 4, 8, 12 et 16 étages. On a supposé que les bâtiments étaient situés à Victoria, Colombie-Britannique, sur un site de class C. Un ensemble de 20 mouvements sismiques du sol a été utilisé pour étudier la performance sismique et la stabilité des structures sélectionnées.

Les bâtiments ont été conçus selon les dispositions pour le calcul par capacité du CNBC 2005 et de la norme CSA-S16S1-05. Des modèles 3D ont été crées en utilisant le logiciel OpenSees. La performance structurale des bâtiments a été examinée à l'aide d'analyses dynamiques non linéaires et d'analyses dynamiques incrémentales.

Les analyses ont démontré que tous les bâtiments étudiés présentent un comportement sismique adéquat. Les valeurs médianes des déplacements inter-étages ont rencontré la limite de 2,5% h_s qui est fixée dans le CNBC 2005 pour des bâtiments d'importance normale (h_s est la hauteur d'étage). Même si ces déformations ont dépassé les valeurs prédites à l'étape de la conception, et même si les bâtiments de 12 et 16 étages ont montré des concentrations des déformations inter-étages sur leur hauteur, les bâtiments de 8, 12 et 16 étages ont montré une comportement très robuste contre l'effondrement global lorsqu'ils ont été soumis aux analyses dynamiques incrémentales. Le niveau de confiance calculé pour les trois bâtiments était de 99,99%, beaucoup plus que la valeur de 90% recommandé par les normes de conception américaines.

Les études ont montré que les diagonales de contreventement devraient offrir une bonne performance contre la rupture par fracture. Les diagonales les plus critiques ont été celles ayant une facteur d'élancement λ autour de 0.75 ($KL/r \approx 55$). Une sollicitation en fatigue

plus faible a été observée pour les diagonales plus trapues ($\lambda \approx 0.60$ et $KL/r \approx 45$) et pour les diagonales plus élancées ($\lambda > 0.90$ et $KL/r > 65$).

Finalement, les analyses ont aussi révélé des déformations permanentes significatives après les séismes dans les bâtiments de 8, 12 et 16 étages. Ces déformations pourraient conduire à des coûts de réparations importants.

Une base de données numérique a été crée pour le développement de protocoles de chargement pour des essais séismiques des diagonales des contreventements en acier utilisés dans les structures contreventées.

Des études futures devraient porter sur la prise en compte du voilement local et de la fracture des diagonales dans le modèle utilisé avec le logiciel OpenSees telle que cela a été proposé dans d'autres études. D'autres études sur des contreventements avec configurations différentes (configuration en X sur un étage, contreventement en chevron, etc.) sont également nécessaires afin de vérifier si les conclusions de cette étude peuvent aussi s'appliquer à ces structures.

ABSTRACT

Since the 1994 Northridge earthquake, concentrically braced steel frames have gained in popularity as lateral load resisting system in seismic areas. Energy dissipation in the system is achieved through inelastic buckling in compression and yielding in tension of the bracing members. Brace fracture under cyclic inelastic loading is however a possibility and may govern the system ductility. In spite of this increasing popularity, very few large-scale tests have been performed so far on these systems and rigorous analytical modeling of braced frames structures with detailing requirements for the bracing members and the connections is also limited. Test validated analytical models of large size bracing members, as typically encountered in multi-storey structures, are needed in order to predict the performance of these structures under severe ground motions.

The main objectives of this project were: (1) to study the overall seismic performance, including global stability, of multi-storey Split-X braced steel frames designed according to NBCC 2005 and CSA-S16S1-05 seismic provisions; and (2) to develop a numerical database that can be used to propose loading protocols for the seismic testing of bracing members used in concentrically braced steel frames.

Parametric studies were carried out in order to evaluate the influence of modelling assumptions when simulating the hysteretic response of steel bracing members with the OpenSees computer software. Comparison between test and analytical results as well as nonlinear dynamic analysis of a simple structure confirmed the capacity of the OpenSees models to predict well the seismic behaviour of low-rise braced steel frame structures.

Thereafter, extended analytical studies were performed on steel structures with Split-X braces. Five building heights were chosen for the study: 2-, 4-, 8-, 12- and 16-storeys

buildings located in Victoria, British Columbia. Twenty ground motions were selected to be applied on the structures in order to study their seismic performance and stability. The buildings were designed following the NBCC 2005 and CSA-S16S1-05 capacity design provisions. Three-dimensional models were created using the OpenSees computer software. The structural performance of the buildings was examined through non-linear dynamic analysis and incremental dynamic analysis.

Good seismic performance was found for all the buildings. The median estimates of the: inter-storey drifts met the 2.5 % limit prescribed in the NBCC 2005 for buildings of normal importance. For all buildings, however, these deformations exceeded the values predicted from response spectrum analysis and the 12- and 16-storey buildings exhibited significant concentration of storey deformations along their height. In spite of these relatively high and non-uniform storey drift values, the 8-, 12- and 16-storey structures, all demonstrated a very robust response against global collapse when subjected to incremental dynamic analysis. The confidence level against this failure mode was equal to 99.99%, well above the recommended minimum value of 90% in U.S. design guidelines.

The study also showed that that the braces exhibit satisfactory performance against fracture. The most critical braces were those with a low slenderness ratio ($KL/r \approx 55$) and relative lower demand was observed on the stockier braces ($KL/r \approx 45$) and on the more slender ones ($KL/r > 65$). Finally, the analyses showed that the 8-, 12- and 16-storey buildings experienced significant permanent storey deformations after design level earthquakes, which could lead to major repair costs. A numerical database was created for use in the development of loading protocols for the seismic testing of bracing members used in concentrically braced steel frames.

Future studies are necessary in order to examine further the effects of residual deformations and the potential for the brace fracture. In addition the findings of this study should be verified for other braced steel frame configurations.

CONDENSÉ EN FRANÇAIS

Les principaux objectifs de ce projet étaient d'étudier la performance séismique globale, y compris que la stabilité, de structures multi-étagées construites avec des contreventements en acier en X sur deux étages et conçues selon les dispositions séismiques du Code National du Bâtiment Canada 2005 et de la norme CSA-S16S1-05. On voulait aussi développer une base de données numérique pouvant être employée pour le développement de protocoles de chargement pour des essais séismiques des contreventements en acier.

Pour atteindre ces objectives, des analyses dynamiques non linéaires ont été effectuées avec le logiciel OpenSees sur des structures de bâtiments de cinq hauteurs différentes représentant des applications typiques de contreventements concentriques en acier utilisés en pratique.

Des études paramétriques ont d'abord été effectuées pour développer et valider un modèle pour les membrures diagonales des contreventements avec le logiciel Opensees, modèle qui a été utilisé par la suite pour réaliser les analyses des structures. Ces analyses de validation ont permis d'évaluer l'influence des hypothèses de modélisation sur le comportement hystérétique des diagonales de contreventements en acier faites de profilés tubulaires de section rectangulaire. Des éléments poutre-poteaux non linéaires ont été utilisés avec une discrétisation par fibres de la section transversale de membrures. Ces études ont montré que le nombre de points d'intégration le long de l'élément a peu d'influence sur la réponse et que des résultats précis peuvent être obtenus avec seulement trois points d'intégration par élément. On a trouvé que la formulation basée sur la force était plus exacte que la formulation basée sur les déplacements et, donc, cette formulation a été retenue même si demandait un temps de calcul plus long. Comme prévu, les erreurs étaient réduites en augmentant le nombre d'éléments ou le nombre de fibres. Les résultats

indiquent qu'une précision suffisante pour des contreventements typiques peut être atteinte si on utilise 8 éléments par membrure ainsi que 16 fibres pour la discrétisation de la section. L'utilisation du modèle de matériel de Giuffré-Menegotto-Pinto a offert une représentation plus réaliste de la réponse hystérétique des contreventements en acier que le modèle bilinéaire. Les comparaisons entre les résultats des essais et des analyses confirment la validité des hypothèses faites pour des structures de faible hauteur. Le modèle a donné des prédictions réalistes pour la réponse hystérétique de contreventements ayant des dimensions, des élancements ou des conditions de retenue différentes. Il est de loin supérieur aux modèles empiriques ou semi-empiriques pour lesquels on a besoin de données expérimentales pour reproduire correctement les propriétés clés de l'élément. Cependant, le modèle a des limitations. Il ne prend pas en considération les effets des contraintes résiduelles dans les membrures (résistance au flambement réduite), et le voilement local des parois de la section et la fracture de l'acier sous sollicitations cycliques ne peuvent être reproduits par le modèle.

Des études paramétriques et comparatives ont été ensuite réalisées afin de valider le deuxième élément d'OpenSees qui à été utilisé dans les modèles de bâtiments, soit l'élément poutre comprenant des articulations plastiques avec une discrétisation par fibres de la section transversale. Cet élément a été utilisé pour la modélisation de toutes les poutres et de tous les poteaux des structures étudiées. Ces études ont montré que le comportement élastique et plastique en flexion d'une poutre de section W, lorsque soumise à des charges concentrées en portée et sollicitée autour de son axe faible, peut être très bien décrit en utilisant une discrétisation de la membrure de neuf éléments et une discrétisation de la section avec dix fibres sur la largeur des semelles et quatre fibres sur la profondeur de l'âme (une fibre sur l'épaisseur de ces composantes). Cependant, la longueur et la position des articulations plastiques influencent le comportement en flexion d'une section. Par conséquent, une validation plus approfondie doit être faite pour la modélisation des poutres fléchies avec ce type d'élément. Des très bons résultats ont été obtenus pour le comportement en flexion-compression d'un poteau soumis à des

moments d'extrémités lorsque l'on utilisait un modèle fait d'un seul élément poutre avec articulations plastiques comparé à un modèle fait de neuf éléments poutre avec des articulations plastiques. Sur cette base, on a décidé d'utiliser un seul élément poutre avec articulations plastiques par membrure pour modéliser les poutres et les colonnes des structures. Une étude a aussi été faite pour examiner l'influence du nombre de fibres utilisées pour discrétiser la section des poteaux. Des résultats très comparables ont été obtenus pour une discrétisation de dix fibres et une discrétisation de vingt fibres d'une section W soumise à une variation linéaire de contraintes. Par conséquent, la discrétisation avec dix fibres a été retenue. OpenSees offre plusieurs possibilités pour décrire l'orientation d'un élément. Ces possibilités ont été étudiées puis validées en comparant avec les résultats de calculs manuel. Finalement, la résistance à l'ultime d'une colonne soumise à de la flexion-compression et modélisée avec des éléments poutre avec articulations plastiques a été comparée à celle prédite avec les équations d'interaction de la norme CAN/CSA S16-01, ceci pour la résistance locale de la section et pour la résistance au flambement de la membrure dans le plan de flexion.

Cinq bâtiments ayant 2, 4, 8, 12 et 16 étages ont été étudiés dans ce projet afin d'étudier la stabilité séismique d'un large éventail de structures multi-étagées construites avec des diagonales de contreventements en acier disposées en X sur deux étages consécutifs (configuration Split-X). On a supposé que les bâtiments étaient situés à Victoria, Colombie-Britannique, sur un site de classe C. Une vue en plan des bâtiments étudiés et l'élévation d'un contreventement Split-X pour le bâtiment de 8 étages sont montrées à la Figure 1. Le contreventement étudié est indiqué sur la vue en plan. Un arrangement structural identique, mais avec des travées supplémentaires donnant des dimensions en plan plus grandes (108,5 m x 108,5 m), a été choisi pour le bâtiment de 2 étages, ceci afin d'obtenir des diagonales de contreventement ayant des sections comparables à celles utilisées dans les autres bâtiments.

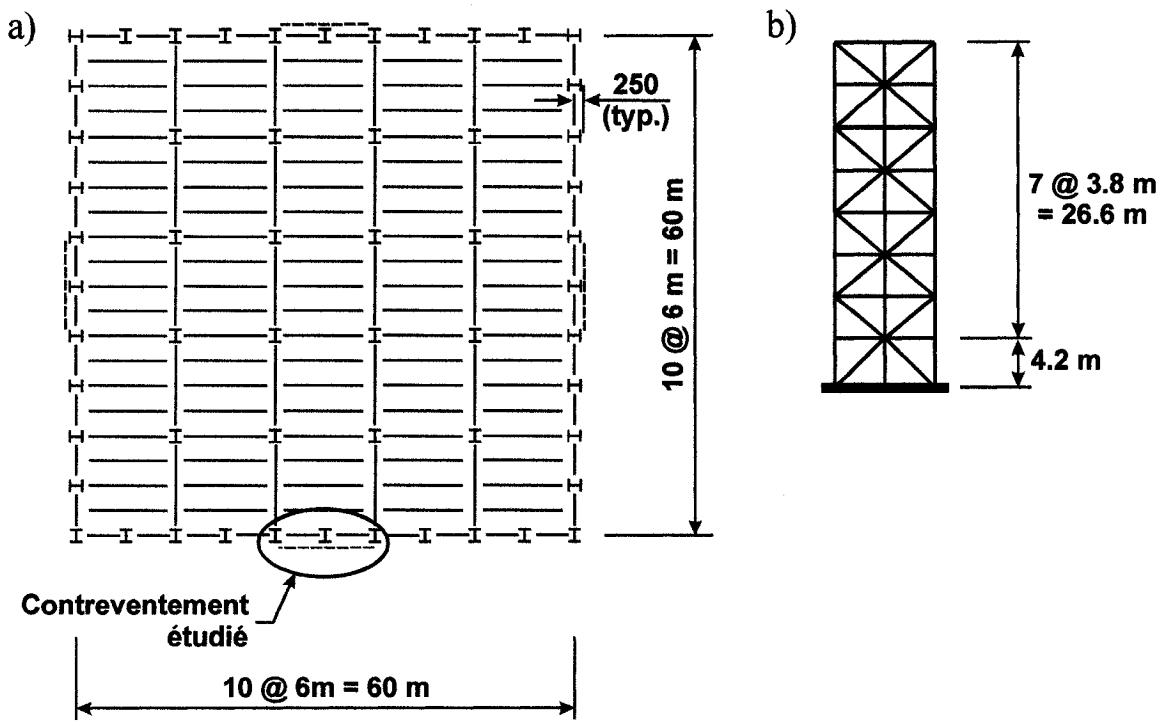

Figure 1. Géométrie des bâtiments étudiés : a) Vue en plan (4, 8, 12 et 16 étages); b) Contreventements "Split-X" pour le bâtiment de 8 étages.

Une conception préliminaire des bâtiments a été d'abord faite, en utilisant la méthode des forces statiques équivalente du CNBC 2005 et en considérant que la moitié de la structure était stabilisée latéralement par un des contreventements en "Split-X". Des contreventements avec ductilité modérée (R_d = 3.0) ont été utilisés pour les bâtiments de 2, 4 et 8 étages. Comme requis dans la norme CSA-S16, des contreventements avec ductilité limitée (R_d = 2.0) ont du être employés pour les bâtiments de 12 et 16 étages en raison de leur plus grande hauteur. Pour la structure 16 étages, les forces séismiques de conception ont été augmentées une autre fois de 26.4 % parce que leur hauteur était plus élevée que 48 mètres.

Une fois la conception préliminaire complétée, on a construit un modèle 3D des structures et on a finalisé la conception à partir des résultats d'analyses dynamiques

spectrales réalisées avec le logiciel Visual Design. Ces analyses ont été réalisées avec le spectre de la ville Victoria du CNBC 2005. La combinaison modale quadratique a été adoptée avec 5% d'amortissement pour chacun des modes Les effets P-Δ ont été pris en considération en amplifiant les effets dus aux charges latérales par le facteur U_2 de la norme CSA-S16. Une excentricité accidentelle de 10% de la dimension du bâtiment a été considérée par l'application, à chaque étage des moments de torsion dans le plan horizontal. Des sections W (ASTM A992) ont été utilisées pour les poutres et les colonnes. Pour les diagonales de contreventement de tous les bâtiments, des sections HSS carrées (ASTM A500, nuance C) ont été employées sauf pour le première étage du bâtiment de 2 étages de même que les niveaux 1 à 7 et 9 du bâtiment de 16 étages où des sections W (ASTM A992) ont été utilisées. Dans le modèle Visual Design, le coefficient de longueur effective des diagonales de contreventement a été supposé égal à 0.9 et on a considéré que leur deux extrémités étaient articulées en flexion dans les deux directions et encastrées pour la torsion. Tous les poteaux ont été posés continus sur la hauteur des bâtiments. Conformément à la norme CSA-S16, les poutres et les colonnes ont été conçues pour les charges de gravité et les efforts axiaux provenant du flambement en compression et de la plastification en traction des diagonales. Ce calcul a été fait manuellement à l'aide d'un chiffrier Excel, à l'extérieur du logiciel Visual Design.

La période latérale fondamentale des bâtiments était plus courte que la limite prescrite par le CNBC 2005 pour tous les bâtiments sauf pour le bâtiment de 2 étages pour lequel la limite supérieure du code a été considérée. Pour tous les bâtiments, l'effort tranchant sismique à la base de la structure obtenu à partir des analyses spectrales a dépassé le minimum prescrit par le CNBC 2005 (80% de l'effort obtenu de l'analyse statique). Aucun ajustement des résultats n'a été nécessaire. Les déplacements inter-étages obtenus de l'analyse spectrale étaient en dessous des valeurs permises par le CNBC 2005 pour des bâtiments d'importance normale.

Des analyses dynamiques non linéaires ont été réalisées avec le logiciel OpenSees sur des modèles réduits étant donné le fait que les bâtiments étaient symétriques. En tirant avantage de la symétrie en plan des structures, on a pu employer des modèles réduites qui comprenaient qu'une demie de chaque structure, c'est-à-dire un seul contreventement Split-X et les colonnes des gravité stabilisée latéralement par ce contreventement (Fig. 2).

Le modèle des diagonales de contreventement et des poteaux ont été ajustés afin d'être le plus représentatif possible des conditions réelles rencontrées dans de vrais bâtiments. Les rigidités en flexion et torsion des goussets ont été considérées dans le modèle, de même que des zones rigides représentant la dimension des poutres, poteaux et assemblages. Cela a donné une valeur d'environ 0.75 pour le coefficient de longueur effective des diagonales. Les colonnes des contreventements ont été considérées continues sur la hauteur des bâtiments, alors que les colonnes de gravité étaient modélisées avec des épissures à chaque deux étages. Pour les diagonales de contreventements, on a considéré un défaut de rectitude initial afin d'obtenir une résistance en compression égale, au maximum, à 110% de la résistance anticipée ($1.2C_u$). Les effets P-delta ont été pris en compte dans les analyses (représentation co-rotationelle) et un amortissement de Rayleigh correspondant à 3% de la valeur critique dans les deux premiers modes de vibration a été considéré.

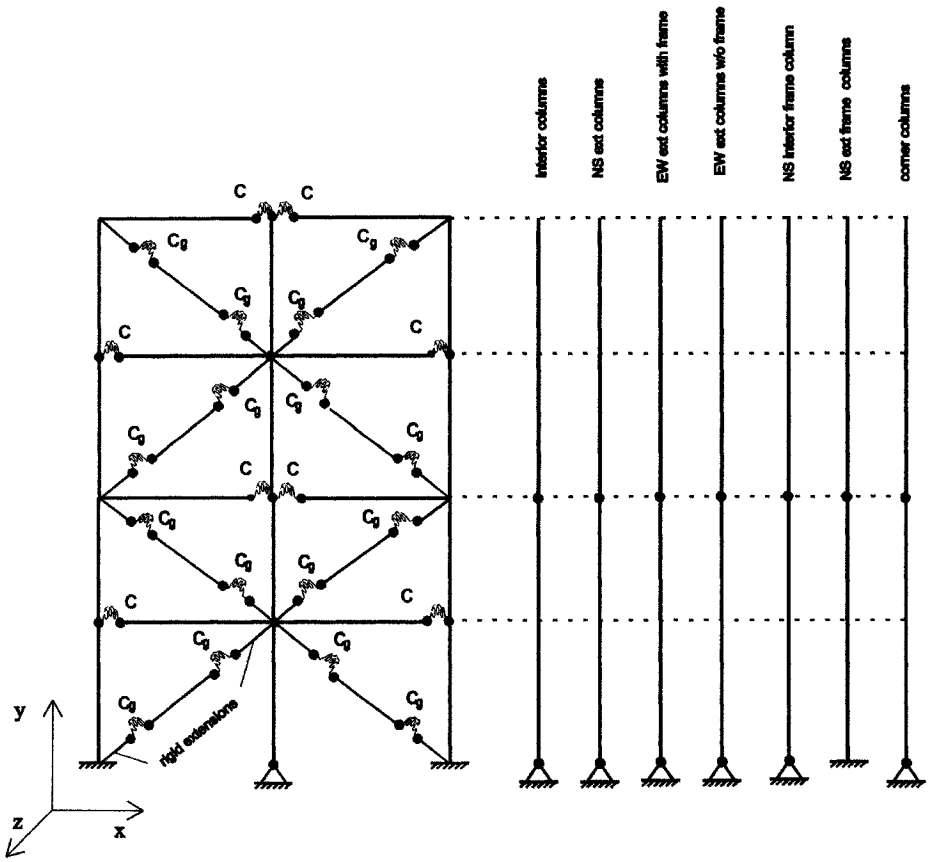

Figure 2. Model OpenSees pour le bâtiment de 4 étages.

Un ensemble de 20 mouvements sismiques du sol (10 de séismes historiques et 10 de séismes artificiels) a été utilisé pour les analyses dynamiques non linéaires. Ces séismes ont été ajustés de façon à ce que leur spectre d'accélération corresponde bien au spectre de conception du CNBC 2005 pour la ville de Victoria. Le comportement sismique des structures (flèches, ductilité des diagonales, etc.) a été examiné sous ces mouvements sismiques. Par la suite, on a étudié la résistance des bâtiments contre l'instabilité globale sous un sous-groupe formé des 10 séismes historiques. Cette vérification a été réalisée en augmentant graduellement l'amplitude des mouvements sismiques.

Sauf pour le déplacement résiduel à la fin des séismes, le comportement sismique des bâtiments a été étudié en utilisant les valeurs de pointe obtenues pendant les séismes pour les differents paramètres de réponse. Pour la vérification de la résistance contre

l'effondrement des bâtiments, on a aussi évalué le niveau de confiance que l'effondrement ne se produise. Les paramètres de réponse utilisés ont été : le déplacement maximal inter-étage Δ/h_s, le déplacement inter-étage résiduel Δ_{res}/h_s, le facteur de concentration de déformations, D_{CF}, et le niveau de ductilité atteints dans les diagonales de contreventements, μ. Le facteur D_{CF} est le rapport entre le déplacement latéral de pointe au niveau du toit, divisé par la hauteur du bâtiment, et le déplacement inter-étage de pointe maximum sur la hauteur du bâtiment. La ductilité des diagonales est le rapport entre la déformation axiale de pointe calculée pendant un séisme et la déformation axiale correspondant à la plastification de l'acier. En examinant les valeurs médianes de ces paramètres sur l'ensemble des séismes, on tire les conclusions suivantes :

- Les déplacements inter-étage maximum (maximum sur la hauteur du bâtiment) augment avec le nombre d'étages, la plus grande valeur ayant été obtenue pour le bâtiment de 16 étages. Ceci signifie que les dommages soufferts par les éléments structuraux et non-structuraux sont les plus grands pour le bâtiment de 16 étages et qu'elles diminuent pour les autres. Les valeurs médianes des déplacements inter-étage sont 2.3 à 1.4 fois plus petites que les limites du CNBC 2005. Elles étaient, par contre, entre 1.17 et 1.8 fois plus grandes que les valeurs obtenues des analyses dynamique spectrales. La différence entre le niveau d'amortissement utilisé dans les analyses spectrales et les analyses non linéaires pourrait contribuer à ces différences.

- La plus grande valeur du déplacement inter-étage résiduel a été obtenue pour le bâtiment de 8 étages tandis que les bâtiments de 12 et 16 étages ont présenté des valeurs trois fois plus petites. Seulement les bâtiments avec 2 et 4 étages ont eu des déplacements inter-étage résiduels en dessous de la tolérance maximale de construction de la norme CSA S16 (0.2%). Une évaluation structurale post-séisme serait donc nécessaire pour les bâtiments plus élevés. Les déplacements résiduels

inter-etages médians subis par tous les bâtiments étaient cependant en dessous de la valeur de 1%.

- Le facteur de concentration de déformation augmente avec le nombre d'étages. Les valeurs médianes obtenues sont comparables à celles prédites à l'aide de modèles proposés dans la littérature pour les bâtiments de 2, 4, et 8 étages. Pour les bâtiments de 12 et de 16 étages, on a obtenu des valeurs jusqu'à 1.3 fois plus élevées que celles prévues.

- Le niveau de ductilité le plus élevé dans les diagonales des contreventements a été observé pour le bâtiment de 12 étages près de la mi-hauteur du bâtiment. On a obtenu des niveaux de ductilité comparables pour les bâtiments de 8 et de 16 étages, mais à des endroits différents : en bas du bâtiment pour le bâtiment de 8 étages et au sommet du bâtiment pour le bâtiment de 16 étages. Les niveaux de ductilité calculés pour les contreventements ont été ensuite comparés avec ces obtenus d'une équation empirique reliant la ductilité à la rupture des diagonales de contreventement HSS. On a constaté que les contreventements ont un comportement satisfaisant contre la rupture des diagonales. Les diagonales les plus critiques sont celles avec une facteur d'élancement adimensionnel, λ, autour de 0.75 ($KL/r \approx 55$) lorsqu'utilisées dans les bâtiments de 2 et 16 étages. Une sollicitation plus faible a été observée pour les diagonales plus trapues ($\lambda \approx 0.60$ et $KL/r \approx 45$) et pour les diagonales plus élancées ($\lambda > 0.90$ et $KL/r > 65$).

La performance contre l'effondrement a été étudiée pour les bâtiments de 8, 12 et 16 étages en utilisant la technique de l'analyse dynamique incrémentale (IDA) et le calcul du niveau de confiance contre l'effondrement. Les analyses ont été faites en utilisant les 10 séismes historiques dont l'amplitude a été modifiée par un facteur S_{FI} qui a été augmenté graduellement de 0.2 jusqu'à 10.0 avec des incréments de 0.2. Les analyses IDA ont montré que tous les bâtiments étudiés sont robustes mais que le comportement différait

d'une structure à l'autre. Le bâtiment de 16 étages s'est effondré pour un facteur d'amplification de 10.0, tandis que les bâtiments de 8 et 12 étages se sont effondrés pour S_{FI} = 5.0 et 8.0 respectivement. De plus, le bâtiment de 8 étages s'est effondré différemment des bâtiments de 12 et 16 étages. Tandis que le premier s'est effondré par la diminution progressive de la rigidité latérale, on a noté que la rupture des autres structures s'est produite lorsque les déplacements inter-étages ont atteint des valeurs excessives, supérieures à 10% h_s. Cette différence de comportement peut être expliquée par les différences au niveau des charges sismiques utilisées pour la conception des trois structures : R_d= 3.0 pour le bâtiment de 8 étages, R_d = 2.0 pour les bâtiments de 12 étages et R_d = 1.58 pour celui de 16 étages, si on tient compte, pour ce dernier, de l'augmentation supplémentaire de 26.4% prescrite par la norme CSA-S16S1-2005.

L'analyse du niveau de confiance contre l'effondrement a été réalisée en se basant sur la procédure proposée dans le document FEMA 350 (FEMA 2000) pour les cadres à nœuds rigides en acier. Le paramètre de confiance λ est le rapport entre la valeur médiane du déplacement inter-étage obtenue des analyses sur la valeur médiane du déplacement inter-étage conduisant à l'effondrement des bâtiments. Les valeurs au nominateur et au dénominateur de ce ratio sont modifiées pour tenir compte de la dispersion et de l'incertitude des résultats, respectivement. Pour les trois bâtiments étudiés, un niveau de confiance de 99.99% a été trouvé, beaucoup plus élevé que la valeur minimale de 90% recommandée par FEMA-350. Ceci signifie que les contreventements concentriques conçus selon les nouvelles dispositions de la norme CSA-S16S1-05 et du CNBC 2005 sont conservatrices.

Une base de données numérique pour le développement de protocoles de chargement pour les diagonales de contreventement a été obtenue en utilisant des paramètres considérés dans l'établissement d'autres protocoles de chargement développés dans le passé. Trois ensembles de résultats des études statistiques sur l'ensemble de 20 séismes ont été considérés pour générer les données : le 50^{ieme} percentile, le 84^{ieme} percentile et la

valeur maximale. Les résultats montrent des variations significatives pour les niveaux de ductilité dans les diagonales des contreventements pour les trois niveaux de probabilité ainsi que pour la hauteur des bâtiments et la position des diagonales (étage) le long de la hauteur des bâtiments.

Même si les résultats obtenus dans cette étude indiquent un comportement sismique adéquat pour le système structural étudié, d'autres études sont nécessaires afin d'améliorer davantage les modèles numériques utilisés et obtenir des données plus concluantes sur les nouvelles dispositions des documents CSA-S16S1-05 et CNBC 2005. Les travaux futurs devraient porter sur la prise en compte du voilement local et de la fracture des diagonales dans le modèle utilisé avec le logiciel OpenSees, tel que cela a été proposé par d'autres (e.g. Jin et El-Tawil, 2003). Des analyses supplémentaires sont aussi nécessaires sur des contreventements concentriques avec des diagonales conçues avec un coefficient de longueur effective plus représentatif de la réalité (autour de 0,75, plutôt que la valeur de 0,9 utilisée dans ce projet). D'autres études sur des contreventements avec configurations différentes (configuration en X sur un étage, contreventement en chevron, etc.) sont également nécessaires afin de vérifier si les conclusions de cette étude peuvent aussi s'appliquer à ces structures. Finalement on devra aussi vérifier que la méthode proposée dans FEMA-350, pour déterminer le niveau de confiance contre l'effondrement des cadres à nœuds rigides en acier, est aussi applicable aux contreventements en treillis en acier.

TABLE OF CONTENTS

LIST OF FIGURES

LIST OF TABLES

LIST OF SYMBOLS

A = area

A_g = gross area

A_t = tributary area of a column

b_f = width of flange

b_W = Whitmore effective width

B_x = ratio at level x used to determine torsional sensitivity

C_e = Euler buckling strength

C_r = factored compressive resistance of member

C_u = brace capacity in compression

C'_u = brace capacity in compression after buckling

d = depth of the section

D_{nx} = plan dimension of building at level x perpendicular to the direction of seismic loading considered

e_x = distance measured perpendicular to the direction of earthquake loading between centre of mass and centre of rigidity at the level considered

E = elastic modulus of steel

F_a = acceleration-based site coefficient

F_t = portion of V to be concentrated at the top of the structure

F_v = velocity-based site coefficient

F_x = lateral force applied to level x

F_y = yield strength

G = shear modulus of steel

h_i, h_n = the height above the base to level i or n

h_s = interstorey height

h_x = the height above the base to level x

I = moment of inertia

I_E = earthquake importance factor of a structure

J = St Venant torsion constant

J_x = numerical reduction coefficient for overturning moment at level x

k = slope of the hazard curve

K = effective length factor

K_X = standard Gaussian variate

KL = effective length

L = length of the brace

M = bending moment

M_f = bending moment in a member

M_p = plastic moment resistance

M_r = factored moment resistance of a member

M_v = factor to account for higher mode effect on base shear

M_w = magnitude of the ground motion

n = parameter for compressive resistance

P_{cr} = elastic buckling load

P_y = yielding load

PGA = peak ground acceleration expressed as a ratio to gravitational acceleration

PS_a = spectral acceleration of the ground motion

PS_v = spectral velocity of the ground motion

r = radius of gyration

R = hypocentral distance of the ground motion

R_d = ductility related force modification factor

R_o = overstrength related force modification factor

R_y = factor applied to F_y to estimate the probable yield stress

$S(T)$ = the design spectral response acceleration

$S_a(T)$ = the 5% damped spectral response acceleration

S_f = scaling factor applied to ground motions to match the 2005 NBCC spectrum

S_{FI} = scaling factor applied to ground motions for incremental dynamic analysis

t_f = thickness of splice

t_g = thickness of gusset plate

T = period in seconds

T_a = fundamental lateral period of vibration of the building

T_{emp} = fundamental lateral period of vibration of the building determined with the formula $0.05h_n$

T_x = floor torque at level x

U_1 = factor to account for moment gradient and for second-order effects of axial force acting on the deformed member

U_2 = amplification factor to account for second-order effects of gravity loads acting on the laterally displaced storey

V = lateral earthquake design force at the base of the structure as determined in Equivalent Static Force Procedure

V_d = lateral earthquake design force at the base of the structure as determined in Dynamic Analysis Procedures

V_e = lateral earthquake elastic force at the base of the structure as determined in Dynamic Analysis Procedures

V_{st} = minimum lateral earthquake force determined in Equivalent Static Force Procedure

W = the weight of the building

W_i, W_x = portion of W which is located at level i or x

Z = plastic section modulus

β = standard deviation of the natural logarithms of the test data

β_U = logarithmic standard deviation

γ = demand variability factor

γ_a = analysis uncertainty factor

δ = brace axial deformation

δ_{ave} = average displacement of the structure at level x

δ_m = brace axial deformation at design

δ_{max} = maximum displacement of the structure at level x

δ_y = brace axial deformation at yield

Δ_f = relative first order lateral displacement of the storey due to factored loads

Δ_o = initial misalignment of the member

λ = slenderness parameter; confidence level

κ = ratio of the smaller factored moment to the larger factored moment at opposite ends of the unbraced length

μ = brace ductility demand

ΣC_f = sum of factored axial compressive loads of all columns in the storey

ΣV_f = sum of factored lateral loads above the storey; total first-order storey shear

ϕ = resistance factor

ϕ_R = global resistance factor

LIST OF APPENDICES

CHAPTER 1. INTRODUCTION

1.1. Generalities

Steel buildings first gained popularity at the beginning of the 20th century and their use expanded significantly after World War II when steel became more available. In the last decades, steel buildings became even more popular as their capabilities increased with improved design due to availability of computer design programs. The popularity of steel building construction can be mainly attributed to the speed of erection and cost savings when compared to more conventional building types such as brick, wood, or concrete.

Building structures generally include two load resisting systems: the gravitational load resisting system and the lateral load resisting system. The minimum steel quantity in a building corresponds to the quantity needed to support the gravity loads. The resistance to the lateral loads due to winds and earthquake requires supplementary quantity of steel, which typically increases exponentially with the number of floors in the building. The lateral resisting systems for steel buildings with moderate height up to 20-40 floors can be divided into three groups: braced frames, moment resisting frames and plate shear walls.

Traditionally it has been recognized that the seismic performance of the concentrically braced steel frames was inferior compared to moment resisting frames. However, the 2004 Northridge earthquake produced unanticipated damages in steel moment resisting frames on the form of brittle failures developing in beam to column connections. This damage was alarming to many structural engineers who started looking for simpler and more economical systems that have a good seismic performance with reduced inter-storey displacements. Some engineers turned to eccentrically braced frames while the majority turned to concentrically braced frames. They were found simpler to design,

cheaper to construct and more resistant to large lateral displacements and brittle connection fracture than the traditional moment-resisting steel frames. Industry experts indicated that concentrically braced frames now represent 40% of the commercial steel construction market in California, while only a decade ago this system represented less than 10% of the construction market.

In Canada, the seismic design of steel buildings must comply with the National Building Code of Canada (NBCC) and the CSA-S16 standard for the design of steel structures. In 2005, a new edition of the NBCC was published (NBCC 2005) that contains several major changes compared to previous editions. In particular, the earthquake hazard level, the seismic maps, the analysis methods and force calculation procedures were entirely revised. Numerous changes have also been introduced in the CSA-S16 standard for the seismic design of seismic force resisting systems, for which ductile behaviour is expected under strong seismic ground motions. The main change was the enforcement of strict capacity design rules for these systems.

In the 2001 edition of the S16 standard (CSA 2001), building height limits were introduced for concentrically braced steel frames. These limits aimed at mitigating the potential for soft-storey response that can lead to large inelastic (ductility) demand in the bracing members and global collapse and dynamic instability (Tremblay 2000, Tremblay and Poncet 2007). In the 2005 edition of the standard (CSA 2005), the height limits were changed from number of storeys to meters. The limits were also relaxed provided that the design seismic forces are increased as a function of the number of meters of height that overpass the 2001 building height limits. The adequacy of these revised provisions for buildings designed according to the new requirements included in the 2005 NBCC had not been validated through extensive nonlinear dynamic analyses.

Bracing members in concentrically braced frames are expected to experience inelastic buckling and tension yielding under strong ground motion. Past tests have shown that

local buckling generally occurs in plastic hinges that typically form upon brace buckling. Large straining develops at these critical locations, which can lead to failure of the braces by fracture upon cyclic response. Past tests indicated that the extent of local buckling and brace fracture are more critical for low slenderness, stocky bracing members, as those encountered in multi-storey buildings.

Limits on the width-to-thickness ratios are specified in CSA S16 to delay and control local buckling response in braces. These limits are more stringent for less slender braces as inelastic brace response is more pronounced for those braces. However, the detailing requirements for bracing members and connections included in CSA S16 are based on inelastic tests performed on small specimens that represent the lower bound of the range of braces actually used in practice (e.g. Black and Popov 1981, Tang and Goel 1987, Tremblay et al 2003). For this reason, a research project has been initiated at École Polytechnique of Montréal to study the cyclic inelastic response of large size, low slenderness bracing members, as used in multi-storey structures. Test specimens include braces with cross-section up to 22800 mm^2 and with dimensionless slenderness parameter $\lambda \leq 0.67$ ($KL/r \leq 50$ for $F_y = 350$ MPa). Selected braces include HSS members with square cross-sections varying from 152x152x9.5 to 305x305x16, HSS members with circular cross-sections varying from 254x9.5 to 324x13 and W shapes from W250x115 to W360x179. The loading protocol to be applied in this test program should reflect the demand anticipated in buildings designed according to recent NBCC and CSA seismic provisions.

1.2. Objectives

The aim of this research project is:

- To study the seismic behaviour of multi-storey buildings with concentrically braced steel frames designed with the new provisions of the 2005 National Building Code of Canada and the CSA-S16S1-05, and

- To obtain a numerical database for the development of test protocols for future experimental studies on large size bracing members used in concentrically braced steel frames.

1.3. Methodology

For attaining the above objectives, it was decided to study the seismic performance of 5 buildings having 2, 4, 8, 12 and 16 storeys. The structures are braced with Split-X concentrically braced steel frames designed according to the latest NBCC and CSA-S16 requirements. In this process, the following methodology was adopted:

- An extended literature review was performed on the OpenSees computer software, the seismic provisions of the 2005 National Building Code of Canada and the seismic design requirements of CAN/CSA S16-01 provisions for concentrically braced steel frames, past research on braced steel frames and past studies on the development of test loading;
- Validation of the OpenSees elements that were used to model the selected buildings by comparing the predicted response with past test results or accepted design equations;
- Preliminary design of the concentrically braced frame structures, following the Equivalent Static Force Procedure (ESFP) of NBCC 2005;
- Final design of the structures using seismic forces obtained from 3D response spectrum analysis of the buildings as well as capacity design seismic detailing requirements;
- Development of the OpenSees models of the selected buildings;
- Selection and scaling of an ensemble of twenty seismic ground motions;
- Nonlinear dynamic analysis under the ground motions scaled to the design level and following the incremental dynamic analysis procedure (total of 852 dynamic time-series non-linear analysis were performed) to study the seismic performance and global stability of the buildings;

- Development of the database on the brace response for the development of test loading protocols.

1.4. Thesis organisation

The thesis is organized in six chapters. The first chapter presents the introduction. The second chapter summarizes the literature review made on the computer software, the code design requirements and past studies on braced steel frames structures and test loading protocols. The third chapter presents the analytical studies performed on steel braces to develop guidelines for modeling their non-linear seismic response using the OpenSees software. The fourth chapter presents analytical studies performed on steel beams and columns in order to validate their model using the OpenSees software. The fifth chapter presents the design and analysis work accomplished on the sample buildings to fulfil the objectives of the project. It starts with the presentation and design of the studied buildings, followed by the selection and scaling of the ground motions, the dynamic analyses and the presentation and discussion of the analysis results. The seismic performance of the structures is discussed and the numerical database for the development of future loading protocols is presented. The conclusions of the studies and recommendations for future work are presented in the sixth chapter.

Chapter 3 of the thesis was prepared with the close collaboration of Professor Antonio Aguero, from Universidad Politécnica de Valencia, Spain, during his stay at École Polytechnique and my research supervisor, Professor Robert Tremblay. Ph.D. student, Charles-Philippe Lamarche also provided assistance for the dynamic analysis of the single-storey frame presented in this Chapter. Chapter 3 is based on the article that was published in the International Journal of Advanced Steel Construction (Aguero et al.,2006). Research associate Martin Lacerte provided assistance in the design and analysis of the buildings presented in Chapter 5.

CHAPTER 2. LITERATURE REVIEW

This chapter presents an extended literature review performed on the OpenSees computer software, the seismic provisions of the 2005 National Building Code of Canada and the seismic design requirements of CAN/CSA S16-01 provisions for concentrically braced steel frames, past research on braced steel frames and past studies on the development of test loading.

2.1. OpenSees – an open source software

2.1.1. Generalities

The software used for the analytical studies in this research project was OpenSees - Open System for Earthquake Engineering Simulation (Mazzoni et al, 2005). Opensees is a software framework using the finite element method to develop applications for the simulation of the performance of structural and geotechnical systems subjected to earthquakes. Its development is sponsored by Pacific Earthquake Engineering Research (PEER) center and it is an open-source software: the code is available at http://opensees.berkeley.edu. Examples are also provided and a forum of discussions has been created to allow the users to interact with each other and with the developers.

The models analysed with OpenSees can be linear or nonlinear, structural and geotechnical. The simulations performed can be static push-over analyses, static reversed cyclic analyses or dynamic time-series analyses.

2.1.2. Past studies using OpenSees

There are several publications in which OpenSees was used for different purposes:

- Uriz (2005) improved and detailed analytical tools for studying the dynamic response of structures and conducted preliminary hazard assessments of concentrically braced steel frames;
- A practical model for the seismic analysis of a steel braced frame was created by Gunnarsson (2005) in order to predict accurately the nonlinear performance evaluation of braced frame systems;

A more detailed description of these two studies above is given in Section 2.3.

- Comparative study between the force based and displacement-based elements implemented in OpenSees was done by Kalkan (2004) using a simple cantilever column and both static and dynamic analyses. The author concluded that in general both elements give similar results, especially when using a fine mesh to model the column or a high number of integration points when using a single element.

2.1.3. Software organisation

Opensees is comprised of a set of modules to create the finite element model, to specify an analysis procedure, to select quantities to be monitored during the analysis, and to prepare the output of the results. This organisation allows users and developers in different fields (engineering, computer science and numerical analysis) to develop and modify specific modules with little influence on other modules and without knowing everything in the framework (McKenna et al., 2004).

The users of OpenSees have to use the Tcl command language (Tcl/TkPrimerhttp:/ /dev.scriptics.com/scripting/primer.html) in order to build the model and the analysis procedure. The Tcl commands are on-line commands and the Tcl language provides

useful programming tools (variable manipulation, mathematical expression evaluation, control structures – if, while, for, procedures and file manipulation) - http://dev.scriptics.com/ scripting/primer.html.
The main advantages of OpenSees are:

- It is a powerful tool for numerical simulation of nonlinear structural and geotechnical systems because of the ever-growing library of materials, elements and analysis commands. One can create his own material, element or analysis tool and incorporate it into OpenSees.
- It is not a black box, it is a useful educational tool for numerical modeling;
- One can describe a structural/geotechnical component at a number of levels: element level (force-deformation model), section level (moment-curvature model) and fiber level (material stress-strain model).

The main features of OpenSees are:

- Models : linear and nonlinear structural and geotechnical models
- Simulations: static pushover analyses, static reversed-cyclic analysis, dynamic time-series analyses (uniform-support excitation and multi-support excitation).

The framework of OpenSees is designed using objects. They represent the governing equations of mechanics and they use algorithms to solve the equations. The high-levelled objects and their relationships in OpenSees are illustrated in Fig. 2.1.3.1.

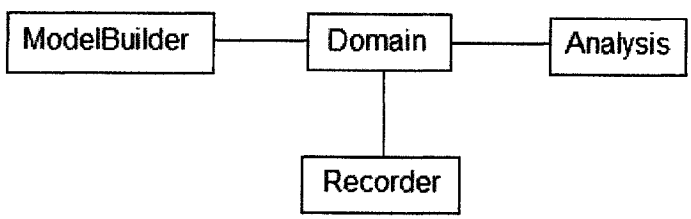

Fig. 2.1.3.1 The main objects in OpenSees
(Mazzoni et al., 2005)

The *ModelBuilder* object constructs the objects of the model (nodes, masses, materials, sections, elements, load_patterns, time_series, transformations, blocks and constraints) and adds them to the *Domain*.

The *Domain* object is responsible with storing the objects created by the *ModelBuilder* and with providing access to the objects for *Analysis* and *Recorder*. The *Domain* object is represented in Fig. 2.1.3.2.

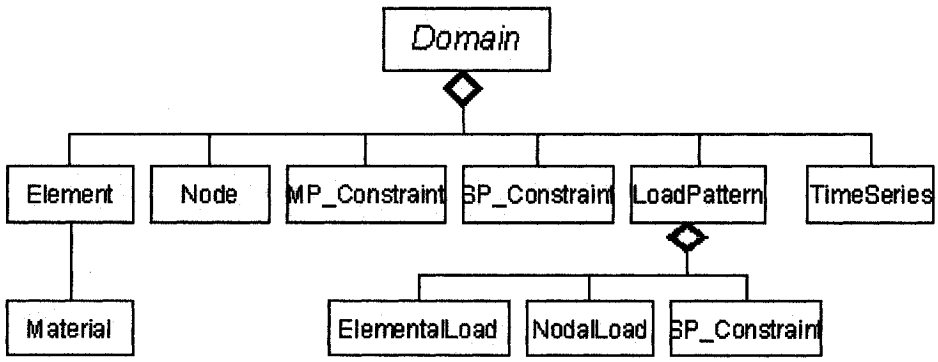

Fig. 2.1.3.2 The *Domain* object
(Mazzoni et al., 2005)

The *Analysis* object performs the analysis, which moves the model from the time state t to the time state $t+\Delta t$. This may vary from a simple static linear analysis to a transient non-linear analysis. Each *Analysis* object is composed from several objects that define how the analysis is performed. This object is presented in Fig. 2.1.3.3.

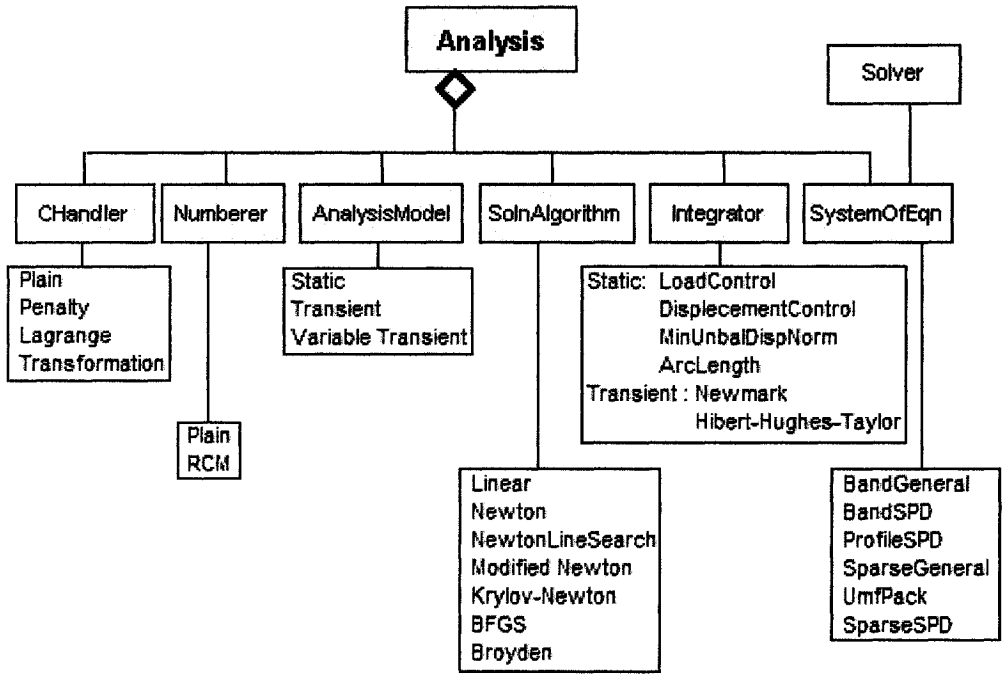

Fig. 2.1.3.3 The *Analysis* object
(Mazzoni et al., 2005)

The *Recorder* object is responsible with monitoring the state of a *Domain* component during the analysis, writing this state to a file or a database at selected intervals during the analysis, plotting and monitoring residuals.

2.1.4. OpenSees objects

One of the key objects of OpenSees is the *Element*. Abstractly, the *Element* provides the resisting force and tangent stiffness matrix for specified displacements to the nodes of the element and is responsible to maintain its state independently of all other objects. In order to compute the resisting forces, the element object must interact with other objects that represent the constitutive behaviour at integration points (McKenna et al, 2004).

The *Element* objects available in OpenSees are:

- Truss Element
- Corotational Truss Element
- Elastic Beam Column Element
- NonLinear Beam-Column Elements
- Zero-Length Elements
- Quadrilateral Elements
- Brick Elements
- FourNodeQuadUP Element
- BeamColumn Joint Element

Only the Elements that are used in this research project are described in the subsequent sections: the Elastic Beam Column Elements, the NonLinear Beam-Column Elements and the Zero-Length Elements.

The Elastic Beam Column Element is used for elements that remain elastic during the analysis or if an elastic analysis is performed. The characteristics of a 3D elastic element depend on the material modulus (Young'modulus and shear modulus), the section area, the moments of inertia about the two local axis of the element and the torsional moment of inertia of the cross-section. The transformation command defines how the element coordinates correlate to the global model coordinates. This element was used in this study to model the rigid extensions at the ends of the braces.

The NonLinear Beam-Column Elements available in OpenSees are the force based elements:

- nonlinearBeamColumn (the plasticity is spread along the element);
- beamWithHinges (the plasticity is concentrated over specified hinge lengths at the element ends and with an elastic interior);

and the displacement based elements:

- dispBeamColumn (distributed plasticity with linear curvature distribution).

The force-based elements were chosen for the analyses performed in this study: the nonlinearBeamColumn elements were used to represent the braces of the frames whereas the beamWithHinges elements were used for the beams and columns of the frames as well as for the gravitational columns. This decision was taken as a result of a comparative study performed between the two formulations presented in Chapter 3.

The characteristics of a nonlinearBeamColumn depend on the number of integration points along the element, the previously defined section of the element, the previously defined coordinate transformation, the maximum number of iterations and the tolerance specified to satisfy the element compatibility. The integration along the length of the element follows the quadrature rule of Gauss-Lobatto, which considers two integration points at the element ends.

For the middle segment of the beamWithHinges element, which is considered as linear-elastic, the characteristics depend on the same properties as for the elasticBeamColumn element. At the element ends, the characteristics depend on the length of the plastic hinges, the previously defined section, the maximum number of iteration and the tolerance limits specified for element compatibility. The mid-point integration is used for this element.

OpenSees provides three types of *sections*: elastic sections (described by geometric and material constants), resultant sections, and fibre sections (the section is discretized in small components, and the general behaviour is obtained by integrating the material stress-strain response of the components). The fibre representation can be used in patches (Fig. 2.1.4.3) and layers, which are subregions with simple, regular shapes (quadrilateral circular or triangular) or individual fibres. For the above-described elements, the

previously defined section is a fibre section. "A section defines the stress resultant force-deformation response at a cross-section of a beam-column or plate element" (Mazzoni et al, 2005).

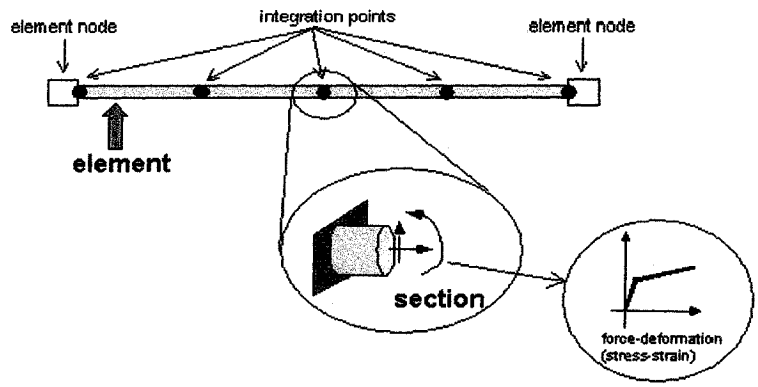

Fig. 2.1.4.1 Section representation
(Mazzoni et al., 2005)

The Bernoulli beam assumptions are considered: plane cross-sections remain plane and perpendicular to the beam axis after the deformation. Longitudinal stress-strain relationships are specified for the fibres. The individual fibres are constructed with the Fiber command (Fig.2.1.4.2) by giving the coordinates of the fibre in the section (local coordinate system), the area of the fibre and the previously defined UniaxialMaterial (to represent the stress-strain relationship for the area of the fibre).

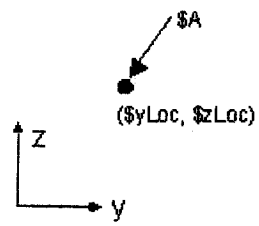

Fig. 2.1.4.2 Fiber Command
(Mazzoni et al., 2005)

The patches can be quadrilateral or circular. The quadrilateral ones are constructed with the Quadrilateral Patch command by giving the previously defined material, the number of fibres in the two directions and the coordinates for each of the four corners of the patch (in the local coordinate system).

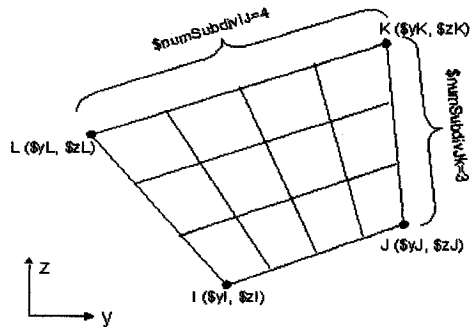

Fig. 2.1.4.3 Quadrilateral Patch
(Mazzoni et al., 2005)

The Zero-Length Elements are used to reproduce force-deformation relationships between DOFs at two points located at the same coordinates. There are three zero length element types in OpenSees:

- The Zero-Length Element, used in this present project, in which "the nodes are connected by multiple *UniaxialMaterial* objects to represent the force-deformation relationship for the element"(Mazzoni et al., 2005);
- The Zero-Length ND Element, in which "the nodes are connected by a single *NDMaterial* object to represent the force-deformation relationship for the element" (Mazzoni et al., 2005);
- The Zero-Length Section Element, in which "the nodes are connected by a single *SectionForceDeformation* object to represent the force-deformation relationship for the element" (Mazzoni et al., 2005).

In this project, the Zero-Length elements were used to model the gusset plates and the splices of the gravitational columns. Their characteristics depend on the previously defined UniaxialMaterials, the material directions and the orientation vectors for the element.

The *Nodes* and the *Masses* objects are responsible for the description of the coordinates of the model nodes and the masses assigned to them.

OpenSees provides two types of *Material* objects: uniaxialMaterial and nDmaterials. The uniaxialMaterial object represents uniaxial stress-strain or force-deformation relationships, while the NDMaterial object represents "stress-strain relationships at the integration points of continuum and force-deformation elements" (Mazzoni et al, 2005). In this project, only uniaxialMaterials were used: the elastic material and one of the FEDEAS (Finite Elements in Design, Evaluation and Analysis of Structures) materials provided in OpenSees: Steel02 Material--Giuffre-Menegotto-Pinto Model with Isotropic Strain Hardening. FEDEAS is a structural element library for linear and nonlinear, static and dynamic analysis of buildings and bridges.

There are Single-Point *Constraints* and Multi-Point *Constraints* in OpenSees. The first type is represented by homogeneous single-point boundary constraints while the second one is represented by multi-point boundary constraints. In this project, the boundary conditions for the frames and the gravity columns were simulated with single point constraints using fix command. The connections between the nodes of zero length elements as well as between the frames and the gravity columns were simulated with multi-point constraints using equalDOF command.

The *Transformation* object in OpenSees is responsible for the transformation of the beam element stiffness and resisting forces from the basic system to the global coordinate system. There are three types of transformations in OpenSees: linear transformation, P-

delta transformation (which takes into account second order P-delta effects) and corotational transformation. The latter was used in the present project in order to account for large deformation effects of the model. In the corotational transformation, a local coordinate system is attached to each element and it moves (translate and rotate) with the element while the global coordinates system is fixed. The deformations of an element can be decomposed in a body-rigid component (identical with the body-rigid motion of the local coordinate system) and a straining component, which is described in the local coordinate system. If the element is small comparing to the deformations and if it is not changing much in shape and size during the deformation process, the element matrices can be written in the local coordinate system. After formulation, the matrices are coordinate transformed from the local coordinate system in the global coordinate system, and assembled in the global stiffness matrix. Therefore, both global stiffness matrix and global equilibrium equations refer to the deformed shape geometry (Cook, 2002).

Another object part of the ModelBuilder is the *Loadpattern* that creates the nodal loads. There are three patterns in OpenSees: a Plain pattern for ordinary loads, a UniformExcitation pattern for the seismic loads and a MultipleSupport pattern for multiple-support excitation imposed to the model. In this project the Plain and the UniformExcitation patterns were used.

All the above objects were used to describe the model that could then be used in the analyses.

The component objects of *Analysis* main object will be described in Chapter 4 together with the OpenSees model for the studied buildings.

The *Recorder* object is used to monitor the results of interest in output files. Once in a file, the results can be easily post-processed and analysed. The component objects of this main object are: Node recorder, EnvelopeNode recorder, Drift recorder, Element

recorder, EnvelopeElement recorder, Display recorder, Plot recorder and Playback command. The Node type records the displacements (translational or rotational), the velocity, the acceleration and the eigenvectors; the Drift type records the displacement drift between two nodes and the Element type records the local forces or global forces for the elements, the force, deformation, stiffness or stress-strain for the sections. These three types of *Recorder* objects were used in the present project.

2.2. Provisions of NBCC 2005 and Supplement No.1 to CSA S16-01 for Type MD Moderately Ductile concentrically braced frames and Type LD Limited Ductility concentrically braced frames

According to the National Building Code of Canada 2005 and the CSA-S16S1-05 (Supplement No.1 to CAN/CSA-S16-01), the seismic design of members and connections of the seismic-force-resisting system of steel framed buildings has to follow capacity design principles in order to resist the maximum anticipated seismic loads. However, these loads need not exceed the values corresponding to $R_dR_o = 1.3$; where R_d is the ductility-related force modification factor that reflects the capability of a structure to dissipate energy through inelastic behaviour and R_o is the overstrength-related force modification factor that accounts for the dependable portion of the reserve strength in a structure.

The part of the structural system considered in design to provide the necessary resistance to the earthquake forces and deformations is called the seismic-force-resisting system. The structural elements that are not part of the seismic-force-resisting system must be capable of supporting the gravitational loads when subjected to seismically induced deformations.

In the capacity design strategy, there are specific elements or mechanisms of the seismic force resisting system that are designed and detailed to dissipate the seismic input energy, while all other elements are sized to ensure that the intended energy dissipation mechanism can be achieved and maintained during the design earthquake. Structural integrity must be maintained during strong ground shaking, and the diaphragms and the load collectors have to transmit the loads from each level to the vertical elements of the lateral load resisting system and to the foundations.

In the 2005 National Building Code of Canada (NBCC 2005), the peak ground acceleration (PGA) and the 5% damped spectral response acceleration values for the reference ground conditions (Site Class C) are given for periods of 0.2 s, 0.5 s, 1.0 s and 2.0 s and they are based on a 2 % probability of exceedance in 50 years. The design spectral acceleration values are determined by applying the appropriate acceleration and velocity based site coefficients F_a and F_v for the site class.

Two methods of analysis for design earthquake actions are described in NBCC 2005: the dynamic analysis and the equivalent static force procedure. The latter can be used only for particular cases such as:

- cases where $I_E F_a S_a(0.2s)$ is less than 0.35;
- regular structures that are less than 60 m in height and that have a fundamental lateral period T_a smaller than 2.0 s in both orthogonal directions; or
- structures with structural irregularities, (except structures with torsional sensitivity), that are less than 20 m in height and have a fundamental lateral period T_a smaller than 0.5 s in both orthogonal directions.

In the equivalent static force procedure, the design earthquake lateral force, V, shall be calculated with the formula:

$$V = \frac{S(T_a)M_v I_E W}{R_d R_o} \qquad (2.2.1)$$

where: S is the design spectral response acceleration, T_a is the building fundamental period used in design determined as $T_a = 0.025\ h_n$ for braced frames, where h_n is the height of the building in meters; M_v accounts for higher mode effects on base shear; the factor I_E reflects the importance category of the building: low (0.8), normal (1.0), schools (1.3) and post disaster buildings (1.5); W is the seismic weight of the building, and R_d and R_o are, respectively, the ductility and the overstrength-related force modification factors which depend on the type of the seismic force resisting systems (SFRS).

In design, it is permitted to use the period from dynamic analysis for T_a, but the period cannot exceed $T_a = 0.05\ h_n$. The value of M_v is 1.0 for braced frames located in Western Canada, where $S_a(0.2s)/S_a(2.0s) < 8.0$, as is the case in this study. When $S_a(0.2s)/S_a(2.0s) \geq 8.0$, M_v is equal to 1.0 for $T_a < 1.0$ s and 1.5 for $T_a > 2.0$ s. Linear interpolation of the product SM_v is permitted for intermediate period values.

NBCC 2005 gives the R_d and R_o values as well as general restrictions for different SFRS categories: steel structures, concrete structures, timber structures and masonry structures. For steel structures, the value of the ductility factor varies from 5.0 (for ductile moment resisting frames) to 1.0 for non ductile systems, and the overstrenght-related force modification factor varies from 1.6 (for ductile frame plate shearwalls) to 1.0.

No height restrictions is prescribed for any steel structures for cases where $I_E F_a S_a(0.2)$ is smaller than 0.35 (except for the SFRS that qualify for $R_d = R_o = 1.0$). In this present project, the seismic-force-resisting system is a Type MD, moderately ductile concentrically braced frames for the 2-, 4-, and 8-storeys buildings and a Type LD, Limited ductility concentrically braced frame for the 12- and 16-storey buildings. According to NBCC 2005, the values of R_d and R_o for those types of SFRS are

respectively equal to 3.0 and 1.3 for Type MD frames and to 2.0 and 1.3 for Type LD frames.

Because the $I_E F_a S_a(0.2)$ value is larger than 0.35 height restrictions of 40 m for Type MD structures and 60 m for Type LD frames apply. According to CSA S16, these maximum heights can be increased if additional requirements are satisfied, as this will be explained below in this chapter. As discussed later, the seismic loads for Type MD and Type LD braced steel frames must be increased for structures taller then 32 m and 48 m, respectively, to mitigate the potential for soft-storey response in these taller buildings.

If $R_d \geq 1.5$, the design earthquake lateral force, V, need not exceed 2/3 the value of V calculated with T_a = 0.2s. However, to account for uncertainty in the response of tall structures, V must not be less than the value of V calculated with T_a = 2.0 s.

In the equivalent static force procedure, the base lateral force V is distributed over the structure height according to:

$$F_x = \frac{(V - F_t)W_x h_x}{\Sigma W_i h_i} \tag{2.2.2}$$

where W_x and W_i are the seismic weights at levels x and i respectively, h_x and h_i are the elevations for the corresponding levels from the base and the force F_t is a concentrated lateral force applied at the roof level for the higher mode effect. This force is given by: $F_t = 0.07 T_a V$, but F_t need not to exceed $0.25V$ and may be taken as zero when $T_a \leq 0.7$ s. The overturning moment caused by the earthquake forces at each level x of the building is given by the relation:

$$M_x = J_x \sum_{i=x}^{n} F_i (h_i - h_x) \tag{2.2.3}$$

where J_x is 1.0 for $h_x \geq 0.6h_n$ and $J+(1-J)(h_x/0.6h_n)$ for $h_x < 0.6h_n$. J is the base overturning moment factor. It depends on the ratio $S_a(0.2s)/S_a(2.0s)$, the type of SFRS

and the fundamental period of the building T_a. The J factor is applied to obtain realistic estimates of the overturning moments computed with the forces F_x, rather than from dynamic analysis. For braced steel frames in western Canada where $S_a(0.2s)/S_a(2.0s) < 8.0$, as is the case in this thesis, the value of J is equal to 1.0 for $T_a < 1.0$ s and 0.8 for $T_a > 2.0$ s. Linear interpolation between these values is permitted for intermediate period values.

According to NBCC 2005, torsional moments must be considered in the design of the structure concurrent with the lateral F_x forces. These moments are due to the eccentricity between the center of mass and the center of rigidity of the building and/or by the accidental eccentricities. The torsional sensitivity of a structure is given for each level x and for each orthogonal direction by the following relation:

$$B_x = \delta_{\max} / \delta_{ave} \tag{2.2.4}$$

where δ_{max} and δ_{ave} are respectively the maximum and average inter-storey drifts at the extreme points of the structure produced by the equivalent static forces acting at distances of $\pm$ $0.10D_{nx}$ from the mass centres of each floor. The maximum of the B_x values is denoted with B. For buildings with $B \leq 1.7$, torsional moments must be applied throughout the building by means of two load cases:

$$T_x = F_x(e_x + 0.1D_{nx}) \text{ and } T_x = F_x(e_x - 0.1D_{nx}) \tag{2.2.5}$$

If $B > 1.7$ and $I_E F_a S_a(0.2s) > 0.35$, the torsional effects must be accounted for through a dynamic analysis.

The dynamic analysis procedure specified in NBCC 2005 consists in the application of one of the following methods:

a) Linear dynamic analysis using either the modal response spectrum or the numerical integration linear time-history method; and
b) Nonlinear dynamic analysis method.

For regular structures, the results of such a dynamic analysis must be scaled such that the base shear from dynamic analysis, V_d, is at least equal to $0.8V$ as defined earlier, unless the dynamic forces exceed those obtained in the equivalent static force procedure. For irregular structures requiring dynamic analysis, the design base shear shall be taken as the largest of the 100% of V as defined earlier and V_d. The base shear V_d is obtained from:

$$V_d = \frac{V_e I_E}{R_d R_0} \tag{2.2.6}$$

where V_e is the elastic base shear obtained from the linear dynamic analysis.

The lateral deflections obtained from a linear elastic analysis with one of the two methods described above must be multiplied with $R_d R_o / I_E$ in order to obtain realistic values, including inelastic deformation effects.

The interstorey deflection at any level shall not exceed $0.025h_s$ for buildings of the normal importance category. For the post-disaster buildings and schools the maximum deflection are $0.01h_s$ and $0.02h_s$ respectively.

Clause 27 in CSA-S16S1-2005 includes general and system specific seismic design provisions aiming at developing the ductility levels intended in NBCC 2005. For capacity design, the expected yield stress of the steel must be taken as equal to $R_y F_y$ with $R_y = 1.1$ (with $R_y F_y \geq 385$ MPa), and the width-to-thickness limits for the energy-dissipating elements shall be calculated using $F_y \geq 350$ MPa.

In calculating the P-Δ effects, the lateral loads must be multiplied by the amplification U_2 coefficient taken as:

$$U_2 = 1 + (\frac{\Sigma C_f R_d \Delta_f}{\Sigma V_f h_s}) \leq 1.4 \qquad (2.2.7)$$

where: ΣC_f is the sum of the axial loads in the columns; R_d is the ductility-related force modification factor; Δ_f is the lateral displacement resulted from a first order analyse; ΣV_f is the sum of the shear loads at the considered floor and h_s the height storey. The structure need to be stiffened if the value of U_2 exceeds 1.4.

Only the S16S1-2005 seismic design requirements applicable to Moderately ductile concentrically braced frames and Limited ductility concentrically braced frames are presented below.

Type MD (moderately ductile) concentrically braced frames can dissipate a moderate quantity of the seismic energy through the yielding and inelastic buckling of the braces. They must be designed with R_d = 3.0 and R_o = 1.3. Four bracing configurations or systems are considered in Type MD concentrically braced steel frames:

- tension-compression bracing system;
- chevron bracing system;
- tension only system; and
- other concentrically braced frame systems that can provide stable inelastic response.

The frames studied herein are of the tension-compression system and only the provisions that are applicable to this system are presented in the following paragraphs.

- Tension-compression bracing systems must not exceed 40 m in height if the specified short-period spectral acceleration ratio $I_E F_a S_a(0.2)$ is greater than 0.35. In addition, when the height exceeds 32 m the factored seismic forces must be increased by 3% per meter of height.

- The diagonal bracing members must have a slenderness ratio (*KL/r*) equal to or less than 200.
- The width-to-thickness ratio is function of the slenderness ratio. When $I_E F_a S_a(0.2) \geq 0.35$, the width-to-thickness ratios must not exceed:
  - When $KL/r \leq 100$: $330/\sqrt{F_y}$ for rectangular and square HSS, $10000/F_y$ for round HSS, $145/\sqrt{F_y}$ for legs of angles or flanges of channels, and Class 1 for other elements;
  - When $KL/r = 200$ Class 1 limits for HSS members, $170/\sqrt{F_y}$ for legs of angles, Class 2 limits for other elements;
  - When $100 < KL/r < 200$ linear interpolation may be used.
- Class 1 HSS can be used when $I_E F_a S_a(0.2) < 0.35$.
- For the brace connections, the eccentricities should be minimized. The factored resistance of the connections must be equal to or exceed both the tension resistance of the bracing member ($A_g R_y F_y$) and 1.2 times the probable compressive resistance of the bracing member. The tensile force must not exceed the combined effect of the gravity load in the bracing and the effects of storey shear corresponding to $R_d R_0 = 1.3$. Redistribution of load due to brace buckling must be considered when computing member forces due to lateral loads corresponding to $R_d R_o = 1.3$.
- The bracing members or their connections, including gusset plates, must be detailed to provide ductile rotational behaviour in or out of plane of the frame. If not, the connections must be sized for the expected flexural capacity of the bracing members.
- For the calculation of the design forces for columns, beams and connections (other than brace connections), the redistribution of loads due to buckling or yielding of the braces must be considered.
- All columns in multi-storey buildings must be continuous and of constant cross-section over a minimum of two storeys. The splices of the columns must have a

factored shear resistance $\geq 0.4/h_s$ times the nominal flexural resistance of the columns; where h_s is the storey height.

- The columns in braced bays shall have a bending resistance $\geq 0.2ZF_y$ in combination with the computed axial loads. They shall also be made of Class 1 or 2 sections.

Type LD (limited ductility) concentrically braced frames can dissipate a limited amount of the seismic energy through the yielding of the braces and classify for $R_d = 2$ and $R_o = 1.3$.

Essentially they must meet all requirements for Type MD braced frames except that:

- Tension-compression bracing system must not exceed 60 m in height, when the short-period spectral acceleration ratio of the building is greater than 0.35. Additionally, for heights greater than 48 meters, the factored seismic forces must be increased by 2% per meter of height.

2.3. Past studies on braced steel frames

The first objective of this research project is to use OpenSees computer software to study the seismic behaviour of braces in split X braced steel frames and the seismic stability of multi-storey Split X braced steel frames. Several past studies addressed the behaviour of braced steel frames.

Tremblay (2000) performed an analytical study on concentrically braced steel frames with 1-, 2-, 4-, 6- and 8-storeys located in western Canada. The objective was to evaluate the influence of the brace slenderness on the building seismic performance. Two braced frame systems were studied: tension-compression bracing and tension-only bracing. The study revealed that large inelastic deformations tend to concentrate in a few stories over the height of the buildings, especially at the top of the 4-storey building and at the upper two levels of the 6- and 8-storey buildings when the tension-only system is used. For the

Ductile Braced frame category specified in Canadian seismic design provisions, the author suggested the following:

- in tension-compression bracing systems non-dimensional brace slenderness parameter, λ (= $KL/r(Fy/\pi^2 E)^{0.5}$) up to 2.65 should be allowed;
- tension-compression bracing systems should be limited to 8 storeys in height, unless it can be shown that a higher structure exhibits a stable inelastic response;
- tension-only bracing systems should be used only in single or two storey buildings with the brace slenderness parameter, λ, less than 2.65. Buildings up to four floors should be allowed if the columns are continuous over the full height of the building.

The provisions in CSA-S16-01 for height limits, *KL/r* limits for braces, and for the continuity of the columns in concentrically braced frames were based on this study.

Tremblay and Robert (2001) studied the seismic behaviour of chevron steel braced frames for buildings of 2-, 4-, 8- and 12-storeys in height located in Vancouver, B.C. Two design philosophies were used. The first one complies with CSA-S16.1-94 provisions for braced frames with nominal ductility (NDBF) for which a force modification factor *R* of 2.0 was specified in the 1995 NBCC (NRCC 1995). In the second design approach, the chevron braced frames were considered as ductile braced frames (DBF) with an *R* factor of 3.0. The beams were strong enough to compensate the loss in brace axial strength due to buckling of the braces. The authors considered three types of chevron braced frames DBF-100, DBF-80 and DBF-60 according to the levels of tension force assumed in the tension braces when designing the beams of the DBF chevron braced frames: 100%, 80% and 60% of the brace yield load.

The study showed that dynamic instability results from large inelastic deformations at given floors due to the degradation of the storey shear resistance after brace buckling has

occurred. This phenomenon is more critical when the building height is increased and it cannot be mitigated by applying current provisions for P-delta effects. Therefore the authors recommended (unless specific analysis is performed to study the system stability) that:

- NDBF system be only used in structures up to 2 storeys. They also may be used in structures up to 4 floors but then, story drift in excess of the current code limits are expected together with high bending moments in the columns.
- The DBF-60 system be only permitted in structures up to 4-storeys
- The DBF-100 system be only permitted in structures up to 8-storeys and up to 12 storeys only if the gravity loads applied to the beams in the bracing bents are small.

Based on this study, the provisions of CSA-S16-01 for height limits and for the design of the beams in chevron braced frames have been elaborated.
In 2004, Tremblay and Poncet studied the seismic stability of multi-storey concentrically braced frames on building heights from 4 to 16 floors located in western Canada. Three types of braced frames were studied: conventional, buckling restrained and dual buckling restrained braced frames. The conventional braced frames were designed according to the proposed NBCC2005 and CSA-S16-01: the use of moderate ductility (MD) braced frames is limited to 8 floors while 12 floors was the limit for the limited ductility (LD) braced frames type.

The study indicated that the potential for dynamic instability increases with the height of the building in conventional Type MD braced frames. More robust performance can be achieved if the lateral resistance is increased in design either by taking into account P-delta effects or by reducing the force modification factor. The authors concluded that the use of the response spectrum analysis method did not improve the seismic stability,

partly because of the 20% reduction in strength permitted by the code when a dynamic analysis method is used.

One year later, the same authors, (Tremblay and Poncet, 2005), studied the influence of mass irregularity on the inelastic seismic performance of eight-storey buildings with concentrically braced frames, also located in western Canada. Three location of mass discontinuity (25%, 50% and 75% of the building height) were considered with two ratios of seismic weight (200% and 300%). The design of the structures was done according to the proposed NBCC 2005 using two analysis methods: the equivalent static force procedure and the response spectrum analysis method. The seismic performance of the buildings was evaluated for two limit states: immediate occupancy (associated to small deflections) and collapse prevention (structural damage is expected and the structure exhibits only residual strength and stiffness).

The authors conclusions were:

- Mass irregularity has limited effects on the elastic response of the buildings for immediate occupancy.
- The eight-storey concentrically braced frame can be designed with the equivalent static force procedure. When a dynamic analysis is performed, the 20% reduction of the design loads could lead to inadequate performance for collapse prevention.
- Mass irregularity does not seem to have significant detrimental effect on the protection level against structural collapse for the structures designed with static analysis. Using the dynamic analyses does not seem to improve the response of buildings with mass irregularity.

The influence of mass irregularity, in terms of location along the height and mass ratios, was also studied by Tremblay et al. (2005). The study involved concentrically braced steel frame buildings of 4-, 8-, 12- and 16-storeys in height located in western and eastern

Canada. Two design methods proposed by NBCC 2005 were used: the equivalent static force procedure (ESFP) and the multi modal response spectrum (dynamic analysis). This study showed that the ESFP procedure can be safely applied to buildings with mass irregularity of up to 300% with the exception of "podium type" buildings that had 50% or more of their mass located in the lower 25% of their height. More economically designs could however be obtained using the dynamic analysis method. For the "podium type" building a dynamic analysis should be performed in order to verify the storey shear forces in the lower levels. It was also observed that the base shear from dynamic analysis, V_d, is more likely to exceed the value of V in western Canada.

Lacerte and Tremblay (2006) studied the inelastic seismic response of multi-storey Split-X concentrically braced steel frames. Structures with 2-, 4-, 8- and 12-storeys in height and located in western and eastern Canada were considered. The buildings were designed according to a preliminary version of NBCC 2005 and according to CSA-S16-01 standard. This preliminary version of NBCC 2005 did not include limit on the design period ($T_a < 0.05h_n$) and no reduction on the earthquake forces corresponding to 2/3 V_f for short period structures. The force modification factors R_d and R_o were considered equal to 3.0 and 1.2 respectively. The equivalent static force procedure was used to distribute the lateral force over the height of the buildings. The study showed that the Split-X concentrically braced frames of 8 floors and taller structures can experience significant concentration of inelastic deformations over their height, which could lead to collapse by dynamic instability. The structures located in western Canada and those with larger gravity loads were more subject to this behaviour when compared to the other ones.

In all the above studies, the nonlinear dynamic analyses were performed using the DRAIN-2D computer software (Powell and Kanaan, 1973) and the braces were modeled using the inelastic brace-buckling element with pinned ends (Element No. 9) developed by Jain and Goel (1978). This is a phenomenological model, i.e. a simple pin ended truss

element to which there were assigned axial hysteretic properties that mimic the observed experimental behaviour. This model is rather simple and has several limitations that can conduct to inaccurate predictions of the structures behaviour.
The SNAP2D (Structural Nonlinear Analysis Program) computer software (Rai, 1996) is an improved version of the DRAIN-2D computer software. It was used by Sabelli (2001) in his research on improving the design and analysis of earthquake-resistant steel braced frames. The brace element (element 09) employs Jain's hysteretic model (Jain, 1987) and has a fracture life-criterion based on tests on steel tubes (Tang, 1989).

In his research, Sabelli made a parallel and comparative study between the seismic behaviour of conventional braced frames (chevron, cross-braced and zipper frames) and buckling restrained braced frames. Two building sizes were used: 3-storey building and 6-storey building, both located in central Los Angeles on a firm soil. The ground motions (twenty records) developed for the SAC model building study were used. The buildings were designed using the NEHRP Recommended Provisions for Seismic Regulations for New Buildings and Other Structures (FEMA, 1997) and the Load and Resistance Factor Design Specification for Structural Steel Buildings (AISC, 1993). Member forces for design were calculated using an equivalent static lateral force based on a response-spectrum corresponding to a hazard of 10 % chance of exceedance in a fifty-year period.

The performance of the cross-braced configuration does not depend much on the beam design criteria, as is the case for chevron-braced frames. Therefore the three-storey crossed braced frame response was less severe than that of the chevron braced frame, even if it experienced some concentration of damage and brace fractures. For the six-storey building, the Split-X cross-braced configuration showed a wider distribution and a greater incidence of brace yielding than the chevron configuration, and an adequate performance with less steel weight. Therefore the author recommended the addition of Split-X and Zipper configurations to the Seismic Provisions for Structural Steel Buildings (AISC, 1997).

Uriz and Mahin (2004) used the nonlinear beam-column element available in the OpenSees software environment. The element is based on an efficient large-displacement formulation. and a fibre representation of the cross-section. Therefore, bi-axial bending and axial load resistance interaction as well as buckling effects can be simulated. They showed that the element is robust and that the results of numerical simulation for a typical square steel tube brace were very close to the experimental ones.

Gunnarson (2005) focused in his research on the numerical evaluation of the seismic performance of Special Concentrically Braced Frames (SCBF) and Buckling Restrained Braced Frames (BRBF). The inelastic response of the braced frame system was investigated using the OpenSees software. Two types of a 3-storey SCBF system were designed: an inverted V bracing frame with zipper columns an X braced frame. The design was done following Appendix B of FEMA 355C, and the equivalent lateral design storey forces were established using the 2000 NEHRP Recommended Provisions for Seismic Regulations for New Buildings and Other Structures (2000). The building was assumed being located in Seattle (site class C) and two ground motions were used for the analyses: the El Centro ground motion and the Newhall ground motion (a near fault type).

The author modeled the frames using the non-linear beam-column element, with fibre section discretization, non-linear geometric formulation and a bi-linear material law. Ten elements were used to model bracing members, beams and columns. The beam and column sections were modeled using 2x10 fibres whereas 10x10 fibres were used for the braces. For the braces, an initial imperfection of $L/500$ was specified, where L is the length of the brace. Geometric nonlinearities of the beams and columns were simulated using a P-delta geometric formulation while a corotational geometric formulation was used in order to model the post buckling behaviour of the braces. The author concluded from his study that:

- Decreasing the slenderness of SCBF braces results in responses closer to BRBF braces (decreasing the slenderness minimizes the differences between the brace buckling and the yielding capacities);
- The performance of properly designed X bracing frame was similar to V inverted bracing;
- OpenSees is a good platform for future research regarding the modelling of structural systems;
- An online database with experimental results should be of great interest to validate models and develop future inelastic models.

OpenSees was also used by Uriz (2005) in an extensive research that focused on two main objectives: 1) to define and improve analytical tools in order to increase the confidence level in studying the seismic behaviour of structures, and 2) to perform a preliminary hazard evaluation on concentrically braced frames (conventional buckling and buckling restrained braces). It is noted that that document was only made available in 2006, after most of this study had been completed. Only the performance based earthquake analysis of steel braced frames by Uriz is presented herein. This analysis was performed using 11 frame models with 3-, 6- and 9-storeys, representative of low- and mid-rise buildings, with different lateral systems and subjected to 60 ground motions representing hazard from frequent to very rare earthquakes. The analytical models were represented by:

- special concentric brace frames with 3 and 6 storeys and chevron bracing configuration with or without net section reinforcement, with or without taking into account fatigue effects and with or without foundation rocking effects;
- buckling restrained brace frames with 3 and 6 storeys with net section reinforcement, taking into account fatigue effects and without foundation rocking effects, and

- moment resisting frames with 3 and 9 storeys with net section reinforcement, taking into account fatigue effects and without foundation rocking effects.

The braces, beams and the columns were modeled with the nonlinear beam-column element that was modified to take into account fracture of the members due to low-cycle fatigue effects. The resistance to fatigue in the model was calibrated on experiments. The Menegotto-Pinto material model was used for the braces, beams and columns. This material model will be described in Chapter 3. Beams and columns were modeled using two nonlinear elements along the member length and three integration points per element. The columns were modeled with initial imperfections and with cross sections discretized in 16 fibers per flange and 4 fibers along the web length. Conventionally buckling braces were modeled using 20 elements along the length and the cross sections dicretized in 16 fibers for the flanges and the web. The brace model allowed out-of-plane brace buckling, assuming end hinging developing in the gusset plates in the "$2t_g$" free length detail suggested in AISC seismic provisions. Rigid end offsets were considered from the beam-to-column centerline intersection point to the middle of the "$2t_g$" fold-line of the gusset plate and the region of the brace that is welded to the gusset plate was modeled as a bare brace. The fatigue parameters used in the brace model were calibrated in static tests. The floors were assumed to act as rigid diaphragms, therefore the out-of-plane displacements of the beams were considered fixed. The torsional properties of the beams and columns were considered rigid. The gravity columns were modeled as a single leaning column pinned at the base, rigidly linked at the lateral displacement of each floor and having the weak-axis property of all the interior columns. Beam with hinges elements were used to model these columns.

The suite of ground motions developed by Somerville (1997) was used for the study, for hazards corresponding to 2%, 10% and 50% probability of exceedence in 50 years. The buildings were assumed to be located on stiff soil in Los Angeles area. The author concluded from this analysis that:

- The low-rise conventional braced structures exhibited poor performance: they had large drifts at the first floor for larger excitations and small drifts demands in the upper floors;
- The rocking foundation models had very large drifts at all floors although the structural system had little damage. For this system, the inter-storey drifts were similar to those anticipated for moment frames;
- The buckling restrained braced frame systems had superior behaviour compared to conventional bracing systems. The median drifts demands were similar to those for the moment frames even though the natural period of vibration was smaller;
- The systems with net section reinforcement, with fatigue effects and without foundation rocking effects behaved poorly, exhibiting instability and collapse; the 6-storey model, though, behaved better than the 3-storey model, suggesting that shorter period structures have a more pronounced tendency for larger drifts.
- The 3-storey model without net section reinforcement was unstable for 30% of the records, twice as much as for a 2-storey model, which illustrates the need for proper detailing;
- P-delta effects were reduced for the braced systems with rigid foundations.

Aguero et al. (2006) investigated the possibility of modeling the seismic inelastic cyclic response of steel bracing members using the OpenSees computer program with the non-linear beam-column elements. Model predictions were compared to individual brace and full-scale frame test results. Realistic previsions, by far superior to using empirical and semi-empirical models, were found. This article was prepared as part of this Master's Thesis work and the work is reported in Chapter 3.

Many studies showed that there are problems with the instability of conventional bracing systems. Therefore a study of the seismic performance of structures designed with the NBCC 2005 and CSA S16-01-05 provisions was needed to verify the adequateness of these provisions. The literature review revealed that the OpenSees computer program is

suitable for adequately reproducing the behaviour of the steel braces and that program was therefore chosen for this project.

2.4. Loading protocols

The second main objective of this research project was the development of a numerical database that can be used to propose loading protocols for the seismic testing of bracing members used in concentrically braced steel frames. For this purpose, nonlinear dynamic analyses were carried out on typical 2, 4, 8, 12 and 16-storey braced frames, as discussed in Chapters 4 and 5. The structural response parameters considered in determination of the loading histories were established by studying the loading protocols elaborated by Tremblay and Bouatay (2002), Krawinkler et al. (2000), Krawinkler et al. (2000), and Sabelli (2001).

2.4.1. Tremblay and Bouatay (2002)

The authors proposed four different loading protocols for the different types of ground motions in North America: crustal events at distance in eastern and western Canada and near-field and subduction earthquakes in western Canada. The protocols were developed based on the results of nonlinear time step dynamic analyses performed on braced steel frames having 2, 4 and 8 storeys built with buckling restrained bracing members exhibiting a bi-linear hysteretic response. The loading histories were established from the axial deformation time history of the bracing members and statistics of brace response parameters. For the 4- and 8-storey buildings only the deformations in the braces at the bottom and top floors were used because these two braces typically experienced the most severe inelastic response in the multi-storey buildings. The parameters considered in the development of the loading protocols were:

- the *peak ductility*, $\mu = \delta_{max} / \delta_y$;

- the *total energy dissipated, EH*, normalized with respect with $P_y\ \delta_y$, $EH/\ (P_y\ \delta_y)$;
- the *fraction of the total energy dissipated* when the brace yields in the same direction as in the inelastic excursion when μ_{max} is reached, $EH_{\mu max}/EH$;
- the *damage index, D*, determined using the linear damage accumulation model by Krawinkler and Zohrei and the rainflow counting method;
- the *time required to dissipate* between 5% and 95% of *EH*, $t_{5\text{-}95}$;
- the *fraction of* $t_{5\text{-}95}$ *required to dissipate* between 5% and 50% of *EH*, $t_{5\text{-}50}/\ t_{5\text{-}95}$;
- the *maximum rate of energy dissipation*, $P_y\ \delta_y/s$;
- the *average rate of energy dissipation*, $EH/\ t_{5\text{-}95}$;
- the *total number of inelastic excursion*, n_i;
- the *numbers of inelastic excursions*, n_0, n_1, n_2,..., and n_9 with an amplitude range of 0-0.5 δ_y, 0.5-1.5 δ_y, 1.5-2.5 δ_y, ..., and 8.5-9.5 δ_y;
- the *number of inelastic excursion having an amplitude greater* than 9.5 δ_y, n_{10}.

The test protocols were developed to reproduce the most critical value of each response parameter while ensuring that the protocols would still represent realistically the observed deformation time histories. While examining the computed responses, the authors realised that it was impossible to achieve this objective with a single brace deformation history because there were significant differences between the effects of each ground motion type, especially for the amplitude and the number of inelastic excursions, the duration of inelastic response and the maximum rate of energy dissipation. Therefore, they developed four types of loading protocols, one for each of the considered ground motion ensembles.

Of interest for the present research project, is the loading protocol that was developed for the west crustal events at distance shown in Fig. 2.4.1, as it corresponds to the case examined in this study.

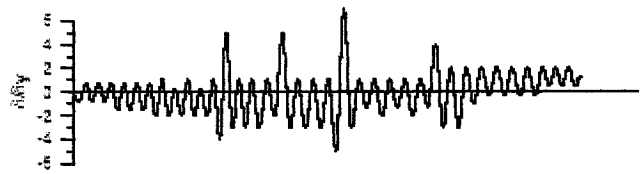

Fig. 2.4.1 Loading protocol for west crustal events at distance

The protocol is made of a suite of sinusoidal curves so that the maximum energy dissipation demand is met in the largest inelastic cycles with the peak ductility demand in the tension side (more critical for fracture).The first and the last three cycles were elastic cycles with amplitude of $\pm 0.75\ \delta_y$, in order to compare the initial stiffness of the specimen with the residual value after the inelastic response. The inelastic cycles were distributed along the time scale in order to reproduce the distribution observed in the analyses and to meet the mean values of $t_{5\text{-}50}/\ t_{5\text{-}95}$. The average rate of energy dissipation $EH/\ t_{5\text{-}95}$ stands on the conservative side because the proposed signal doesn't contain any intermediate elastic cycles (its duration $t_{5\text{-}95}$ is shorter than that obtained in the sample buildings).

2.4.2. Krawinkler et al. (2000)

Krawinkler et al. (2000) used the results of the analyses by Medina and Krawinkler (1999) to develop loading histories for the SAC Joint Venture for the seismic performance testing of steel moment resisting frame components and assemblies. A large number of nonlinear time history analyses were used to predict the connection demands based on which the loading protocols were developed. The authors proposed two different types of loading histories for testing the beam-to-column subassemblies. The first one, the basic loading history, should be employed for tests in which the ground motion that controls the design causes several cycles of damaging response and is not of the near-fault type. The second one, the near-fault loading history, is utilised for large displacement pulses.

The following presentation of the authors' development of a loading protocol focuses on the basic loading protocol, because the ground motions considered in the present project are not of the near-fault type. The deformation parameter used to control the loading protocol was the inter-storey drift angle, θ, defined as the inter-storey displacement over the storey height. The authors considered that this is the best choice for steel moment resisting frames because the storey drift angle value in a given earthquake is not very sensitive to the number of storeys or to subjective design decisions, and also because extensive analytical studies (Gupta and Krawinkler, 1999) showed that this parameter can be bracketed, except in extreme cases.

The model buildings used in their studies were the SAC model buildings: 3-, 9- and 20-storey steel moment resisting frames designed for Los Angeles and for Seattle. The results of the SAC ground motion record sets for 10% and 2% in 50 years were used. The emphasis was put on the L.A buildings in the development of the basic loading history and the predictions of interstory drift angle demands were based on 2D analyses. The damaging excursions were found by applying the simplified rainflow cycle counting method to the deformation histories obtained from the analyses. Cycle counting is necessary for converting the response time history of the inter-storey drift angle into a series of cycles from which the loading history can be obtained. Rainflow cycle counting method means re-arranging the response history in order to obtain the largest possible deformation ranges and the smaller excursions to be interruptions of larger ones. The history starts always with the maximum amplitude point and the end of the moved-up portion is connected artificially with the beginning of the time history. This method is a compromise because the damage due to the largest excursion is realistically represented in one direction and overestimated in the other. The history resulting from this method has only full cycles. The basic loading history was based on the following demand parameters:

- N_t, the *number of cycles* with deformation range bigger or equal to 0.005;

- θ_{max}, *maximum deformation* experienced during the seismic response;
- $\Delta\theta_{max}$, *maximum deformation range* (peak-to-peak) experienced during the seismic response;
- $\Delta\theta_2$, *second largest deformation range* experienced during the seismic response;
- $\Delta\theta_3$, *third largest deformation range* experienced during the seismic response;
- $\Delta\theta_i$, *deformation range of cycle i* experienced during the seismic response;
- $\Sigma\Delta\theta_i$, *sum of deformation ranges* bigger or equal to 0.005;
- $\Delta\theta_{pi}$, *plastic deformation range* of cycle i ($=\Delta\theta_i - 2\theta_y$);
- $\Sigma\Delta\theta_{pi}$, *sum of the plastic deformation ranges*;
- N_p , *number of inelastic cycles* (cycles with amplitude $>\theta_y$).

All the above demand parameters for the basic loading history were derived from series of ordered deformations ranges, $\Delta\theta_i$, for each floor of each structure and each ground motion record. A loading history cannot cover all possible cases (ground motion characteristics, structural configurations and failure modes). It has to be rationalized in order to be used for a general performance evaluation, at various performance levels and in different seismic regions. The loading history has to represent a reasonable and generally conservative demand on N_t, $\Delta\theta_i$ and $\Sigma\Delta\theta_i$ which means an average number of damaging cycles and a conservatively representation of the cumulative deformation range. Considerations should be given to the cycles with relatively large deformation ranges and to a conservative representation of the plastic deformation ranges. The statistical evaluation of the demand parameters was made only on "critical" stories of each structure. These were found to be the 3rd story and the 9th story for the structures of 3 and 9 floors regarding the largest values of the θ_{max}, $\Delta\theta_{max}$ and $\Sigma\Delta\theta_i$.

The results are presented for 50, 75 and 90 percentiles, for three record sets 10% in 50 years (20 records), 2% in 50 years (20 records) and 2% in 50 years (10 records representing 10 fault normal components of 2% in 50 years records) and for the following parameters N_t, θ_{max}, $\Delta\theta_{max}$, $\Delta\theta_2/\ \Delta\theta_{max}$, $\Sigma\Delta\theta_i$ and $\Sigma\Delta\theta_{pi}$. The following considerations

were made in order to establish the number of cycles and the deformation ranges in the basic loading history:

- Only symmetric cycles are performed, with an amplitude equal to one half the deformation range $\Delta\theta_i$;
- For a selected number of cycles N_t :
  - the *cumulative distribution function* (*CDF*) of the test loading history is below the *CDF* of the $\Delta\theta_i$ points from the analyses for the 10% and 2% in 50 years sets of ground motions;
  - the sum of the deformation ranges of the loading history is larger than the demands on $\Sigma\Delta\theta_i$ for the appropriate percentiles and ground motion sets.

The loading history was developed using the analysis results for inter-storey drift angle at the 3rd floor of the 3-story L.A. building, which exhibited the largest demand levels. That history was then checked against the demand observed at the 9th floor of the 9-storey L.A. building. For the basic loading history, the authors considered the following values as target values for the demand parameters:

- the number of damaging cycles, N_t, is set to 30, being assumed that every cycle with $\Delta\theta > 0.005$ can cause damage;
- the maximum deformation range, $\Delta\theta_{max}$, is set to 0.0504 (the 90th percentile value) for the 10% in 50 years records (0.06 for the loading history), and to 0.0838 (the 75 percentile) for the 2% in 50 years records (0.08 for the loading history);
- the maximum deformations θ_{max}, where obtained : 10% set θ_{max}= 0.0332
  2% set θ_{max}= 0.0522
  2%-10 set θ_{max}= 0.0534

  The authors did not consider as a problem the fact that the latter two values exceeded the maximum test amplitude (0.04) because: 1) the damage is proportional to the

range, not with the amplitude, and 2) the largest value for θ_{max} was obtained for near-fault ground motions.

- the cumulative deformation ranges, $\Sigma\Delta\theta_i$, were found :

  10% set $\Sigma\Delta\theta_i$= 0.47

  2% set $\Sigma\Delta\theta_i$ = 0.487 (for 90th percentile $\Sigma\Delta\theta_i$ = 0.602)

  2%-10 set $\Sigma\Delta\theta_i$ = 0.420 (for 90th percentile $\Sigma\Delta\theta_i$ = 0.702).

Additional considerations were regarded when developing the loading histories:

- the number of small cycles is greater than the number of large cycles
- for small cycles the step increment should be small, and for large cycles it can increase; and
- the steps should be such that the second and the third largest deformation ranges to be conservatively reproduced.

The basic loading history is illustrated in Fig. 2.4.2.

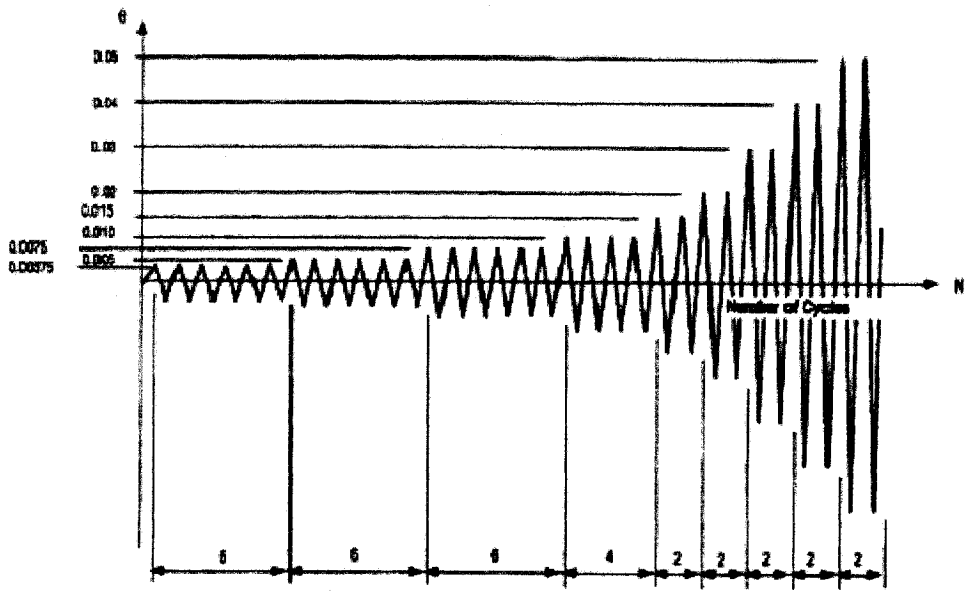

Fig. 2.4.2 Basic loading history.
Deformation parameter is inter-story drift angle

It is composed of 32 cycles in 7 steps:
- 6 cycles with peak drift angle $\theta = 0.00375$
- 6 cycles with $\theta = 0.005$
- 6 cycles with $\theta = 0.0075$
- 4 cycles with $\theta = 0.01$
- 2 cycles with $\theta = 0.015$
- 2 cycles with $\theta = 0.02$
- 2 cycles with $\theta = 0.03$

In a test, the loading history should be continued following the established pattern (additional steps with 2 cycles at each step and with increments in θ of 0.01) until severe strength deterioration is observed (the resistance at peak deformation is less than 30% of the maximum resistance).

Even if it was developed for steel moment resisting frames, that SAC loading protocol was used in experimental tests on steel braces realised as part of recently completed NSF/NEESR project by B.V. Fell and A.M. Kanvinde at the University of California, Berkeley.

2.4.3. Krawinkler et al.(2000)

Krawinkler et al. give recommendations for quasi-static experimentations on components of woodframe structures and for shaking table experiments on wooden houses. The authors also developed loading histories based on the results of nonlinear dynamic analysis on hysteretic systems. They developed deformation controlled loading histories for ordinary ground motions and for near fault ground motions as well as forced controlled loading histories.The interest for the present research project is on basic loading histories, and hence, only this part of the report is presented.

The set of ground motions utilised for the development of the basic loading history had a probability of exceedance of 10% in 50 years for the Los Angeles area. A total of 20 records were used in order to obtain stable statistical estimates: median and 84th percentile. It was decided to use single story wooden buildings and to place the emphasis on the hysteretic systems represented by plywood shear panels. The pattern for the basic loading history is Fig. 2.4.3.

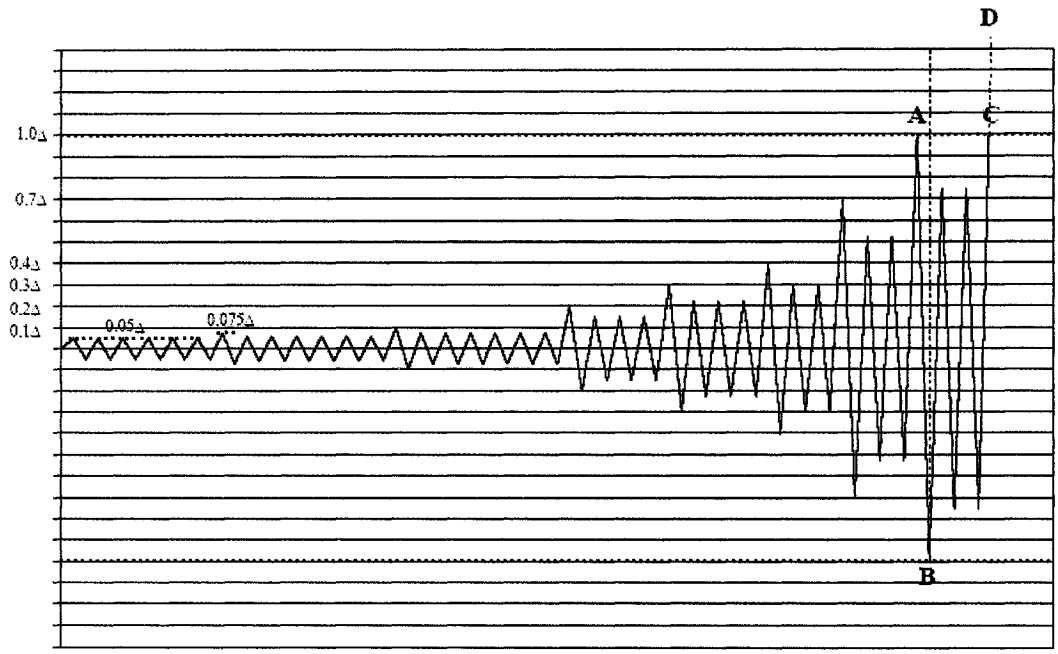

Fig. 2.4.3 Loading history for basic cycling load test

It is formed of:

- 6 cycles of 0.05Δ amplitude
- a primary cycle of 0.075Δ amplitude
- 6 trailing cycles (with an amplitude of 75% from the preceding primary cycle)
- a primary cycle of 0.1Δ amplitude
- 6 trailing cycles
- a primary cycle of 0.2Δ amplitude
- 3 trailing cycles

- a primary cycle of 0.3Δ amplitude
- 3 trailing cycles
- a primary cycle of 0.4Δ amplitude
- 2 trailing cycles
- a primary cycle of 0.7Δ amplitude
- 2 trailing cycles
- a primary cycle of 1.0Δ amplitude
- 2 trailing cycles
- increasing steps with an increase of 0.5Δ in amplitude (one primary cycle with an amplitude increased with 0.5Δ from the previous one, followed by two trailing cycles).

The reference deformation Δ is the maximum deformation (displacement, drift angle, rotation, etc) that a specimen can sustain according to applicable system specific acceptance criteria. It may vary from a specimen to another or can be fixed during a testing program. The general guidelines given by the authors are:

- the monotonic deformation capacity, Δ_m, (found from a monotonic test) is defined as the deformation for which the applied load drops, for the first time, below 80% of the maximal load applied;
- the use of a specific fraction of Δ_m, $\gamma\ \Delta_m$, as reference for the basic cyclic load test. The coefficient γ accounts for the difference in the deformation capacity between a monotonic test and a cyclic test, and it was set for the beginning at 0.6.

The authors considered that the peak values of displacement amplitudes and corresponding ductility ratios do not give insight into the loading history that should be applied in a test. Therefore, the basis for the development of representative loading histories was given by the damage mechanism, which causes stiffness degradation and

strength deterioration under cyclic loading. The following concepts were considered in this development:

- the *damage*, which is defined by the full deformation range (peak-to-peak) of damaging excursion;
- all *excursion above a threshold level* were considered; (the threshold level is the smaller of δ_y or $\Delta\ \delta_{max}/20$ where $\Delta\ \delta_{max}$ is the maximum range that the component experience without significant deterioration in strength);
- *individual excursions* were extracted from response histories and ordered by means of the rainflow cycle counting method;
- *large excursions* are emphasized in the loading history;
- the relative amount of damage caused by an excursion depends on the *deformation range* of the excursion, $\Delta\delta$, the *mean deformation* of the excursion and the sequence in which large and small excursions are applied to the component.
- the *number of damaging excursions*, N, the deformation ranges of the excursions, $\Delta\delta_i$, and the sum of the deformation ranges, $\Sigma\Delta\delta_i$;
- *medians and 84th percentile values* of the largest, second largest, third largest, etc, response excursion obtained from time history analysis and rainflow cycle counting.

In order to derive statistical information for deciding the number and sequence of excursions that will form the loading history, the following process was implemented:

1. Nonlinear time history analyses were performed on structural systems with sets of ground motions;
2. Three evaluations were performed: one for the entire displacement response history, one for the pre-peak response history and the third one for the primary excursions alone;

3. The rainflow cycle counting was performed for each time history response in order to obtain a series of excursions with well defined properties; these excursions are ordered in decreasing magnitude and only those which are larger than the threshold value are considered;
4. For each structural system and set of ground motions, statistical values (median and 84th percentile) for the following response parameters were determined:
   - for each of the ordered excursion : - the deformation range ($\Delta\delta_i$)
     -the mean deformation ($\Delta\delta_{mean,i}$)
   - for partial sums of ranges, the cumulative deformation ranges ($\Delta\delta_{max} + \Delta\delta_2$, $\Delta\delta_{max} + \Delta\delta_2 + \Delta\delta_3$, etc, up to the sum of all damaging excursions);
5. All the statistical information is presented in tables and graphics;
6. A backward process was used for structuring the loading protocol: the largest deformation amplitude, Δ, becomes the parameter function on which all the other excursions are expressed as fractions.

Large differences were obtained between median and 84th percentile response values. Therefore, the authors decided to use 84th percentile response values in order to arrive at conservative estimates of the number of excursion and their relative ranges. The loading protocols developed by the authors represent the seismic demands imposed by Californian earthquakes on woodframe buildings.

2.4.4. Sabelli (2001)

A loading protocol for buckling restrained braced frames was developed by Sabelli (2001). Analytical studies were performed on braced frame buildings with three and six storeys using the nonlinear analysis computer program SNAP-2DX (Rai, 1996). A total of 20 records were used, two each for ten recorded ground motions (one fault-normal, one fault parallel), for the 10% chance of exceeding in 50 years. Parallel sets of analyses were performed on the same buildings using ground motions developed to represent

hazard level of 2% chance of exceedence in 50 years and 50% chance of exceedence in 50 years. The ground motions were selected to represent a range of earthquakes that might occur at the building site during a period of time, and therefore, the results were very different from record to record. Maximum and cumulative inelastic deformations were needed in order to characterise the performance and to develop loading protocols for establishing brace qualification criteria and statistical information on the system demand, both for the inter-storey drift and for the brace demand. The response parameters statistically studied in order to develop the loading protocol were:

- the mean peak lateral floor displacement;
- the mean of the largest inter-story drift values – it was observed that the peak drift demand was much higher in the lower three stories than in the upper levels;
- the residual displacement present in the building – it represents about 40 – 60 % of the maximum displacement attained.
- the cumulative ductility developed by the buckling restrained braces.

The developed loading protocol comprises the following cycles:

- 6 cycles of loading at deformation $\Delta_b = \Delta_{by}$
- 4 cycles at deformation $\Delta_b = 0.50\Delta_{bm}$
- 4 cycles at deformation $\Delta_b = 1.0\Delta_{bm}$
- 2 cycles at deformation $\Delta_b = 1.5\Delta_{bm}$
- Additional complete cycles at deformation $\Delta_b = 1.0\Delta_{bm}$, until the cumulative inelastic axial deformation is at least 140 times the yield deformation;

where Δ_b is the total brace axial deformation, Δ_{bm} is the value of Δ_b corresponding to the design storey drift, Δ_{by} is the value of Δ_b corresponding to the first significant yielding of the specimen. For the calculation of Δ_{bm}, the design story drift shall be ≥ 0.01 times the storey height but not greater than 5 Δ_{by}.

That loading protocol was adopted in the 2005 AISC seismic provisions for steel buildings (AISC 2005) with the following modifications: the number of cycles was kept constant at 2 for all the steps, 2 cycles of $\Delta_b = 2.0\Delta_{bm}$ were added and the additional complete cycles must be at deformation $\Delta_b = 1.5\Delta_{bm}$ until the cumulative inelastic deformation is at least 200 times the yield deformation.

CHAPTER 3. HSS BRACE MODEL USING OPENSEES

This chapter presents the results of a collaborative study that was performed by the author, Antonio Aguero and Robert Tremblay to develop and validate a model for steel bracing members with the OpenSees computer program. Ph.D. candidate Charles-Philippe Lamarche also contributed to the dynamic analysis of the building sample described at the end of this chapter. This work was presented in an article that has been published in 2006 in the International Journal of Advanced Steel Construction (Aguero et al., 2006). The figures and tables presented in this chapter are taken from the paper. The text essentially corresponds to the text of the article.

3.1. Introduction

Bracing members in braced steel frames are expected to experience several cycles of inelastic buckling and tensile yielding when the structure is subject to strong seismic ground motions (Fig. 3.1).

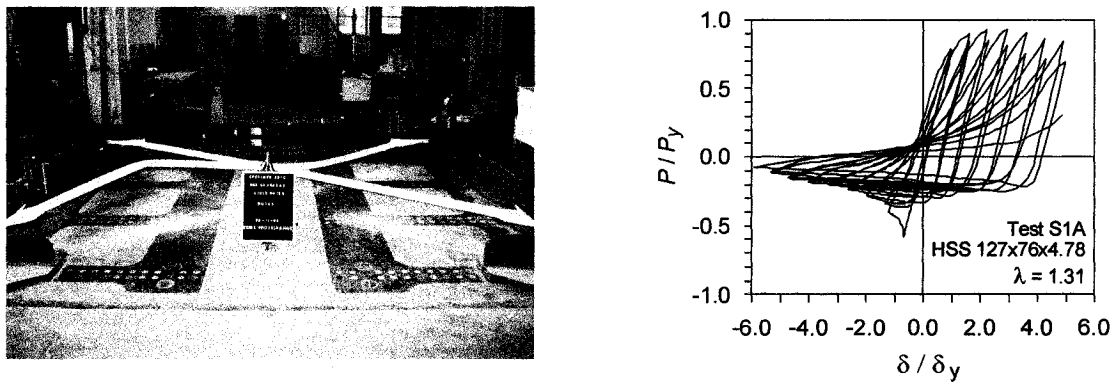

Fig. 3.1 Typical hysteretic response of steel bracing members
(adapted from Tremblay et al. 2003)

When modeling the behaviour of braced frames under seismic loading, the type of brace model and related numerical aspects must therefore be carefully selected such that

accurate results can be obtained while minimizing the computational costs. The objective of this chapter is to develop guidelines for modeling the non-linear seismic response of steel braces using the OpenSees analysis environment.

3.2. Force based elements versus displacement based elements. Parametric study.

A first parametric study was performed to compare the efficiency of the force-based and displacement-based element formulations available in the OpenSees nonlinear beam-column element. The force based formulation was implemented in OpenSees to eliminate the drawbacks and the limits of the displacement based formulation (describing elements with plastic hinges and the softening behaviour) (Kalkan, 2004). Displacement-based elements specify an approximate displacement field along the element while force-based elements interpolate internal forces. The main advantage of the force-based element versus the displacement-based element is "the ability of using one element to represent the material non-linear behaviour of a beam-column element, compared with several displacement-based elements for a single member" (Scott, 2004).

A corotational framework was used to model the nonlinear geometric behaviour, and spread of inelasticity was accounted for through fibre discretization of the cross-section with bi-linear hysteretic material behaviour with isotropic and kinematic strain hardening. In the analyses, an initial sinusoidal out-of-straightness with maximum amplitude corresponding to $1/500^{th}$ of the brace length was specified. The tolerance was set to 10^{-7} and the step size of 0.1 mm was used. The analyses were performed for the brace specimen S2A tested by Tremblay et al. (2003). This brace has a rectangular tubular cross-section (HSS 102x76x4.8) with a steel Young's modulus, E, of 185 GPa and steel yield stress, F_y, of 381 MPa. The slenderness parameter of the brace, $\lambda = (P_y/P_{cr})^{0.5}$, was equal to 1.56, where P_y and P_{cr} are the yielding load and the elastic buckling load of the brace, respectively. The number of elements along the brace length, n_e, was varied (n_e = 4, 8, 16, 24, and 32) as well as the number of integration points per element, n_i (n_i = 4, 5

and 6). A total of 16 fibres were used for modeling the cross-section, as illustrated in Fig 3.2.1.a. Figure 3.2.1.b shows typical hysteresis responses obtained from computation. The brace was considered pined-pined and its length was set equal to the effective length of the brace, $L = KL$.

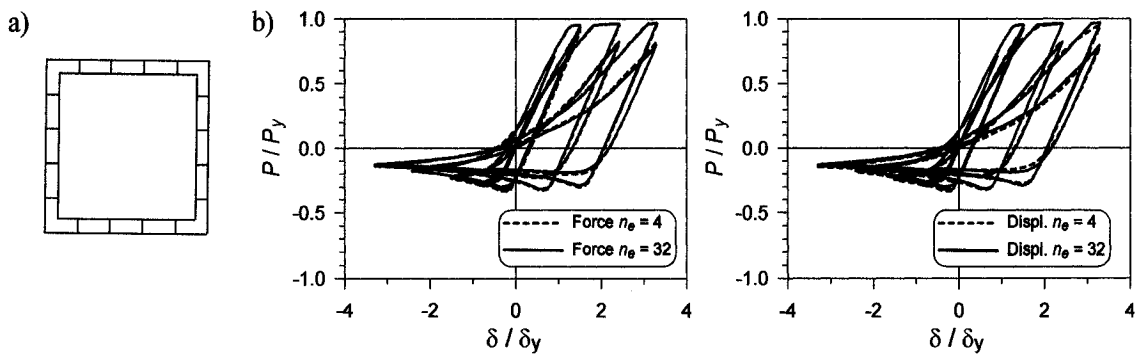

Fig. 3.2.1 a) Fibre discretization; b) Typical hysteretic responses from computation

The computational work was performed with a Pentium 4 with 2.8 GHz and 1.0 Gb RAM. The computation time is given in Fig. 3.2.2.a as a function of the number of elements and integration points. As shown, the computational effort increases nearly linearly with the number of elements but is not influenced by the number of integration points. For this particular example, it was found that the force based formulation required between 40% and 50% more calculation time than the time needed with the displacement based formulation. In the parametric study, it was observed that the sequence of analyses had an influence on the computational time when using the Tcl programming language.

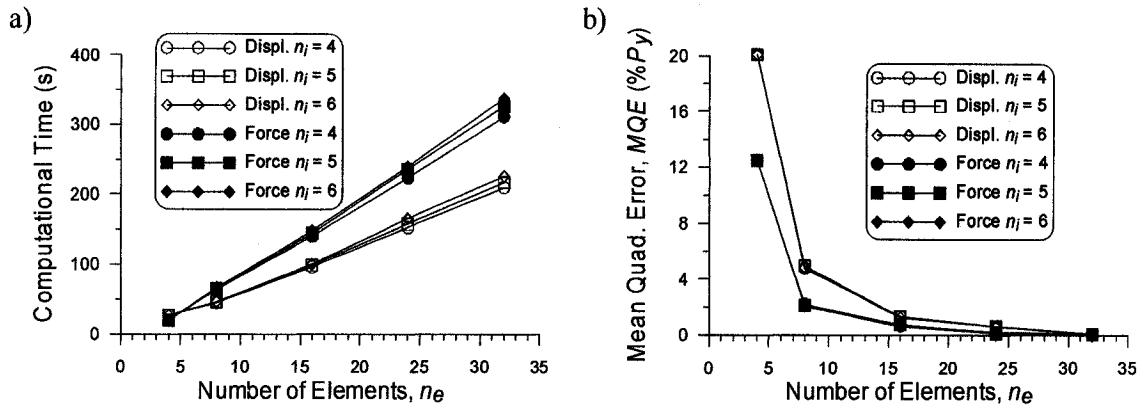

Fig. 3.2.2 Influence of the element formulation, n_e and n_i on: a) Computational time; b) Mean quadratic error, *MQE*

The mean quadratic error on the force developed by the brace element was determined using $MQE = [\Sigma(P_i - P_{ie})^2/n]^{0.5}$, where P_i and P_{ie} are respectively the force estimates at every calculation step with a given (n_e, n_i) combination and with n_e = 32 and n_i = 6, respectively, and n is the number of calculation steps. Figure 3.3.2.b shows the variation of *MQE* with parameters n_e and n_i, expressed as a percentage of P_y, and the numerical results are presented in Table 3.2.1. As anticipated, the error decreases with the number of elements. Again, the number of integration points had limited impact on the quality of the results. The figure clearly shows that a force based formulation leads to more accurate results. Such a convergence is in agreement with previous studies (e.g., Barbato and Conte, 2004).

Table 3.2.1 Mean Quadratic Error Values (% P_y)

n_e	Displacement based elements			Force based elements		
	$n_i = 4$	$n_i = 5$	$n_i = 6$	$n_i = 4$	$n_i = 5$	$n_i = 6$
4	20.10	20.12	20.00	12.50	12.46	12.40
8	4.80	4.95	4.86	2.22	2.12	2.10
16	1.32	1.29	1.27	0.68	0.74	0.65
24	0.61	0.61	0.61	0.19	0.15	0.14
32	0.02	0.04	0.00	0.05	0.05	0.00

3.3. Parametric study using the force based formulation

3.3.1. Influence of modeling parameters

A second parametric study was carried out, this time using only the force based formulation. The influence of brace slenderness was examined by carrying out analyses on three braces with different cross-sections and effective lengths. The properties of the braces are given in Table 3.3.1.1. All members were tubular steel shapes with square cross-sections made of ASTM A500 Grade C steel with $F_y = 345$ MPa and $E = 200$ GPa.

Table 3.3.1.1 Brace properties

Shape	A (mm^2)	$I_x = I_y$ (10^6 mm^4)	r (mm)	KL (mm)	KL/r	λ
305x305x16	16100	222	118	4460	37.8	0.5
203x203x9.5	6490	40.3	78.9	5964	75.6	1.0
102x102x6.4	2110	3.16	38.7	5855	151.3	2.0

The same initial out-of-straightness conditions as considered in the previous study were also specified in this second series of analyses. However, the uniaxial Giuffre-Menegotto-Pinto (GMP) steel material with kinematic and isotropic hardening was used to simulate Bauschinger effect under cyclic loading.

The input data for the Steel02 Giuffré-Menegotto-Pinto (GMP) material are: F_y, E, b, R_0, c_1, c_2, a_1, a_2, a_3, a_4 where: F_y is the yield strength; E is Young's modulus; $b = E_p/E$ is the strain hardening ratio; R is an exponent that controls the transition between elastic and hardening branch (the suggested values are between 10 and 20); c_1 and c_2 are parameters for the change of R with cyclic loading (suggested values of 0.925 respective 0.15); a_1 is an isotropic hardening parameter, which reflects the increase of compression yield envelope as proportion of yield strength after a plastic strain of a_2 ε_y; a_2 is an isotropic hardening parameter; a_3 is an isotropic hardening parameter, which reflects the increase

of tension yield envelope as proportion of yield strength after a plastic strain of $a_4\ \varepsilon_y$; a_4 is an isotropic hardening parameter (Mazzoni et al., 2005).

The properties specified for this model were based on the load-deformation response measured on the core of buckling restrained bracing members subjected to quasi-static cyclic tests (Tremblay et al. 2004) and the values used the above mentioned parameters where: b = 0.01, R = 20, c_1 = 0.925, c_2 = 0.15, a_1 = a_3 = 0.0000001 and $a_2 = a_4$ = 0.0000002. The nonlinear equation proposed by Menegotto and Pinto (1973) to characterise the reinforcing steel is:

$$\sigma^* = b\varepsilon^* + \frac{(1-b)\varepsilon^*}{(1+\varepsilon^{*R})^{1/R}} \tag{3.3.1}$$

where σ^* and ε^* are the effective strain and stress, and they are function of the unload/reload interval, b is the ratio between the initial and final tangent stiffness and R is a parameter that defines the shape of the unload curve. This equation was used to describe the unloading response of a material model proposed by Filipou et al (1983) and incorporated in OpenSees. The Giuffré-Menegotto-Pinto Model is represented in Figure 3.3.1.1.

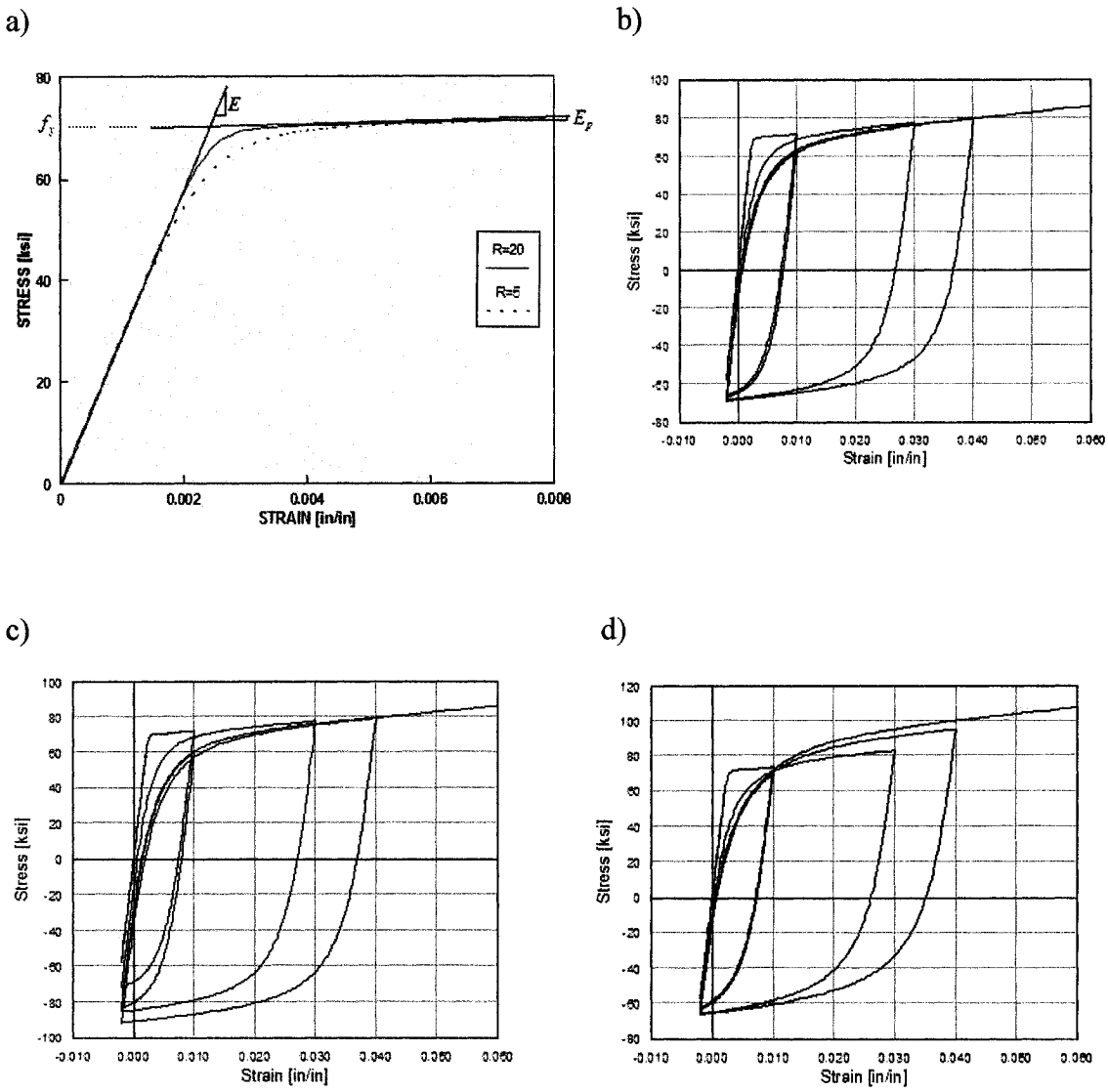

Fig. 3.3.1.1 Steel02 Material

a) Material parameters for the monotonic envelope; b) Hysteretic behaviour of model w/o isotropic hardening; c) Hysteretic behaviour of model with isotropic hardening in compression; d)Hysteretic behaviour of model with isotropic hardening in tension (Mazzoni et al., 2005)

In Figure 3.3.1.2, the experimental measurements are compared to the analytical predictions from the bi-linear model used in the previous study and the GMP model. As

shown, the second model reflects better the cyclic hysteretic behaviour of steel material. Figure 3.3.1.3 compares the response obtained using the bilinear and the GMP hysteretic brace model. When compared to typical measured response (see Fig 3.1), the latter provides a better representation of actual brace behaviour with smoother transitions between elastic and inelastic stages.

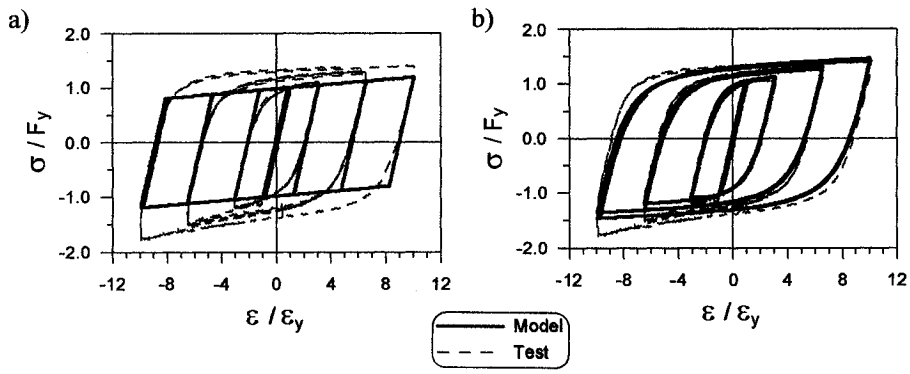

Fig. 3.3.1.2 Steel material models:
a) Bi-linear model; b) Giuffré-Menegotto-Pinto model

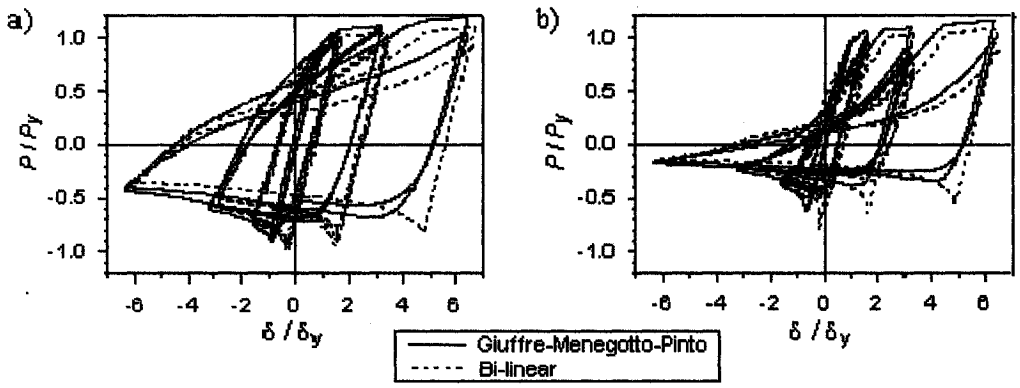

Fig. 3.3.1.3 Comparison of the predicted response
obtained from the Giuffre-Menegotto-Pinto and bi-linear steel models
for: a) $\lambda = 0.5$; and b) $\lambda = 1.0$ ($n_e = 8$ and $n_f = 16$, $n_i = 3$)

The test loading protocol proposed for buckling restrained braces (AISC 2005) was applied in the study: 6 cycles at a brace axial deformation, δ, equal to δ_y, 4 cycles at δ = 0.5 δ_m, 4 cycles at δ = 1.0 δ_m, and 2 cycles at δ = 2.0 δ_m, where δ_y is the axial deformation at yield and δ_m is the brace deformation at design storey drift, δ_m = 3.2 δ_y. Modeling parameters that were varied included the number of elements along the brace length (n_e = 4, 8, 16 and 32) and the number of fibres used to define the cross-section, n_f = 8, 12 and 16. Prior to performing the study, preliminary analyses were carried out for the brace with intermediate slenderness (λ = 1.0) with n_i = 3 and 4 (number of integration points per element). No significant differences could be observed for the *MQE* and the total energy dissipated by the brace computed with these two n_i values. Therefore the number of integration points was set equal to 3.

A total of 8 response parameters describing the brace hysteresis were examined: 1) the buckling load at first occurrence of buckling, P_{u0}; 2) the buckling load in the first cycle at δ = 1.0 δ_m, P_{u1}; 3) the energy dissipated up to and including the 4th cycle at δ = 1.0 δ_m, E_{h1}; 4) the energy dissipated at the end of the test loading protocol, E_{h2}; 5) the brace deformation when developing P_y in the first cycle at δ = 1.0 δ_m, δ_{y1}; 6) the compressive resistance at peak negative deformation in the first cycle at δ = 1.0 δ_m, P_1; 7) the brace out-of plane deformation at peak negative deformation in the first cycle at δ = 1.0 δ_m, Δ_1; and 8) the brace out-of- plane deformation at peak negative deformation in the first cycle at δ = 2.0 δ_m, Δ_2.

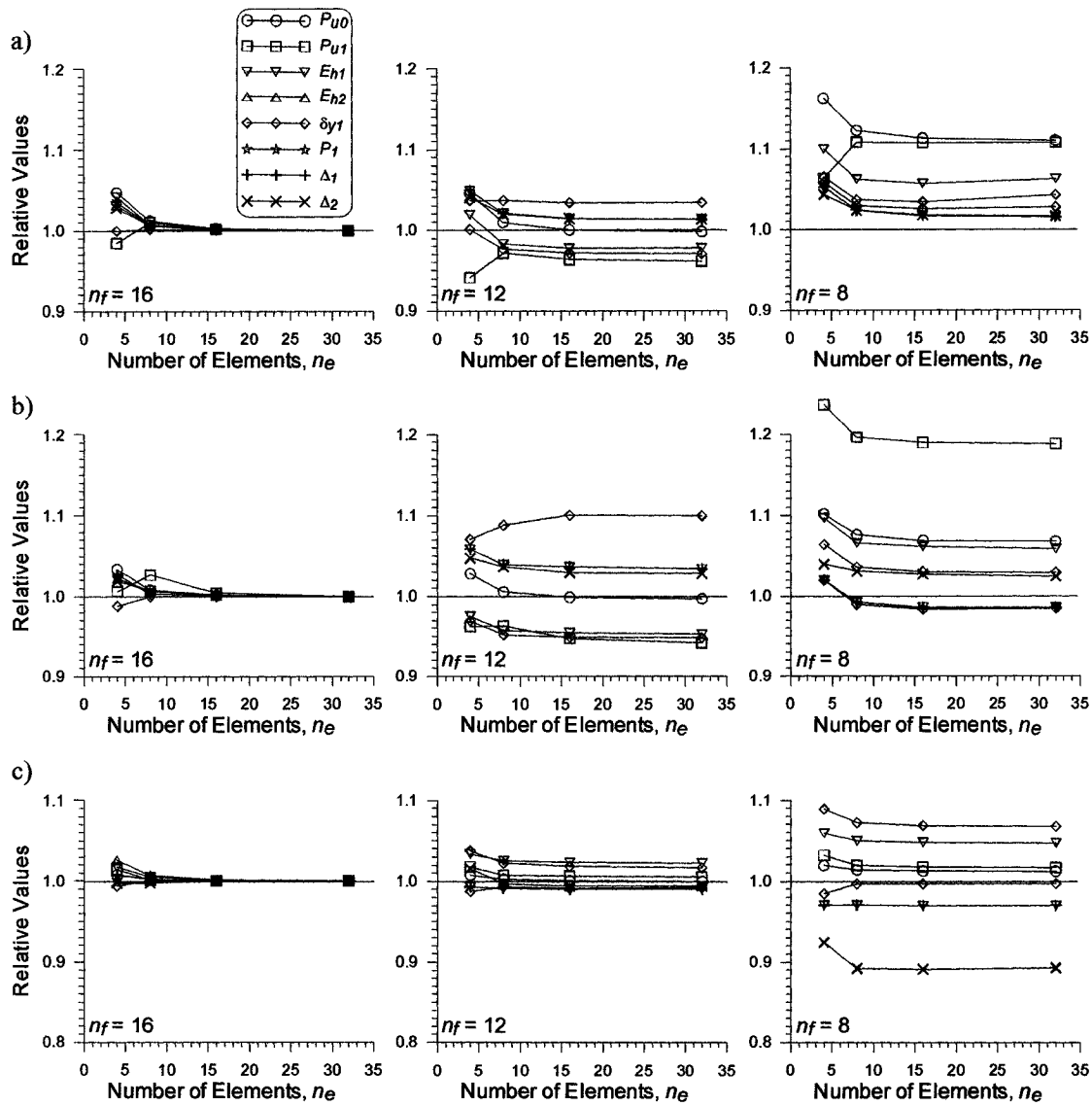

Fig. 3.3.1.4 Influence of n_e and n_f on brace response parameters for: a) $\lambda = 2.0$; b) $\lambda = 1.0$; and c) $\lambda = 0.5$

In Fig. 3.3.1.4, the variation of the 8 brace response parameters as a function of n_e and n_f is presented for each brace slenderness. For each brace slenderness, the results have been divided by the values obtained with the highest level of discretization, i.e. using n_e = 32 and n_f = 16. Clear trends can be observed from these plots: the quality of the results is maintained when the number of elements is reduced from 32 to 8 but degrades

significantly if the number of fibres is reduced from 16 to 8. For $n_f = 16$, discretizing the brace members with 8 elements instead of 32 elements resulted in errors of only 1% or less for all parameters except for P_{u1} for $\lambda = 1.0$ in which case the error reached 3%. The same trend is observed for other values of n_f. Conversely, the loss in accuracy can reach up to 10% (δ_{y1} for $\lambda = 1.0$) or 5% (other response parameters or slenderness) when n_f is reduced from 16 to 12 and n_e is kept equal to 32. Much larger errors are observed if n_f is reduced further from 12 to 8. It is noted, however, that the stockiest brace is less sensitive to a reduction in the number of fibres (error less than 3% when n_f is reduced from 16 to 12 and n_e is reduced from 32 to 8).

3.3.2. Influence of loading sequence

The analyses on the three bracing members were redone under two additional loading sequences: the quasi-static cyclic test protocol recommended by the European Convention for Constructional SteelWork (ECCS, 1991) and the brace test displacement history developed by Tremblay and Bouatay (2002) for braced steel frames exposed to crustal and sub-crustal earthquakes in western Canada (WC protocol). The response under the AISC loading protocol is also investigated for comparison. The three displacement sequences are illustrated in Figure 3.3.2.1. The history of the energy dissipated, E_H, as a function of the cumulated imposed displacement, $\Sigma\delta$, in each loading protocol is used to evaluate the validity of the modeling assumptions. The stockier ($\lambda = 0.5$) and the most slender ($\lambda = 2.0$) braces are examined. Two different models are considered: a simple but still accurate model as per previous studies with $n_e = 8$, $n_f = 16$, and $n_i = 3$, and a more refined model with $n_e = 32$, $n_f = 16$, and $n_i = 4$. As shown in Fig. 3.3.2.1, the simple model predicts equally well the brace energy dissipation capacity, regardless of the model assumptions and the applied loading history. The total energy dissipation capacity is compared in Table 3.3.2.1. Again, negligible differences are found between the two models.

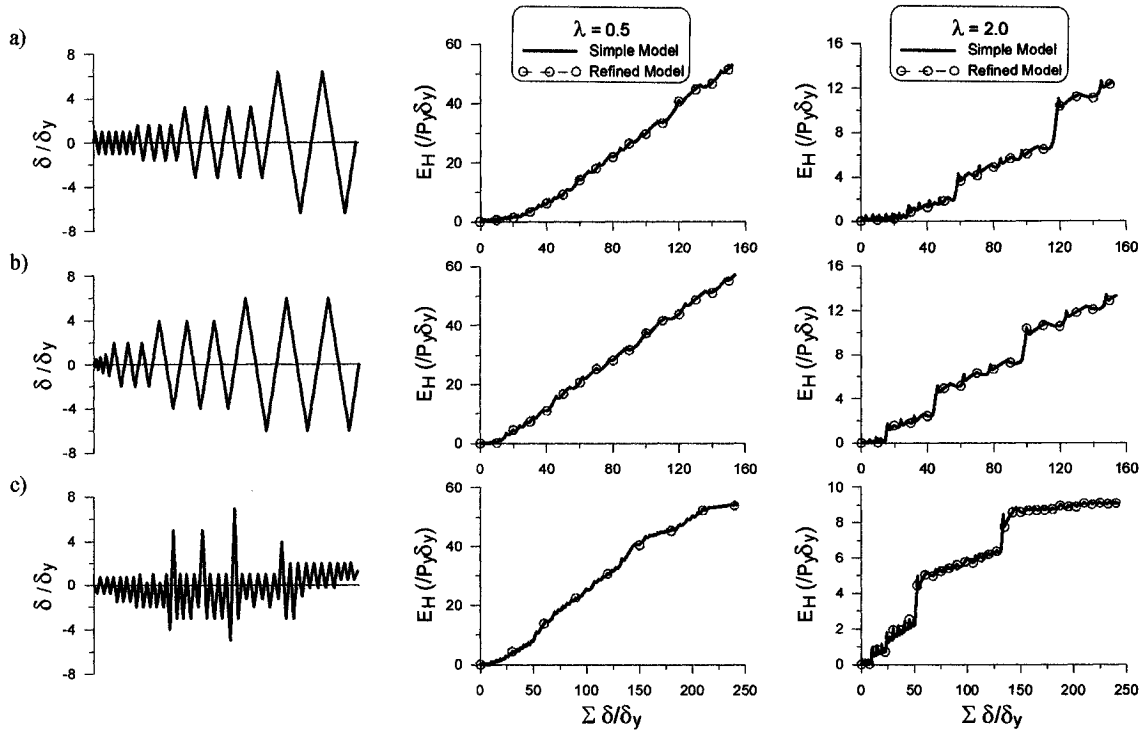

Fig. 3.3.2.1 Influence of test displacement protocol on brace energy dissipation: a) AISC displacement protocol; b) ECCS displacementprotocol; and c) WC displacement protocol

Table 3.3.2.1 Total E_H ($/P_y\delta_y$)

Brace λ	Model	Loading protocol		
		AISC	ECCS	WC
0.5	Simple	52.77	57.19	54.03
	Refined	52.38	56.78	53.67
2.0	Simple	12.50	13.30	9.07
	Refined	12.43	13.23	9.04

3.4. Comparison with brace test results

3.4.1. Description of braces

The force based formulation is used further to reproduce the hysteretic response of four rectangular HSS bracing members from different test programs. The properties of the braces are given in Table 3.4.1.1. Specimens S2-A and S1QB were tested by Tremblay et al. (2003) while tests on Specimens 1B and 2 were respectively performed by Shaback and Brown (2003) and by Haddad (2004). The cross-sectional flexural properties, I and r, are those associated with the plane of buckling observed in the tests. The δ_y values are reference yield deformations defined in each of the studies. Initial out-of-plane imperfections at mid-length of the braces, v_0, as assumed in the analyses, are also given in the table.

Table 3.4.1.1 Test brace properties

Shape	A (mm^2)	I ($10^6 mm^4$)	r (mm)	L (mm)	E (GPa)	F_y (MPa)	δ_y (mm)	v_0 (mm)
(S2A) 102x76x4.8	1550	2.18	37.5	4614	185	381	7.79	4.6
(S1QB) 127x76x4.8	1790	3.78	45.9	4614	198	395	7.93	4.6
(1B) 127x127x8	3620	8.36	48.0	3401	191	421	8.30	3.0
(2) 152x152x8	4430	15.1	58.4	4900	190	467	10.5	3.0

According to current seismic design practice, brace connections must be detailed to allow ductile rotational response upon brace buckling. For single gusset plate connections, end rotations due to out-of-plane brace buckling can be easily accommodated in the gusset plates by introducing a free hinge length between the brace end and the line of restraint (see Fig. 3.4.1.1a). It is recommended that the length of the free hinge region be equal to two times the gusset plate thickness, t_g (Astaneh et al., 1985). This detail was adopted in

the three test programs, as shown in Fig. 3.4.1.1b for the tests by Tremblay et al. (2003), and the length L in Table 3.4.1.2 corresponds to the brace length between hinge center lines.

Table 3.4.1.2 Test brace connection and slenderness properties

No.	C_g (kN-m/rad)	K ( )	KL (mm)	KL/r	λ	L_c (mm)	M_{pg} (kN-m)
S2A	63 (75)[1]	0.88	4051	108	1.56	19200 (16132)	3.68
S1QB	62 (75)[1]	0.93	4277	93.2	1.32	36210 (29940)	3.68
1B	1150	0.75	2545	52.6	0.79	4165	10.9
2	1290	0.76	3727	63.4	1.01	6672	12.1

[1]Value for upper brace end, value in brackets for lower brace end.

Such a detail induces rotational restraint at the brace ends, and plastic hinging is anticipated in the gusset plates when large brace out-of-plane deformations develop after brace buckling in compression (see Figs. 3.4.1.1b and 3.4.1.1c). Using the flexural stiffness of the gusset plate assembly, C_g, the brace effective length including end restraint effects can be determined from classical elastic stability theory (Chajes 1974). Table 3.4.1.2 gives the values of C_g for each of the test specimens as well as the resulting slenderness parameters. For these braces, the parameter K varies from 0.75 to 0.93. In view of the key role of the brace effective slenderness on the cyclic hysteretic response of bracing members, these end condition effects must be properly modeled when reproducing brace test results or predicting the brace response in actual building structures. Three different approaches are presented in the following sub-sections to account for the rotational restraint induced by the gusset plates.

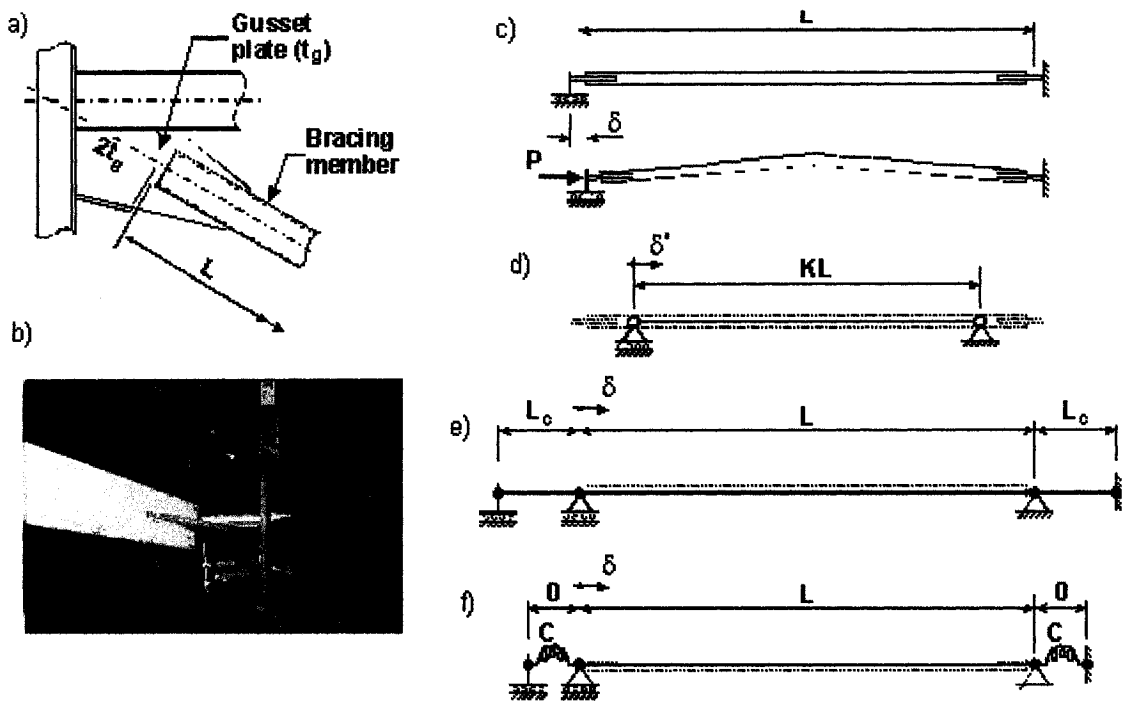

Fig. 3.4.1.1 Brace end connections

a) Typical brace connection; b) Plastic hinge in gusset plate upon brace buckling; c) Brace and gusset plate responses upon brace buckling; d) Brace model with length = KL; e) Brace model with extended brace segments; f) Brace model with zero-length end rotational springs

3.4.2. Brace model with effective length KL

In the first modeling approach, a pin-ended brace is used with a length equal to the brace effective length *KL* see Fig. 3.4.1.1d). In Fig. 3.4.2.1, the predicted response with $n_f = 16$, $n_i = 3$, and $n_e = 8$ is compared to the test measurements for Specimens S2A and 2. Similar results were obtained for the other two test braces or when using a larger number of elements (n_e greater than 8). Hysteretic responses are compared using two sets of parameters for the Giuffre-Menegotto-Pinto material model. The curves on the left hand side were obtained with the same parameters as defined in the previous section, i.e. with

R_0 = 25 and both isotropic and kinematic strain hardening properties. In the second comparison, the parameter R_0 was reduced to 20 and isotropic hardening was omitted (a_1 to a_4 = 0.0). It can be seen that using a lower R_0 value with more progressive yielding response resulted in a better match with the measured response for the post-buckling resistance upon reloading in compression at large deformations. When isotropic hardening was specified, the predicted yield tensile resistance of the braces was found to increase with the number of cycles, which was not the case for the test specimens. As shown, a material model without isotropic hardening seems to be more appropriate. This modified GMP material model is used in the remaining of the paper.

Although the GMP steel model nicely reproduces the transition between tension and compression responses, it must be realized that it has inherent limitations such that it will not be possible to fully characterize brace cyclic inelastic response. For instance, residual stresses are not included in the model. This results in a stiffer response in the first, small deformation cycles, as well as in a higher compression load at first occurrence of buckling. Local buckling and brace fracture cannot be reproduced either. Therefore, the predicted response is typically too optimistic near the end of a test.

The pin-ended brace model of length *KL* also has important drawbacks, which may preclude its use in seismic building analysis. One of these limits is the fact that the length of the brace model does not correspond to the actual brace length in the structure. This requires the use of rigid extension members and the brace axial stiffness will not be representative of the actual bracing member stiffness. In the individual brace analyses carried out herein, the test loading protocol was multiplied by *K* before it was applied to the numerical model. Therefore, the same elastic and inelastic deformation demand was imposed in both the test and model braces. This cannot be done so simply in a building analysis. A second main shortcoming of the *KL* model is the fact that such a model will always underestimate the out-of-plane brace deformations due to the shorter brace length, as illustrated for Braces S2A and 2 in Fig. 3.4.2.1c. This affects the brace post-buckling compression capacity as well as the resistance of the member upon straightening the

brace in tension. Finally, a model based on the effective length cannot capture the energy dissipation through plastic hinge rotations that develop in the gusset plates, at the braces ends.

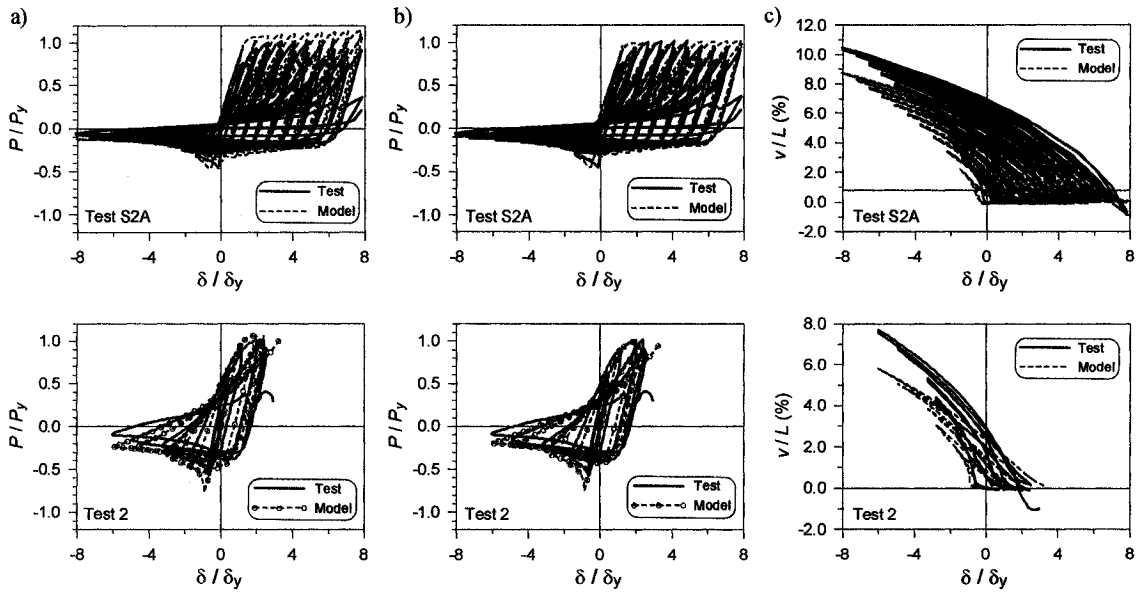

Fig. 3.4.2.1 Comparison between test and pin-ended model with length *KL*
a) Hysteretic response with $R_0 = 25$, $a_1 = a_3 = 0.00001$, and $a_2 = a_4 = 0.00002$; b) Hysteretic response with $R_0 = 20$ and a_1 to $a_4 = 0.0$; c) Out-of-plane response at brace mid-length with $R_0 = 20$ and a_1 to $a_4 = 0.0$

3.4.3. Brace model with end extensions

The problems of the *KL* model associated with the difference between actual and model brace lengths can be partly overcome by using the model shown in Fig. 3.4.1.1e. In this model, the rotational restraints at the brace ends are included by adding fictitious brace extensions of length L_c at both ends of a brace model having the actual brace length. The vertical displacements at the outer ends of these extensions must be restrained. For simplicity, the flexural stiffness (*EI*) of the bracing member can be assigned to the extensions. If pinned connections are specified at the outer ends of the extensions, the

length L_c can then be taken equal to $3EI/C_g$. The L_c values so computed for the four brace specimens are given in Table 3.4.1.2, and Figure 3.4.3.1 compares the response of Specimen S2A obtained from this model to the test results and the predictions from the *KL* model. All calculations were carried out with $n_f = 16$, $n_i = 3$, and $n_e = 8$.

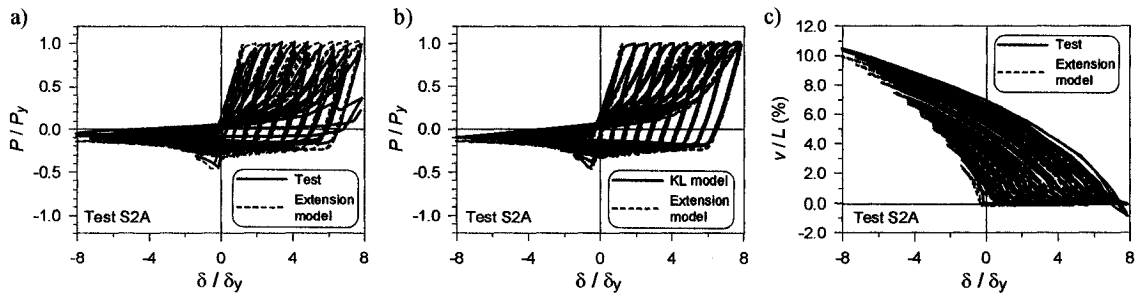

Fig. 3.4.3.1 Response of Specimen S2A using the brace model with end extensions a) Comparison between test and predicted hysteretic responses; b) Comparison of the hysteretic responses predicted by the *KL* and the extension brace models; c) Comparison between test and predicted out-of-plane responses at brace mid-length

As shown, both the *KL* model and the model with extensions give virtually the same response for this specimen. The use of brace extensions however permits to reproduce adequately the out-of-plane deformations (Fig.3.4.3.1c). It must also be noted that the energy dissipation in the gusset plates can be included in this model by specifying the plastic moment resistance of the gusset plates for the extension members. In the analysis of actual braced frame structures, however, the modeling of the extensions and the support conditions at the outer ends of the brace extensions can still represent a challenge for the analyst and a more convenient model should be developed for that purpose.

3.4.4. Brace model with rotational spring

In the third option, the flexural restraint at brace ends is incorporated by means of zero-length rotational springs. The simplest models would include linear elastic springs with a stiffness C_g. More sophisticated representation can be however considered to reproduce the hysteretic response of the gusset plates under the successive bending cycles imposed at every brace load reversal. Such a refined modeling is adopted herein. The flexural stiffness and strength of the gusset plates were given to the rotational springs (C_g and M_{pg} in Table 3.4.1.2) and the GMP steel model that was used for the braces was also applied for the gussets.

In this model, the brace length corresponds to the actual brace length and flexural strength is assigned to the gusset plates. In frame analysis, torsional restraint of the brace and gusset plates can also be included when out-of-plane buckling is studied. Brace torsional properties must then be added to the fibre nonlinear beam-column element using the aggregation tool in OpenSees. One limitation of the model is that the flexural strength of the rotational spring does not vary with the axial load applied by the brace to the gusset plate. Therefore, the spring resistance in the model can be overestimated when high axial loads are transmitted by the gusset, as is the case when tension yielding develops in the braces. Figure 3.4.4.1a shows the predicted M-θ hysteretic response of the upper gusset plate of Specimen S2A. The predicted and measured rotations are also compared for this specimen. Again, n_f = 16, n_i = 3, and n_e = 8 were used in these calculations. Due to its limitations, the model tends to overestimate the end rotations at large brace deformations, as a result of the permanent rotation gradually developing upon load reversals due to too high flexural capacity. However, the very good match between test and predicted axial and out-of-plane brace responses in Figs. 3.4.4.1c and 3.4.4.1d indicate that this error has limited impact on brace overall behaviour.

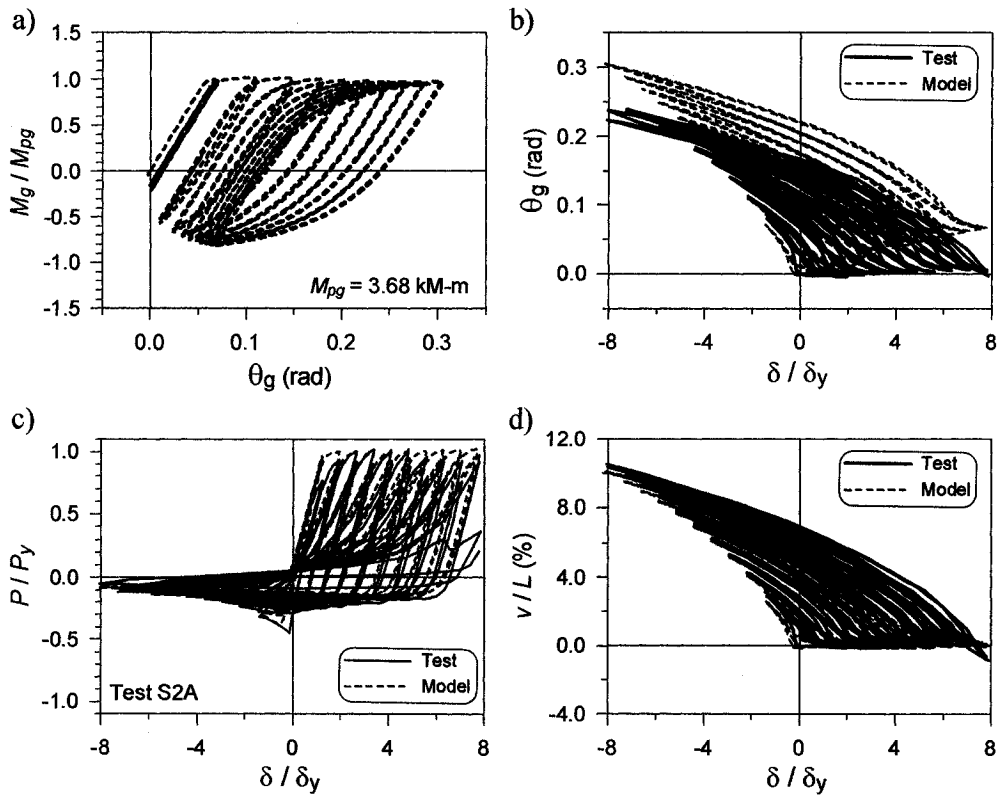

Fig. 3.4.4.1 Validation of the response of Specimen S2A from the model with rotational end springs (n_f = 16, n_i = 3, n_e = 8):

a) Upper gusset plate moment-rotation hysteresis; b) Comparison of test and predicted upper gusset plate rotation; c) Comparison of test and predicted brace hysteretic axial response; and d) Comparison of test and predicted brace out-of-plane response

Figure 3.4.4.2 compares the predicted hysteretic and out-of-plane responses of the three remaining brace specimens. Again, excellent match is obtained in all cases except for the axial load prediction during the large positive deformation excursion tension for Specimen SQ1B. This difference can be attributed to the methodology used to measure F_y in the tests (2% offset method), as this approach does not capture well progressive yielding including residual stress effects observed in HSS members. The figure also shows that the model can overestimate the peak compression brace resistance at first buckling, likely because residual stresses are not included in the model. Again, degradation of brace tension capacity due to local buckling and fracture of the material is

not captured by the model. Table 3.4.4.1 compares the test and predicted total energy dissipated by the brace up to the point of zero deformation in the last tension half-cycle before fracture. As shown, the models generally underestimate the energy dissipated by the braces, especially for Specimen S1QB due to the error in predicting the measured yield tensile resistance. The results show that little error is made when using 8 elements to discretize the braces.

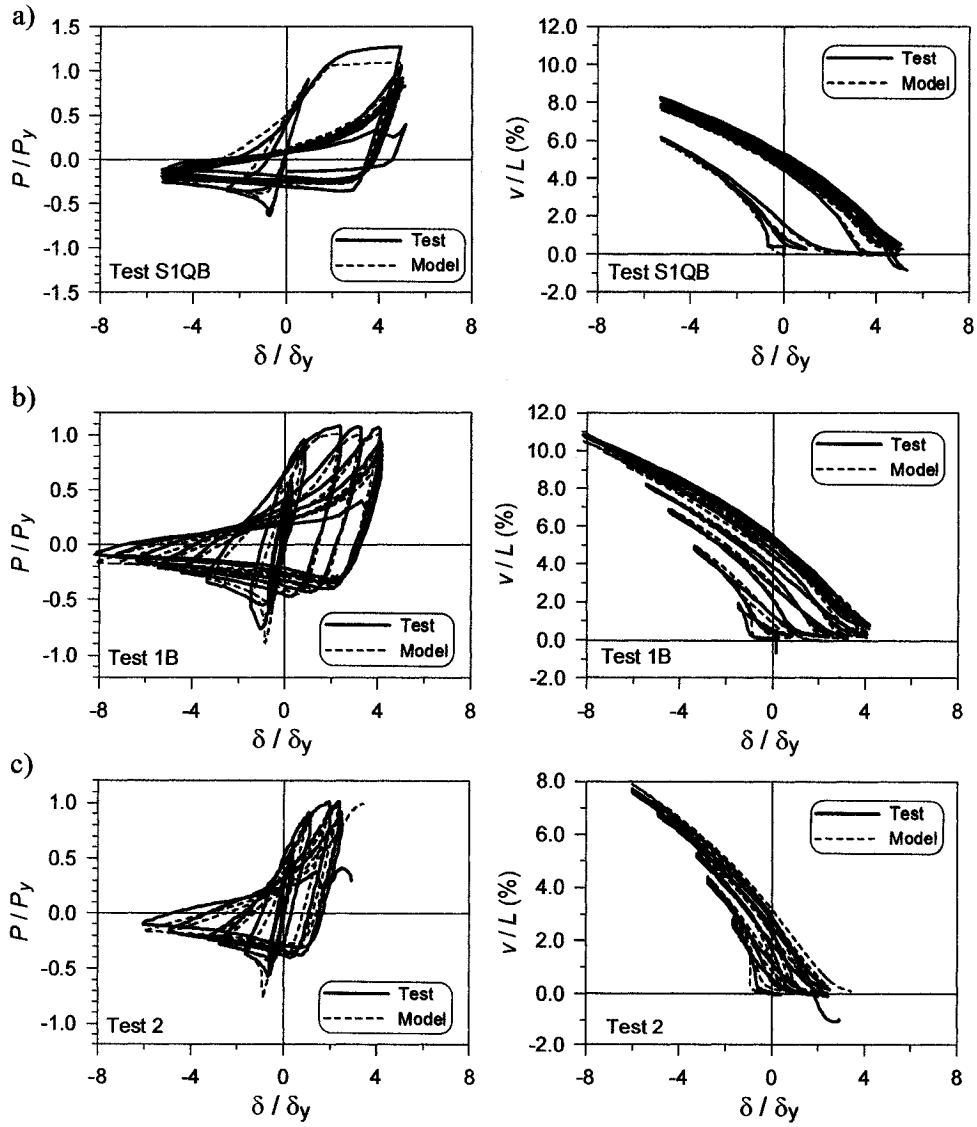

Fig. 3.4.4.2 Comparison between test and predicted brace hysteretic axial and out of-plane responses
for Specimens: a) S1QB; b) 1B; and d) 2

Table 3.4.4.1 Total $E_H(/P_y\delta_y)$

Case	Brace Specimen			
	S2A	S1QB	1B	2
Test	40.13	18.21	27.4	12.0
$n_e = 8$	40.51	14.5	23.4	8.57
$n_e = 16$	40.27	14.44	23.3	8.46
$n_e = 32$	40.24	14.42	23.25	8.45

3.5. Inelastic frame analysis

3.5.1. Comparison with test results

The overall response of the test X-braced frame by Tremblay et al. (2003) with Specimen X6-C is compared to that of the model analysis. The frame is shown in Fig. 13a. True-pinned connections were built at the column bases and at the beam-to-column joints such that the applied lateral load was entirely resisted by the braces. The braces were HSS 64x64x4.8 with the following properties: A = 1060 mm^2, r = 23.6 mm, F_y = 397 MPa, E = 189 GPa, KL/r = 89.8, λ = 1.31, and J = 995x10^3 mm^4. At brace intersection, one brace was continuous whereas the other brace was interrupted. However, as shown in the figure, full torsional and flexural continuity was provided between the two brace segments through welding and connecting plates. The braces were connected at their ends by means of gusset plates 300 mm wide by 9.5 mm thick. At the lower brace ends, the gusset plates were connected to the frame columns. At the top ends, they were connected to the beam only. Beam and column properties are given in Fig.3.5.1.1b. For this frame, the yield storey shear, V_y, is defined as the sum of the horizontal components of the brace tension yield capacity: V_y = 674 kN, and the yield storey drift, Δ_y = 12.1 mm.

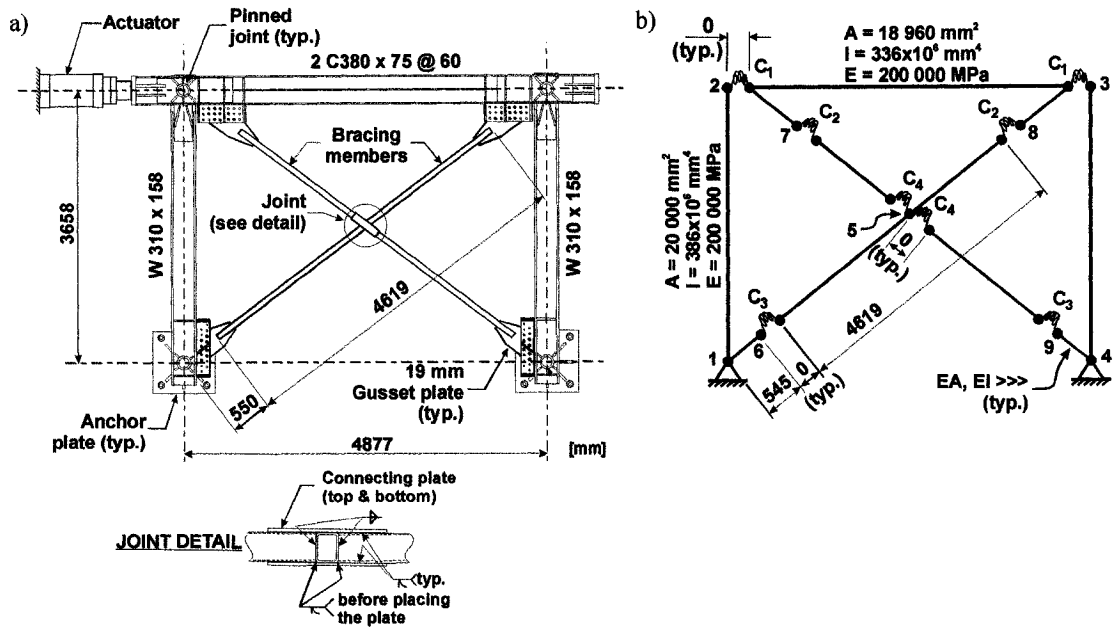

Fig. 3.5.1.1 1 Full scale frame test

a) Test Setup for Specimen X6-C (adapted from Tremblay et al., 2003);

b) Frame model

A general-purpose model was developed with rotational springs at beam-to-column joints (C_1), and springs with rotational and torsional properties at brace ends (C_2 and C_3) and at the connection between the two braces (C_4). For this particular test application, $C_1 = 0$, $C_2 = 29$ kN-m/rad (flexure) and 45 kN-m/rad (torsion), and $C_3 = 37$ kN-m/rad (flexure) and 45 kN-m/rad (torsion). The flexural capacity of springs C_2 and C_3 was set equal to 2.045 kN-m. Springs C_4 was given infinite stiffness and strength in flexure and torsion. In this model, torsional properties of the brace had to be added to the fiber beam-column brace elements. The frame was subjected to symmetrical displacement protocol with stepwise incremental amplitudes. The braces were modeled using the GMP steel material with the properties as defined in the previous section. The parameters $n_f = 16$ and $n_i = 4$ were used, and the number of elements in each of the half-brace segment was varied as followed: $n_e = 2$, 4, 8, and 16.

Figures 3.5.1.2a to 3.5.1.2c compare the measured and predicted lateral load-lateral deformation response of the frame as well as the out-of-plane deformation response at the middle of the lower half-brace segment of the continuous brace and at the brace intersection point. The results shown were obtained using 4 elements for each of the half-brace segments. Excellent agreement is found between the experimental and computed results. Figures 3.5.1.2d and 3.5.1.2e show the influence of the number of elements on the global hysteretic response and the energy dissipated by the frame, E_H. The cumulated energy dissipation in the test was equal to 26.09 $V_y\Delta_y$. The analysis results are 23.81, 22.68, 22.22, and 22.20 $V_y\Delta_y$ with n_e = 2, 4, 8, and 16, respectively. These results again show that a total of 8 elements per brace would be adequate to properly reproduce the behaviour of braces of this type.

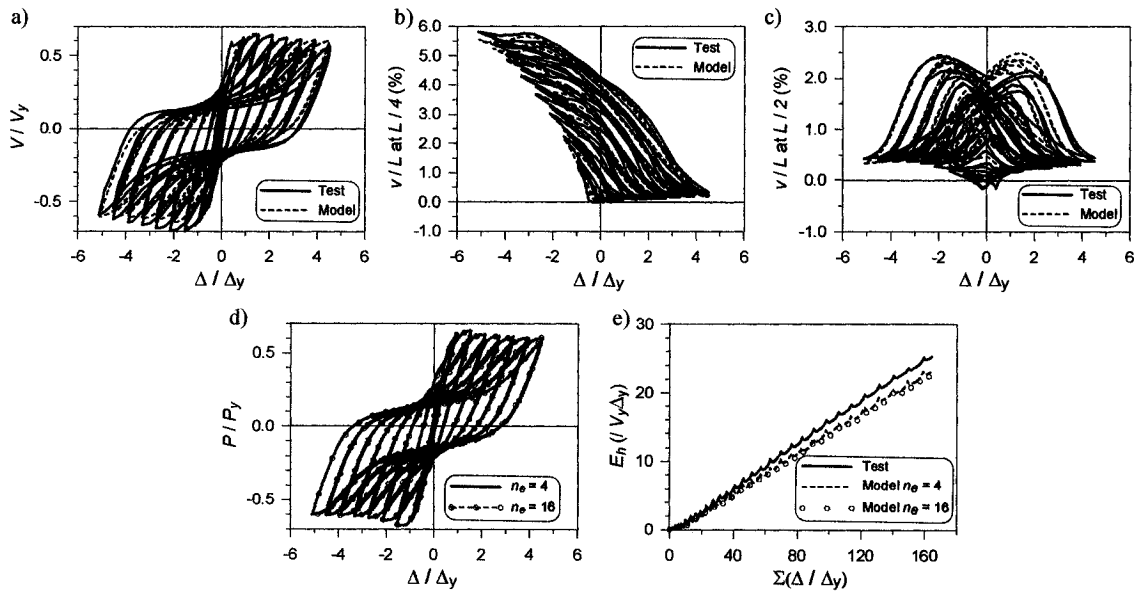

Fig. 3.5.1.2 Response of test frame X6-C

a) Comparison between test and predicted (n_e = 4) lateral load-lateral deformation hysteretic responses; b) Out-of-plane deformation response at the lower half-brace segment; c) Out-of-plane deformation response at the brace intersection point; d) Influence of n_e on the lateral load-lateral deformation response prediction; e) Influence of n_e on the energy dissipation prediction

3.5.2. Seismic analysis

The response of an actual single-storey X-braced steel frame subjected to earthquake is examined to assess the validity of the model for inelastic seismic response analysis. The building is 45 m x 45 m x 3.658 m tall. It is located in Victoria, B.C., Canada, on a stiff soil site. The design is performed according to the provisions of the 2005 National Building Code of Canada and CSA-S16-01 Standard. Steel with nominal F_y = 345 MPa(and actual F_y = 385 MPa) E = 200 000 MPa, and G = 77 GPa is used for all members. For simplicity, the roof diaphragm is assumed infinitely stiff and the total seismic weight (5508 kN) is concentrated at the roof level. A single braced bay, 9.0 m wide, is used on each of the exterior walls and tension-only design was assumed. The bracing members are HSS 102x102x6.4 with the following properties: A = 2170 mm^2, r = 38.6 mm, KL/r = 113, λ = 1.50, J = 5320x10^3 mm^4. The braced bay columns are HSS 152x152x4.8 (A = 2570 mm^2, I = 9.27x10^6 mm^4) and the beams are W460x60 (A = 7590 mm^2, I = 255x10^{6}mm^4). The base of the columns is assumed to be pinned and simple shear connections are used between the beams and the columns. The fundamental period of the structure is 0.55 s if the compression braces are neglected. It reduces to 0.38 s when the contribution of the compression braces is included.

The model in Fig. 3.5.1.1b can be employed for this structure. Spring C_1 is set to zero. Springs C_2 and C_3 both have a flexural stiffness of 173 kN-m/rad and a flexural strength of 5.42 kN-m for out-of-plane bending. They were considered as infinitely stiff for in-plane bending and their torsional stiffness were set equal to 216 kN-m/rad for C_2 and 227 kN-m/rad for C_3. Spring C_4 was defined as fully rigid in all three rotational axes, assuming the same type of connection as in frame X6-C. The rigid extensions at the lower and upper brace ends are respectively 353 mm and 843 mm.

The analysis is carried out under a record from the 1994 M7.0 Northridge earthquake (Station Standford University, Comp. 0°). The record is scaled by 1.43 to match the design spectrum and to account for accidental eccentricity. The same brace model was

used with n_f = 16, n_i = 4, and n_e = 4, 8, and 16. The tolerance was set to 10^{-3} and the Newton-Raphson with line search algorithm was adopted to improve the convergence. Time step values, Δt, of 0.01 s and 0.001 s were used. In analyses performed with time steps longer than 0.01 s, convergence could not be reached upon first brace buckling. Mass proportional Rayleigh damping was used with 5% in the first structure mode (T_1 = 0.38s).

Figures 3.5.2.1a compares the time history of the roof horizontal displacement for the two time steps and n_e = 4 and 16. The time history of the energy dissipated in the system for Δt = 0.01 s is also given in the figure. Figure 3.5.2.1b shows the hysteretic response obtained for n_e = 4 when using Δt = 0.01 and 0.001 s, showing the effect of brace response degradation on the lateral strength and stiffness of the frame under cyclic loading. For Δt = 0.01s, the total energy dissipated by the braces with ne = 4, 8, and 16 is respectively equal to 6.27, 6.28 and 6.29 $V_y\Delta_y$. For Δt = 0.001 s and n_e = 4, E_H = 6.36 $V_y\Delta_y$. All these results clearly indicate that good predictions can be achieved for typical braced frames like the one studied herein by using a time step of 0.01 s and 4 elements per half-brace segment.

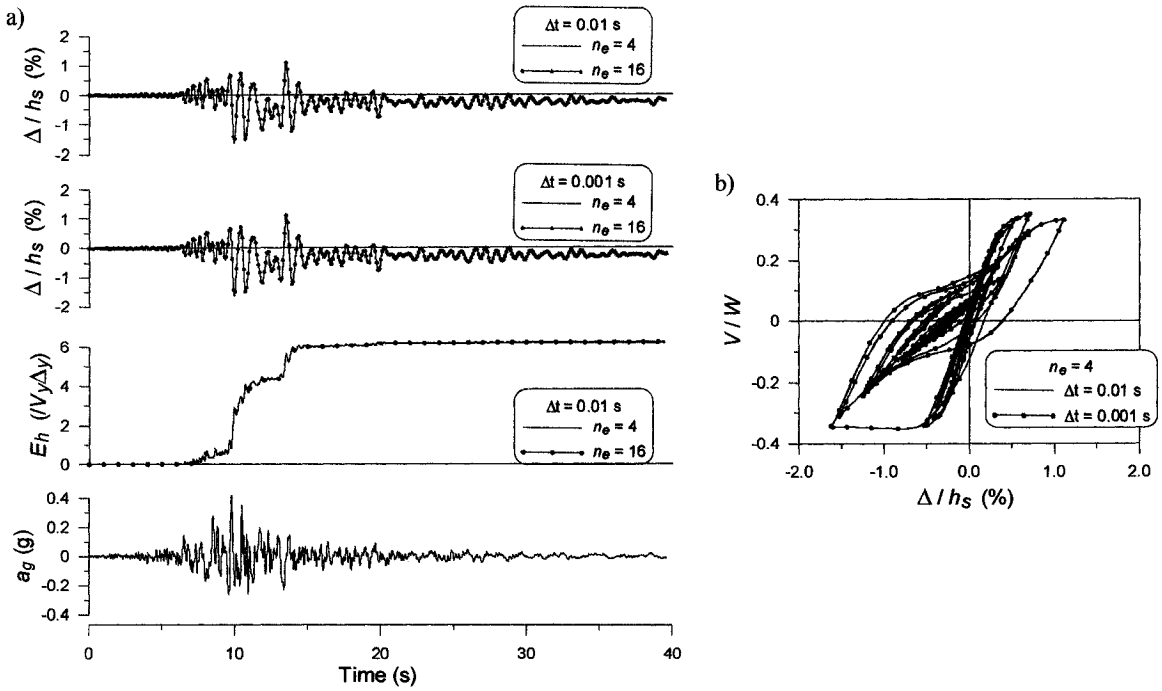

Fig. 3.5.2.1 Seismic response of a single-storey X-braced steel frame building:
a) Time history of roof displacement and dissipated energy;
b) Influence of time step on base shear-roof displacement hysteretic response.

3.6. Conclusions

The first objective of this research project was to use OpenSees computer software for studying the seismic behaviour of braces in Split-X braced steel frames and the seismic stability of multi-storey Split-X braced steel frames. The study reported in this Chapter permitted to develop and validate a brace model that was used later for the analysis of brace frame building structures with the OpenSees program.

Parametric studies were carried out to evaluate the influence of modeling assumptions when simulating the hysteretic response of steel bracing members with the OpenSees finite element computer software. Nonlinear beam-column elements were used with a

fiber representation of member cross-sections. The study showed that the number of integration points per element has limited influence on the response and that accurate results could be obtained with three integration points. For a given set of parameters, the force based formulation was found to provide higher accuracy compared to the displacement based formulation. This formulation should therefore be preferred, even if it requires longer computational time. As expected, the errors were found to reduce when increasing the number of elements or the number of fibres. The results indicate that sufficient accuracy can be achieved for typical bracing members if 8 elements per brace member were used together with 16 fibers for cross-section discretization. The use of the Giuffré-Menegotto-Pinto constitutive model was also found to provide a more realistic representation of the brace hysteretic response compared to the simpler bi-linear model. Comparisons between test and predicted results as well as simple dynamic seismic analysis confirm the appropriateness of these modeling assumptions for typical low-storey braced frame applications.

The brace model was found to give realistic predictions of the hysteretic response of braces having different sizes, slenderness ratios or end restraint conditions. This is by far superior to using empirical or semi-empirical models which specific test data are needed to adequately reproduce key response properties. However, the brace modeling considered in this study still has some limitations. For instance, it does not account for residual stress effects on compression strength at first buckling, and local buckling effects and brace fracture cannot be reproduced by the model.

CHAPTER 4. VALIDATION OF THE BEAM WITH HINGES ELEMENT FROM OPENSEES

In the building models to be studied in Chapter 5, the nonlinear beam-column element of OpenSees was used only for the bracing members. To ease and speed the analyses, a simpler element of OpenSees, the Beam with Hinges element was used for modeling the columns and beams of the braced frame as well as the gravitational columns. This element considers the plasticity to be concentrated over specified hinge lengths at the element ends. The elastic properties of the element are integrated only over the middle segment of the beam, which is considered to be linear elastic. Forces and deformations of the inelastic regions are sampled at the hinge midpoints, using mid-point integration (Mazzoni et al., 2005). Prior to constructing the building models, the Beam with Hinges element was validated through simple cases, and this validation process is described in this chapter.

4.1. Plastic analysis of a beam with hinges element using OpenSees

A W 360x196 section (Fig. 4.1.3) made from ASTM A992 steel with F_y = 385 MPa and E = 200000 MPa was used for the first study. The uniaxial elastic perfectly plastic material (Fig. 4.1.1) was used to describe the nonlinearity of the material with the plastic strain ε_P = 0.001925 (=385/200000) and the initial strain ε_0 = 0.

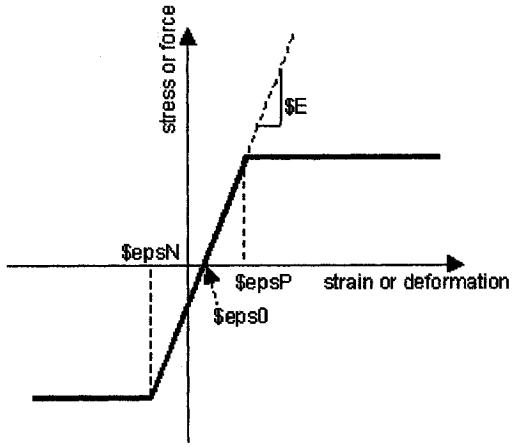

Fig. 4.1.1 Elastic perfectly plastic material (OpenSees manual)

A simple model of a beam fixed at both ends and composed of nine elements was considered. Two equally spaced vertical concentrated loads were applied on the beam (Fig.4.1.2). The loads were set equal to the plastic limit load for the section: $P = \frac{6M_p}{l}$; where $M_p = Z_y F_y$ is the plastic moment of the section (Appendix I).

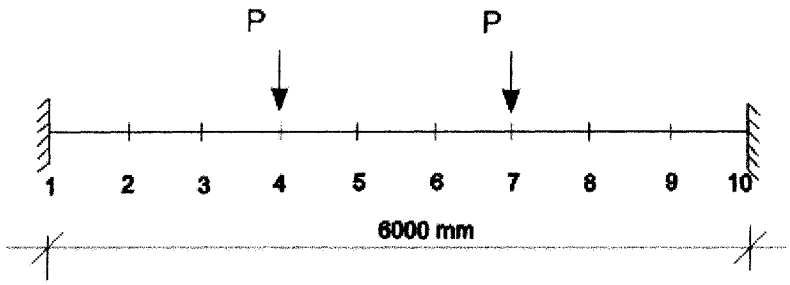

Fig. 4.1.2 Beam model for the plastic analysis

A corotational coordinate transformation was used in order to take into account large deformations. The cross-section was divided in three rectangular patches: two for the flanges and one for the web (Fig. 4.1.3). The patches were discretized into fibres with quadrilateral shapes both for the web and the flanges. Plastic hinges of 200 mm length

(approx. half of the cross-section depth) were considered for the beam with hinges element.

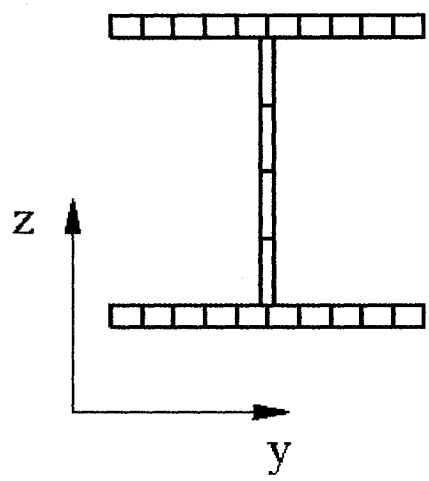

Fig. 4.1.3 Section discretization for the plastic analysis

A total of ten fibres were used along the width of each flange and four fibres over the height of the web. The beam was oriented such that the applied concentrated loads produce bending about the weak (z) axis. This justifies the larger number of fibres used for the flanges compared to the web.

A Newton with line search solution algorithm was selected in the Opensees library to achieve rapid convergence (Mazzoni et al., 2005). This solution algorithm uses an energy increment test and the tolerance was set equal to 0.001 with a maximum of 500 iterations. A single load step is performed for the vertical loads using the OpenSees LoadControl integrator. The equations are formed using a sparse symmetric scheme, so the system was SparseGeneral. The equations were numbered using the RCM (reverse Cuthill McKee) numberer and the constraints were represented with the Plain constraint handler, which enforces homogeneous single-point constraints (homogeneous boundary conditions).

In Chapter 3, it was found, that good results could be obtained when modeling bracing members with a series of 8 nonlinear beam column elements. Therefore, the validation of

the Beam with Hinges element was started using nine elements (the number 9 was selected to have a symmetric vertical load pattern). The load-displacement response shown in Fig. 4.1.4 was obtained with the model. The displacement is calculated at node 4, Δ_4.

Thereafter, a theoretical elastic-plastic analysis was done into two phases: first, the load amplitude and the beam deflection corresponding to the development of plastic hinges at the beam supports were determined, and, second, the loads corresponding to the development of two additional plastic hinges under the concentrated loads were determined. The deflection of the beam under this ultimate loading condition was then calculated and compared in Table 4.1.1 with the numerical results from OpenSees. The detailed calculations are presented in Appendix I. Good agreement can be observed between the two methods. Based on these results, it can be concluded that the flexural behaviour of the beam can be very well described using a nine-element discretization and the chosen section discretization.

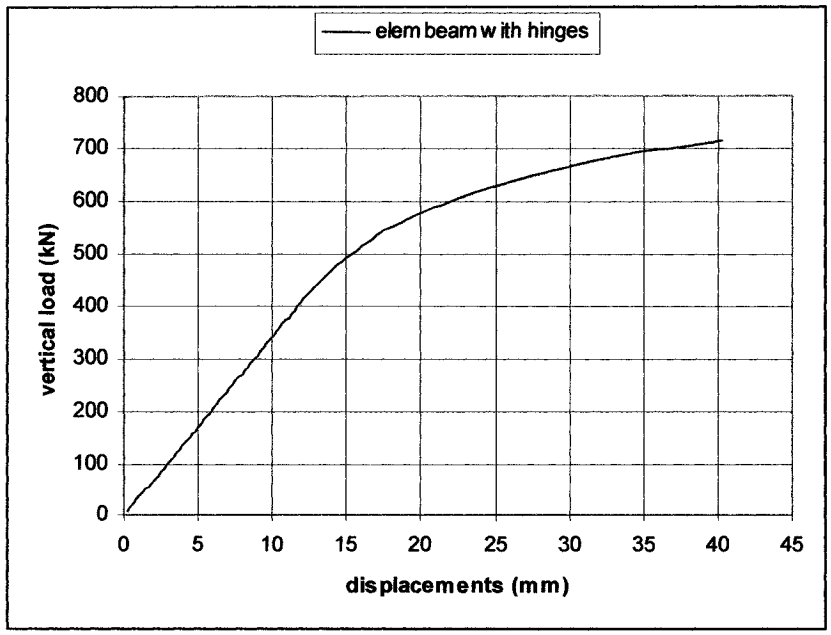

Fig. 4.1.4 Load-displacement diagram for a beam with hinges element

Table 4.1.1 Comparison between beam deflections Δ_4 at ultimate load from OpenSees and theoretical plastic analysis

	Theoretical analysis	OpenSees analysis	Difference
P=716.1kN : Δ_4 (mm)	41.67	40.32	3 %

Thereafter, the influence of the length of the plastic hinge and the influence of the coordinate transformation on the deflection of the beam was studied. Three lengths of plastic hinges were used: very short (0.01 mm), approximately half of the section depth (200 mm) and the full section depth (372 mm). Linear and corotational coordinate's transformations were used. Two equally spaced vertical concentrated loads equal to the ultimate load (716.1 kN) were applied on the beam. The beam was thereafter modeled using elastic beam column elements, in order to compare the obtained values. Table 4.1.2 presents the beam displacement of node 4 for the different hypothesis.

Table 4.1.2 Parametric study on the influence of the plastic hinge length

Elements	Plastic hinges (mm)		Linear transformation	Corotational transformation
Beam with Hinges	All the elements	0.01	20.84	21.14
		200	45.64	40.32
		372	36.54	34.02
Elastic Beam Column	-		20.84	20.76

As can be seen from the table, the length and the position of the plastic hinges influence the flexural behaviour of the beam. For the corotational transformation, the deflection of the beam is smaller than for linear transformation (except for the case where the plastic hinges are very short). This can be explained by the fact that part of the load is resisted by

membrane action when the corotational transformation is specified. It can be also seen from the table that using Beam with Hinges elements with very short plastic hinges or Elastic Beam Columns to model a beam in flexion gives similar results, which means that a realistic plastic hinge length must be specified to obtain adequate plastic rotation response when yielding develops in the cross-section fibres. Therefore, a careful validation has to be made when modelling beams in flexure using the Beam with Hinges elements.

4.2. Parametric studies

The columns and the beams in the building model will be subjected only to end moments, with no concentrated loads along the member length. Therefore, in this section, the possibility of using only one Beam with Hinges element (Model 2) by comparing it with a nine-element solution (Model 1) was studied, as shown in Fig. 4.2.1.

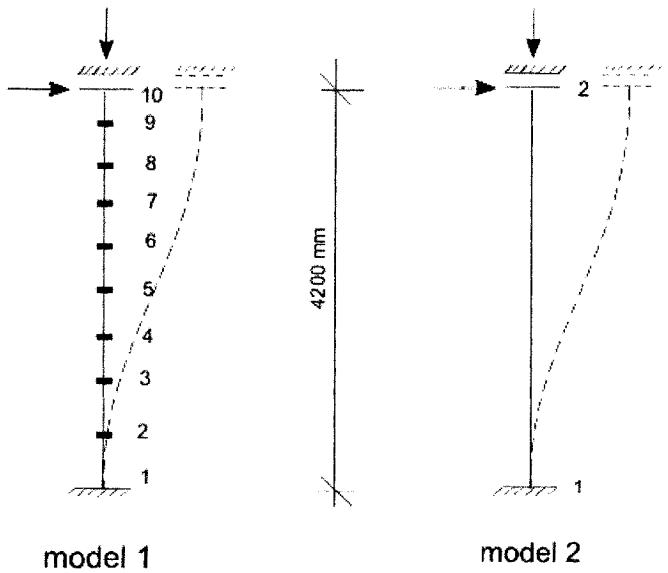

Fig. 4.2.1 Beam with hinges model for parametric studies

The column model is fixed at the bottom end and free but guided at the top end. The member was subjected to an initial compression load and to a gradually lateral displacement at the top end.

A W310 x 129 section made from ASTM A992 steel with F_y = 385 MPa and E = 200000 MPa was used. The uniaxial elastic perfectly plastic material of Fig. 4.1.1 was used again to describe the nonlinearity of the material. The member was bent about its weak axis and the fibre representation of the cross-section used in the previous section was used again in this study. In both models, the length of the plastic hinges was set equal to the depth of the cross-section.

A Newton solution algorithm was used. This solution algorithm uses a Norm displacement increment test which checks the positive force convergence if the second norm of the displacement increment is less than the tolerance (10^{-8}). The equations are formed using a BandGeneral scheme, which constructs a un-symetric banded system of equations. The equations are numbered using the Reverse Cuthill-McKee numberer. The constraints are represented with a Transformation constraint handler.

A single load step is performed for the axial load using the LoadControl integrator. Subsequently, the axial load is kept constant and a new load pattern with a linear time series and horizontal loads acting at node 10 in Model 1 (or node 2 in Model 2) is added to the model. The time in the domain is set to zero and the integrator is changed to DisplacementControl to impose nodal displacements and the static analysis is followed by a pushover analysis. A reference force of 1000 kN is defined in the linear time series. For this reference load, the DisplacementControl integrator determines the load increment necessary to increase the horizontal displacement at node 10 (or 2) with 0.1 mm increments. A total of 2350 analysis steps were performed in this new analysis.

As shown in Fig. 4.2.2 the results are very close. On this basis, it was concluded that a single Beam with Hinges element could be used to model the beams and columns of the braced frames as well as the gravity columns.

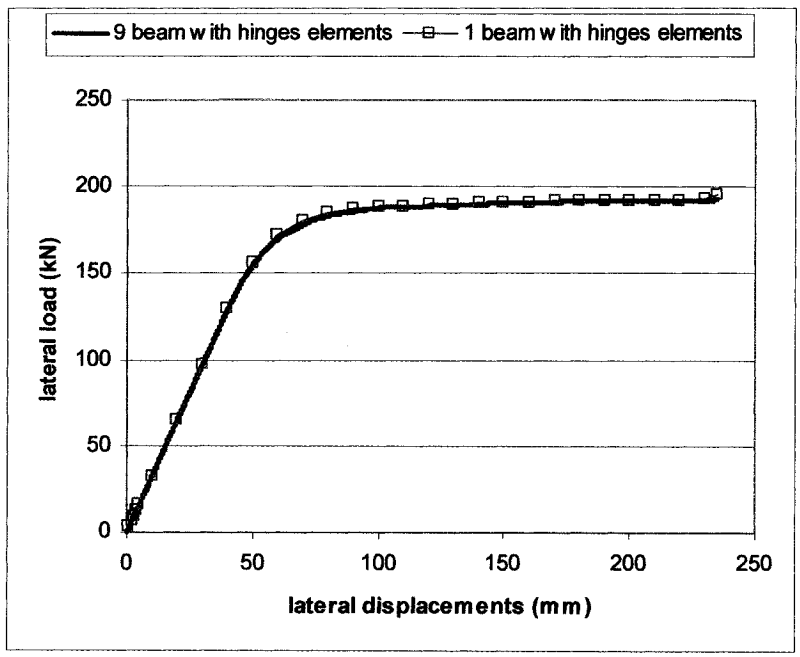

Fig. 4.2.2 Influence of the number of Beam with Hinges elements on the column

A second verification was performed to study the influence of the number of fibres in the patches used to discretize the cross-section of the Beam with Hinges element. As before, the section was divided into three rectangular patches, two for the flanges and one for the web, but the number of elements in the flange patches was varied: 5, 10 and 20 fibres as shown in Fig. 4.2.3.

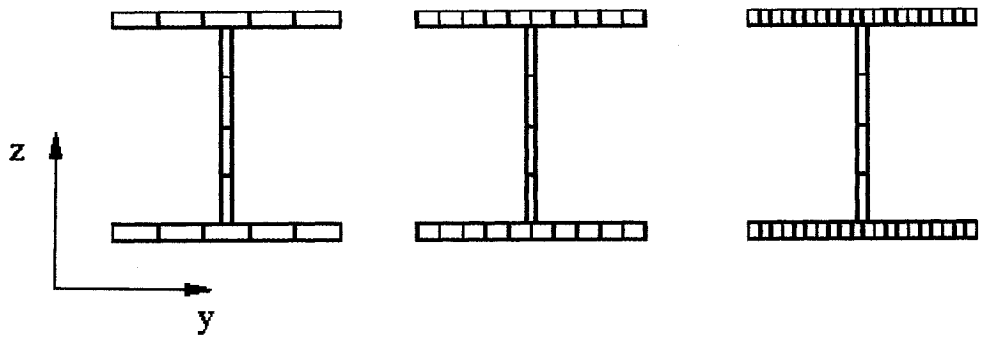

Fig. 4.2.3 Flanges discretization using 5, 10 and 20 fibres

The number of fibres in the web patch was kept constant at 4 over the height of the web. It is noted that only one fibre could be used for the web discretization in this orientation. Model 2 with one Beam with Hinges element column model was used for these calculations. The analysis parameters were also kept the same. The resulting load-displacement diagrams for the three discretizations are presented in Fig. 4.2.4.

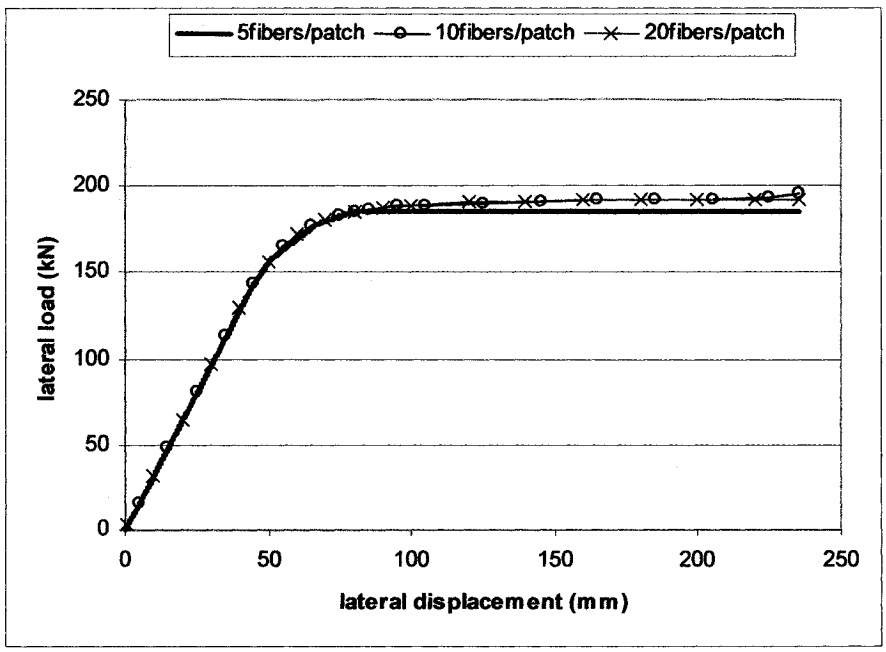

Fig. 4.2.4 Comparative load-displacement diagrams for number of fibres parametric study

As shown, the transition between elastic and plastic responses in the load-displacement curve with 5 fibres is not as smooth as the ones computed when 10 and 20 fibres were used. The results for 10 and 20 fibres are nearly identical and a discretization with 10 fibres for the patches subjected to varying stress distribution upon member bending was adopted to model all Beam with Hinges elements in the building models.

4.3. Element orientation

A fixed-fixed beam, composed of two Beam with Hinges elements, and subjected to a vertical load applied at mid-span was considered to verify the influence of the orientation of the element. The section W 360x196 and the same material as used in the first study were considered again for this analysis. Ten load steps of 100 kN were considered for the vertical load using the LoadControl integrator. All the components of the analysis are the same as those assumed in the first study.

There are two possibilities for changing the orientation of a three dimensional element in OpenSees, either by changing the description of the fibres in the patches according to the new orientation of the axis, or by changing the vectors vecxz that define the x-z plane of the local coordinate system.

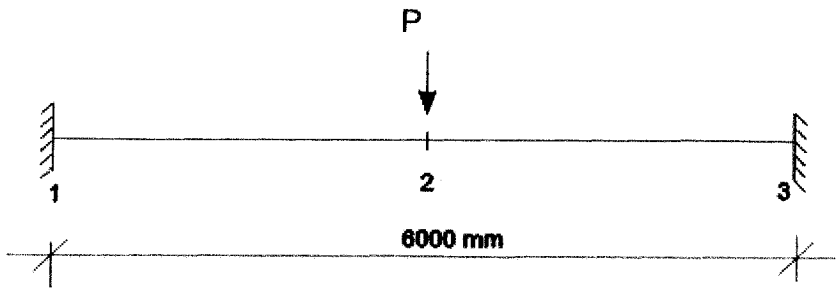

Fig. 4.3.1 Beam model for element orientation study

The beam is bent about its weak axis if it is described weak axis (Fig. 4.3.2.a) and the values for the vecxz vectors are 0 0 1. The orientation of the beam can be changed either by changing the description (describing it strong axis - Fig. 4.3.2.b, with vecxz values 0 0 1), or by maintaining the same description (weak axis) and changing the vectors vecxz to 0 -1 0.

The fibre discretization adopted in the previous study was used again herein, with 10 fibres perpendicular to the plan of bending for the flange patches and 4 fibres for the web patch.

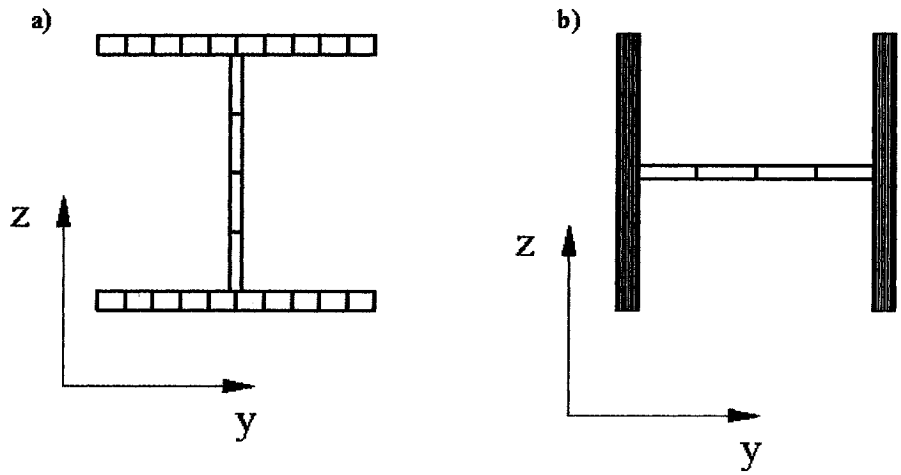

Fig. 4.3.2 Beam orientation a) Weak axis, b) Strong axis

The analysis results are compared to hand calculations using elastic beam formulas. Table 4.3.1 compares the mid-span deflection under a load of 100 kN.

Table 4.1.3.1 Comparison of the beam deflection from beam formula and OpenSees analysis for different element orientations

	Weak axis (mm)	Strong axis (mm)
Hand calculations $\Delta_{max} = \frac{Pl^3}{192EI}$	2.456	0.884
OpenSees - Weak axis description Vecxz 0 0 1	2.465	
OpenSees - Weak axis description Vecxz 0 -1 0		0.886
OpenSees - Strong axis description Vecxz 0 0 1		0.886

As shown, the differences between the hand calculations and OpenSees analyses are very small (0.2 % and 0.3 %). In fact, it was found that these differences correspond to the differences between the values of the moment of inertia calculated by OpenSees from the fibre cross-section representation and the ones given in the Steel Handbook (2004).

4.4. Element validation

Model 2 in Fig. 4.2.1 was used to validate the Beam with Hinges element to reproduce the response of an axially loaded column including large translational displacement effects. The fibre discretization of the section was as shown in Fig.4.3.2.a, with the section bent about the weak axis. Experimental results of the nonlinear behaviour of the columns were not available. Therefore, the validation was done by comparing the OpenSees results with the CAN/CSA S16-01 strength and stability provisions for members subjected to axial compression and bending moments.

The same W310 x 129 section and material properties as used before were assumed for this study. Two coordinate transformations methods were used: the linear transformation when studying the cross-sectional strength, and the corotational transformation for the overall member strength and stability.

A Newton solution Algorithm was used because of the material nonlinearities. The solution algorithm uses an Energy increment test which checks the positive force convergence if half of the inner-product of the displacement increment and the unbalanced force is less than the tolerance (10^{-3}). The equations are formed using a SparseGeneral scheme and are numbered using the Reverse Cuthill-McKee numberer. The constraints are represented with a Transformation constraint handler.

A single load step is performed for the axial load using the LoadControl integrator. The time in the domain is then set to 0.0 and the axial load is kept constant. A new load pattern with a linear time series and horizontal loads acting at node 2 is added to the model. The integrator is changed to DisplacementControl to impose nodal displacements and the static analysis is followed by a pushover analysis. A reference force of 1000 kN is defined in the linear time series. For this reference load, the DisplacementControl integrator determines the load increment necessary to increase the horizontal displacement at node 2 with 0.01 mm increments. A maximum of 21000 analysis steps were performed in this new analysis.

According to CAN/CSA S16-01, the capacity of Class 1 and Class 2 sections of I shaped members required to resist both bending moments and axial compressive forces is checked using the following interaction equation:

$$\frac{C_f}{C_r} + \frac{0.85U_{1x}M_{fx}}{M_{rx}} + \frac{\beta U_{1y}M_{fy}}{M_{ry}} \leq 1.0, \qquad (4.4.1)$$

where C_f and M_f are the maximum load effects including stability effects. These stability effects can be included by amplifying the translational load effects from a first order analysis with the factor U_2:

$$U_2 = \frac{1}{1-[\frac{\Sigma C_f \Delta_f}{\Sigma V_f h}]} \tag{4.4.2}$$

Only the weak axis behaviour was studied, therefore the equation 4.1.4.1 can be rewritten as:

$$\frac{C_f}{C_r} + \frac{\beta U_{1y} M_{fy}}{M_{ry}} \leq 1.0 \tag{4.4.3}$$

According to S16-01 standard, the member capacity should be examined for:

a) cross sectional strength, with β=0.6, and

$$U_{1y} = \left[\frac{\omega_1}{1-\frac{C_f}{C_e}}\right] \tag{4.4.4}$$

where $\omega_1 = 0.6 - 0.4\kappa \geq 0.4$ because the element is subjected to end moments only, κ is the ratio between the moments at the two ends of the element and C_e is the Euler load, $C_e = \pi^2 EI/L^2$. For the case studied herein, κ = 1.0 (equal moments at both ends), ω_1 = 0.4 and C_e = 11190 kN (I = 100 x 10^6 mm^4).

b) overall member strength, with $\beta = 0.6 + 0.4\,\lambda_y$.

In addition, the member should meet the criterion: $\frac{M_{fy}}{M_{ry}} \leq 1.0$. (4.4.5)

where M_{ry} is the factored bending resistance.

Pairs of compression and lateral loads were applied to the column model. The compression load C_f was expressed as a fraction of the column squash load, $C_y = AF_y$, for the cross-sectional strength study and as a fraction of the ultimate column buckling

strength, $C_u = AF_y(1+\lambda^{2n})^{-1/n}$, for the overall member strength study. The parameter β was set equal to 0.6 and U_1 and U_2 were considered equal to 1.0 for the cross-sectional strength study. For the overall member strength study, β was taken as the minimum between 0.85 and 0.6 + 0.4 λ_y, where λ_y is the column dimensionless slenderness parameter. For the column studied, λ_y = 0.75 and β was equal to 0.60 and 0.85 for the cross-sectional strength study and the overall member strength study, respectively. The bending moments M_f, were then determined from equation 4.4.3, for values of C_f/C_y and C_f/C_u varying from 0.0 to 1.0. Note that C_r and M_r in this equation were respectively taken equal to C_y (or C_u) and M_{py} (= Z_yF_y).

For the OpenSees analysis, the horizontal forces V_f that correspond to the moments determined from equation 4.4.3 were calculated ($V_f = 2M_f/L$) and then imposed at node 2 of the column. For the overall member strength, U_2 was included in the calculation of the horizontal forces V_f ($V_f = 2M_f/U_2L$). For each pair of C_f and V_f, the Opensees model was used to determine the value of the bending moment for which the yielding started in the end plastic hinges. The ratios of these moment values over the plastic moment ($M_p = ZF_y$) were then represented graphically as a function of the C_f/C_y ratios in Figure 4.4.1.

Tables 4.4.1 and 4.4.2 compare the theoretical results using the S16 equations to the results obtained from the OpenSees analyses. Table 4.4.1 presents the results for the cross-sectional strength check while Table 4.4.2 presents the results for the overall member strength verification. The ratios of these moment values over the plastic moment ($M_p = ZF_y$) were then represented graphically function of C_f/C_y ratios in Figure 4.4.1.

The interaction equation in the CSA-S16 standard (equation 4.4.3) is a simplified representation of the actual column response and, hence, do not allow an accurate verification of the OpenSees results. In order to obtain a better comparison reference the quadratic interaction formula proposed by Beaulieu et al (2003) was also used:

$$\frac{M_{ucy}}{M_{py}} = 1.19\left[1-\left(\frac{C}{C_y}\right)^2\right] \tag{4.4.6}$$

This equation was proposed to approximate the cross-section strength interaction for Class 1 and Class 2 of I shaped members required to resist both bending moments and axial compressive forces when the bending is about the weak axis. All the calculations for the cross-section strength check were redone using this equation and the results are plotted in Figure 4.4.1. It can be seen that the OpenSees results are very close to the theoretical values.

Table 4.4.1 Verification of cross sectional strength for bending with compression

S16-01								OpenSees
C_f/C_y	C_f(kN)	U_1	U_2	M_f (kNm)	C_f/C_y	M_f/M_p	V_f (kN)	M_f/M_p
0.00	0	1.00	1.00	635892	0.00	1.67	303	
0.10	635	1.00	1.00	572303	0.10	1.50	273	1.05
0.20	1271	1.00	1.00	508713	0.20	1.33	242	1.05
0.30	1906	1.00	1.00	445124	0.30	1.17	212	1.04
0.40	2541	1.00	1.00	381535	0.40	1.00	182	1.00
0.50	3176	1.00	1.00	317946	0.50	0.83	151	0.91
0.60	3812	1.00	1.00	254357	0.60	0.67	121	0.79
0.70	4447	1.00	1.00	190768	0.70	0.50	91	0.64
0.80	5082	1.00	1.00	127178	0.80	0.33	61	0.45
0.90	5717	1.00	1.00	63589	0.90	0.17	30	0.22
1.00	6353	1.00	1.00	0	1.00	0.00	0	

Table 4.4.2 Verification of overall member strength for bending with compression

S16-01								OpenSees
C_f/C_u	C_f(kN)	U_1	U_2	M_f (kNm)	C_f/C_y	M_f/M_p	V_f (kN)	M_f/M_p
0.00	0	0.40	1.00	1122162	0.00	2.94	534	
0.10	478	0.42	1.04	966847	0.08	2.53	441	1.04
0.20	955	0.44	1.09	821111	0.15	2.15	358	1.04
0.30	1433	0.46	1.15	684951	0.23	1.80	284	1.03
0.40	1910	0.48	1.21	558369	0.30	1.46	221	1.01
0.50	2388	0.51	1.27	441364	0.38	1.16	165	0.99
0.60	2865	0.54	1.34	333936	0.45	0.88	118	0.95
0.70	3343	0.57	1.43	236086	0.53	0.62	79	0.87
0.80	3820	0.61	1.52	147813	0.60	0.39	46	0.79
0.90	4298	0.65	1.62	69118	0.68	0.18	20	0.67
1.00	4775	0.70	1.74	0	0.75	0.00	0	0.44

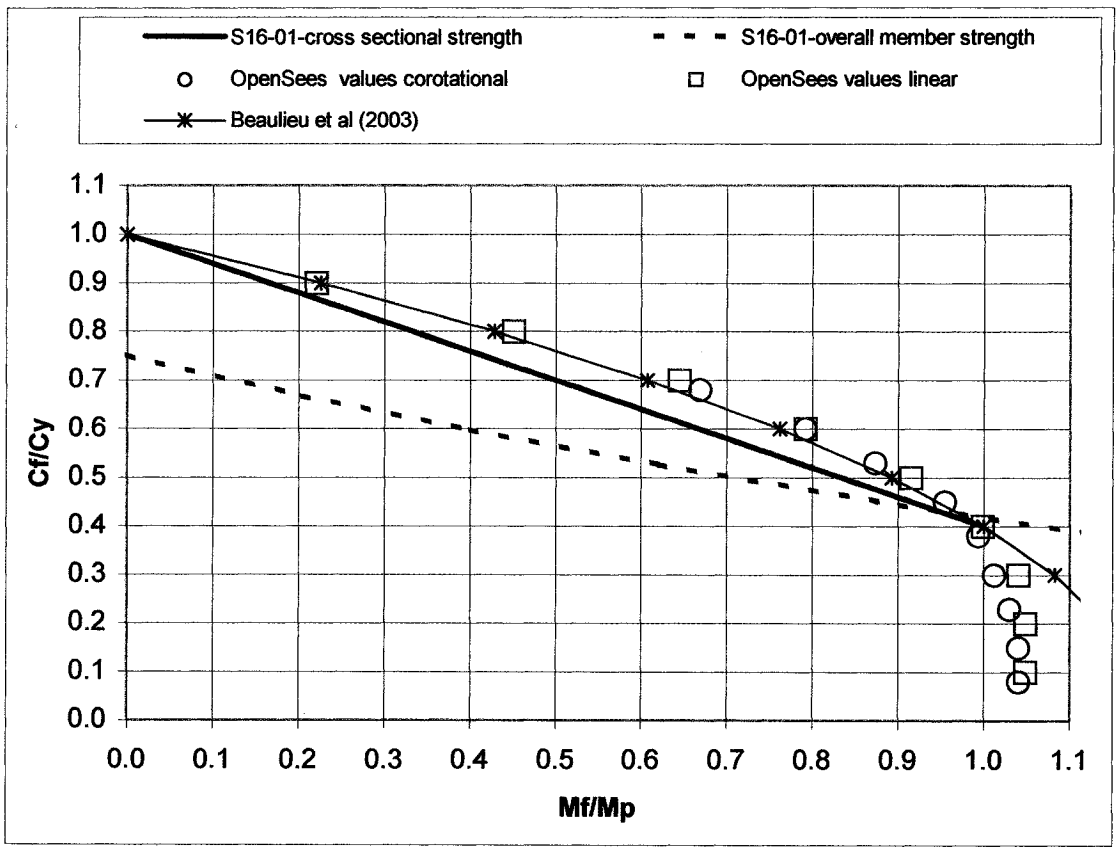

Fig. 4.4.1 Interaction curves for the W 310x129 section

4.5. Conclusions

The parametric and comparative studies realized in this chapter showed that:

- The elastic and inelastic flexural behaviour of W shape beams bent about their weak axis can be very well described using a nine-element discretization and a section discretization with ten fibres along the width of the flanges and four fibres over the height of the web. It was found though that the length and the position of the plastic hinges influence the flexural behaviour of the beam. Therefore, careful validation has to be made when modelling beams in flexure using the Beam with Hinges elements.
- Very close results were obtained when modelling a column with nine Beam with Hinges element and with one Beam with Hinges element. Therefore, it was decided to use a single Beam with Hinges element for modeling the beams and columns of the frame and also the gravity columns.
- Very close results were obtained when using ten fibres and twenty fibres discretizations of the portions of a W-shape section subjected to a linear stress variation. Therefore, a discretization with 10 fibres for these portions of W-shape sections was adopted to model all Beam with Hinges elements.
- The Beam with Hinges element orientation was validated, by comparing different methods with hand calculations.
- Finally, the single Beam with Hinges element model in OpenSees was found to predict well the capacity of a member subjected to axial load in compression combined with bending moments when comparing with the CAN/CSA S16-01 cross-section strength and overall member strength requirements.

CHAPTER 5. ANALYSES AND DISCUSSION OF RESULTS

This chapter describes the design and analysis work that was performed to assess the seismic performance of 2- to 16- storey concentrically braced steel frames designed according to current CSA-S16 seismic provisions. The first section of the chapter presents the assumptions and procedure used for the design of the sample buildings. The second section of the chapter presents the OpenSees analytical model developed for the studied buildings. This is followed by a description of the selected ground motions records. Afterwards, the results of the nonlinear dynamic analysis are presented, together with the overall seismic performance, including stability, of the studied buildings. Lastly, the results of the analysis are used to develop a statistical database of the brace axial deformation demand that can be used for the development of a loading protocol.

5.1. Building geometry and design

The studied buildings were 2-, 4-, 8-, 12- and 16- storey in height and were assumed to be located in Victoria, British Columbia, on a Site Class C. The plan view of the building structures is shown in Fig. 5.1.1.a for the 4- to 16-storey structures and in Fig.5.1.1.b for the 2-storey building. The structures are symmetrical in plan and they are braced by two concentrically braced steel frames in each orthogonal direction to resist the lateral loads. A Split-X system (concentrically braces over two floors) was chosen for the braced frames with braces acting in tension and compression. The elevation of the 8-storey frame is illustrated in Fig. 5.1.1.c. A storey height of 3.8 m was adopted for all floors except the first one which was 4.2 m tall. The same geometry was adopted for all structures. Therefore, the building heights, h_n, were 8.0, 15.6, 30.8, 46.0 and 61.2 m for the 2-, 4-, 8-, 12- and 16-storeys buildings.

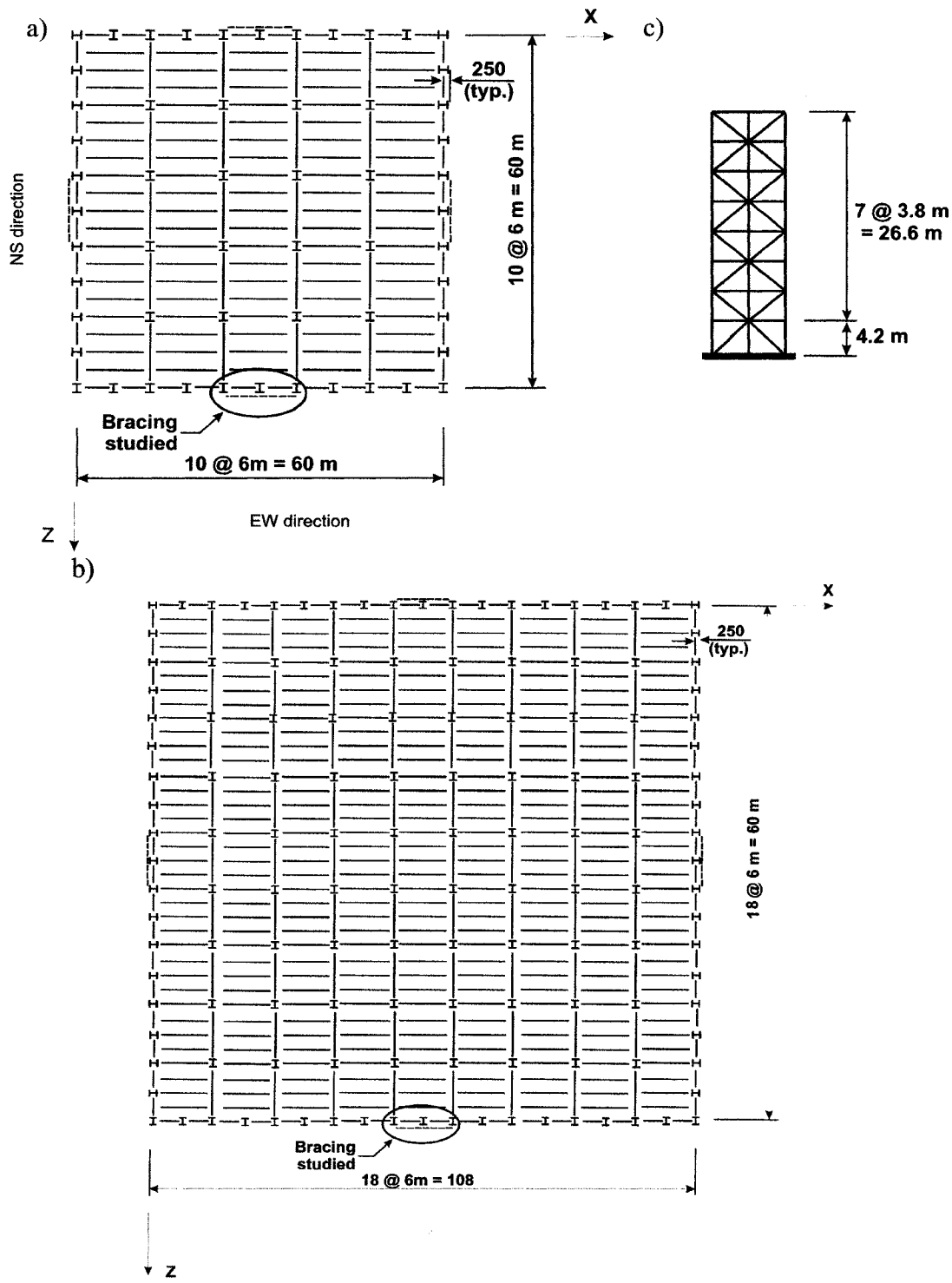

Fig. 5.1.1 Buildings studied:

a) Plan view (4-, 8-, 12- and 16-storey buildings); b) Plan view (2-storey building);

c) Braced frame elevation (8-storey building)

The reason for adopting larger plan dimensions for the 2-storey building (3.21 times larger in area compared to the other structures) was to obtain braces with large cross-sections and low slenderness, as was the case for the other structures.

In the CSA-S16 Standard (CSA 2005), the height limit for Type MD braced frame structures is 40 m. Hence, the 12- and 16-storey buildings were considered as Type LD frames with $R_d = 2.0$, while all the other ones were considered as Type MD with $R_d = 3.0$. The height of the 16-storey building was equal to 61.2 m, which approximately corresponds to the height limit for Type LD frames. For that building, the earthquake loads had to be increased by 26.4%, which corresponds to an increase of 2% per meter of height beyond 48 m (increase = 2.0% x (61.2 m – 48.0 m) = 26.4%), resulting in an equivalent R_d factor of 1.58 (= 2.0 / 1.264).

The design gravity loads were as follows: gravity dead load (D) and snow load (S) of 2.0 kPa and 1.08 kPa at the roof level, gravity dead load (D) and live load (L) of 3.5 kPa and 2.4 kPa at the floor levels. The partitions and the exterior walls were 1.0 kPa. For the 4-storey and taller buildings, the seismic weights for half the floor area were: 4384 kN at the top floor, 7780kN at the intermediate floors and 7805 kN at the first floor. For instance, for the intermediate floors, *W/frame* = 0.5 x [60.5 x 60.5 x (3.5 + 0.5) + 4 x 60.5 x 1.0 x 3.8] = 7780 kN.

A preliminary design of the structures was performed using the equivalent static force procedure (ESFP) of NBCC 2005, the buildings being regular and with a maximum height up to 60 m. The minimum earthquake lateral force is given by equation 2.2.1 (Section 2.2), including the upper and lower limits for short period and long period buildings, respectively. The values of the 2% in 50-year uniform hazard spectral ordinates, S_a, for the site of Victoria are given in Table 5.1.1 and the graphical representation is given in Fig. 5.3.1. The structures are assumed to be on a Site Class C and the foundation factors F_a and F_v are both equal to 1.0. The design spectrum ordinate,

S, for a given period was therefore obtained directly by linear interpolation between these S_a values.

Table 5.1.1 Uniform Hazard Spectral Ordinates for Victoria, B.C.

T(sec)	S_a(g)
0.0	1.2
0.2	1.2
0.5	0.82
1.0	0.38
2.0	0.18
4.0	0.09

The design period T_a was taken equal to 2 x 0.025 h_n, where h_n is the building height as permitted in NBCC for braced steel frames. For braced steel frames located in western Canada, the M_v factor is equal to 1.0 and the buildings were assumed to be of the normal importance category with $I_E = 1.0$.

In the equivalent static force procedure (ESFP), the base lateral force V is distributed over the height of the building according to the equation 2.2.2 (chapter 2.2). In the preliminary design, the loads were reduced by 20% (= $0.8V$) in anticipation of the 20% reduction that was made at a later stage in design, when the response spectrum analysis was used. The reduced forces were however increased by 10% to account for in-plane accidental eccentricity effects.

Only the response of the buildings in the X direction (E-W) was studied. However, the bracing bents acting in both orthogonal directions were designed in order to adequately represent the torsional response of the structure in the 3D dynamic analysis that was performed later in the design. Following the capacity design principles, the braces of the bracing bents were sized first, considering that the storey shear at every level was entirely resisted by axial forces in the braces. The story shears were amplified to account for the P-delta effects using the U_2 factor (equation 2.2.7, chapter 2.2) and brace axial load estimates due to gravity loading (D+0.5L) were added. The design of the braces was

governed by compression, the section of the braces being chosen in order to have the smallest weight per unit length. A value of 0.9 was used for the brace effective length factor. In the E-W bracing bents, the braces at the second floor of the 2-storey building, all braces in the 4-, 8-, and 12-storey structures, and the braces at the 8th floor and above the 9th level in the 16-storey building were made of ASTM A500 gr. C square steel tubes (F_y = 345 MPa). The remaining braces for the 2-storey building (at the first floor) and 16-storey structure (from the first floor to the 7th floor) were made of ASTM A992 steel (F_y = 345 MPa) W shapes.

Beams and columns were subsequently designed to resist gravity loads together with the maximum brace forces expected to develop upon inelastic response. W shapes made of ASTM A992 steel (F_y = 345 MPa) were used for the beams and columns. First, the gravity loads in the columns were determined using the reduction factor for the live loads $F = 0.3 + \sqrt{9.8/A_t}$ where A_t is the tributary area of the column. Thereafter, the effect of the lateral loads was calculated considering three cases:

- assuming buckling of all of the compression braces and tension yielding in all the tensioned braces in the storeys above the level under consideration,
- assuming that all compression braces in the storeys above the level under consideration impose their reduced post-buckling strength while tension braces still develop their full yielding capacity, and
- assuming that R_d times the lateral seismic loads were applied to the building.

For the buildings studied, the brace tension forces from the last case were found to exceed the tension capacity of the braces at every floor, and hence only the first two cases were in fact considered. Gravity load effects on the columns were determined assuming that all the loads were carried by the columns after inelastic response has developed in the braces. Following CSA-S16-01 requirements, the columns were verified as beam-columns. The columns were bent about their weak axis and, hence, the check was performed for the cross-section strength and the overall member strength in the plane of

bending. Class 1 or 2 sections were selected and the same section was kept over two consecutive floors.

The beams were first designed to resist the gravity loads combination 1.25 D + 1.5 L. Thereafter, they were verified as beam-columns, following CSA S16-01 provisions, considering the gravity load due to D + 0.5 L and the largest of the compression forces arising from the brace force patterns described above. The beams were verified only for the cross-section strength and the overall member strength in the plane of bending; assuming that they were laterally supported by the floor slabs.

After completion of the preliminary design based on the NBCC equivalent static force procedure, three-dimensional dynamic analysis of the structures was performed with the Visual Design software. An iterative design process was carried out, using the member cross-sections from the preliminary design as the starting point, until convergence was achieved for the brace cross-sections. The response spectrum analysis method was used with the design spectrum values, *S(T)*, described earlier. The complete quadratic modal combination approach was adopted with 5% of the critical damping for each of the modes. Accidental eccentricity was included in the computer program by applying horizontal and in-plane torsional moment at every level equal to the horizontal seismic force at the level times 10% of the building plan dimension along the Z direction. P-delta effects were also included in the analysis by amplifying the lateral load effects by the CSA-S16 U_2 factor. Notional loads accounting for initial imperfections were not applied as the analytical model used to asses the performance of the structure assumes no imperfections. According to NBCC 2005 provisions, the results of the spectrum analysis were scaled such that the base shear from dynamic analysis V_d is equal to or exceeds $0.8V$, as permitted for regular structures.

In the Visual design model, the base of the columns of the bracing bents was assumed to be fixed while the gravity columns were modelled with pinned bases. The columns were

continuous over two consecutive floors and the splice connections were assumed to exhibit full flexural strength and stiffness continuity. Pinned connections were used between the beams and the columns. The braces were pin connected to the framing members and an effective length factor $K = 0.9$ was considered. The slabs were modeled using the "joist floor" elements included in the program (the joists span in the X direction in Fig. 5.1.1). The slabs were considered as rigid diaphragms at each level and the gravity loads were considered as uniformly distributed over their areas.

There are two possibilities for the design of steel structures using the Visual Design program: either by letting the program selecting the elements automatically from an internal section's library according to the desired standard or by asking the program to perform a code check of member cross-sections previously selected by the user. The program calculates the maximum forces and displacements according to the chosen code provisions (NBCC 2005). Unfortunately, at the time this work was performed, the capacity design procedure had not been implemented in the Visual Design software and an iterative manual analysis-design procedure had to be performed in order to fulfill the CSA-S16 capacity design requirements for the seismic force resisting systems. An EXCEL worksheet was created in order to calculate the forces induced by the braces upon buckling and yielding in the beams and the columns of the bracing bents. The spreadsheet was also developed to design these members to meet the above described beam-column requirements.

The member cross-sections obtained from the preliminary design were used to create the first model of each of the buildings in Visual Design. A first 3-D dynamic analysis was performed on the structures. The program was adjusted to perform a code check (verification only) for the members of the bracing bents and to automatically select the required shapes for the rest of the structure. With the brace forces obtained from this analysis, the brace sections were chosen on a minimum weight basis. The EXCEL worksheet was then used to determine the brace capacity at buckling, after buckling and

at yielding in order to design the columns and the beams of the bracing bents. With these new sections, a second dynamic analysis was performed on the structure following the same procedure: a code check for the concentrically braced frame members and automatic design of the other members. The above-described procedure was repeated until the convergence was reached when the brace sections did not need to be changed from one analysis to the next. For each building, it was necessary to perform up to 4-5 iterations to reach the convergence for the forces in the braces. Figure 5.1.2 shows the final choice of sections, as obtained at the end of the iterative dynamic analyses/dynamic procedure.

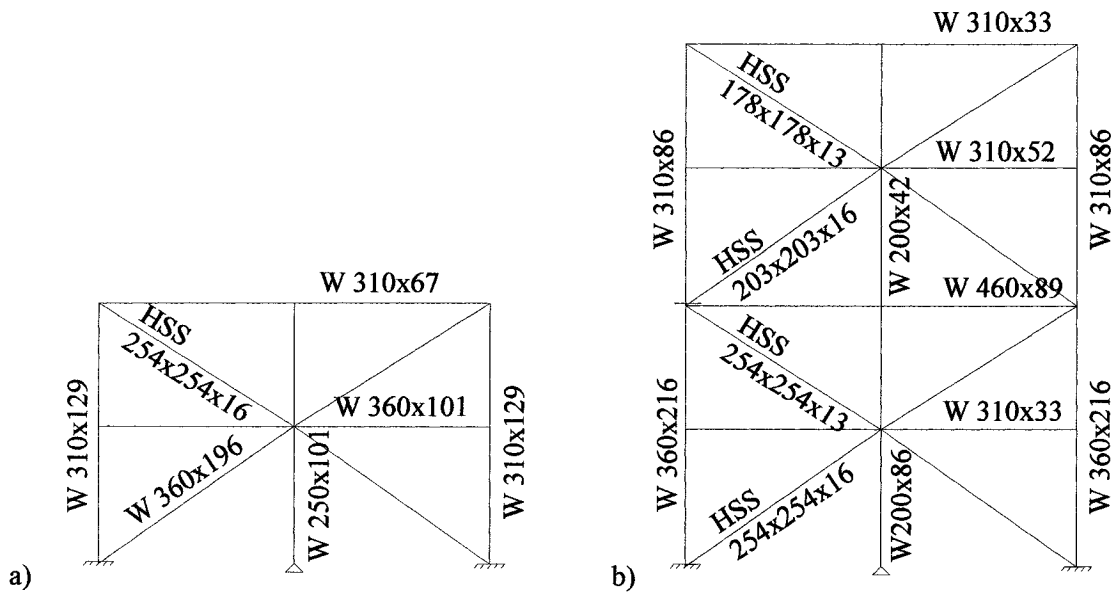

Fig. 5.1.2 Brace, beam and column sections for the studied buildings
a) 2-storey building; b) 4-storey building;

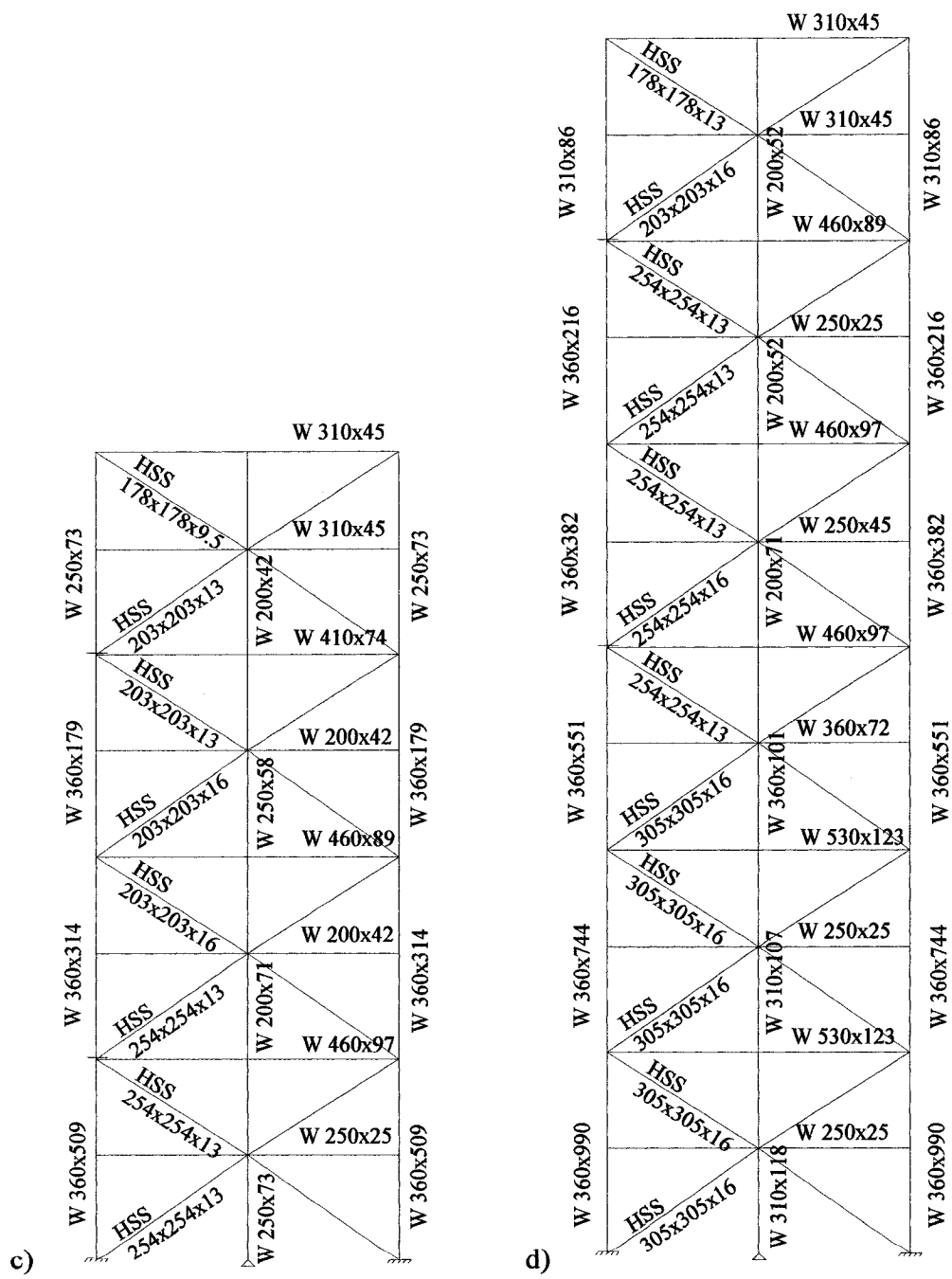

Fig. 5.1.2(cont'd) Brace, beam and column sections for the studied buildings; c) 8-storey building; d) 12-storey building

e)

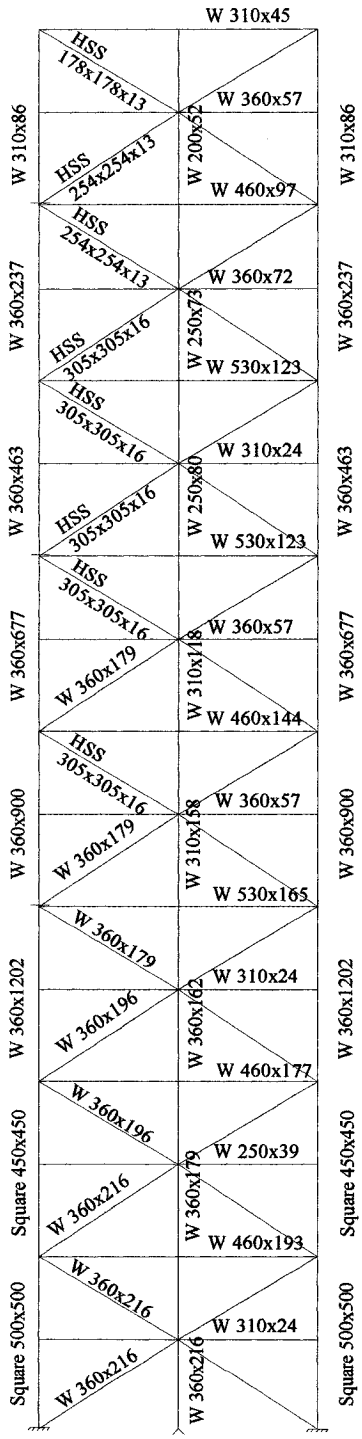

Fig. 5.1.2(cont'd) Brace, beam and column sections for the studied buildings: e) 16-storey building.

Table 5.1.1 gives the modal properties of the buildings studied for the number of modes required to reach 90% of the total mass of the structures in both orthogonal directions (Carr, 1994). In the table, T is the period of the mode, W is the total seismic weight for the entire building and W_x/W corresponds to the mass participation ratio for the mode of vibration in the E-W direction. For the 2-storey building, 6 modes of vibration had to be used to perform the analysis. The required number of modes for the 4-, 8-, 12- and 16-storey structures were respectively equal to 8, 10, 12 and 16.

Table 5.1.2 summarizes the calculation of the base shear force values for each orthogonal direction. In the Table, T_{emp} is the period from the empirical formula ($T_{emp} = 0.05\ h_n$), T_1 is the computed first mode period (Table 5.1.1), T_a is the design period, V is the base shear obtained from the equivalent static force procedure, V_e is the elastic base shear from response spectrum analysis, and V_d is the dynamic base shear, $V_d = V_e I_E/R_d R_o$. Regarding the design periods of the buildings, only the period of the 2-storey building exceeded the NBCC limits ($0.05h_n$) and that upper limit was therefore used as the design period. As can be seen, the value of V_d exceeded $0.8V$ for all buildings and no adjustment (scaling) of the spectrum analysis results was needed.

Table 5.1.1 Mass participation ratios for the first six (or eight) modes of vibration

Building	R_d	i	T	DIR	W (kN)[1]	W_x/W
2	3.0	1	0.47	X	76361	86.6%
		2	0.46	Z		86.6%
		3	0.29	Torsion		86.6%
		4	0.23	X		100%
		5	0.23	Z		100%
		6	0.14	Torsion		100%
4	3.0	1	0.75	Z	55468	0%
		2	0.72	X		83.3%
		3	0.47	Torsion		83.3%
		4	0.28	Z		83.3%
		5	0.27	X		95.5%
		6	0.18	Torsion		98.5%
8	3.0	1	1.53	X	117677	78.1%
		2	1.50	Z		78.1%
		3	1.00	Torsion		78.1%
		4	0.54	X		92.3%
		5	0.53	Z		92.3%
		6	0.35	Torsion		92.3%
12	2.0	1	2.15	X	179885	72.2%
		2	2.10	Z		72.2%
		3	1.38	Torsion		72.2%
		4	0.74	X		89.6%
		5	0.71	Z		89.6%
		6	0.47	Torsion		89.6%
		7	0.41	X		94.2%
		8	0.39	Z		94.2%
16	1.58	1	2.53	X	242098	68.8%
		2	2.52	Z		68.8%
		3	1.61	Torsion		68.8%
		4	0.83	X		87.6%
		5	0.81	Z		87.6%
		6	0.52	Torsion		87.6%
		7	0.45	X		92.8%
		8	0.44	Z		92.8%

[1]Total floor area (for all bracing bents in each direction)

Table 5.1.2 Base shear forces for the buildings studied
(values for the entire building)

n	R_d	T_{emp} (s)	T_1 (s)	T_a (s)	Dir	V (kN)	$0.8V$ (kN)	V_e (kN)	V_d (kN)	V_{chose} (kN)
		0.40	0.47	0.40	X	15664	12531	57998	14871	14871
2	3.0	0.40	0.46	0.40	Z	15664	12531	59068	15146	15146
		0.78	0.75	0.75	Z	8541	6833	28280	7251	7251
4	3.0	0.78	0.72	0.72	X	8961	7169	30232	7752	7752
		1.54	1.50	1.50	Z	8437	6750	29480	7559	7559
8	3.0	1.54	1.53	1.53	X	8251	6601	29000	7436	7436
		2.30	2.10	2.10	Z	12454	9963	31328	12049	12049
12	2.0	2.30	2.15	2.15	X	12454	9963	31105	11963	11963
		3.06	2.53	2.53	X	21216	16973	38231	18613	18613
16	1.58	3.06	2.52	2.52	Z	21216	16973	38499	18743	18743

Table 5.1.3 presents the characteristics of the buildings in the X direction: the steel tonnage for one of the bracing bents studied, the maximum values over the building height of the P-delta amplification factor U_2, the torsion amplification factor for the bracing bents studied and the maximum intrestorey drift ratio (Δ/h_s) over the building height. The torsion parameter corresponds to the increase in the first floor brace axial loads due to earthquake loading when comparing the results of the 3D analysis performed for the following two conditions: in-plane torsional response of the building released and restrained, respectively. The storey drift values are those obtained from the spectrum analysis and include inelastic effects as well as in-plane torsional effects. The U_2 factor and storey drift values at every floor of the structures are given in Appendix II (Table II.1).

As shown, the U_2 amplification factor is less than the CSA S16-01 limit of 1.4 and the interstorey drift values are less than the NBCC 2.5% h_s limit for all buildings. Hence,

none of the structures needed to be stiffened. Torsional effects were close to the 10% assumed in the preliminary design. These factors are used later in the scaling of the ground motion records.

Table 5.1.3 Characteristics of buildings

n	Steel tonnage (t)	U_2 max ( )	Torsion factor ( )	Δ/h_s max (%)
2	9.51	1.04	1.10	0.93
4	13.19	1.05	1.10	0.87
8	33.41	1.13	1.11	0.95
12	78.49	1.10	1.06	1.01
16	115.16	1.09	1.11	0.99

The time history nonlinear dynamic analyses of the above-presented braced frames were performed using the OpenSees software and ground motions ensemble comprising 20 records.

5.2. OpenSees model for the studied buildings

The OpenSees models represented one-half of the building structure. It included one of the two braced frames studied as well as all the gravity columns laterally stabilized by that braced frame. For simplicity, identical columns were lumped together in the model, resulting in seven different column types: one for the interior columns, three for the exterior columns (one for the columns in the N-S direction and two for the columns in E-W direction), one for each interior and exterior columns of the braced frames acting in the N-S direction, and one for the corner columns. The 4-storey building model is shown in Fig. 5.2.1.

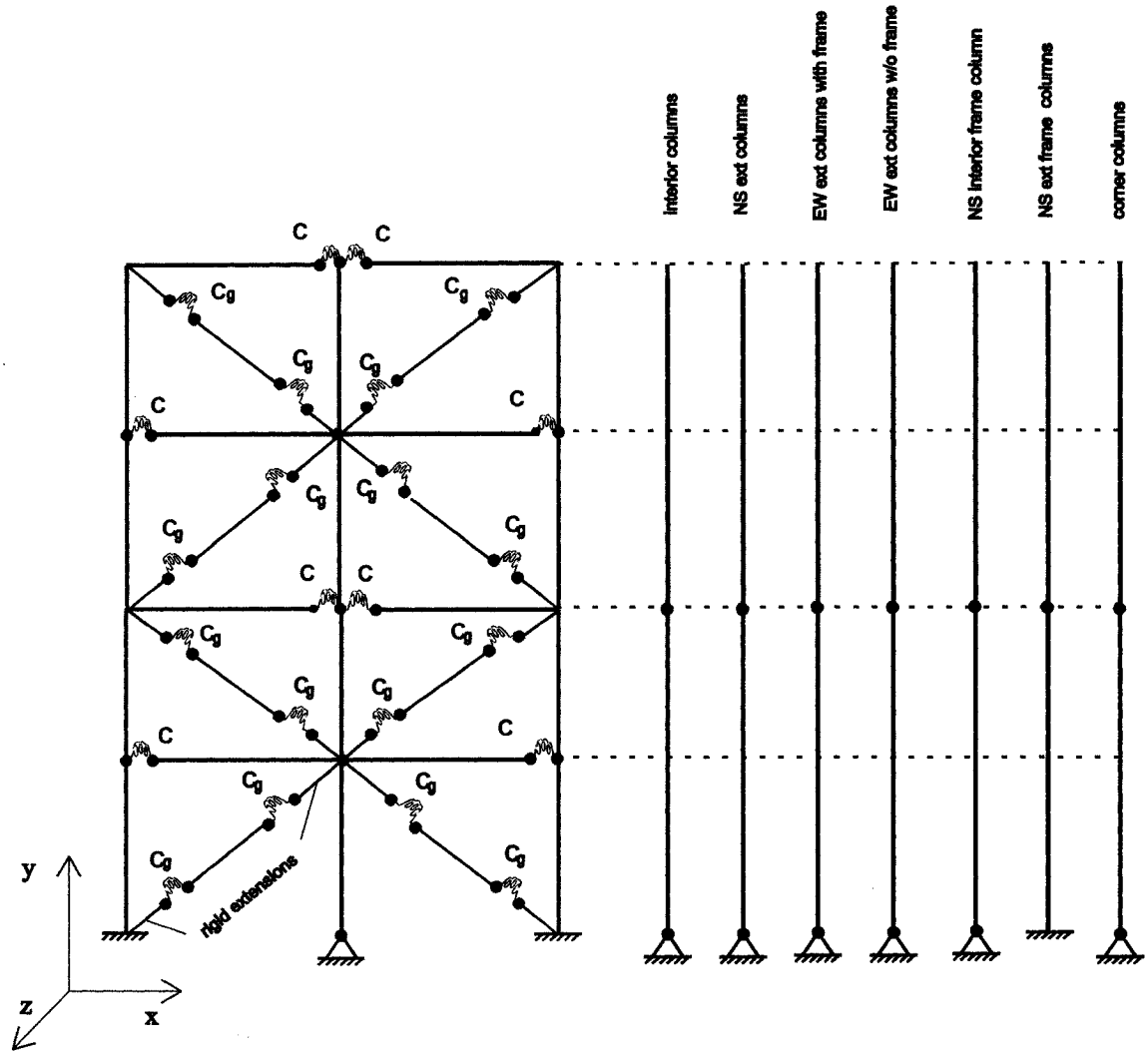

Fig. 5.2.1 OpenSees model for the 4-storey building

Although all members were arranged in only one plane (x-y plane), a three-dimensional model was used to represent the out-of-plane (Z direction) initial imperfection and out-of-plane buckling response of the bracing members. A half-sine deformed shape was specified for the brace initial imperfection. The amplitude of the initial imperfection at the brace mid-length, δ_0, was adjusted iteratively until the compression strength of each of the braces as modelled was equal to a maximum of 110 % of $1.2C_u$ for the braces,

where $C_u = AF_y(1+\lambda^{2n})^{-1/n}$, λ being calculated with R_yF_y and n = 1.34. This verification was performed using the OpenSees model including the actual size and the flexural stiffness of the gusset plate end connections, as discussed below. The model was also used to evaluate the effective brace slenderness ratio in order to compare with the K value of 0.9 assumed in design. The calculations were performed for the 8-storey building and are presented in Appendix VIII. The K factor was found to vary between 0.71 and 0.82 over the 8 floors, with an average value of 0.77.

The brace characteristics and the resulting imperfection amplitudes considered are given in Tables 5.2.1 to 5.2.5. In the tables, the K factor is taken as 0.9 and the length L corresponds to the o/c brace dimensions. As shown, initial imperfection of $L/250$ and $L/200$ were needed to obtain realistic values of the brace buckling load. These values are larger than the out-of-straightness limit of $L/500$ implicit in the CSA-S16 column curve. One reason for the difference is the shorter actual effective length factor of the braces compared to the value used to calculate $1.2C_u$ at the design stage. Another reason for the required large imperfection values is the fact that residual stresses are not included in the brace model.

Table 5.2.1 Characteristics and imperfections of the braces for the 16-storey building

Floor	Brace	1.2 C_u (kN)	AF_y	λ	KL/r	δ_0
16	HSS 178x178x13	1455	2839	1.26	96	200
15	HSS 254x254x13	3313	4212	0.86	65	250
14	HSS 254x254x13	3313	4212	0.86	65	250
13	HSS 305x305x16	5656	6300	0.72	55	250
12	HSS 305x305x16	5656	6300	0.72	55	250
11	HSS 305x305x16	5656	6300	0.72	55	250
10	HSS 305x305x16	5656	6300	0.72	55	250
9	W 360x179	6620	8653	0.88	67	250
8	HSS 305x305x16	5656	6300	0.72	55	250
7	W 360x179	6620	8653	0.88	67	250
6	W 360x179	6620	8653	0.88	67	250
5	W 360x196	7286	9488	0.88	67	250
4	W 360x196	7286	9488	0.88	67	250
3	W 360x216	8412	10436	0.83	63	250
2	W 360x216	8412	10436	0.83	63	250
1	W 360x216	8195	10436	0.86	65	250

Table 5.2.2 Characteristics and imperfections of the braces for the 12-storey building

Floor	Brace	1.2 C_u (kN)	AF_y	λ	KL/r	δ_0
12	HSS 178x178x13	1455	2839	1.26	96	200
11	HSS 203x203x16	2425	4023	1.11	84	200
10	HSS 254x254x13	3313	4212	0.86	65	250
9	HSS 254x254x13	3313	4212	0.86	65	250
8	HSS 254x254x13	3313	4212	0.86	65	250
7	HSS 254x254x16	4004	5161	0.87	66	250
6	HSS 254x254x13	3313	4212	0.86	65	250
5	HSS 305x305x16	5656	6300	0.72	55	250
4	HSS 305x305x16	5656	6300	0.72	55	250
3	HSS 305x305x16	5656	6300	0.72	55	250
2	HSS 305x305x16	5656	6300	0.72	55	250
1	HSS 305x305x16	5542	6300	0.74	56	250

Table 5.2.3 Characteristics and imperfections of the braces for the 8-storey building

Floor	Brace	1.2 C_u (kN)	AF_y	λ	KL/r	δ_0
8	HSS 178x178x9.5	1159	2197	1.24	94	200
7	HSS 203x203x13	2030	3294	1.09	83	200
6	HSS 203x203x13	2030	3294	1.09	83	200
5	HSS 203x203x16	2425	4023	1.11	84	200
4	HSS 203x203x16	2425	4023	1.11	84	200
3	HSS 254x254x13	3313	4212	0.86	65	250
2	HSS 254x254x13	3313	4212	0.86	65	250
1	HSS 254x254x13	3224	4212	0.89	67	250

Table 5.2.4 Characteristics and imperfections of the braces for the 4-storey building

Floor	Brace	1.2 C_u (kN)	AF_y	λ	KL/r	δ_0
4	HSS 178x178x9.5	1159	2197	1.24	94	200
3	HSS 203x203x16	2425	4023	1.11	84	200
2	HSS 254x254x13	3313	4212	0.86	65	250
1	HSS 254x254x16	3894	5161	0.90	68	250

Table 5.2.5 Characteristics and imperfections of the braces for the 2-storey building

Floor	Brace	1.2 C_u (kN)	AF_y	λ	KL/r	δ_0
2	HSS 254x254x16	4004	5161	0.87	66	250
1	W 360x196	7083	9488	0.91	69	250

Two types of material were used in the model: the uniaxial elastic material and the uniaxial Steel02 Giuffré-Menegotto-Pinto material. A uniaxial material is represented by uniaxial stress-strain (or force-deformation) relationships. The elastic material behaviour depends only on the Young's modulus and is represented in Fig.5.2.2. The characteristics of the GMP material were presented in Section 3.3.1.

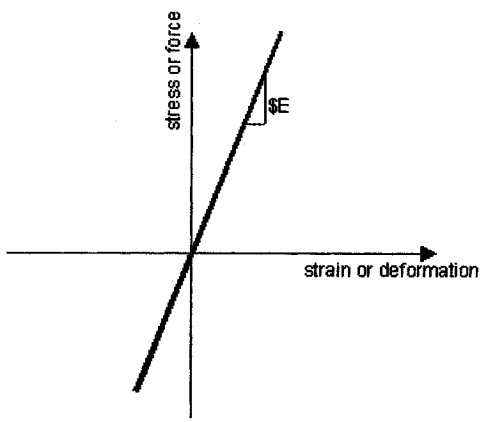

Fig. 5.2.2 Elastic material

Large deformation analysis was performed using the co-rotational formulation for the transformation of the element stiffness and resisting forces from the local system to the global coordinate system.

Nonlinear beam-column elements with plasticity spread along the length of the element were used to model the braces. Each brace was modeled using eight elements with the cross-section divided into sixteen fibres and four integration points per element, as it was concluded in Chapter 3. An exception was made at the first floor of the 2-storey building and at the first nine floors of the 16-storey buildings, where braces were made of W sections. For those braces, the cross-section fibre discretization described in Chapter 4 of the beams and columns was used. The torsional stiffness of the braces was included using the Section Aggregator object of OpenSees (Mazzoni et al., 2005). This object permits to combine previously defined uniaxial materials in a single section. Two tasks can be performed using this command:

- group previously defined uniaxial materials in order to describe a resultant section; and/or
- add to an existing section another uniaxial material.

The latter feature was used to take into account the torsional properties of the braces. A previously defined uniaxial elastic material was added to the existed fibre section of the braces in which the interaction between the axial force and flexure was already considered.

The beams and the columns were modeled using the Beam with Hinges element described and validated in Chapter 4. The length of the plastic hinges was considered equal to the height of the section of the beam and of the column respectively. Out-of-plane displacements of the beams were assumed to be constrained by the rigid diaphragms of the slabs at each floor. Torsional response of the beams and columns, including the gravity columns, was prevented using the same Section Aggregator object:

a very rigid uniaxial material was added to the existing fibre section of the beams and columns. Beams in the braced frames were assumed to be rigidly connected to the columns at brace connection locations. Other beam-to-column connections were assumed to be pinned. These pinned connections were modeled using zero-length rotational spring elements with only the rotation around the axis normal to the plane of the frame being permitted.

The actual dimensions and thickness of the gusset plates at each floor were established using the Whitmore and Thornton assumptions. Whitmore (1952) defined the effective width (b_w) of a gusset plate "as the length of the line passing through the bottom row of fasteners and intercepted by two 30° lines originated at the outside fasteners of the first row". The buckling strength of the gusset plate is calculated by considering a uniform distributed yielding stress of the material along the effective width. This method overestimates the strength of the gusset. An alternative method proposed by Thornton (1984) is to consider imaginary column strips of unit width below the Whitmore width. The buckling strength of the gusset plate is estimated based on the Whitmore width and the compressive resistance of the imaginary columns. Thornton suggested that the longest of the three lines L_1, L_2, L_3 in Fig. 5.2.3 should be considered as the critical effective length. In this study, the Whitmore width was determined as the length of the line passing through the end of the brace and intercepted by two 30° lines starting from the intersection of the brace and the gusset plate. The critical length L_c was taken as the average of the three values L_1, L_2, and L_3 as recommended in several design guidelines (e.g. Cochran and Honeck 2004). Experimental results by Lin et al. (2005) concluded that the effective length factor K for the column strips could be considered equal to 2.0, Thornton suggested a value of 0.65. In this project a value of K equal to 1.2 was considered.

The gusset plates were designed with the "$2t_g$" free length detail allowing hinges to form in the gusset upon out-of-plane buckling of the braces. Rigid extensions were considered

from the beam-to-column centerline intersection points to the brace fold line location in the gusset plates. These extensions were modeled using elastic beam column elements with infinite stiffness and strength. The length of these rigid extensions was determined from the geometry of the beams, columns and braces at each floor. Detailed calculations are given in Appendix III. Zero length rotational elements were used to connect the braces to the rigid extension elements. The rotational spring elements were oriented along the local axis of the braces using orientation vectors, as detailed in Appendix IV, and the spring stiffness in each direction was representative of the in-plane and out-of-plane gusset plate bending stiffness.

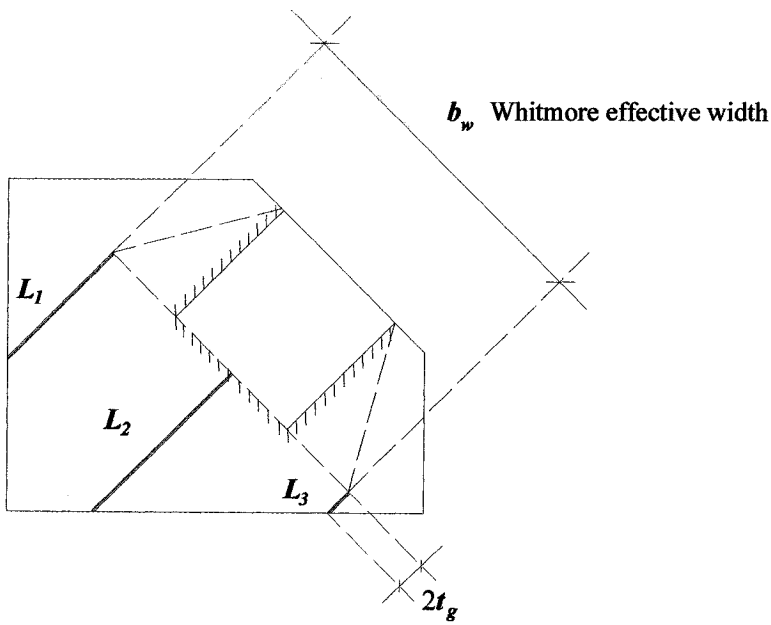

Fig. 5.2.3 Whitmore effective width and Thornton method

The gusset plates were assumed to be made of steel with F_y = 345 MPa. Their thickness was determined from the most severe from the two following conditions:

- the gusset plate resistance in tension $T_r = \phi F_y b_w t_g$ must exceed the capacity in tension of the brace $P_{y\ brace} = AR_y F_y$;
- the gusset plate resistance in compression $C_r = \phi A F_y (1 + \lambda^{2n})^{-1/n}$, where $\lambda = \frac{KL_c}{t_g}\sqrt{\frac{12F_y}{\pi^2 E}}$, must exceed the expected capacity in compression of the brace $P_{max} = 1.2C_u$.

The detail of the gusset plate design at each floor of each building is described in Appendix V. The plate thickness values varied from 26 mm to 42 mm. Zero-length rotational springs were used between the rigid extensions and the ends of the bracing member and the nonlinear beam column elements to reproduce the flexural and torsional gusset plate properties. The out-of-plane bending stiffness and torsional stiffness of the rotational springs were respectively calculated using the following formula: $C_f = 1.5\frac{EI}{2t_g}$ in flexure and $C_t = \frac{GJ}{2t_g}$ in torsion. In these equations, t_g is the thickness of the gusset plate, I and J are the flexural and torsional moments of inertia of the gusset plate, respectively. The flexural capacity of the gusset plates was taken equal to: $M_p = \frac{1}{4} b_w t_g^{\ 2} F_y$.

The gravity columns were modeled as single leaning columns. They were constrained to have the same lateral displacements as the braced frame columns, assuming rigid diaphragm effect of the slabs at every floor using the equalDOF command. Their flexural properties were established based on the orientation and the bending axis properties of each of the column types.

As it can be seen in Fig. 5.2.1, the outer braced frame columns were assumed to be fixed at their bases whereas other column bases were assumed to be pinned. Full continuity

was considered for the splices of the three braced frame columns as well as for the columns of the N-S bracing bents.

The gravity columns were modeled with zero-length rotational springs reproducing the column splices at every second floor. For these rotational springs, a flexural capacity equal to 10% of the smallest of the flexural resistance of the two column shapes was considered and a flexural stiffness was calculated as a function of the column orientation (strong axis or weak axis).

For the strong axis orientation the stiffness was equal to $C_{x-x} = \frac{EAd^2}{L}$, where A is the area of the splice plates connecting the two flanges of the column members, $A = b_f t_{splice}$, where t_{splice} is the thickness of the splice plates, b_f is the width of the column flange, and L is the vertical distance between the first bolt rows located on either side of the column splice. For the weak axis orientation, the rigidity was equal to $C_{y-y} = \frac{9}{16}\frac{EAb_f^2}{L}$, where $A = \frac{b_f}{2} t_{splice}$. Detailed calculations are presented in Appendix VI.

In the model, the capacities of all members and connections were determined using an expected yield strength value of 380 MPa.

Masses representing the seismic weight at each floor were assigned at the braced frame nodes and Rayleigh damping equal to 3% of critical damping in the first two modes of vibration was specified. An example of damping calculation is presented in Appendix VII. The value of 3% of critical damping was selected from a survey of several past studies that summarized as follows:

- Foutch, et al (1987) determined the damping and the periods of the first few modes of a 6 floors concentrically braced steel frame structure using vibration tests. The damping found in the lowest 3 modes was 2%.

- Bertero, et al (1989) studied a 0.3 scaled shake table model of a 6-storey concentrically steel braced frame subjected to 20 simulated ground motions. Prior to these tests, flexibility tests as well as free and forced vibration tests were conducted to measure the initial dynamic characteristics of the model. The damping values found: 1.29%, 0.67% and 0.54% in the first 3 mode free vibration and 1.56%, 0.72% and 0.63% in the first 3 mode-forced vibrations.

- Bard, et al (1991) measured the damping ratios of several buildings using multi-sensor in-situ testing, in both longitudinal (L) and transversal (T) directions:
  5.8% (L) and 3.6% (T) for 1st mode of a 4 floors building;
  2.9% (L) and 4.9% (T) for 1st mode of a 6 floors building; and
  3.0% and 2.4% (L), 1.3% and 2.2% (T) for 1st mode of a 13 floors building, under two different ground motions events.

- Chen et al (1992) studied a 47-story steel structure in San Francisco and the free vibration damping ratio obtained from recorded data were 2.0%-2.6% for the EW moment frame direction and 1.7%-2.0% for the NS braced frame direction.

- For the same 47-floor building in San Francisco, Çelebi (1993) determined from system identification procedures (input-output data the following damping values for the NS and respectively, EW direction of the building: 2.5% and 3.7% for 1st mode; 2. 2 % and 2.8% for the 2nd mode; and 1.4% and 3.6% for the 3rd mode.

Once the model was created, the *Analysis* object could be described in order to perform the analysis.

For each ground motion, the analysis of the models was conducted into two steps. In the first step, a single load pattern with linear time series and vertical nodal loads applied at each node of the braced frame and of the gravity columns was used to apply the gravity loads on the structure. The gravity load included the permanent dead load plus 50% of the floor live load and 25% of the roof snow load. In the second step, a second load pattern consisting of a uniform excitation load pattern, with an acceleration record specified at a base node was used to apply the earthquake excitation.

The equations were numbered using an RCM (inverse Cuthill-McKee) numberer, which optimizes the node numbering in order to reduce the storage bandwidth. This method outputs an error message when the structure is disconnected. The constraints were enforced in the analysis using the transformation method. This method transforms the stiffness matrix by condensing out the constrained degrees of freedom. This approach was used because it is recommended in transient analyses. The system of equations was formed using a SparseGeneral scheme and was factored and solved during the analysis using the SuperLU solver.

The Solution Algorithm determines the sequence of steps for solving the equations for the non-linear dynamic analysis. The model contains material and geometric non-linearities and a solution algorithm of the Newton type was first considered. However, this approach was found to lead to convergence problems, and the more advanced Newton with Line Search algorithm procedure was chosen. This algorithm uses the Newton-Raphson method with line search to advance to the next step.

The solution algorithm uses a convergence test that checks the energy increment if the product of displacement increment and the unbalanced force is less than a specified tolerance at the end of an iteration step.

The integrator for the analysis was of type Load Control with a load step increment of 0.1. The role of the integrator is to determine the step for the time $t+dt$, to specify the tangent matrix and the residual vector at any iteration and to determine the corrective step based on the displacement increment.

Once the components of the analysis are defined, the analysis object is created. For the static analyses, a series of 10 steps are used in order to load the model with the desired gravity loads. After the gravity load analysis has been performed the gravity loads are set to constant and the time is set to 0. A new Newmark-Beta type integrator is defined, with $\gamma = 0.5$ and $\beta = 0.25$. Transient analyses are then performed with a time step of 0.005 s and the number of the time steps varying depending on the duration of the chosen earthquake record.

Table 5.2.6 presents the fundamental periods T_1 found for the OpenSees model and for the three-dimensional Visual Design model for the studied buildings. The values are very close, which means that the OpenSees model reproduces well the three-dimensional Visual Design model.

Table 5.2.6 Visual Design vs OpenSees fundamental periods of the buildings

	2	**4**	**8**	**12**	**16**
Visual Design	0.47	0.72	1.53	2.15	2.53
OpenSees	0.48	0.73	1.59	2.17	2.67

5.3. Ground motion records

Twenty ground motions were used in this project to study the behaviour of the buildings: ten signals as recorded in past natural earthquakes and ten simulated ground motion time histories. These motions have magnitude-distance characteristics that are compatible with the dominant scenarios governing the 2% in 50 year hazard for Vancouver and other western Canadian cities (Halchuk and Adams 2004, Tremblay and Atkinson 2001) as given in Table 5.3.1. The selected signals are also representative of Site Class C conditions assumed in design with shear wave velocity between 360 and 760 m/s.

Table 5.3.1 Scenario events for the selection of compatible time histories

	Moderate earthquakes at **short** distance		**Large** earthquakes at **long** distance	
City	Magnitude (Mw)	Hypocentral distance (km)	Magnitude (Mw)	Hypocentral distance (km)
Victoria	6.5	30	7.2	70

These two scenario events only cover the hazard form crustal and subcrustal earthquakes. The scenario of great Mw 8.5 earthquakes along the Cascadia subduction zone was not considered in this study.

The ten historical earthquake records (H01 to H10) were selected from the Pacific Earthquake Engineering Research Center (PEER) database. They are described in Tables 5.3.2 and 5.3.3. The ten simulated motions (A01 to A10) are described in Table 5.3.4.

The tables give the magnitude, the hypocentral distance, R, the peak horizontal acceleration (PHA) and the peak horizontal velocity (PHV) of the time histories. Each ground motion was scaled such that its 5% damped acceleration response spectrum matches, on average, the 2005 NBCC design spectrum for Victoria. The scaling factor, S_f, is given in the tables. It is noted that the PHA and PHV values in the tables are for the unscaled motions. The scaling factor was obtained by successive iterations until the area under the curve of the two spectra was equal for the period range between 0.25 s and 4.0 s. The area under the spectra was obtained by numerical integration using the trapezoidal method between the two period integration bonds. These limits were established by inspecting the period range over which the two spectra are most superposed.

In the selection and scaling processes, the relative velocity spectra of the scaled ground motions were also computed and compared to the design velocity spectrum, S_v, for the site ($S_v = S \times T/2\pi$). For some of the ground motions, the scaling factor was slightly adjusted to achieve a better match between the ground motion and design velocity spectra. Figures 5.3.1 to 5.3.6 present the acceleration and velocity spectra of all scaled ground motions. It is noted that the scaling factor was considered as a criterion in the ground motion selection process as the objective was to obtain the smallest possible scaling factor for the selected records.

Table 5.3.2 Characteristics of the short distance historical earthquakes

No	Event	Magn.	*R* (km)	Station	Dir. (°)	*PHA* (g)	*PHV* (m/s)	S_f (_)
H01	Jan. 17, 1994 Northridge	MW 6.7	44	Castaic, Old Ridge Rd	90	0.568	0.53	**0.8**
H02	Jan. 17, 1994 Northridge	MW 6.7	30	Santa Monica City Hall	360	0.369	0.251	**1.4**
H03	Jan. 17, 1994 Northridge	MW 6.7	34	Los Angeles Baldwin Hills	360	0.167	0.176	**2.1**
H04	Feb. 9, 1971 San Fernando	MW 6.6	31	Castaic, Old Ridge Rd	291	0.268	0.259	**1.6**
H05	Jan. 17, 1994 Northridge	MW 6.7	26	Pacific Palisades-Sunset	280	0.197	0.149	**2.5**

Table 5.3.3 Characteristics of the long distance historical earthquakes

No	Event	Magn.	*R* (km)	Station	Dir. (°)	*PHA* (g)	*PHV* (m/s)	S_f (_)
H06	Apr. 25, 1992 Cape Mendocino	MW 7.0	52	Eureka - Myrtle & West	90	0.178	0.283	**1.5**
H07	Oct. 18, 1989 Loma Prieta	MW 7.0	54	Stanford Univ.	360	0.29	0.28	**1.2**
H08	Oct. 18, 1989 Loma Prieta	MW 7.0	100	Presidio	90	0.2	0.34	**1.4**
H09	Apr. 13, 1949 West.Wash.	MW 7.1	76	Olympia, Test Lab	86	0.28	0.17	**1.6**
H10	June 28, 1992 Landers	MW 7.3	93	Barstow	90	0.135	0.258	**2.2**

Table 5.3.4 Characteristics of the ten artificial earthquakes

No	Event	Magn.	*R* (km)	*PHA* (g)	*PHV* (m/s)	S_f (_)
A01	W60201	MW 6.0	20	0.167	0.199	**2.6**
A02	W60202	MW 6.0	20	0.203	0.338	**2.6**
A03	W65301	MW 6.5	30	0.534	0.566	**1.1**
A04	W65302	MW 6.5	30	0.537	0.613	**1.1**
A05	W65501	MW 6.5	50	0.259	0.283	**1.2**
A06	W65502	MW 6.5	50	0.279	0.309	**1.2**
A07	W72301	MW 7.2	30	0.936	1.32	**0.4**
A08	W72302	MW 7.2	30	0.649	0.841	**0.4**
A09	W72701	MW 7.2	70	0.246	0.297	**1.2**
A10	W72702	MW 7.2	70	0.259	0.239	**1.2**

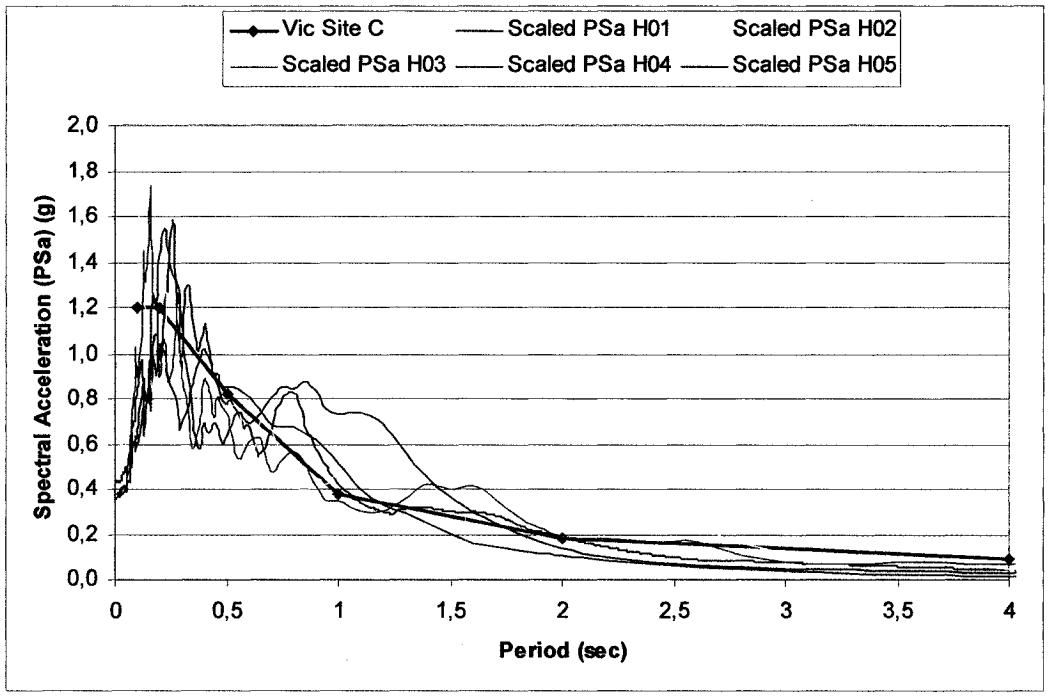

Fig. 5.3.1 Scaled acceleration spectra for historical short distance earthquakes

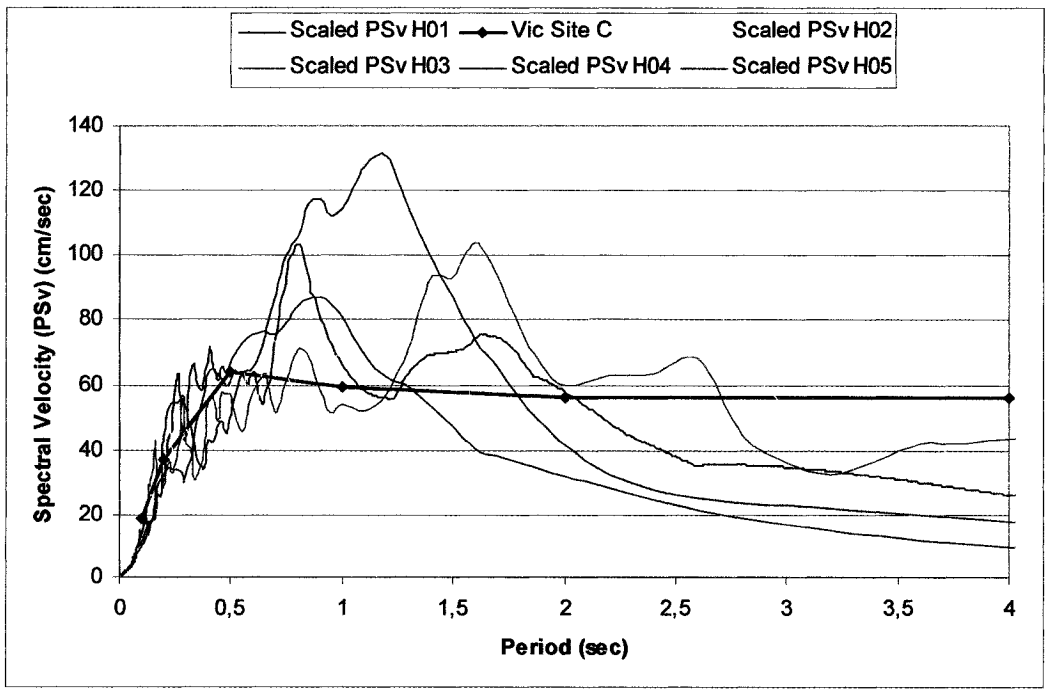

Fig. 5.3.2 Scaled velocity spectra for historical short distance earthquakes

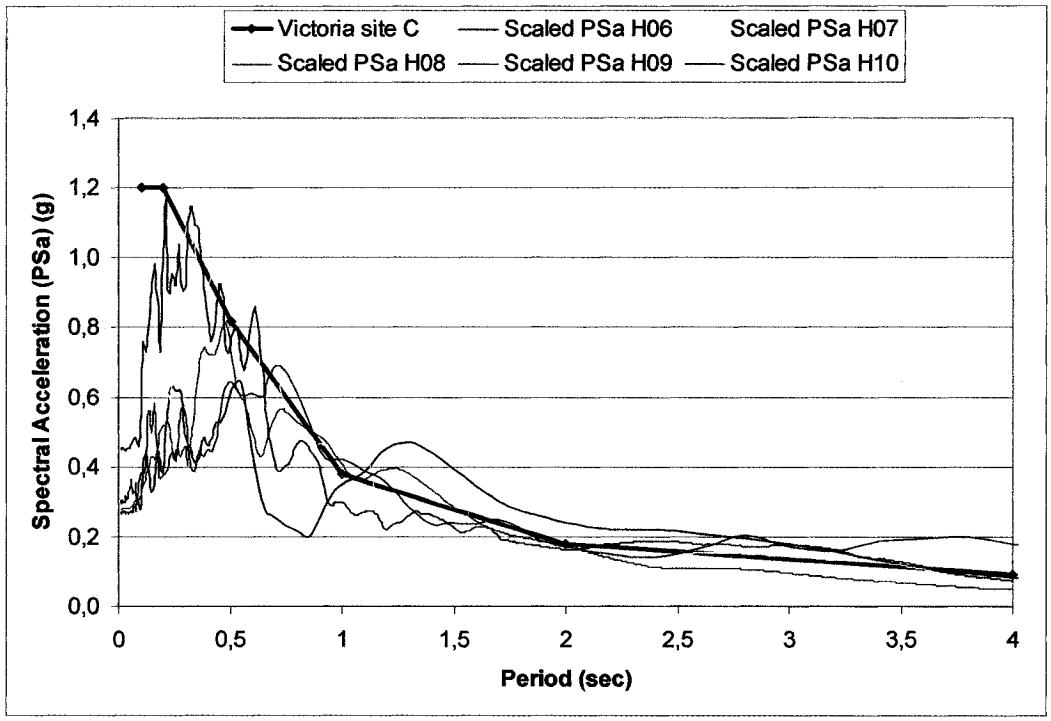

Fig. 5.3.3 Scaled acceleration spectra for historical long distance earthquakes

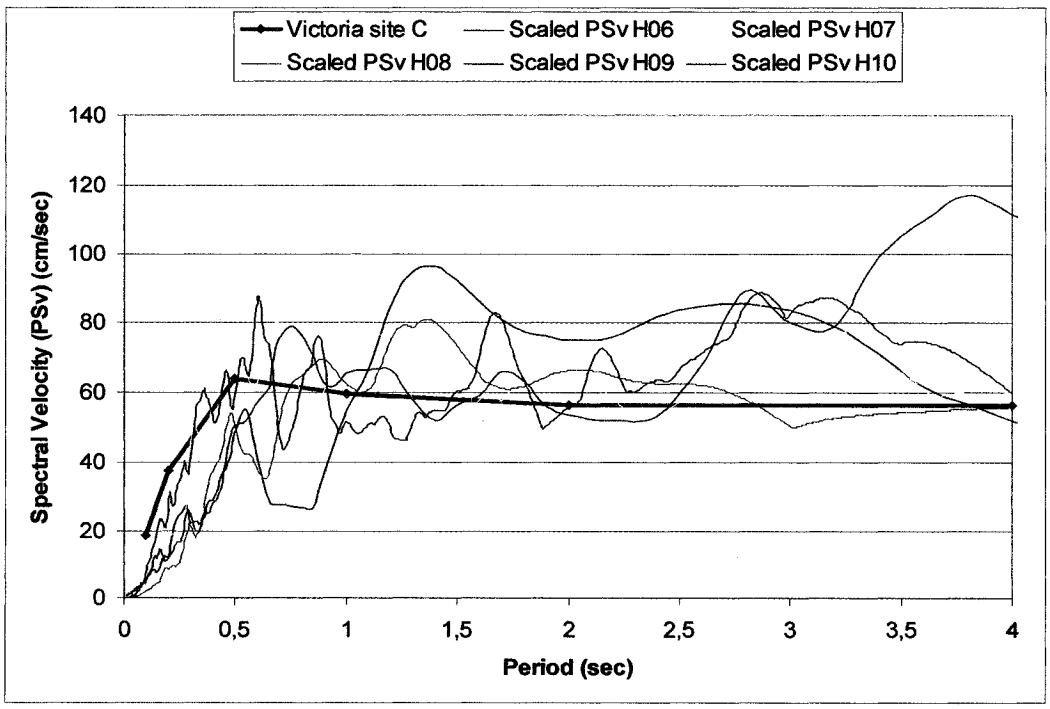

Fig. 5.3.4 Scaled velocity spectra for historical long distance earthquakes

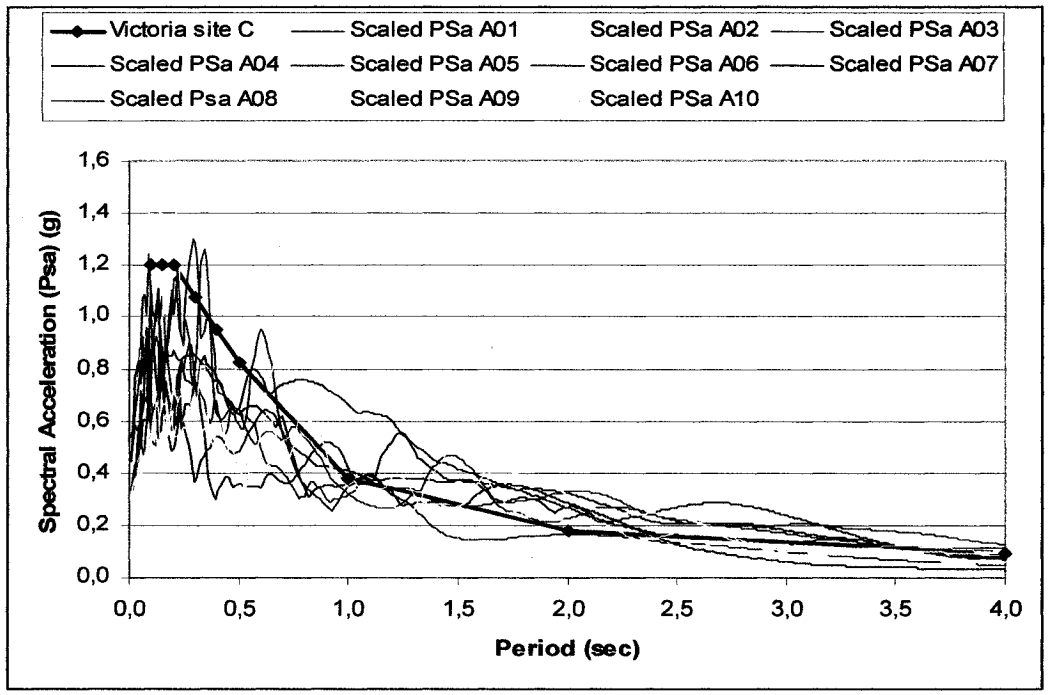

Fig. 5.3.5 Scaled acceleration spectra for artificial earthquakes

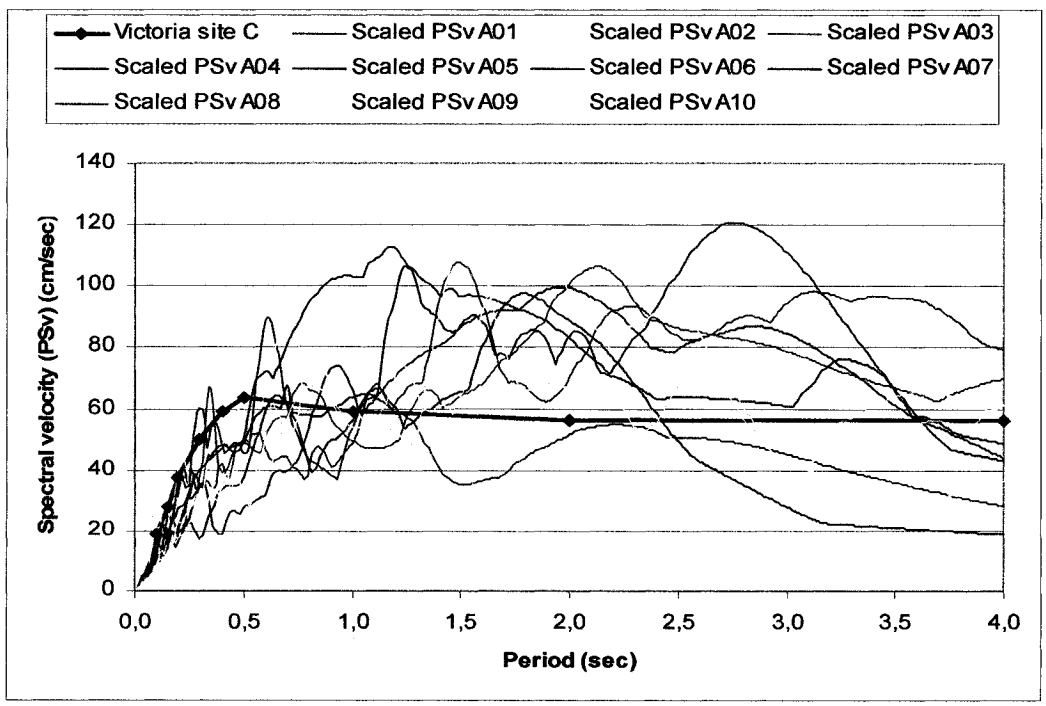

Fig. 5.3.6 Scaled velocity spectra for artificial earthquakes

For consistency with the design, the ground motions were then amplified to account for the building torsional response. The torsion amplification factors are those given in Table 5.1.3.

5.4. Nonlinear Dynamic Analysis

Two series of analysis were carried out in order to fulfill the objectives of this project: 1) dynamic analysis under the twenty selected earthquake ground motions (H01- H10 and A01-A10) scaled as described above, and 2) incremental dynamic analysis using a shortened version of the historical earthquake records (denoted HS01-HS10).

The first series of analyses was used to evaluate the seismic behaviour of the buildings and obtain a numerical database for the development of the test loading protocol, while the second series was used to determine the performance of the buildings against global collapse. The second series of analyses is described in Section 5.5.

The seismic behaviour of the five buildings was evaluated by examining the following peak response parameters:

- the peak story drift angle, Δ/h_s
- the residual story drift angle, Δ_{res}/h_s
- the drift concentration factor, D_{CF}
- the brace ductility demand, μ

The four parameters were evaluated at every floor of the buildings. The peak and the residual story drift angles permit the evaluation of the damage suffered for both the structural and non-structural elements. For each ground motion, the maximum value of these two parameters was kept along the height of the building. Statistics of these values

(the 50th percentile, the 84th percentile, and the maximum values) for each building are presented in Table 5.4.1:

Table 5.4.1 Statistics of the peak and residual storey drift angle values

Number of floors	Peak storey drift angle Δ/h_s (%)			Residual storey drift angle Δ_{res}/h_s (%)		
	50th	**84th**	**Max**	**50th**	**84th**	**Max**
2	1.08	1.49	3.51	0.16	0.35	0.68
4	1.08	1.63	3.41	0.17	0.45	0.82
8	1.40	2.17	4.23	0.92	1.50	3.45
12	1.59	2.48	4.61	0.32	0.60	3.29
16	1.78	2.20	2.70	0.30	0.59	1.08

As can be seen from the median values presented in the table, the peak storey drift angle increases with the building height and even though the maximum storey deformations are observed in the 16-storey building, the 8-storey building experienced the most significant residual storey deformations, almost 3 times larger than those computed for the 12- and 16-storey buildings. NBCC 2005 does not give acceptance criteria for the residual storey drift angle parameter. However, the CSA-S16 maximum erection tolerance is 0.2 %, which means that buildings with residual storey drift angles larger than this value will need post-earthquake structural evaluation to verify if they can provide adequate level of safety with such a permanent deformation. Regarding this residual performance criterion, the 8-, 12- and 16-storey buildings would need post-earthquake structural evaluation.

The median values of the peak story drift angles were considered for comparison of the nonlinear response history procedure with the values recommended by NBCC 2005 and the values predicted by the initial response spectrum analysis. The reason for choosing the median estimates rather than the 84th percentile or maximum values, is that the ASCE 7-05 Standard (ASCE, 2005), the 2003 NEHRP (National Earthquake Hazards Reduction

Program) document (Building Seismic Safety Council, 2003) and FEMA 356 document (Federal Emergency Management Agency) (FEMA 356, 2000) all recommend for the response parameters from nonlinear dynamic analyses that: "if at least seven ground motions are analyzed, the design values of member forces, Q_E, member inelastic deformations, γ, and story drift, Δ, shall be permitted to be taken, respectively, as the average of the scaled Q_{Ei}, γ_i, and Δ_i values determined from the analyses."

NBCC 2005 limits the interstorey deflections to $0.025h_s$ for all the buildings, except for post-disaster buildings and schools. As can be seen from Table 5.4.1 the median values of the peak interstorey drift angles are smaller than NBCC 2005 limits while the maximum values are much larger than those permitted, especially for the 12-storey building.

The values obtained from the response spectrum analysis in the design, the predicted values, are shown in Table 5.4.2. These values are between 1.17 and 1.8 times smaller than the median values obtained from the dynamic analyses:

Table 5.4.2 Design values for peak storey drift angles

Number of floors	**2**	**4**	**8**	**12**	**16**
Peak story drift angle Δ/h_s (%)	0.93	0.87	0.95	1.01	0.99

The drift concentration factor is used to evaluate the structure capacity to mitigate de soft storey mechanism and to mobilize the energy dissipation capacity of the structure (Tremblay et al. 2005). It corresponds to the ratio between the maximum peak story drift angle along the building height and the peak overall roof deformation angle, $D_{CF} = (\Delta / h_s)/(\Delta_{roof} / h_n)$ (Paulay and Priestley, 1992; Kimura et al. 2002), as shown in Fig. 5.4.1.

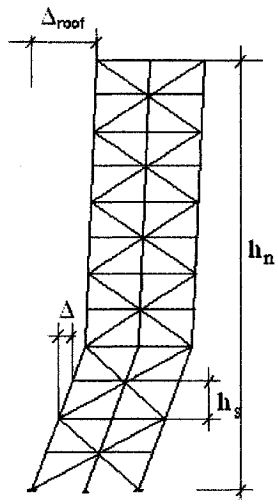

Fig. 5.4.1 Drift concentration factor

A value of D_{CF} close to 1.0 indicates that all floors are equally deformed and that the storey deformations are comparable to the average deformation of the building (there is no soft-story). For braced steel frames, the amount of drift concentration depends on the continuity of the columns and on the flexural stiffness. If the columns are continuous and infinitely rigid, the D_{CF} will be equal is unity.

Expressions to predict the D_{CF} values for multi-storey buildings with continuous columns were proposed in past research. McRae et al (2004) suggested that the D_{CF} in braced steel frames could be calculated with the following formula:

$$DCF = \max\left\{\frac{1+0.64(\mu-1)^{0.5}(1-\beta'/3)\left(\frac{\beta'^{0.319}}{\alpha^{0.223}}\right)N^{0.35}}{\mu^{0.5}(1-\beta'/3)};1+\frac{7\beta N^2}{120\left(\alpha+\frac{\beta N^2}{15}\right)}\right\} \qquad (5.4.1)$$

where N is the number of storeys, α is the column stiffness ratio (the sum of the flexural stiffness of all columns at the first level relative to the bracing bent lateral stiffness at that

level), β is the vertical distribution of the lateral resistance of the seismic force resisting system, μ is the expected global ductility level and β' is the frame strength distribution parameter for frame with discrete number of storeys. That last parameter can be calculated with the formula:

$$\beta' = \left(1 - \frac{1.3}{N}\right)\beta^{(1.25+(0.5/N))} \tag{5.4.2}$$

The values obtained with this model for the buildings studied herein are presented in Table 5.4.3. These values are referred to Ref.1 in the table. A second method, proposed by Miranda (1999), is based on the global ductility level, μ, the number of levels, N, and the governing deformation mode of the structure (shear or flexure). The following formula was used to calculate the drift concentration factor values for the studied buildings:

$$IDR_{\max} = \beta_2 \beta_4 \frac{u_{roof}}{H} \tag{5.4.3}$$

where $\beta_4 = 1 + \frac{\mu}{30} + \frac{N}{200}$. The factor β_2, depends on the deformation mode of the structure and an intermediate value of 1.6 was adopted. The values from this method are referred to as Ref.2 in Table 5.4.3.

For both the above-mentioned methods, the global ductility level, μ, was taken equal to the ductility factor R_d used in design.

The 50th percentile, the 84th percentile, and the maximum values of D_{CF} for each building and all ground motions are compared to the reference values in Table 5.4.3. As can be noticed, the predicted values for the 2-, 4- and 8-storey buildings are very close to the values obtained from the nonlinear dynamic analyses. For the 12- and 16-storey buildings, the predicted D_{CF} values are exceeded.

Table 5.4.3 Drift concentration factors

Number of floors	Drift concentration factor D_{CF}				
	50th	**84th**	**Max**	**Ref.1**	**Ref.2**
2	1.4	1.6	1.6	1.8	1.8
4	1.7	1.9	2.0	1.8	1.8
8	1.9	2.1	2.2	1.8	1.8
12	2.4	2.7	2.9	1.9	1.8
16	2.5	3.0	5.6	2.0	1.8

The brace peak ductility demand, μ, was determined for each floor of each of the five buildings for all the 20 ground motions (H01-H10 and A01-A10). The ductility was computed by dividing the peak axial deformation of the brace by the brace deformation at yield. The latter corresponds to the brace length between the hinge lines in the gusset plates times the expected yield strain of the material (= 0.0019 = 380 MPa/200000MPa). The maximum, 50th percentile and 84th percentile values of the ductility at every building floor are presented in Table 5.4.4.

Table 5.4.4 Brace ductility demand

Number of floors		Max μ	50th percentile μ	84th percentile μ
2	2	2.50	1.33	1.92
	1	11.08	3.09	4.82
4	4	2.77	1.27	2.14
	3	2.47	1.67	2.34
	2	8.84	2.88	4.89
	1	8.58	2.14	3.39
8	8	1.16	0.66	0.77
	7	1.87	0.94	1.63
	6	3.67	2.11	3.15
	5	4.65	2.37	3.59
	4	8.59	2.90	4.73
	3	13.81	2.98	6.27
	2	10.84	3.74	5.78
	1	8.61	2.35	3.90

Table 5.4.4(cont'd) Brace ductility demand

Number of floors		Max μ	50th percentile μ	84th percentile μ
12	12	0.78	0.57	0.63
	11	3.17	1.39	2.28
	10	2.08	1.13	1.63
	9	8.48	3.06	4.05
	8	12.19	3.52	6.12
	7	15.01	4.07	7.40
	6	9.39	3.38	5.19
	5	5.62	1.03	2.10
	4	1.24	0.94	1.07
	3	3.47	2.10	2.50
	2	4.13	1.87	2.91
	1	2.31	1.39	1.82

Table 5.4.4(cont'd) Brace ductility demand

Number of floors		Max μ	50th percentile μ	84th percentile μ
16	16	1.93	0.92	1.43
	15	3.01	1.01	1.93
	14	6.99	3.63	5.38
	13	4.05	0.92	1.66
	12	3.28	0.95	1.5
	11	5.39	1.52	3.36
	10	4.78	1.55	3.19
	9	6.12	1.06	4.08
	8	7.87	1.99	4.10
	7	5.54	1.66	3.50
	6	4.56	1.32	2.51
	5	3.40	1.23	2.12
	4	5.32	1.16	1.85
	3	3.98	1.17	1.82
	2	3.91	1.13	1.49
	1	1.66	1.05	1.39

Figures 5.4.2 to 5.4.6 represent graphically the brace ductility demand. It can be seen that the ductility demand for the 2-, 4- and 8-storey buildings is higher in the lower floors. For the 12-storey building, the demand is more pronounced near the mid-height of the building whereas it is highest at the top of the building for the 16-storey structure. When examining the median values, one can also observe that the maximum ductility demand on the braces is almost the same (around 3.7) for the 8-storey and 16-storey buildings. Their location in the building is however different: near the base (2nd floor) for the 8-storey building and near the top (14th floor) for the 16-storey building. For the 12-storey

building the median ductility demand is a little higher (4.07) and is localised at half of the building height.

For this reason, only the braces that have experienced the highest demand were taken into account when performing the statistical studies for the determination of a test loading protocol: the first and second floor for the 2- and 4-storey buildings, the first 4 floors for the 8-storey building, the 6th, 7th, 8th and 9th floors for the 12-storey building and the 7th, 8th, 9th and 14th floors for the 16-storey building.

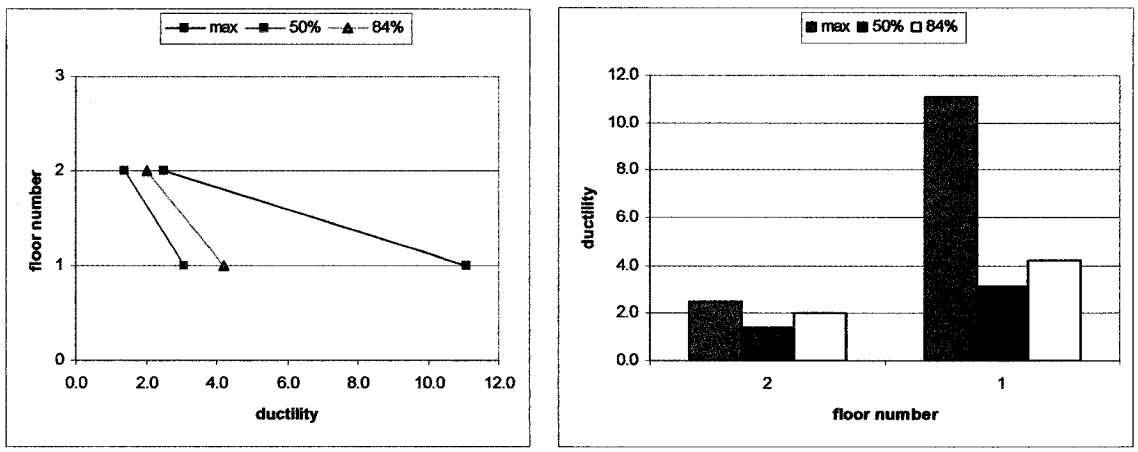

Fig. 5.4.2 Ductility demand in the 2-storey building

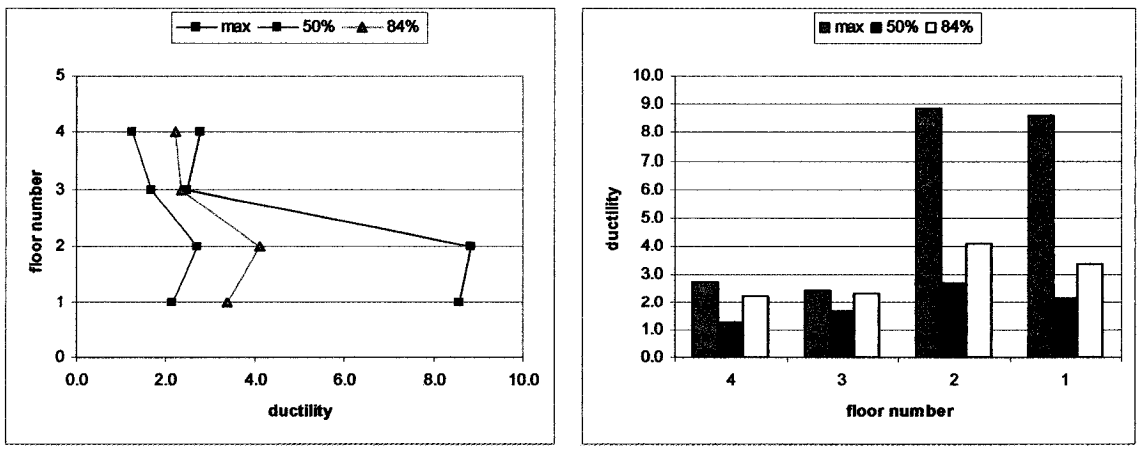

Fig. 5.4.3 Ductility demand in the 4-storey building

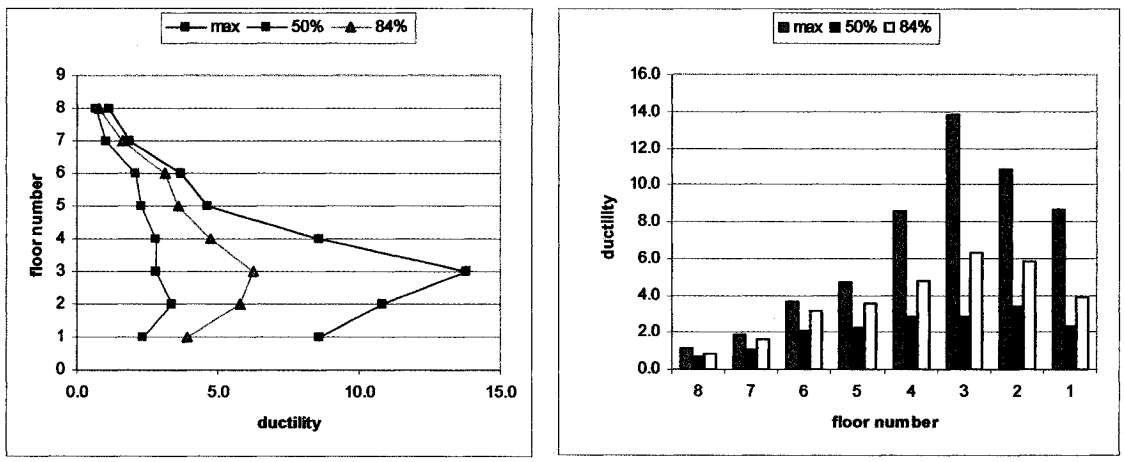

Fig. 5.4.4 Ductility demand in the 8-storey building

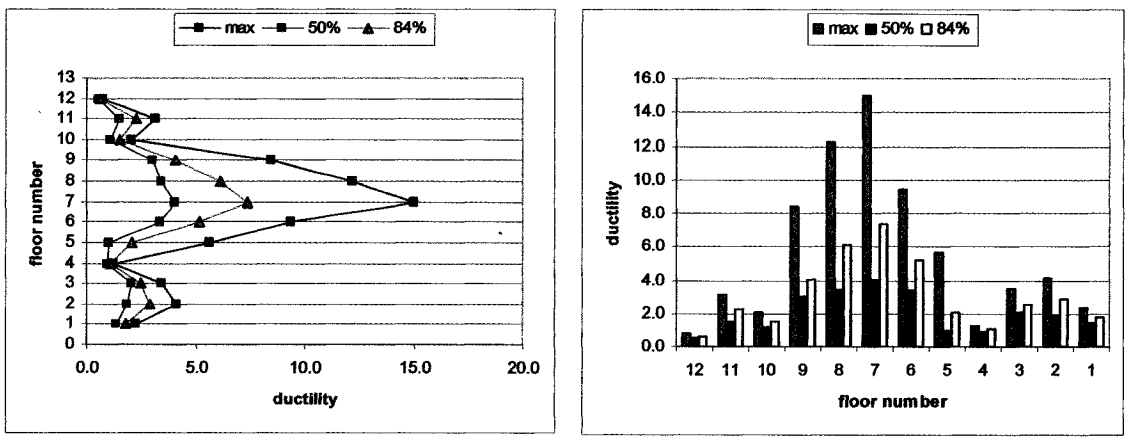

Fig. 5.4.5 Ductility demand in the 12-storey building

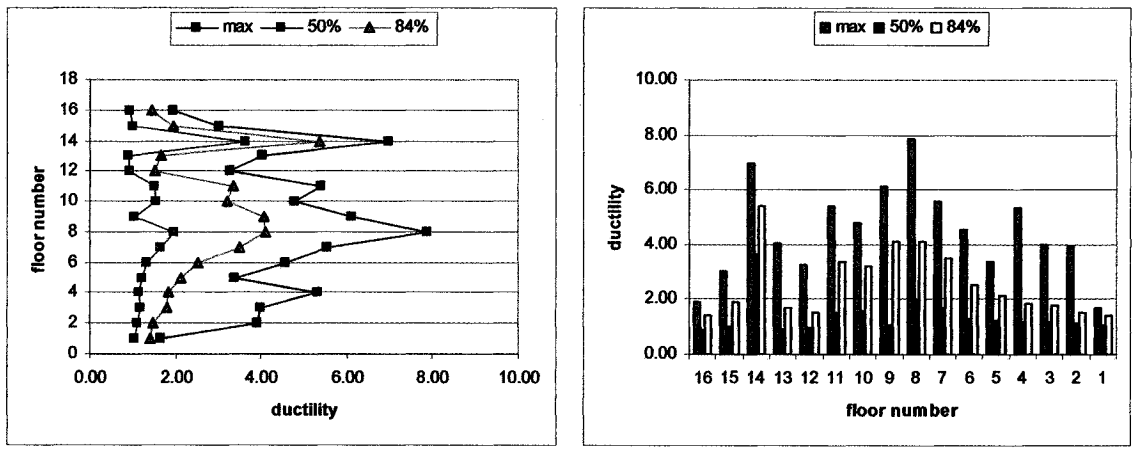

Fig. 5.4.6 Ductility demand in the 16-storey building

The brace ductility demand was thereafter compared to the empirical expression proposed by Tremblay (2002) for the average brace ductility at fracture, μ_f:

$$\mu_f = 2.4 + 8.3\lambda \tag{5.4.4}$$

The ductility μ_f represents the sum of the peak ductility in compression μ_c and in tension μ_t and it is a function of brace slenderness λ. Figure 5.4.7 presents the 50th percentile values of the peak ductility demand for all the braces from all five buildings. It presents also the mean ductility value from the equation 5.4.4 as well as the mean +/- one standard deviation to reflect the scatter in test results. In this figure it is assumed that the braces experienced the same ductility in compression and tension, and hence $\mu_f = 2 \times \mu$. The brace slenderness λ, was calculated with an effective length factor K = 0.75 which represents more closely the designed end-conditions, as was discussed in Section 5.2. It is shown in the figure that the braces generally exhibit satisfactory performance against fracture and that the most critical braces are those with λ in vicinity of 0.75 ($KL/r \approx 55$) used mostly in 2- and 16-storey buildings. Relatively lower demand compared to brace ductility capacity was observed for the stockier braces ($\lambda \approx 0.60$, $KL/r \approx 45$) and on the more slender ones ($\lambda > 0.90$, $KL/r > 45$).

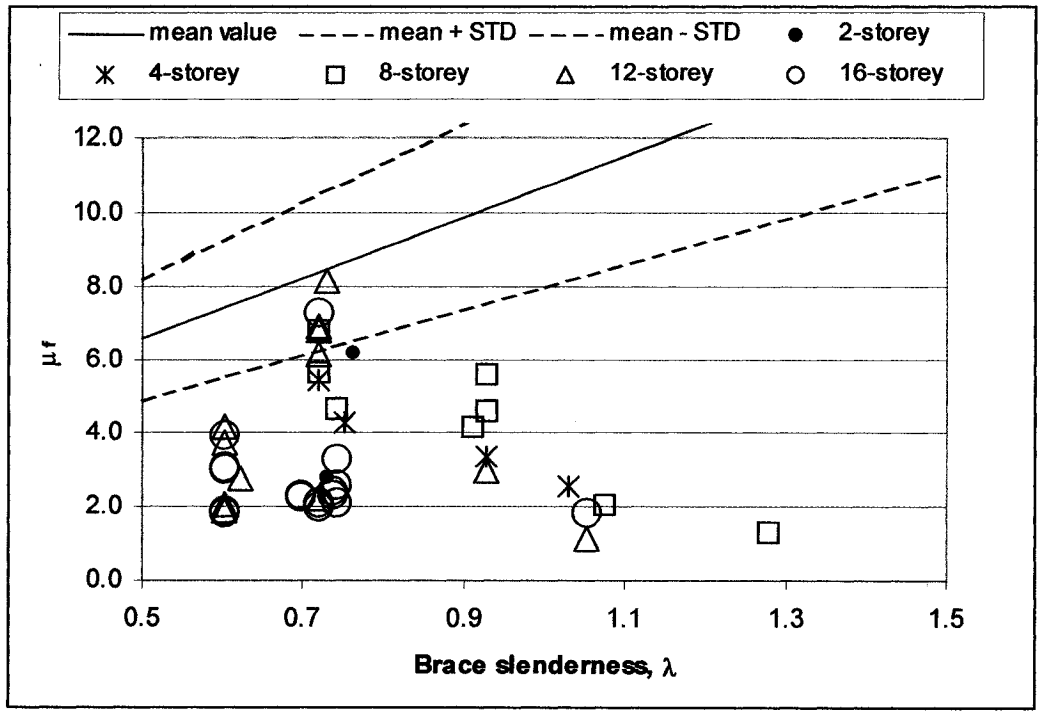

Fig. 5.4.7 Peak ductility demand in braces vs anticipated brace ductility at fracture

5.5. Incremental Dynamic Analysis

5.5.1. Behaviour of the buildings

The buildings with 8, 12 and 16 stories were studied to evaluate their performance against global collapse by instability using the incremental dynamic analysis (IDA) procedure. The IDA is a parametric analysis method that involves subjecting a structural model to ground motions that are scaled to multiple levels of intensity to produce curves of response parameters versus intensity level (Vamvatsikos and Cornell, 2002). This method has been recently adopted by the U.S. Federal Emergency Management Agency (FEMA) as the state of art method to determine the global collapse capacity.

In the procedure, an additional scaling factor, S_{FI} was applied to the ground motions as scaled for matching the design spectrum. The scaling factor S_{FI} increased stepwise in increments of 0.2 until collapse of the structures occurred by dynamic instability. The results of incremental dynamic analyses are generally presented on the form of IDA curves giving the maximum peak storey drift value at any storey obtained for each S_{FI} value. IDA curves are plotted with the S_{FI} factor along the Y-axis, which leads to "load-deformation" type response curves. The IDA procedure is applied individually for each ground motion of an ensemble. If needed, statistics of the storey drift values for all ground motions can be computed at every S_{FI} ordinate, which permits to obtain median or higher percentile IDA curves for the ground motion ensemble.

Dynamic instability is considered to have occurred when the building reached a 10 % interstorey drift at any level over its height, or when the tangent slope of the curve of the ground motion intensity S_{FI} versus the maximum peak interstorey drift reached a value smaller than 20 % of the initial elastic slope of that curve (between 0 and $S_{FI} = 0.2$). This 20% tangent slope approach is proposed in FEMA-350. It means that significant flattening of the curve is an indicator of dynamic instability.

A smaller ground motion ensemble comprising the 10 natural (historical) ground motions described in the Section 5.3 was used for these analyses. In addition, the ground motions were shortened in duration (HS01-HS10 vs H01-H10) such that the energy developed by the reduced time histories was at least 95 % of the total energy produced by the original ground motion. The reason for using fewer and shorter ground motions was the very large number of analyses needed and the computational time required for each of these analyses. For instance, a total of 23 analyses for each ground motion were necessary to achieve dynamic instability for the 8-storey building. For the 12- and 16-storey buildings, this number increased to 38 and 47 analyses, respectively.

The IDA curves for the three buildings studied and their tendencies given by the 50th and 84th percentile for the ensemble of the ground motions are presented in Figures 5.5.1.1 to 5.5.1.3:

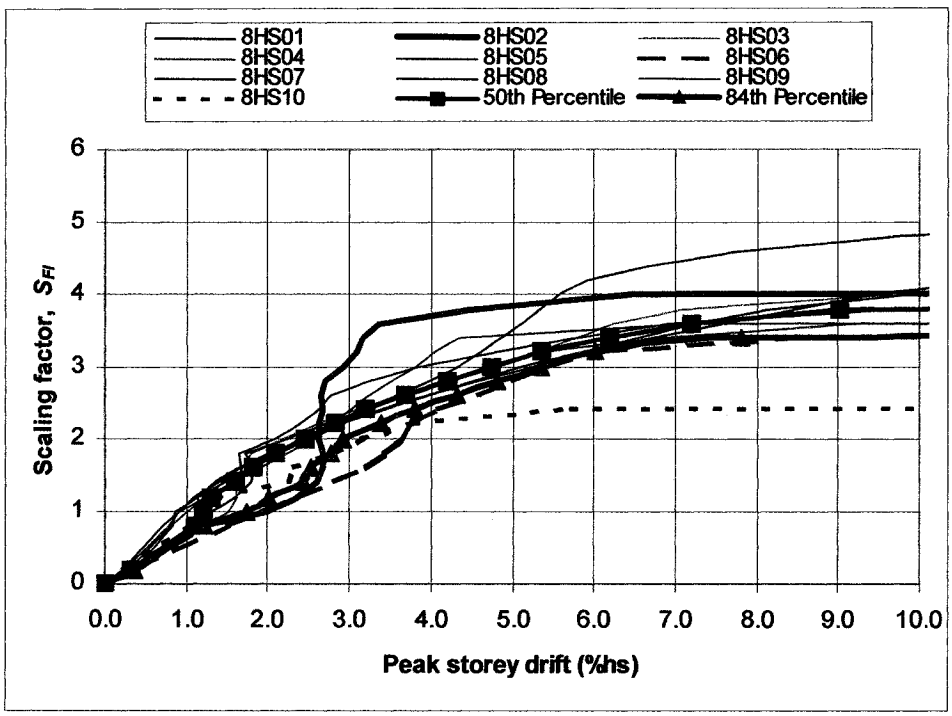

Fig. 5.5.1.1 Incremental dynamic analysis curve for 8-storey building

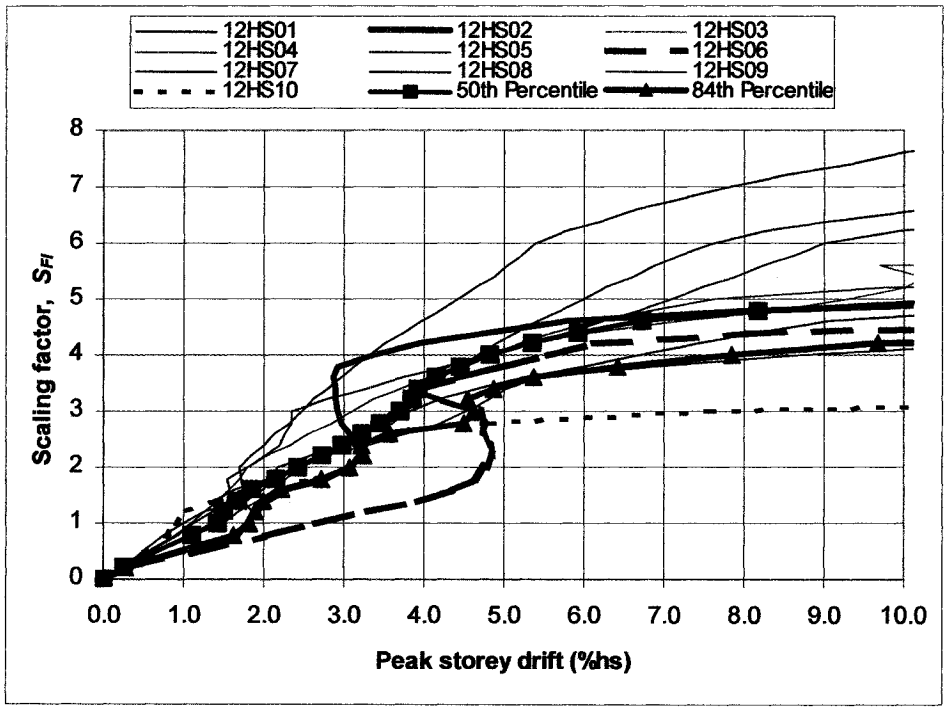

Fig. 5.5.1.2 Incremental dynamic analysis curve for 12-storey building

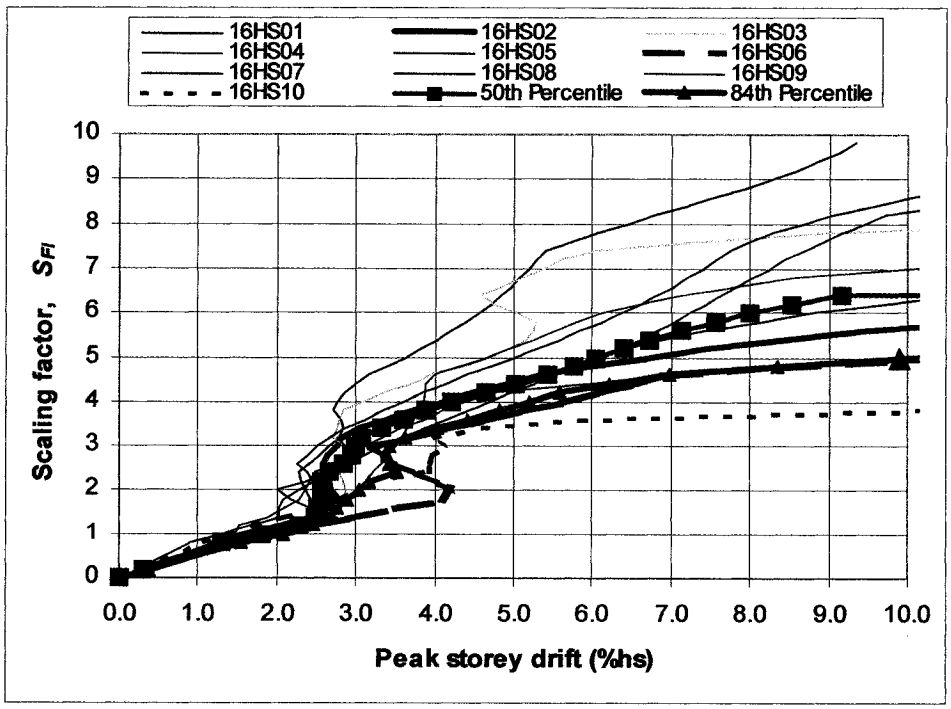

Fig. 5.5.1.3 Incremental dynamic analysis curve for 16-storey building

One can observe that all of the curves exhibit an elastic linear region. This portion ends at $S_{FI} \approx 0.8$ (drift = 1.0% h_s) for the 8-storey building, and at $S_{FI} \approx 1.0$ for the 12-storey and 16-storey buildings. The end of the elastic linear region corresponds to storey drifts of 1.5% h_s and 2.0% h_s respectively for the 12-and 16-storey structures. This region terminates when the first non-linearity appears, which means that the non-linearity appears sooner in the 8-storey building compared to the 12- and 16-storey structures.

Upon increasing S_{FI}, the 8-storey building curves generally exhibit gradual softening response except for the HS01 and HS02 ground motions, for which some hardening response (S-shape) can be observed. For the 12-storey building, more IDA curves present strong hardening: HS01, HS02, HS05 and HS06, while all the curves present severe hardening for the 16-storey building, except for the HS09 and HS10 ground motions. This pronounced hardening behaviour means that the structures experience acceleration of the damage up to a given S_{FI} value beyond which deceleration of the damage occurs such that the accumulation of the damage is stopped and even reversed when increasing further the ground motion amplitudes, pulling the IDA curve in the opposite direction. These results seems to indicate that ground motions HS01 and HS02 were the least damaging among the 10 earthquakes considered and that HS09 and HS10 were the most destructive time histories.

The behaviour of the three buildings studied is compared using the 50th and the 84th percentile IDA curves in Figures 5.5.1.4 and 5.5.1.5.

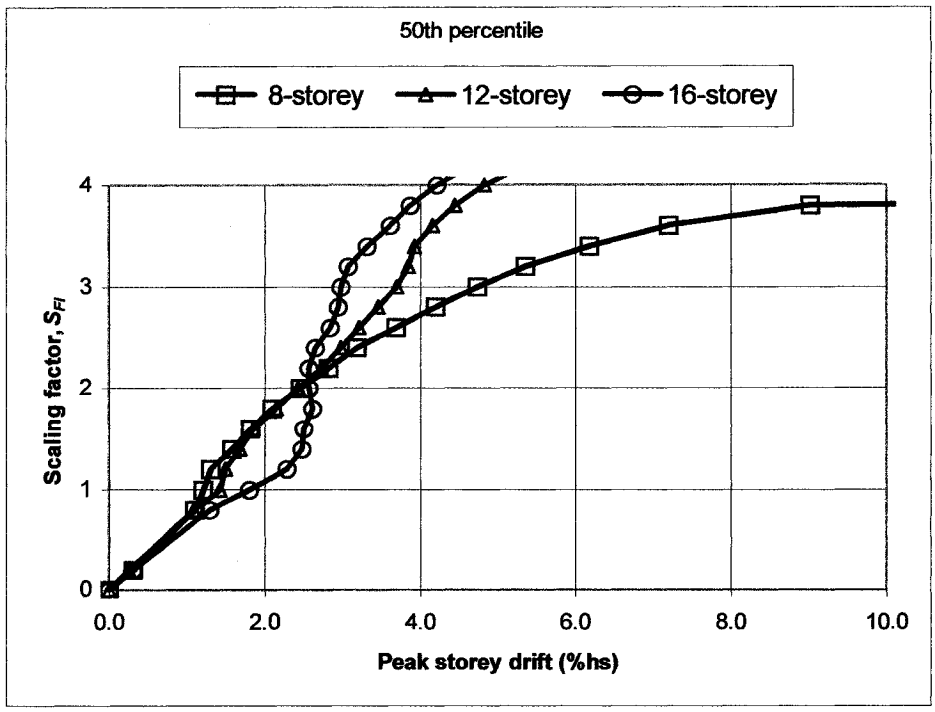

Fig. 5.5.1.4 50th percentile IDA curves for the buildings studied

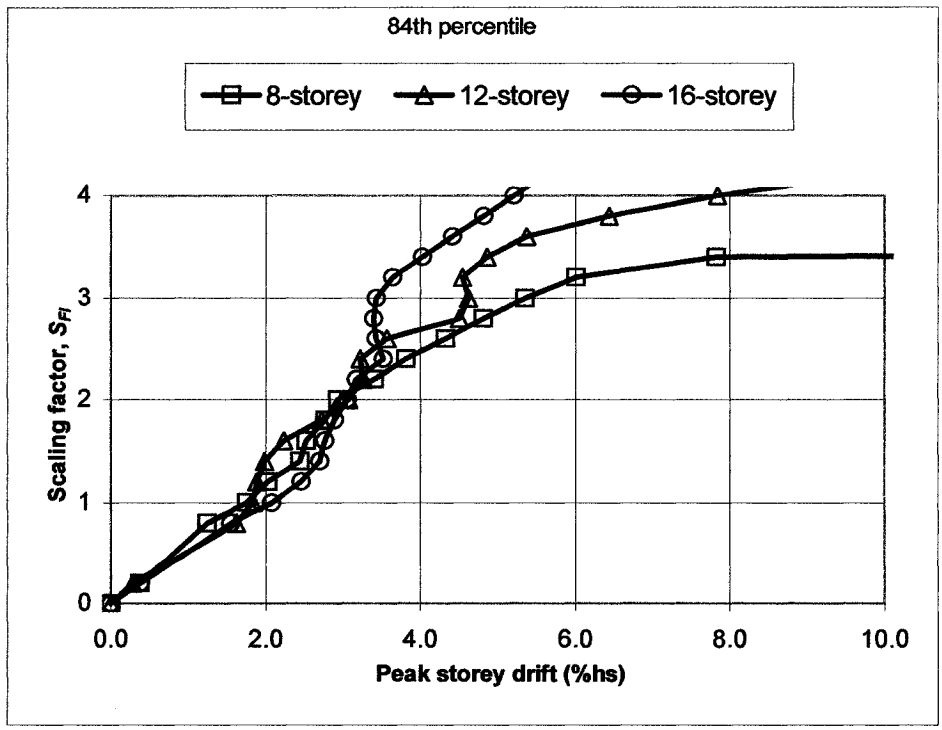

Fig. 5.5.1.5 84th percentile IDA curves for the buildings studied

As shown, the studied buildings exhibit different responses upon increasing ground motion amplitudes up to dynamic instability. The 8-storey building reached instability by gradually flattening of the IDA curve for 8 of the ground motions. The 12-storey and 16-storey buildings exhibited this response for only 5 and 4 ground motions, respectively. They also showed different resistance levels against collapse: the 8-stories buildings collapsed before a scaling factor S_{FI} = 5.0 whereas S_{FI} values up to 8.0 and 10.0 were reached for the 12-storey and 16-storey building, respectively. This can be explained by the more conservative design rules for the 12 and 16-storeys buildings. Both structures were designed for higher design factored seismic forces because of their height. In addition, their period was longer than 2.0 s, which means that the minimum earthquake load determined with S(2.0s) was applied for these two structures.

Another way of studying the behaviour of the buildings is to look at the variation of the peak storey drifts along the height of the buildings when increasing the intensity of a ground motion. As earthquake HS10 was found to be one of the more critical ground motions, the building's behaviour was first examined for this ground motion. Figures 5.5.1.6 to 5.5.1.8 present these responses.

In the 8-storey building, the deflections increased more in the upper levels (6^{th} floor) until S_{FI} reached the value of 1.2. Beyond this amplitude, the deflection at the 6^{th} storey remained nearly constant, whereas the deflection became larger in the bottom levels (2^{nd} and 3^{rd}) to eventually lead to collapse at the 3^{rd} level.

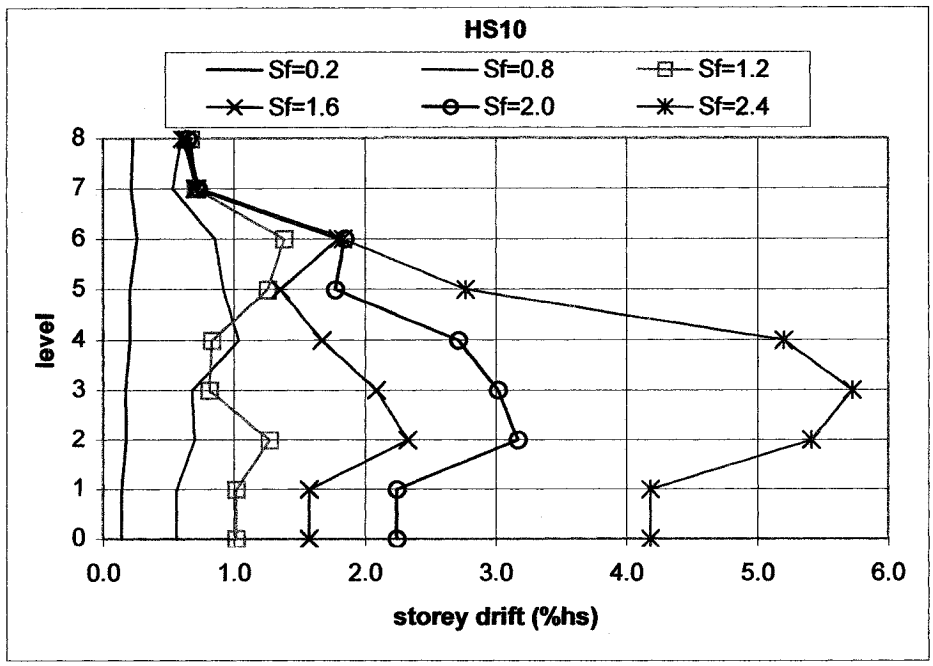

Fig. 5.5.1.6 Peak storey drift under HS10 ground motion for 8-storey building

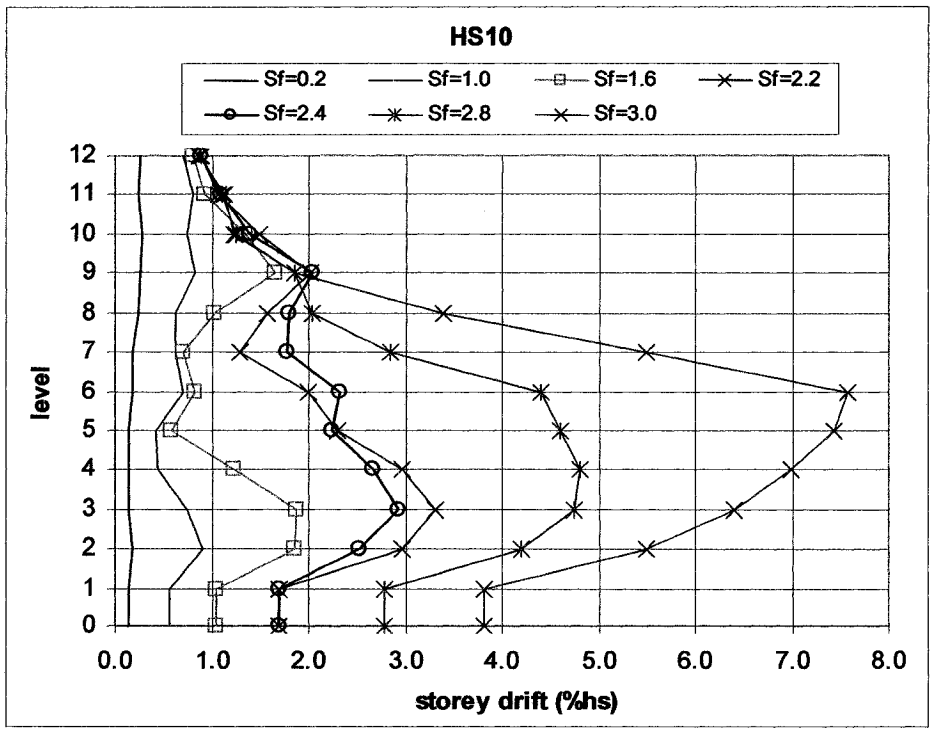

Fig. 5.5.1.7 Peak storey drift under HS10 ground motion for 12-storey building

The 12-storey building has a different behaviour (Fig. 5.5.1.7). Until S_{FI} reaches the value of 1.0, the deflection in the bottom levels (2nd floor) is larger than in the upper levels (9th floor). The deflections in these levels become equal at S_{FI} = 1.6. For higher values of S_{FI} the largest deflection is observed at the 3rd floor, then at the 4th and eventually at the 6th level where collapse finally took place.

The behaviour of the 16-storey building (Fig.5.5.1.8) is similar to that of the 8-storey building at low S_{FI} values, with larger deflections in the upper part of the building (14th floor) up to S_{FI} = 1.8. Under higher ground motion amplitude, the deflections in the bottom part of the building then increased more rapidly with a larger increase at the 5th floor, moving then at the 4th and 3rd floors, then at the 4th floor, with collapse eventually taking place at the 5th floor. One can notice that the deflections in the upper part of the building increased slowly and remained at maximum at the 14th floor for high S_{FI} values.

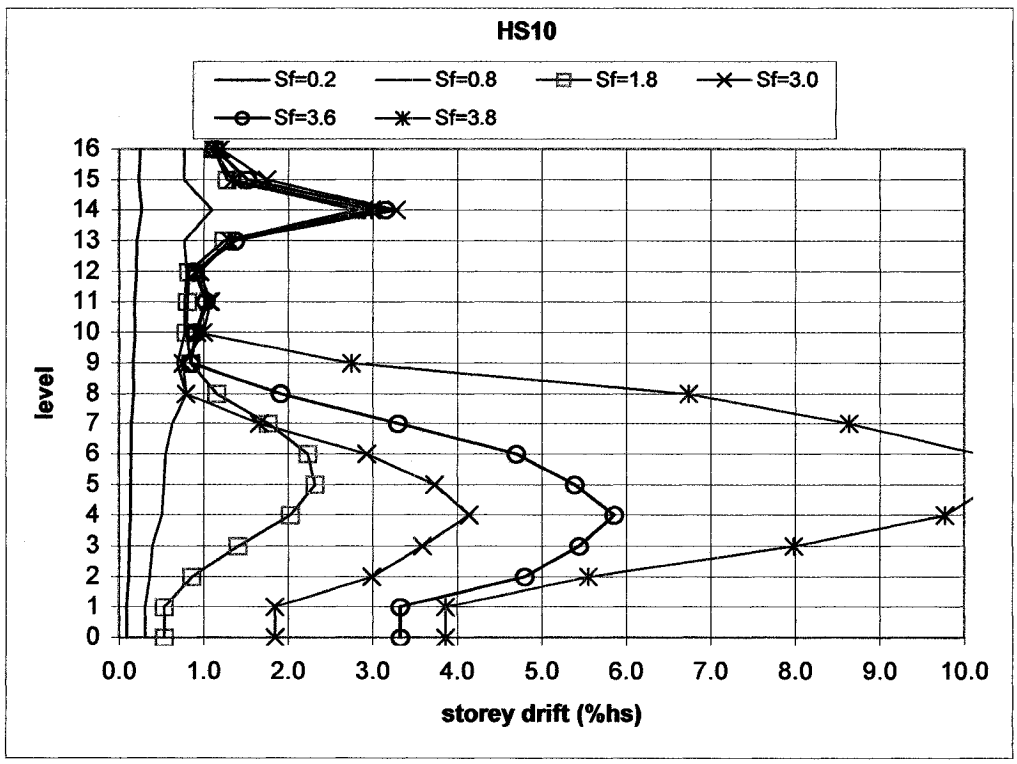

Fig. 5.5.1.8 Peak storey drift under HS10 ground motion for 16-storey building

For this HS10 ground motion it can be concluded that the collapse took place in the lower third of the structure for the 8- and 16-storey buildings and near mid-height of the structure for the 12-storey building.

Two other ground motions (HS02 and HS06) were chosen to study further the variation of the peak storey drift along the height of the buildings when increasing the intensity of the ground motion. These records were selected because they produced strong hardening response (S-shape) for the 12- and 16-storey buildings, as can be observed in Figures 5.5.1.2 and 5.5.1.3. The behaviour of the 8-, 12-, and 16-storey buildings under the HS02 and HS06 ground motions is presented in Figures 5.5.1.9 to 5.5.1.14.

The figures show the behaviour of the buildings up to $S_{FI} = 3.0$ for the 8-storey building and up to $S_{FI} = 4.0$ and 4.6 for the 12- and 16-storey structures, respectively. This permits to observe the hardening of the buildings under these two ground motions. For the 8-storey building and the HS02 ground motion (Fig. 5.5.1.9), this hardening behaviour can be observed in the first three floors, where the storey drift between S_{FI} = 1.4 to 2.6 decreases with an increase of the ground motion intensity. Thereafter, the storey drifts increase when the ground motion intensity is increased. Eventually, the building collapses at the 3rd floor. For the same building, under the HS06 ground motion, (Fig. 5.5.1.10), the hardening behaviour can be observed in the upper floors (5, 6, 7 and 8). Starting at S_{FI} = 2.0, the storey drift values decrease under increasing ground motion intensity. These storey drift values are then maintained until collapse of the building takes place at the 2nd floor at a ground motion intensity $S_{FI} = 3.6$.

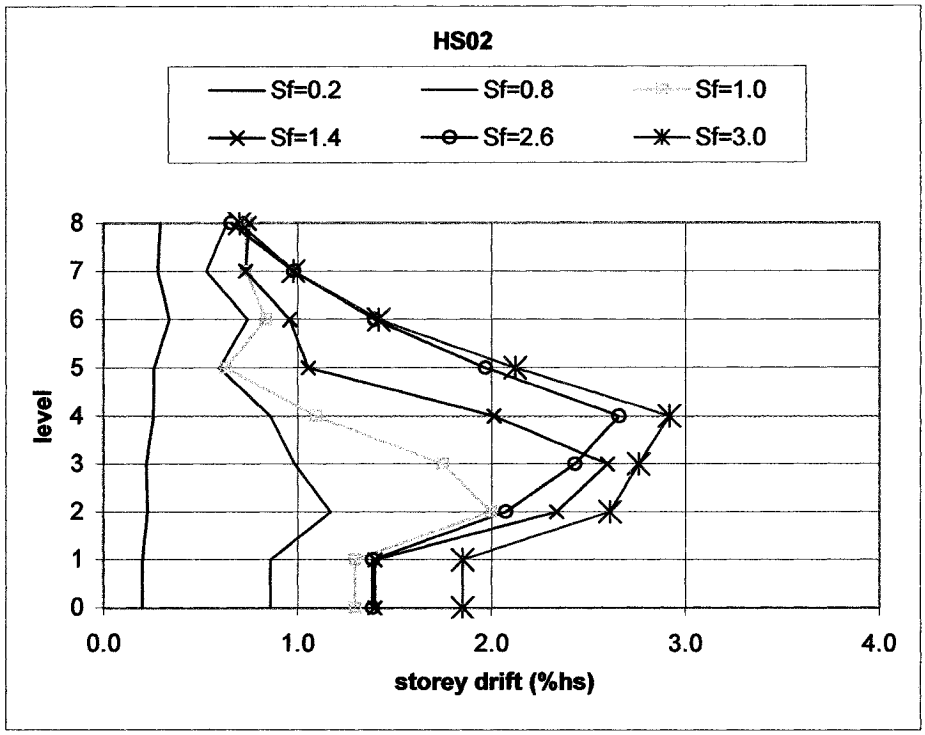

Fig. 5.5.1.9 Peak storey drift under HS02 ground motion for 8-storey building

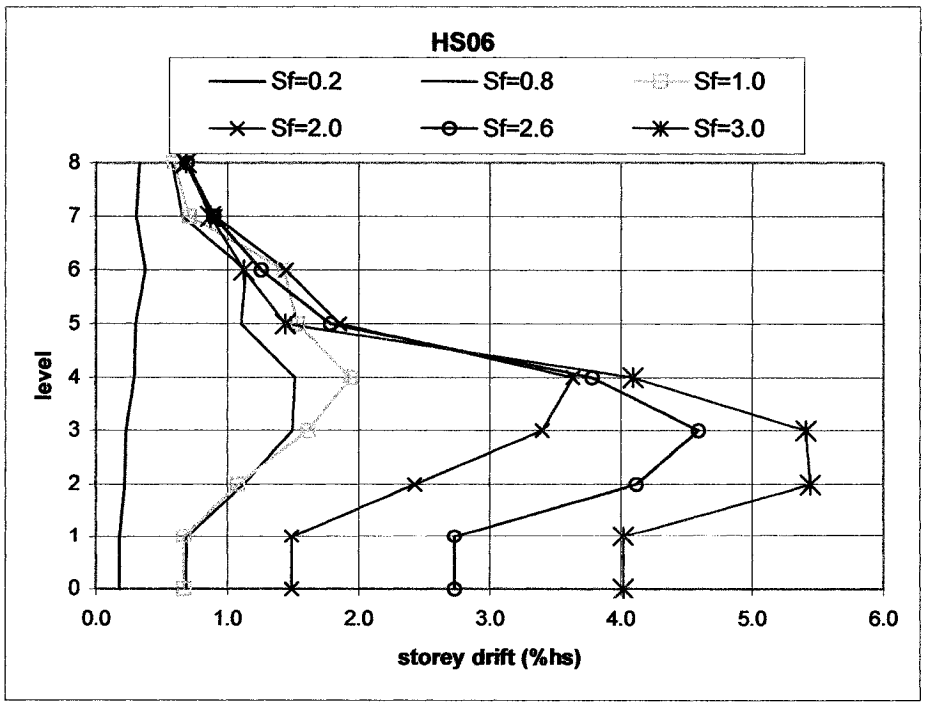

Fig. 5.5.1.10 Peak storey drift under HS06 ground motion for 8-storey building

The 12-storey building exhibited hardening response in the upper floors (7th, 8th and 9th floor) under the HS02 ground motion (Fig. 5.5.1.11) for S_{FI} between 3.0 and 4.0. Beyond this value, the storey drift values remain almost the same in the upper part of the building, whereas they gradually increase in the lower part of the building until collapse of the building occurs at the 4th floor for an S_{FI} coefficient of 5.0. The HS06 ground motion (Fig. 5.5.1.12) induces a similar hardening response of the building in the upper floors (6th, 7th and 8th floor) at S_{FI} of 3.0. The most pronounced hardening response is observed approximately at an S_{FI} value of 4.0, after which the storey drifts increase along the whole building but with a faster rate in the lower floors. Finally, the collapse is observed at the 3rd floor of the building for an S_{FI} coefficient of 4.6.

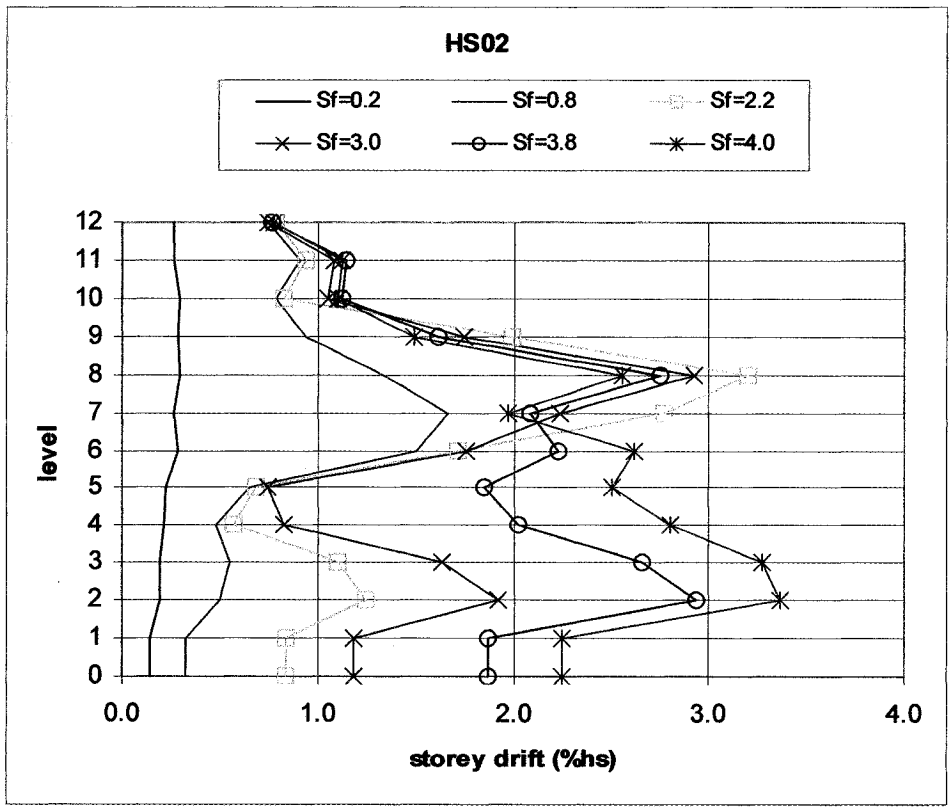

Fig. 5.5.1.11 Peak storey drift under HS02 ground motion for 12-storey building

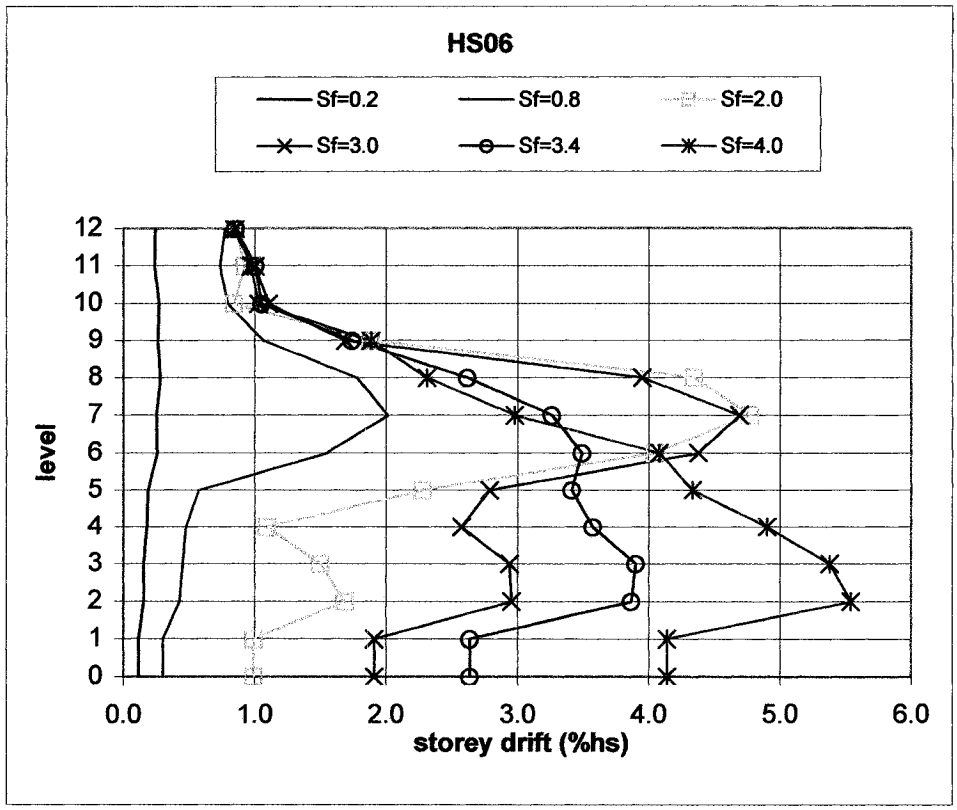

Fig. 5.5.1.12 Peak storey drift under HS06 ground motion for 12-storey building

A hardening response can be very well observed in the upper half of the 16-storey building under the HS02 and HS06 ground motions (Fig. 5.5.1.13 and 5.5.1.14). For the HS02 ground motion, the building experiences hardening between the 9th and 14th floors for S_{FI} values between 1.4 and 4.6. The collapse of the building took place at the 4th floor at an S_{FI} value of 5.8. Under the HS06 ground motion, the 16-storey building experiences hardening over more than half of the building - from the 7th floor up to the top - for values of S_{FI} between 2.0 and 4.0. The building eventually collapsed at an S_{FI} value of 5.0 at the 4th floor.

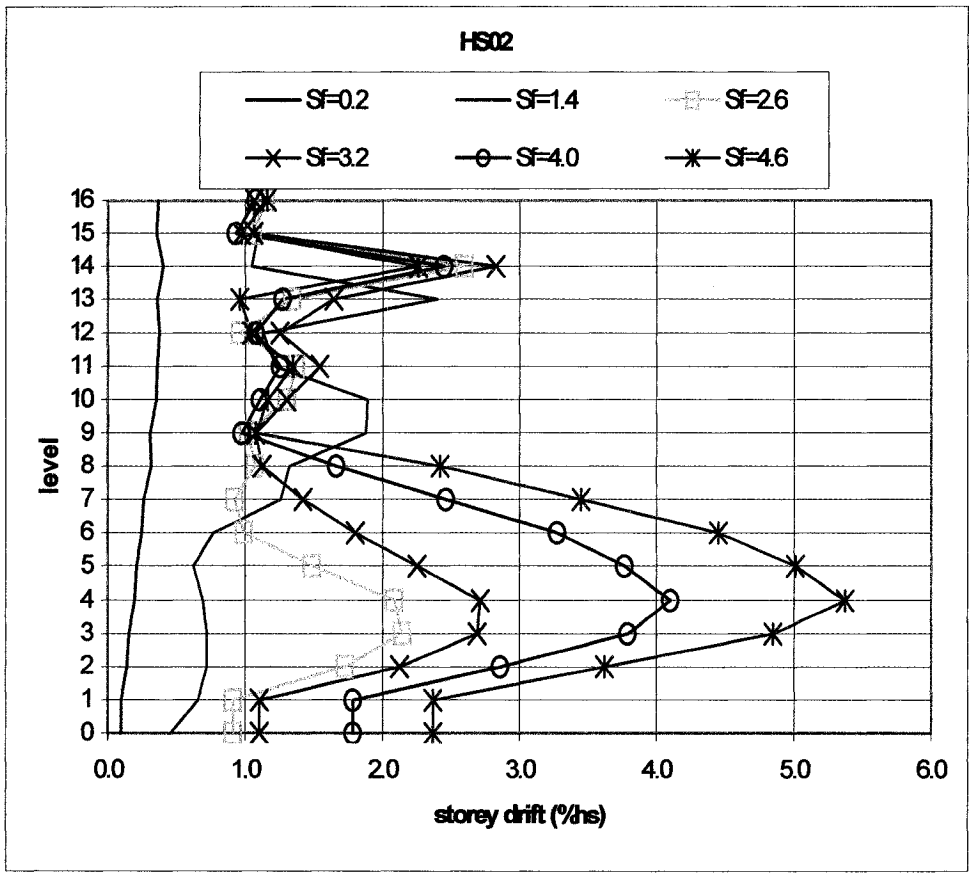

Fig. 5.5.1.13 Peak storey drift under HS02 ground motion for 16-storey building

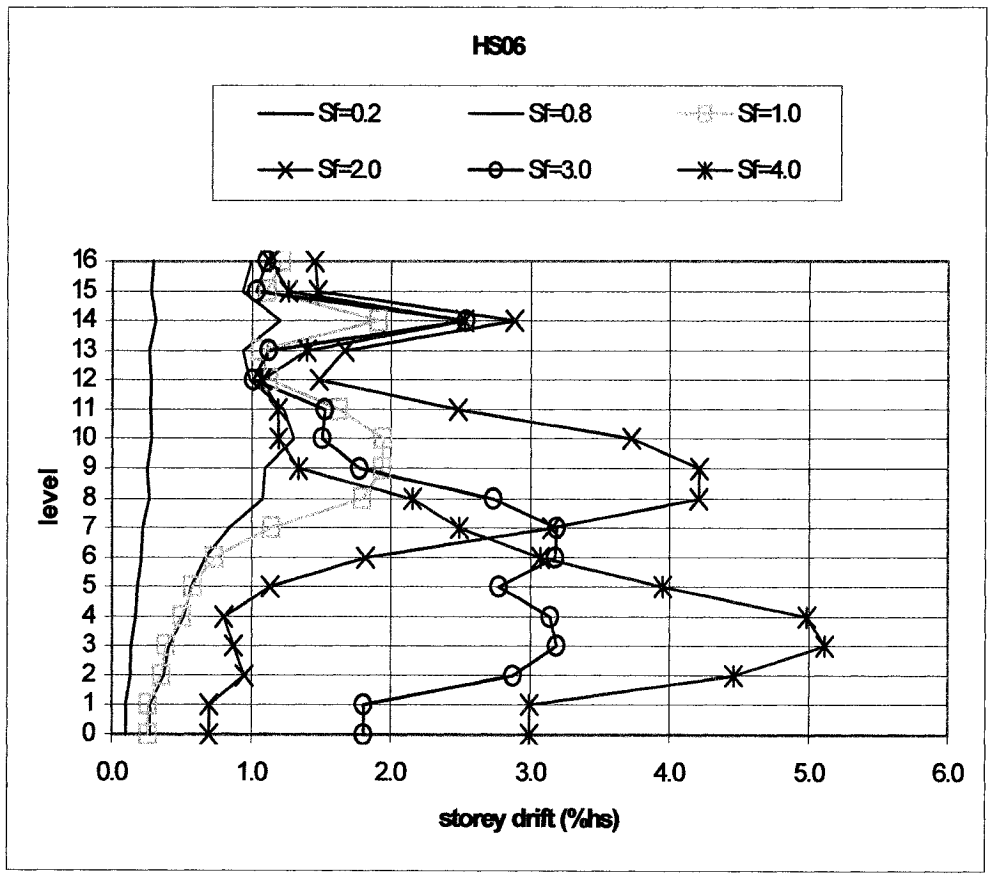

Fig. 5.5.1.14 Peak storey drift under HS06 ground motion for 16-storey building

The difference between the behaviour of the buildings under the ground motions presented herein could be seen from the beginning on the IDA curves in Fig. 5.5.1.1 to 5.5.1.3; the more pronounced S-shaped is the IDA curve, the more hardening response experienced by the building. This hardening behaviour could be explained by the fact that once inelastic response initiates in a part of a building, it is possible that the dynamic behaviour of the building is modified and the member forces gradually increase in another part of the building when S_{FI} is increased. This behaviour is more pronounced in the taller buildings because there are more floors and hence offer more chances to this behaviour to occur.

The hardening response has positive consequences on the structure behaviour; the structure becomes stiffer because of the redistribution of the inelastic deformations over the building height for various S_{FI} values.

5.5.2. Confidence level against global collapse

In order to obtain more conclusive remarks on the seismic performance of concentrically braced steel frames designed with the new provisions of the CAN/CSA-S16-01 Standard and the National Building Code of Canada 2005, the confidence study against global collapse described in FEMA-350 document for steel moment resisting frames was adapted to the braced steel frames as proposed by Tremblay and Poncet (2005).

The parameters identified in the FEMA procedure for determining the level of confidence in a building's ability of meeting the desired design objectives are the interstorey drift, the column axial load and the column splice tension. These parameters should be evaluated independently and the controlling parameter is the one that results in the calculations of the lowest confidence for building performance. In this project, the confidence study for the braced steel framed buildings was done only using the interstorey drift parameter. It must also be noted that the results only represent estimates as the FEMA procedure was developed for steel moment resisting frames and may not be directly applicable to braced steel frames.

Following this method, the confidence level is determined through the confidence index parameter, λ, which is an evaluation of the factored demand to capacity ratio, given by:

$$\lambda = \frac{\gamma\gamma_a D}{\phi C} \qquad (5.5.2.1)$$

where D is the interstorey drift demand on the structure calculated from structural analysis and C is the capacity of the structure against global instability based on the

interstorey drift demand. In this study, D is the median estimate of the maximum interstorey drift at S_{FI} = 1.0 and C is the median estimate of the interstorey drift at collapse. The other parameters are defined as follows:

γ is the demand variability factor that accounts for the different responses exhibited by a structure under different ground motion records. It is calculated using the relation:

$$\gamma = e^{\frac{k}{2b}\beta_{DR}^2} \tag{5.5.2.2}$$

where k is the logarithmic slope of the hazard curve

b is a coefficient that is normally = 1.0 and represents the increase in the demand as a function of the hazard, and

β_{DR} is the standard deviation of the natural logarithms of the demand parameters i.e., the interstorey drift in this project;

γ_a is an analysis uncertainty factor that takes the values 1.06 for 8- and 12-storey buildings (mid-rise structures) and 1.10 for the 16-storey building (high-rise structures). These values are proposed in FEMA 350 for steel moment resisting frame buildings;

ϕ is a resistance factor, determined using the formula:

$$\phi = \phi_U \phi_R = e^{-\frac{k}{2b}\beta_U^2}\phi_R \tag{5.5.2.3}$$

where ϕ_R is the global resistance factor due to randomness in the global collapse capacity and is given by the equation:

$$\phi_R = e^{-\frac{k}{2b}\beta^2} \tag{5.5.2.4}$$

β_U is the logarithmic standard deviation related to uncertainty in analytical prediction, with values of 0.2 for mid-rise structures (4 to 12 storeys) and 0.25 for high-rise structures (> 12 storeys);

and β is the standard deviation of the natural logarithms of the test data.

The slope of the hazard curve, denoted k, was calculated with the formula given in FEMA-350 (5.5.2.5) except that the spectral response accelerations at 1.0 s, as proposed in FEMA were replaced by the spectral response accelerations at 2.0 sec because the periods of the buildings studied are closer to 2.0 s. Hence, k was obtained from:

$$k = \frac{\ln\left(\frac{H_{S2(10/50)}}{H_{S2(2/50)}}\right)}{\ln\left(\frac{S_{2(2/50)}}{S_{2(10/50)}}\right)} = \frac{1.65}{\ln\left(\frac{S_{2(2/50)}}{S_{2(10/50)}}\right)} \qquad (5.5.2.5)$$

where $S_{2(10/50)}$ and $S_{2(2/50)}$ are the spectral amplitudes at T = 2.0 s for 10% in 50 years and 2% in 50 years hazard levels, respectively. These two values were obtained from Adams and Halchuk (2003): $S_{2(10/50)}$ = 0.095 g and $S_{2(2/50)}$ = 0.18 g. The parameters $H_{S2(10/50)}$ and $H_{S2(2/50)}$ respectively correspond to the probabilities of exceedance of 10% in 50 years ($H_{S2(10/50)}$ = 0.0021) and 2% in 50 years ($H_{S2(2/50)}$ = 0.0004). Using these values k = 2.4.

Once λ is determined, the confidence level can be established using the following equation:

$$\lambda = e^{-\beta_{UT}\left(K_X - \frac{k}{2b}\beta_{UT}\right)} \qquad (5.5.2.6)$$

where: K_X is the standard Gaussian variate associated with probability x of not being exceeded as a function of number of standard deviations above or below the mean found in standard probability tables,

β_{UT} was considered equal to 0.4 for the 8- and 12-storey buildings, and 0.5 for the 16-storey building, as recommended by FEMA-350 for special moment resisting steel frames,

and the others parameters were defined earlier.

The values obtained for all of the above coefficients and for the resulting confidence levels for the studied buildings are presented in Table 5.5.2.1. FEMA-350 recommends values for the parameters to be used in the calculation of the confidence level for special moment resisting frames. These values are presented in Table 5.5.2.2, including the minimum accepted level of confidence against collapse. Table 5.5.2.1 shows that braced steel frames designed in accordance with the new provisions of CSA-S16S1-05 and NBCC2005 have a very high level of confidence against global collapse and fulfill the minimum recommended confidence level value.

Table 5.5.2.1 Confidence level for collapse prevention

Coefficient	Number of floors		
	8	12	16
C (% h_s)	7.874	9.884	10.000
D (% h_s)	1.213	1.425	1.806
b	1.0	1.0	1.0
k	2.4	2.4	2.4
β	0.209	0.243	0.221
β_U	0.2	0.2	0.25
β_{UT}	0.38	0.475	0.475
β_{DR}	0.303	0.329	0.194
ϕ_R	0.949	0.932	0.943
ϕ_U	0.953	0.953	0.928
ϕ	0.905	0.888	0.875
γ	1.117	1.139	1.046
γ_a	1.06	1.06	1.10
λ	0.200	0.198	0.229
K_X	4.685	3.976	3.673
Confidence level	**99.99%**	**99.99%**	**99.99%**

When comparing the two tables, it is noted that the values obtained in this study for the confidence level parameters for concentrically braced frames are close to the values recommended by FEMA-350 for steel moment-resisting frames (γ for 8 and 12 floors and γ_a for 8 floors). For some of the values, the tendency is the same as that given by FEMA-350 (values decreasing when increasing the number of floors, as is the case for ϕ), whereas others have opposite trends (values of γ and γ_a increase when increasing the number of floors).

Table 5.5.2.2 FEMA-350 Recommended values of confidence level for collapse prevention

Coefficient	Number of floors	
	Mid-rise structures 4-12 stories	High-rise structures greater than 12 stories
β_{UT}	0.38	0.475
β_U	0.2	0.25
ϕ	0.85	0.75
γ	1.2	1.5
γ_a	1.06	1.10
Confidence level	**> 90%**	**>90%**

5.6. Database for the development of a test loading protocol

5.6.1. Parameters

From the loading protocols developed in the past and described in detail in Section 2.4, several conclusions were made in order to elaborate a numerical database to be used for the development of a loading protocol for the seismic testing of bracing members used in concentrically braced steel frames.

- The parameters considered in the development of the loading protocols were:
  - the peak ductility: $\mu = \delta_{max} / \delta_y$;
  - the number of small deformation excursions with amplitude between 0.5 δ_y and 1.0 δ_y, N_t 0.5 δ_y;
  - the number of small deformation excursions with amplitude between 1.0 δ_y and 1.5 δ_y, N_t 1.0 δ_y;
  - the number of small deformation excursions with amplitude between 1.5 δ_y and 2.0 δ_y, N_t 1.5 δ_y;
  - ...
  - the number of small deformation excursions with amplitude greater than 5.0 δ_y, N_t 5.0 δ_y;
  - the largest deformation range experienced during the seismic response, Range 1;
  - the second largest deformation range experienced during the seismic response, Range 2;
  - ...
  - the fifth largest deformation range experienced during the seismic response, Range 5;
- The demand parameters were derived for all the buildings studied (2-, 4-, 8-, 12- and 16-storeys) and all the 20 ground motions selected.

In these calculations, δ_y is the brace deformation at yield, as defined in Section 5.4 for the calculation of the brace ductility demand. The deformation ranges Range 1 to Range 5 are expressed in terms of brace ductility (δ/δ_y). The number and amplitude of the deformation ranges were obtained from the time histories of brace axial deformations modified with the simplified rainflow counting method proposed by Uriz (Uriz, 2005).

5.6.2. Statistical studies

Regarding the statistical studies, the conclusions made from studying the loading protocols developed in the past were:

- The statistical evaluation of the demand parameters was made for the braces with the highest demand: the first and second floor for the 2- and 4-storey buildings, the first 4 floors for the 8-storey building, the 6th, 7th, 8th and 9th floors for the 12-storey building and the 7th, 8th, 9th and 14th floors for the 16-storey building as was shown in Section 5.4.
- The 50th percentile, the 84th percentile and the maximum estimates of the demand parameters were determined for each brace for the entire ensemble of 10 historical ground motions and 10 artificial ground motions.

The computed values are presented in Tables 5.6.2.1 to 5.6.2.3. Tables 5.6.2.4 to 5.6.2.6 present the average values of the three demand estimates for all braces in each building.

Past loading protocols were developed using different values for statistical estimates: median, 84th percentile and 90th percentile. In this project it was decided to provide the median, the 84th percentile and the maximum values such that the variability in the demand is well characterized. As can be seen from the tables below, there are significant differences between the three estimates. For instance, the 50th percentile, 84th percentile and the maximum ductility demand reach 4.1, 7.4, and 15.0, respectively. There are also

large variations within the same ensemble or between the different building heights. For example, regarding the 50th percentile demand estimates in Table 5.6.2.4, the number of small deformation excursions decreases with an increase of the number of floors of the buildings until a value of δ_y of 2.0. The same tendency is observed for the 84th percentile demand estimates but only until 1.0 δ_y, whereas for the maximum demand estimates is not applicable. On the other hand, the 84th percentile and the maximum demand estimates give more information regarding the deformation excursions with amplitudes larger than 3.0 δ_y. These variations will need to be accounted for when developing the test loading protocol.

Table 5.6.2.1 50^{th} percentile values of the demand parameters for all 20 ground motions

	2 floors		4 floors		8 floors				12 floors				16 floors			
	1st	2nd	1st	2nd	1st	2nd	3rd	4th	6th	7th	8th	9th	7th	8th	9th	14th
δ/δy max =	3.1	1.3	2.1	2.9	2.3	3.4	2.8	2.8	3.4	4.1	3.4	3.1	1.7	2.0	1.1	3.6
Nt 0.5 δy =	20	25	19	18	16	11	11	10	10	8	11	14	9	11	8	12
Nt 1.0 δy =	11	8	8	7	6	7	5	4	5	3	5	6	4	5	3	6
Nt 1.5 δy =	5	3	3	4	3	3	3	2	2	2	2	1	1	2	1	3
Nt 2.0 δy =	2	1	1	2	2	1	1	1	1	1	1	1	0	0	0	2
Nt 2.5 δy =	1	0	0	1	1	1	0	1	1	1	1	1	0	0	0	1
Nt 3.0 δy =	1	0	1	0	0	1	1	1	0	1	0	0	0	0	0	1
Nt 3.5 δy =	1	0	0	0	0	0	0	0	0	0	0	0	0	0	0	0
Nt 4.0 δy =	0	0	0	1	0	0	0	0	0	0	0	0	0	0	0	0
Nt 4.5 δy =	0	0	0	0	0	0	1	0	0	0	0	0	0	0	0	1
Nt 5.0 δy =	0	0	0	0	0	0	0	0	1	0	1	0	0	0	0	0
Range 1	4.8	2.4	3.5	4.3	4.1	4.9	5.1	4.1	5.4	4.9	5.1	4.1	2.6	3.2	1.8	6.0
Range 2	2.8	1.9	2.4	2.7	2.4	3.7	2.5	2.1	3.7	2.5	2.6	2.3	2.0	2.2	1.5	4.0
Range 3	1.6	1.3	1.4	1.5	1.1	1.2	1.0	1.0	1.7	1.1	1.2	1.2	1.1	1.2	0.8	1.4
Range 4	1.2	0.9	1.0	0.9	0.5	0.6	0.4	0.5	0.5	0.4	0.4	0.5	0.6	0.7	0.4	0.8
Range 5	1.1	0.9	0.8	0.6	0.4	0.6	0.3	0.3	0.2	0.1	0.2	0.2	0.3	0.3	0.1	0.5

Table 5.6.2.2 84^{th} percentile values of the demand parameters for all 20 ground motions

	2 floors		4 floors		8 floors				12 floors				16 floors			
	1st	2nd	1st	2nd	1st	2nd	3rd	4th	6th	7th	8th	9th	7th	8th	9th	14th
δ/δy max =	4.2	2.0	3.4	4.4	3.9	5.8	6.3	4.7	5.2	7.4	6.1	4.0	3.5	4.1	4.1	5.4
Nt 0.5 δy =	36	35	29	26	24	24	23	24	23	15	15	22	20	24	17	20
Nt 1.0 δy =	17	12	14	13	14	12	12	6	8	7	9	9	7	6	4	8
Nt 1.5 δy =	8	5	7	7	6	5	4	3	4	4	5	3	3	3	3	5
Nt 2.0 δy =	5	2	5	5	5	3	3	2	2	2	3	3	2	2	2	4
Nt 2.5 δy =	3	1	1	2	1	2	1	2	1	1	3	2	1	1	1	4
Nt 3.0 δy =	2	0	1	1	1	1	2	2	1	1	2	1	1	1	0	2
Nt 3.5 δy =	1	0	1	1	1	1	1	1	1	0	1	1	0	1	0	2
Nt 4.0 δy =	1	0	0	1	1	1	1	1	1	1	1	1	0	1	0	1
Nt 4.5 δy =	1	0	0	1	0	1	1	0	1	1	0	1	0	0	0	2
Nt 5.0 δy =	2	0	0	2	0	3	2	2	2	3	2	0	0	1	1	4
Range 1	7.5	3.0	4.6	6.1	5.8	8.7	8.2	6.7	8.0	9.1	9.2	5.0	4.6	5.8	5.6	8.8
Range 2	5.1	2.4	4.1	4.5	4.1	6.8	6.9	4.9	6.6	7.4	7.1	3.6	4.3	4.5	3.9	5.4
Range 3	4.4	1.9	2.2	2.1	2.4	2.8	3.2	2.0	3.5	3.1	3.1	2.2	1.7	2.2	1.3	3.1
Range 4	1.9	1.5	1.6	1.6	1.2	2.2	1.2	1.7	1.3	1.1	1.5	1.1	1.4	1.8	1.1	1.9
Range 5	1.6	1.3	1.2	1.0	0.8	1.2	0.7	1.1	0.7	0.6	0.9	0.7	0.8	1.1	0.7	1.0

Table 5.6.2.3 Maximum values of the demand parameters for all 20 ground motions

	2 floors		4 floors		8 floors				12 floors				16 floors			
	1st	2nd	1st	2nd	1st	2nd	3rd	4th	6th	7th	8th	9th	7th	8th	9th	14th
δ/δy max =	11.1	2.5	8.6	8.8	8.6	10.8	13.8	8.6	9.4	15.0	12.2	8.5	5.5	7.9	6.1	7.0
Nt 0.5 δy =	43.0	49.0	48.0	43.0	55.0	58.0	49.0	48.0	29.0	26.0	21.0	30.0	30.0	27.0	25.0	32.0
Nt 1.0 δy =	23.0	21.0	18.0	19.0	21.0	23.0	14.0	12.0	21.0	17.0	16.0	19.0	8.0	11.0	8.0	15.0
Nt 1.5 δy =	17.0	9.0	13.0	13.0	7.0	7.0	5.0	8.0	7.0	5.0	7.0	10.0	6.0	5.0	5.0	7.0
Nt 2.0 δy =	6.0	3.0	7.0	9.0	7.0	5.0	5.0	6.0	5.0	6.0	6.0	5.0	3.0	2.0	6.0	11.0
Nt 2.5 δy =	8.0	3.0	3.0	7.0	3.0	3.0	2.0	3.0	3.0	2.0	4.0	3.0	2.0	3.0	2.0	7.0
Nt 3.0 δy =	7.0	4.0	4.0	2.0	3.0	3.0	3.0	2.0	3.0	3.0	2.0	4.0	3.0	2.0	2.0	4.0
Nt 3.5 δy =	3.0	0.0	3.0	3.0	2.0	2.0	2.0	3.0	2.0	2.0	2.0	6.0	1.0	2.0	1.0	5.0
Nt 4.0 δy =	3.0	0.0	1.0	2.0	2.0	2.0	2.0	3.0	2.0	2.0	1.0	2.0	2.0	1.0	1.0	2.0
Nt 4.5 δy =	2.0	0.0	1.0	1.0	1.0	1.0	3.0	1.0	1.0	2.0	2.0	2.0	1.0	1.0	1.0	2.0
Nt 5.0 δy =	12.0	0.0	9.0	9.0	6.0	7.0	7.0	7.0	7.0	8.0	7.0	4.0	2.0	2.0	2.0	9.0
Range 1	13.6	4.0	10.2	10.8	10.5	15.4	16.6	11.9	12.3	17.0	15.5	9.4	8.3	10.3	7.7	9.7
Range 2	12.8	3.0	10.0	10.5	9.0	14.2	14.7	10.4	10.3	13.5	12.8	7.7	4.4	5.2	6.7	8.1
Range 3	8.9	2.4	6.0	7.2	8.7	11.1	12.6	8.5	8.3	12.3	10.8	7.5	3.1	4.3	3.1	4.5
Range 4	7.8	1.8	3.5	4.9	3.5	3.9	4.1	4.3	2.9	4.9	3.6	3.4	1.8	2.4	2.2	4.4
Range 5	5.7	1.5	3.4	4.1	1.6	2.1	2.0	2.9	1.6	1.3	1.5	3.3	1.1	1.8	0.9	1.5

Table 5.6.2.4 Average values of the 50th percentile demand estimates for each building

AVERAGE	2 floors	4 floors	8 floors	12 floors	16 floors
δ/δy max =	2.2	2.5	2.8	3.5	2.1
Nt 0.5 δy =	22.0	18.5	11.9	10.6	9.9
Nt 1.0 δy =	9.3	7.3	5.4	4.8	4.5
Nt 1.5 δy =	3.8	3.5	2.6	1.6	1.6
Nt 2.0 δy =	1.5	1.5	1.1	1.0	0.5
Nt 2.5 δy =	0.5	0.5	0.8	0.8	0.3
Nt 3.0 δy =	0.5	0.5	0.4	0.1	0.3
Nt 3.5 δy =	0.3	0.0	0.0	0.0	0.0
Nt 4.0 δy =	0.0	0.5	0.0	0.0	0.0
Nt 4.5 δy =	0.0	0.0	0.1	0.0	0.1
Nt 5.0 δy =	0.0	0.0	0.0	0.3	0.0
Range 1	3.6	3.9	4.5	4.9	3.4
Range 2	2.3	2.6	2.7	2.8	2.4
Range 3	1.5	1.4	1.1	1.3	1.1
Range 4	1.1	0.9	0.5	0.5	0.6
Range 5	1.0	0.7	0.4	0.2	0.3

Table 5.6.2.5 Average values of the 84th percentile demand estimates for each building

AVERAGE	2 floors	4 floors	8 floors	12 floors	16 floors
δ/δy max =	3.1	3.9	5.2	5.7	4.3
Nt 0.5 δy =	35.5	27.4	23.7	18.7	20.2
Nt 1.0 δy =	14.4	13.5	10.9	8.2	6.2
Nt 1.5 δy =	6.5	7.0	4.5	4.0	3.5
Nt 2.0 δy =	3.5	5.0	3.2	2.5	2.5
Nt 2.5 δy =	2.0	1.5	1.5	1.7	1.7
Nt 3.0 δy =	1.0	1.0	1.5	1.3	1.0
Nt 3.5 δy =	0.5	1.0	1.0	0.8	0.7
Nt 4.0 δy =	0.5	0.5	1.0	1.0	0.5
Nt 4.5 δy =	0.5	0.5	0.5	0.8	0.5
Nt 5.0 δy =	1.0	1.0	1.8	1.7	1.5
Range 1	5.3	5.3	7.4	7.8	6.2
Range 2	3.7	4.3	5.7	6.2	4.5
Range 3	3.1	2.2	2.6	3.0	2.1
Range 4	1.7	1.6	1.6	1.2	1.6
Range 5	1.5	1.1	1.0	0.7	0.9

Table 5.6.2.6 Average values of the maximum demand estimates for each building

AVERAGE	2 floors	4 floors	8 floors	12 floors	16 floors
δ/δy max =	6.8	8.7	10.5	11.3	6.6
Nt 0.5 δy =	46.0	45.5	52.5	26.5	28.5
Nt 1.0 δy =	22.0	18.5	17.5	18.3	10.5
Nt 1.5 δy =	13.0	13.0	6.8	7.3	5.8
Nt 2.0 δy =	4.5	8.0	5.8	5.5	5.5
Nt 2.5 δy =	5.5	5.0	2.8	3.0	3.5
Nt 3.0 δy =	5.5	3.0	2.8	3.0	2.8
Nt 3.5 δy =	1.5	3.0	2.3	3.0	2.3
Nt 4.0 δy =	1.5	1.5	2.3	1.8	1.5
Nt 4.5 δy =	1.0	1.0	1.5	1.8	1.3
Nt 5.0 δy =	6.0	9.0	6.8	6.5	3.8
Range 1	8.8	10.5	13.6	13.5	9.0
Range 2	7.9	10.2	12.1	11.1	6.1
Range 3	5.7	6.6	10.3	9.7	3.7
Range 4	4.8	4.2	3.9	3.7	2.7
Range 5	3.6	3.8	2.2	1.9	1.3

5.7. Conclusions

In order to study the seismic stability of multi-storey Split-X braced steel frames for a large range of structures, five buildings having 2-, 4-, 8-, 12- and 16-storeys were examined in this project.

A preliminary design of the buildings was first completed using the equivalent static force procedure of NBCC 2005. The design was then finalized using the dynamic response spectrum analysis with the Visual Design computer software.

In the spectral analyses, the complete quadratic modal combination approach was adopted with 5% of the critical damping for each of the modes. The fundamental lateral periods of the buildings were found to be shorter than the NBCC 2005 limit for all the

buildings except for the 2-storey one for which the NBCC upper limit on the period applied. P-Δ effects were taken into account by amplifying the lateral load effects by the CSA-S16 U_2 factor. A 10% accidental excentricity was considered and was included in the analysis by applying horizontal and in-plane torsional moments. The base shear obtained from the spectral analyses exceeded the NBCC 2005 minimum value, for all the buildings, and no adjustment of the results was needed. The effective length factor of the braces was taken equal to 0.9 in the design and the braces were considered pinned in bending in both directions and fixed in torsion. The columns were considered fixed for both bending and torsion. They were also continuous over the buildings height.

Nonlinear dynamic analyses of the structures were performed using the OpenSees computer software. The OpenSees model included one bracing bent as well as all the building columns braced by that bracing bent. In these analyses, the brace model and the column model were adjusted in order closely represent the actual conditions in a building. The braces were carefully modelled with the nonlinear beam column elements described in Chapter 3. An out-of-plane initial imperfection was considered in order to develop a brace buckling load not exceeding 110% of the expected brace compression strength ($1.2C_u$). The flexural and torsional stiffness of the gusset plates were considered in the OpenSees model. This resulted in brace effective length factors approximately equal to 0.75. The bracing bent columns were considered as continuous over the height of the buildings, whereas the gravity columns were modeled with splices at every second floor. Rayleigh damping with 3% critical damping in the first two modes was specified in the OpenSees model. The nonlinear dynamic analyses were performed under 20 selected and scaled ground motions to study the peak response parameters. Thereafter the performance of the structures against global instability under incrementally increasing ground motion amplitudes was examined.

The peak response parameters considered were the peak story drift angle, Δ/h_s, the residual story drift angle, Δ_{res}/h_s, the drift concentration factor, D_{CF}, and the brace ductility demand, μ.

Based on the median estimates of these response parameters, it can be concluded that:

- The peak storey drift angle generally increased with the number of storeys, and the maximum value was obtained for the 16-storey building. This means that the damage suffered by both the structural and non-structural elements would more likely be more important for the 16-storey building and that the damage level would decrease with a reduction of the number of floors. The median values of the peak interstorey drift angles were between 2.3 and 1.4 times smaller than the NBCC 2005 limits. However, they were between 1.17 and 1.8 times larger than the values obtained by the response spectrum analyses. The differences in the level of damping assumed in the spectral and nonlinear dynamic analyses likely contributed to these differences in storey drift predictions.
- The maximum value for the residual story drift angle was found for the 8-storey building. The values obtained for the 12- and 16-storey buildings were nearly three times less than the 8-storey building results. This shows that the 8-storey building is returning less to its undeformed position. Only the 2- and 4-storey buildings experienced residual storey drift angles that were within the CSA S16 maximum erection tolerance of 0.2% for out-of-plumbness. The taller structures would need post-earthquake structural evaluation. All the buildings experienced median residual storey drift angles less than 1%.
- The values found for the drift concentration factor D_{CF} generally increase with the number of floors. When compared with predicted values obtained from models available in the literature, the D_{CF} values were very close to the predictions for the 2-, 4- and 8-storey buildings but exceeded by 1.3 the values found in literature for the 12- and 16-storey buildings.
- The 12-storey building exhibited the largest brace ductility demand in the mid-height portion of the building. The 8- and 16-storey buildings showed similar ductility levels but at different locations: near the building base for the 8-storey building and near the top of the building for 16-storey building. The most critical floors were the 7^{th} for the 12-storey building and the 2^{nd} and 14^{th} floors for the 8-

and 16-storey buildings, respectively . The brace ductility demand was thereafter compared to an empirical expression that had been proposed to predict brace failure due to fracture. It was found that the braces would generally exhibit satisfactory performance against fracture. The most critical braces were those with λ in the vicinity of 0.75 (KL/r $\approx$ 55) used mostly in the 2- and 16-storey buildings. Relatively lower brace ductility demand was observed for the stockier braces ($\lambda \approx 0.60$, $KL/r \approx 45$) and for the more slender ones ($\lambda > 0.90$, $KL/r > 65$).

The performance against collapse of the 8-, 12- and 16-storey buildings was studied using the incremental dynamic analyses (IDA) and a confidence level parameter. The IDA analyses showed that the 16-storey building collapsed at a scaling factor of 10.0, while the 12- and the 8-storey buildings collapsed at a scaling factor of 8.0 and 5.0 respectively. The 8-storey building collapse mode was different from the one observed for the 12- and 16-storey buildings: while the first one collapsed by gradually degradation of the lateral stiffness, the other ones collapsed when reaching excessive values of maximum interstorey drift (more than $10\%h_s$), beyond which when the model may not be trustworthy. This difference in global stability response can be partly explained by the differences in the design of the buildings. The 8-storey building was designed as a Type MD frame with $R_d = 3.0$, whereas the 12- and 16-storey buildings were designed with lower ductility-related force modification factor, $R_d = 2.0$. In addition the design seismic forces had to be amplified up to $R_d = 1.58$ for the 16-storey building because of its larger height, as required in CSA S16S1-05.

The detailed response of the buildings under selected ground motions was examined at different ground motion amplitudes, especially to study the hardening behaviour of the buildings under these ground motions.

The confidence level against global stability was determined by adapting the procedure described in the FEMA-350 document for steel moment resisting frames. For all the three

buildings, the confidence level was found to be equal to 99.99%, which is much more than the minimum value of 90% recommended in FEMA - 350. This means that concentrically braced steel frames designed in accordance with the new provisions of CSA-S16S1-05 and NBCC 2005 are conservative. Further studies are required in order to decide if the new provisions of the codes need to be revised, especially because the procedure described in FEMA-350 has been developed for steel moment resisting frames, not for concentrically braced steel frames.

A numerical database for the development of test loading protocols was obtained following the parameters considered in the development of past loading protocols. Three sets of results from the statistical studies were computed which can be used in the formulation of future loading protocols: the 50^{th} percentile, the 84^{th} percentile and the maximum values. The results show significant variations in the brace demand between these three probability levels as well as between the different buildings and the vertical position of the braces in the buildings.

CHAPTER 6. COCLUSIONS AND RECOMMENDATIONS

6.1. Conclusions

The main objectives of this project were to use the OpenSees computer software to:

- Study the overall seismic performance, including the global stability against collapse, of multi-storey Split-X braced steel frames designed according to NBCC 2005 and CSA-S16S1-05 seismic provisions, and
- Develop a numerical database that can be used in the development of loading protocols for the seismic testing of bracing members used in concentrically braced steel frames.

Parametric studies were first carried out to evaluate the influence of modeling assumptions when simulating the hysteretic response of rectangular HSS steel bracing members with the OpenSees finite element computer software. Nonlinear beam-column elements were used with a fibre representation of the member cross-section. These studies showed that:

- the number of integration points per element has a limited influence on the response and that accurate results could be obtained with three integration points;
- for a given set of parameters, the force based formulation was found to provide higher accuracy compared to the displacement based formulation. This formulation should therefore be preferred, even if it requires longer computational time;
- as expected, the errors were found to reduce when increasing the number of elements or the number of fibres. The results indicate that sufficient accuracy can be achieved for typical bracing members if 8 elements per brace member were used together with 16 fibres for cross-section discretization;
- the use of the Giuffré-Menegotto-Pinto constitutive model was found to provide a more realistic representation of the brace hysteretic response compared to the simpler bi-linear model;

- comparisons between test and predicted results as well as simple dynamic seismic analysis confirm the appropriateness of these modeling assumptions for typical low-rise braced frame applications;
- the brace model was found to give realistic predictions of the hysteretic response of braces having different sizes, slenderness ratios or end restraint conditions. This is by far superior to using empirical or semi-empirical models for which specific test data are needed to adequately reproduce key response properties. However, the brace modeling considered in this study still has some limitations. For instance, it does not account for residual stress effects on the compression strength at first buckling, and local buckling effects and brace fracture cannot be reproduced by the model.

Thereafter, parametric and comparative studies were realized in order to validate the OpenSees element used to model the beams and the columns of the bracing bents as well as the gravitational columns of the studied buildings. This element is the Beam with Hinges element. It has elastic axial and flexural response between plastic hinges located at the member ends. A fibre representation of the member cross-section is used for the element. These studies showed that:

- The elastic and inelastic flexural behaviour of W shaped beams bent about their weak axis under concentrated loads can be very well described using a nine-element discretization and a section discretization with ten fibres along the width of the flanges and four fibres over the depth of the web. It was found that the length and the position of the plastic hinges influence the flexural behaviour of the beam. Therefore, careful validation has to be made when modelling beams in flexure using the Beam with Hinges elements.
- Very close results were obtained when modelling a column subjected to axial compression and end moments with nine Beam with Hinges elements and with only one Beam with Hinges element. Therefore, it was decided to use a single

Beam with Hinges element for modeling the beams and columns of the braced frames as well as the gravity columns.

- Very close results were obtained when using ten-fibre and twenty-fibre discretizations of the portions of a W-shape cross-section subjected to a linear stress variation. Therefore, a discretization with 10 fibres for these portions of W-shaped members was adopted to model all Beam with Hinges elements.
- The Beam with Hinges element orientation was validated by comparing different methods with hand calculations.
- Finally, the single Beam with Hinges element model in OpenSees was found to predict well the capacity of a member subjected to axial load in compression combined with end bending moments when comparing with published axial load bending moment interaction equations for cross-section strength and overall member strength.

A total of five buildings having 2-, 4-, 8-, 12- and 16-storeys were examined in this project to study the seismic response and stability of multi-storey Split-X braced steel frames for a large range of structures.

A preliminary design of the buildings was first completed using the equivalent static force procedure of NBCC 2005. The design was then finalized using the dynamic response spectrum analysis with the Visual Design computer software.

In the spectral analysis, the complete quadratic modal combination approach was adopted with 5% of the critical damping for each of the modes. The fundamental lateral periods of the buildings were found to be shorter than the NBCC 2005 limit for all the buildings except for the 2-storey one for which the NBCC upper limit on the period applied. P-Δ effects were taken into account by amplifying the lateral load effects by the CSA-S16 U_2 factor. A 10% accidental eccentricity was considered and was included in the analysis by applying horizontal in-plane torsional moments at every level. For all buildings, the base

shear obtained from spectral analysis exceeded the NBCC 2005 minimum value of 80 % of the base shear from static analysis. Hence, no adjustment of the analysis results was needed. An effective length factor equal to 0.9 was assumed in the design of the braces. In the Visual Design model, the brace ends were considered as pinned in bending in both directions and fixed in torsion. The column bases were considered to be fixed for both bending and torsion. The columns were also assumed as continuous over the building height.

Nonlinear dynamic analysis of the structures was performed using the OpenSees computer software. The OpenSees model included one bracing bent as well as all the building columns braced by that bracing bent. In these analyses, the brace model and the column model were adjusted in order closely represent the actual conditions in a building. The braces were carefully modelled with the nonlinear beam column elements described in Chapter 3. An out-of-plane initial imperfection was considered in order to develop a brace-buckling load not exceeding 110% of the expected brace compression strength (1.2 C_u). The flexural and torsional stiffness of the gusset plates were considered in the OpenSees model. This resulted in brace effective length factors approximately equal to 0.75. Rigid members were also used at the brace ends to reproduce the actual beam-column joint dimensions. The bracing bent columns were considered as continuous over the height of the buildings, whereas the gravity columns were modeled with rotationally flexible splices at every second floor. Rayleigh damping with 3% critical damping in the first two modes of vibration was specified in the OpenSees model. The nonlinear dynamic analyses were performed under 20 site representative scaled ground motions to study the peak response parameters. Thereafter the performance of the structures against global instability was examined under incrementally increasing ground motion amplitudes for a subset of 10 time histories from past earthquakes.

The response parameters considered were the peak story drift angle, Δ/h_s, the residual story drift angle, Δ_{res}/h_s, the drift concentration factor, D_{CF}, and the peak brace ductility demand, μ.

Based on the median estimates of these response parameters, it can be concluded that:

- The peak storey drift angle generally increased with the number of storeys. This means that the damages suffered by both the structural and non-structural elements would more likely be more important for the 16-storey building and that the damage level would decrease with a reduction of the number of floors. The median values of the peak interstorey drift angles were 2.3 to 1.4 times smaller than the NBCC 2005 limits of 2.5%h_s. However, they were between 1.17 and 1.8 times greater than the values obtained from response spectrum analysis at the design stage. The differences in the level of damping assumed in the spectral and nonlinear dynamic analyses likely contributed to these differences in storey drift predictions.
- The 8-storey building experienced the maximum value of residual story drift angle. The values obtained for the 12- and 16-storey buildings were nearly three times lower than for the 8-storey building results. This shows that that the 8-storey building is returning less to the undeformed position. Only the 2- and 4-storey buildings experienced residual storey drift angles that were within the CSA-S16 maximum erection tolerance of 0.2% for out-of-plumbness. The taller structures would need post-earthquake structural evaluation. All the buildings experienced median residual storey drift angles less than 1%.
- The values of the damage concentration factor D_{CF} generally increase with the number of floors. When compared with predicted values obtained from models available in the literature, the D_{CF} values were very close to the predictions for the 2-, 4- and 8-storey buildings but exceeded by 1.3 the values found in literature for the 12- and 16-storey buildings.
- The 12-storey building exhibited the largest brace ductility demand and the highest demand was located in the mid-height portion of the building. The 8- and 16-storey buildings showed similar ductility levels but at different locations: near the building base for the 8-storey building and near the top of the building for 16-storey building. The most critical floors were the 7^{th} for the 12-storey building

and the 2nd and 14th floors for the 8- and 16-storey buildings, respectively. The brace ductility demand was thereafter compared to an empirical expression that had been proposed to predict the failure of braces due to fracture. It was found that the braces would generally exhibit satisfactory performance against fracture. The most critical braces were those with λ in the vicinity of 0.75 (KL/r $\approx$ 55) used mostly in the 2- and 16-storey buildings. Relatively lower brace ductility demand was observed for the stockier braces ($\lambda \approx 0.60$, $KL/r \approx 45$) and for the more slender ones ($\lambda > 0.90$, $KL/r > 65$).

The performance against collapse of the 8-, 12- and 16-storey buildings was studied using the incremental dynamic analyses (IDA) and a confidence level parameter against global instability. The IDA analyses showed that the 16-storey building collapsed at a scaling factor of 10.0, while the 8- and the 12-storey buildings collapsed at a scaling factor of 5.0 and 8.0 respectively. The 8-storey building collapse mode was different from the one observed for the 12- and 16-storey buildings: while the first one collapsed by gradually degradation of the lateral stiffness, the other ones collapsed when reaching excessive values of maximum interstorey drift (more than 10%h_s), beyond which when the model may not be trustworthy. The difference in global stability response can be explained partly by the differences in the design of the buildings. The 8-storey building was designed as a Type MD frame with $R_d = 3.0$, whereas the 12- and 16-storey buildings were designed with a lower ductility-related force modification factor, $R_d = 2.0$. In addition the design seismic forces had to be amplified up to $R_d = 1.58$ for the 16-storey building because of its larger height, as required in CSA S16S1-05.

The detailed response of the buildings under selected ground motions was examined at different ground motion amplitudes, especially to study the hardening behaviour of the buildings under these ground motions.

The confidence level against global stability was determined by adapting the procedure described in the FEMA-350 document for steel moment resisting frame structures. For all three buildings, the confidence level was found to be equal to 99.99%, which is much higher than the minimum value of 90% recommended in FEMA-350. This means that concentrically braced steel frames designed in accordance with the new provisions of CSA-S16S1-05 and NBCC 2005 are conservative.

A numerical database for the development of test loading protocols was obtained following the parameters considered in the development of past loading protocols. Three sets of results from the statistical studies were computed which can be used in the formulation of future loading protocols: the 50^{th} percentile, the 84^{th} percentile and the maximum values. The results show significant variations in the brace demand between these three probability levels as well as between the different buildings and the vertical position of the braces in the buildings.

6.2. Recommendations

Although useful results showing a good seismic performance for multi-storey concentrically braced steel frames were obtained in this project, further studies and research work are necessary in order to improve the models used in this project and to better evaluate the seismic behaviour of braced steel frame structures designed according to the new provisions of CSA16-01 and NBCC 2005. The future work should comprise:

- The implementation in OpenSees software of a damage model that will consider local buckling effects as well as brace fracture, such as the one proposed by Jin and El-Tawil (2003).
- Supplementary analyses on tall concentrically braced steel frames buildings with braces designed with a more realistic estimate of the effective length factor (0.75 versus the value of 0.9 that was assumed in this study).

- Analyses of other braced frame configurations (single-storey X bracing, chevron bracing, etc.) should be performed to verify that the conclusions of this study could be extended to all concentrically braced frames permitted in CSA-S16.
- Further studies are also necessary to verify that the procedure described in FEMA-350 originally developed for steel moment resisting frames is equally applicable to concentrically braced steel frames.

REFERENCES

ADAMS, J., ATKINSON, G.M, (2002). "Development of seismic hazard maps for the proposed edition of the National Building Code of Canada", Canadian Journal of Civil Engineering, 30: 255-271.

ADAMS, J. and HALCHUCK, S. (2003). "Fourth generation seismic hazard maps of Canada: Values for Canadian localities intended for the 2005 National Building Code of Canada", Open File 4459, Geological Survey of Canada, Ottawa, ON.

AGUERO, A., IZVERNARI, C., and TREMBLAY, R. (2006). "Modelling of the Seismic Response of Concentrically Braced Steel Frames using the OpenSees Analysis Environment", International Journal of Advanced Steel Construction, 2, 3, 242-274.

AISC. (2005). ANSI/AISC 341-05. "Seismic Provisions for Structural Steel Buildings (Draft September 10, 2004)", American Institute of Steel Construction. Chicago, Il.

ARCHAMBAULT, M.H., (1995). "Étude du comportement séismique des contreventements ductiles en X avec profiles tubulaires en acier", Rapport No. EPM/GCS-1995-09, École Polytechnique de Montréal.

ASCE (2005). "ASCE/SEI 7-05, Minimum Design Loads for Buildings and Other Structures", American Society of Civil Engineers, Reston, VA.

ASTANEH-ASL, A., GOEL, S.C. and HANSON, R.D. (1985). "Cyclic Out-of-Plane Buckling of Double-Angle Bracing", Journal of Structural Engineers, ASCE, 111, 1135-1153.

ATKINSON, G.M., BERESNEV, I.A., (1997). "Compatible ground-motion time histories for new national seismic hazard maps", Canadian Journal of Civil Engineering, 25:305-318.

BARD, P.Y., AFRA, H. and ARGOUL, P. (1991). "Seismic response of buildings during earthquakes: experimental results from strong motion data", Proceedings of the International Workshop on Seismology and Earthquake Engineering, Mexico City, 149-175.

BARBATO, M. and CONTE, J.P. (2004). "Finite Element Response Sensitivity Analysis: a Comparison Between Force-Based and Displacement-Based Frame Element Models", Computer Methods in Applied Mechanics and Engineering, 194, 1479-1512.

BEAULIEU, D., PICARD, A., TREMBLAY, R., GRONDIN, G. and MASSICOTTE, B. (2003). "Calcul des charpentes d'acier", Institut Canadien de la Construction en Acier.

BERTERO, V.V., UANG, C.M., LLOPIZ, C.R. and IGARASHI, K. (1989). "Earthquake simulator testing of concentric braced dual system". Journal of Structural Engineering, Vol. 115, No. 8.

BUILDING SEISMIC SAFETY COUNCIL for the Federal Emergency Management Agency (2003). "NEHRP Recommended Provisions for Seismic Regulations for New Buildings and Other Structures (FEMA 450)", Washington, D.C.

CARR, A.J. (1994). "Dynamic Analysis of Structures", Bulletin of the New Zealand National Society for Earthquake Engineering, Vol.27, No.2.

CHAJES, A. (1974). "Principles of Structural Stability Theory", Prentice-Hall, Inc., Englewood Cliffs, NJ.

CHEN, C.C., BONOWITZ, D., ASTANESH-ASL, A. (1992). "Studies of a 49 story instrumented steel structure shaken during the Loma Prieta earthquake", Report No. UCB/EERC-92/01, Earthquake Engineering Research Center, University of California at Berkeley.

ÇELEBI, M.(1993). "Seismic response of eccentrically braced tall building", Journal of Structural Engineering, Vol. 119, No. 4, Paper No. 3841.

COOK, R.D, MALKUS, D.S, PLESHA, M.E., WITT, R.J., (2002). "Concepts and Applications of Finite Element Analyses", Forth Edition, John Wiley & Sons Inc., USA.

COCHRAN, M.L. and HONECK, W.C. (2004). "Design of Special Concentric Braced Frames. Steel Tips", Structural Steel Education Council, Moraga, CA.

CSA (2001). "CAN/CSA-S16-01, Limit States Design of Steel Structures", Canadian Standard Association, Toronto, ON.

CSA (2005). "S16S1-05 Supplement No.1 to CAN/CSA-S16-01, Limit States Design of Steel Structures", Canadian Standard Association, Rexdale, ON.

ECCS (1986). "ECCS – TWG 1.3 Seismic Design Recommended Testing Procedure for Assessing the Behaviour of Structural Steel Elements under Cyclic Loads", European Convention for Constructional Steelwork, Technical Committee - Structural safety and loading, Brussels, Belgium.

FELL, B.V., MYERS, A.T., DEIERLIN G.G., and KANVINDE, A.M., (2006). "Testing and Simulation of Ultra-Low Cycle Fatigue and Fracture in Steel Braces", 8th National Conference on Earthquake Engineering, San Francisco, April 2006.

FEMA 350 (2000). "FEMA-350, Recommended Seismic Design Criteria for new Steel Moment-Frame Buildings", Prepared by the SAC Joint Venture for the Federal Emergency Management Agency, Washington, DC.

FEMA 356 (2000). "Prestandard and Commentary for the Seismic Rehabilitation of Buildings", Prepared by American Society of Civil Engineers for the Federal Emergency Management Agency, Washington, DC.

FILIPPOU, F.C., POPOV, E.P. and BERTERO, V.V. (1983). "Modelling of Reinforced Concrete Joints under Cyclic Excitations", ASCE Journal of Structural Engineering, Vol. 109, No. 11.

FOUTCH, D.A, GOEL, S.C. and ROEDER C.W. (1987). "Seismic testing of full-scale steel building ", Journal of Structural Engineering, Vol. 113, No. 11, Paper no. 21935.

GUNNARSSON, I.R. (2005). "Numerical Performance Evaluation of Braced Frame Systems", Master of Science Thesis, Civil Engineering, University of Washington.

HADDAD, M. (2004). "Design of Concentrically Braced Steel Frames for Earthquakes", Ph.D. Thesis, Dept. of Civil Eng., Univ. of Calgary, Calgary, AL.

HALCHUK, S., ADAMS, J. (2004). "Deaggregation of seismic hazard for selected Canadian cities", 13th World Conference on Earthquake Engineering, Vancouver, Canada. Paper No. 2470.

HANDBOOK OF STEEL CONSTRUCTION - Eighth Edition (2004), Canadian Institute of Steel Construction, Toronto, ON.

HEIDEBRECHT, A.C. (2003). "Overview of Seismic Provisions of the Proposed 2005 Edition of the National Building Code of Canada", Canadian Journal of Civil Engineering, , 30, 241-254.

JIN, J. and EL-TAWIL, S. (2003). "Inelastic Cyclic Model for Steel Braces", Journal of Engineering Mechanics, ASCE, 129, 5, 548-557.

KALKAN, E. (2004). "Force-based vs. Displacement-based Elements", Department of Civil and Environmental Engineering, University of California Davis.

KRAWINKLER, H., GUPTA, A., MEDINA, R. and LUCO, N. (2000). "Loading Histories for Seismic Performance Testing of SMRF Components and Assemblies", SAC Joint Venture – Report No. SAC/BD-00/10.

KRAWINKLER, H., PARISI, F., IBARRA, L., AYOUB, A. and MEDINA, R. (2000) "Development of a testing protocol for wood frame structures", CUREE Publication No.W-02.

LACERTE, M. and TREMBLAY, R. (2006). "Making Use of Brace Overstrength to Improve the Seismic Response of Multi-Storey Split-X Concentrically Braced Steel Frames", Canadian Journal of Civil Eng. (in press).

LIN, M.L., TSAI, K.C, HSIAO, P.C and TSAI C.Y. (2005). "Compressive behaviour of buckling-restrained brace gusset connections", The First International Conference on Advances in Experimental Structural Engineering AESE 2005, July 19-21, 2005, Nagoya, Japan.

MAZZONI, S., McKENNA, F., FENVES, G.L. (2005). "OpenSees Command Language Manual", http://opensees.berkeley.edu.

MENEGOTTO, M., and PINTO, P.E. (1973). "Method of analysis for cyclically loaded R.C. plane frames including changes in geometry and non-elastic behaviour of

elements under combined normal force and bending", Proc. IABSE Symposium on Resistance and Ultimate Deformability of Structures Acted on by Well Defined Repeated Loads, 15-22.

MIRANDA, E. (1999). "Approximate Seismic Lateral Deformation Demands in Multistory Buildings", Journal of Structural Engineering, Vol.125, No.4, Paper No. 16012.

MACRAE, G.A., KIMURA, Y. and ROEDER, C. (2004). "Effect of Column Stiffness on Braced Frame Seismic Behaviour", Journal of Structural Engineering, Vol.130, No.3.

MCKENNA, F. and FENVES, G.L. (2004). "Open System for Earthquake Engineering Simulation (OpenSees)", Pacific Earthquake Engineering Research Center (PEER), University of California, Berkeley, CA. (http://opensees.berkeley.edu/index.html).

NBCC (2005), "National Building Code of Canada 2005, 12th ed", National Research Council of Canada, Ottawa, ON.

PAULAY, T., and PRIESTLEY, M.J.N. (1992). "Seismic design of reinforced concrete and masonry buildings", Wiley Interscience Publication, John Wiley & Sons, Inc.

PEER - Pacific Earthquake Engineering Research Center Strong Motion Database [on line] http://peer.berkeley.edu.

PONCET, L. and TREMBLAY, R. (2004). "Seismic Performance of Multi-Storey Concentrically Braced Steel Frames with Mass Irregularity", 13th World Conference on Earthquake Engineering, Vancouver, Canada. Paper No. 2896.

SABELLI, R. (2001). "Research on Improving the Design and Analysis of Earthquake-Resistant Steel-Braced Frames", EERI/FEMA NEHRP Fellowship Report No. PF2000-9, Oakland, CA.

SCOTT, M.H., FRANCHIN P., FENVES L. and FILIPPOU F.C. (2004). "Response Sensitivity for Nonlinear Beam-Column Elements", Journal of Structural Engineers, Vol. 130, No. 9.

SHABACK, J.B. and BROWN, T. (2003). "Behaviour of square hollow structural steel braces with end connections under reversed cyclic axial loading", Canadian Journal of Civil Engineering, 30, 745–753.

THORNTON, W.A. (1984). "Bracing connections for heavy constructions", Eng. J. AISC 1984; 21(3):139-48.

TREMBLAY, R. (2000). "Influence of Brace Slenderness on the Seismic Response of Concentrically Braced Steel Frames", Proc. STESSA 2000 Conf., Montréal, Canada, 527-534.

TREMBLAY, R. (2002). "Inelastic seismic response of steel bracing members", Journal of constructional steel research 58 (2002) 665-701.

TREMBLAY, R., ARCHAMBAULT, M.A., and FILIATRAULT. A. (2003). "Seismic Performance of Concentrically Braced Steel Frames made with Rectangular Hollow Bracing Members", Journal of Structural Engineers, ASCE, 129:12, 1626-1636.

TREMBLAY, R. and BOUATAY, N. (2002). "Loading Protocols for the Seismic Testing of Ductile Bracing Members in Concentrically Braced Steel Frames", Proc. 12th European Conf. on Earthquake Eng., London, UK, Paper No. 480.

TREMBLAY, R., MERZOUQ, S., IZVERNARI, C., and ALEXIEVA, K. (2005). "Application of the Equivalent Force Procedure for the Seismic Design of Multi-Storey Buildings with Vertical Mass Irregularity", Canadian Journal of Civil Engineering, 32, 3, 561-568.

TREMBLAY, R., PONCET, L., BOLDUC, P., NEVILLE, R., and Devall, R. (2004). "Testing and Design of Buckling Restrained Braces for Canadian Application", Proc. 13th World Conference on Earthquake Eng., Vancouver, BC, Paper no. 2893.

TREMBLAY, R. and PONCET, L. (2004). "Improving the Seismic Stability of Concentrically Braced Steel Frames", Proc. 2004 SSRC Annual Technical Session & Meeting, Long Beach, CA, 19-38.

TREMBLAY, R. and PONCET, L. (2005). "Seismic Performance of Concentrically Braced Steel Frames in Multi-Storey Buildings with Mass Irregularity", Journal of Structural Engineering, ASCE, 131, 9, 1363-1375.

TREMBLAY, R. and PONCET, L. (2007). "Improving the Seismic Stability of Concentrically Braced Steel Frames", Eng. Journal (in press).

TREMBLAY, R. and ROBERT N. (2001). "Seismic Performance of Low- and Medium-Rise Chevron Braced Steel Frames", Canadian Journal of Civil Engineering, 28, 4, 699-714.

URIZ, P. and MAHIN, S.A. (2004). "Seismic Performance Assessment of Concentrically Braced Steel Frames", 13th World Conference on Earthquake Engineering, Vancouver, B.C., Canada, Paper No.1639.

URIZ, P. and MAHIN, S. A. (2004). "Seismic performance Assessment of Concentrically braced steel Frames", Proc. 13th World Conference on Earthquake Eng., Vancouver, BC, Paper No. 1639.

URIZ, P. (2005). "Towards Earthquake Resistant Design of Concentrically Braced Steel Structures", Ph.D. Thesis, Engineering-Civil and Environmental Engineering, Graduate Division, University of California, Berkeley, CA.

VAMVATSIKOS, R and CORNELL, A. (2002). "Incremental dynamic analysis", Earthquake Engineering and Structural Dynamics, 31: 491-514.

WHITMORE, R.E. (1952). "Experimental investigation of stresses in gusset plates", Bulletin No. 16, Engineering Experiment Station, University of Tennessee.

APPENDIX I.

Plastic analysis of the section W 360x196

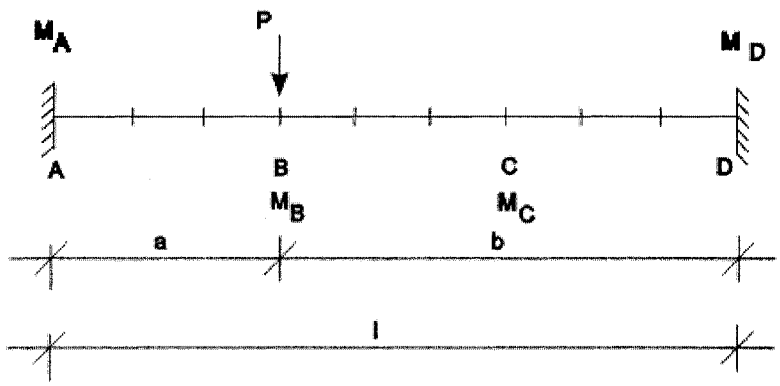

Fig.I.1 Geometry of the beam studied

For a load applied at point B at 1/3 of the beam span, l: $b = 2a$, so $a = l/3$ and $b = 2l/3$

At point A: $M_A = \frac{Pab^2}{l^2} = \frac{4}{27}Pl$

At point B: $M_B = \frac{Pa^2b}{l^2} = \frac{2}{27}Pl$

At point C: $M_C = \frac{2Pa^2b^2}{l^3} = \frac{8}{81}Pl$

and at point D: $M_D = \frac{1}{81}Pl$

If a second load is applied at point C located at $2l/3$, using the superposition principle we obtain the bending moments:

$$M_A = M_B = \frac{2}{9}Pl \ , \ M_C = M_D = \frac{1}{9}Pl$$

So, at the end of Phase I, the first two plastic hinges will appear at the ends of the beam under the loads P_1 applied at points B and C equal to:

Phase 1 : $$P_1 = \frac{9M_p}{2l} = 4.5\frac{M_p}{l}$$

In order to have plastic hinges at points C and D, the additional load P_2 must be applied at points B and C on the beam with hinges at both ends, as shown in Fig. I.2:

Fig.I.2 Additional loads applied in phase 2

The load P_2 is obtained by taking the total moment at points B and C from Phases 1 and 2 equal to M_p of the beam:

Phase 2 $$\frac{P_2 l}{3} = M_p - \frac{P_1 l}{9} = M_p - \frac{M_p}{2} \quad \text{so,} \quad P_2 = 1.5\frac{M_p}{l}$$

The plastic limit load is then, $P = P_1 + P_2 = 6\frac{M_p}{l}$.

For the load P_1 the displacements at points B and C were calculated also using the superposition principle using the formulas:

$$\Delta_{B1} = \Delta_{C1} = \frac{Pa^3b^3}{3EIl^3} + \frac{Pa^2x^2}{6EIl^3}(3bl - 3bx - ax)$$, where $x = b/2$ and $P = P_1$

The additional displacements at points B and C due to the load P_2 were calculated with the formulas:

$$\Delta_{B2} = \Delta_{C2} = \frac{Pa}{6EI}(3lx - 3x_2 - a^2)$$, where $x = a$ and $P = P_2$

The properties of the beam studied are: l = 6000 mm, E = 200000 Mpa, I = 229 x 10^6 mm^4 and M_p = 716.1 kNm. Using these values, the following numerical values were obtained:

Table I.1 Computed plastic loads and associated beam deflections at point B

P_1 (kN)	P_2 (kN)	Δ_{B1} (mm)	Δ_{B2} (mm)	Δ_{Btot} (mm)
537	179	15.62	26.05	41.67

The load-displacement diagram from this plastic analysis is shown in Fig.I.3:

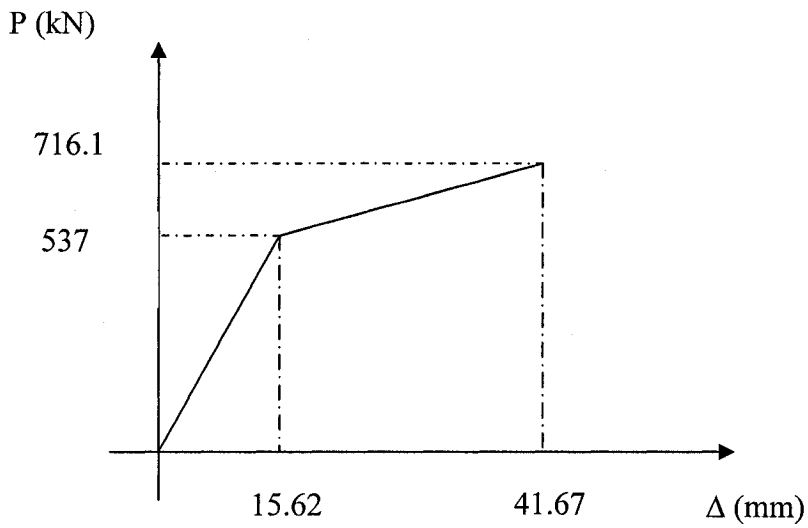

Fig. I.3 Computed load-deflection response (deflection at point B)

APPENDIX II.

U_2 values and interstorey drift values at each floor for all buildings

Table II.1 gives the deflection and P-delta effect parameters produced by the Visual Design program. The values are those obtained from the response spectrum analysis in t the storey height,he last design iteration. In the table, height is the height at the building at each storey, Bx is the ratio maximum storey displacement/the average displacement at level x used to determine the torsional sensitivityof the building, Δmx is the corrected interstorey dieflections in order to take into account the ductility of the structure, θx is the stability factor and $U_2 = 1+ \theta x$ is the amplification factor for taking into account the P-delta effects.

Table II.1 Deflection and P-delta parameters from response spectrum analysis

Building	Height (m)	Bx	Δ mx (mm)	hs (mm)	drift (%)	θx	U_2
2 floors	8.00	1.11	35.24	3800	0.93	0.03	1.03
	4.20	1.10	29.87	4200	0.71	0.04	1.04
	15.60	1.12	24.89	3800	0.65	0.02	1.02
4 floors	11.80	1.12	29.59	3800	0.78	0.04	1.04
	8.00	1.11	33.17	3800	0.87	0.05	1.05
	4.20	1.11	28.37	4200	0.68	0.05	1.05
	30.80	1.13	29.70	3800	0.78	0.04	1.04
	27.00	1.13	33.16	3800	0.87	0.06	1.06
	23.20	1.12	36.27	3800	0.95	0.09	1.09
	19.40	1.12	32.56	3800	0.86	0.10	1.10
8 floors	15.60	1.12	33.42	3800	0.88	0.11	1.11
	11.80	1.12	31.13	3800	0.82	0.11	1.11
	8.00	1.12	32.34	3800	0.85	0.13	1.13
	4.20	1.12	28.00	4200	0.67	0.10	1.10

Table II.1(cont'd) Deflection and P-delta parameters from response spectrum analysis

Building	Height (m)	Bx	Δ mx (mm)	hs (mm)	drift (%)	θx	U_2
	46.00	1.14	31.74	3800	0.84	0.03	1.03
	42.20	1.14	34.84	3800	0.92	0.05	1.05
	38.40	1.14	38.22	3800	1.01	0.07	1.07
	34.60	1.13	36.58	3800	0.96	0.08	1.08
	30.80	1.13	34.85	3800	0.92	0.09	1.09
12 floors	27.00	1.13	28.94	3800	0.76	0.09	1.09
	23.20	1.13	30.61	3800	0.81	0.10	1.10
	19.40	1.12	24.44	3800	0.64	0.09	1.09
	15.60	1.12	24.34	3800	0.64	0.09	1.09
	11.80	1.12	23.40	3800	0.62	0.09	1.09
	8.00	1.12	24.36	3800	0.64	0.09	1.09
	4.20	1.11	19.55	4200	0.47	0.07	1.07
	61.20	1.14	31.45	3800	0.83	0.02	1.02
	57.40	1.14	35.32	3800	0.93	0.04	1.04
	53.60	1.14	37.53	3800	0.99	0.05	1.05
	49.80	1.13	33.88	3800	0.89	0.06	1.06
	46.00	1.13	35.64	3800	0.94	0.07	1.07
	42.20	1.13	33.48	3800	0.88	0.08	1.08
	38.40	1.13	33.19	3800	0.87	0.08	1.08
16 floors	34.60	1.13	28.13	3800	0.74	0.08	1.08
	30.80	1.13	29.00	3800	0.76	0.09	1.09
	27.00	1.12	24.06	3800	0.63	0.07	1.07
	23.20	1.12	23.57	3800	0.62	0.08	1.08
	19.40	1.12	20.99	3800	0.55	0.07	1.07
	15.60	1.12	20.82	3800	0.55	0.07	1.07
	11.80	1.11	18.56	3800	0.49	0.06	1.06
	8.00	1.11	18.76	3800	0.49	0.06	1.06
	4.20	1.11	14.43	4200	0.34	0.04	1.04

APPENDIX III.

Length of the rigid connection at the brace ends

The details of the gusset plate connection at the lower and upper ends of a brace to a beam-to-column joint are given in Fig.III.1.

a)

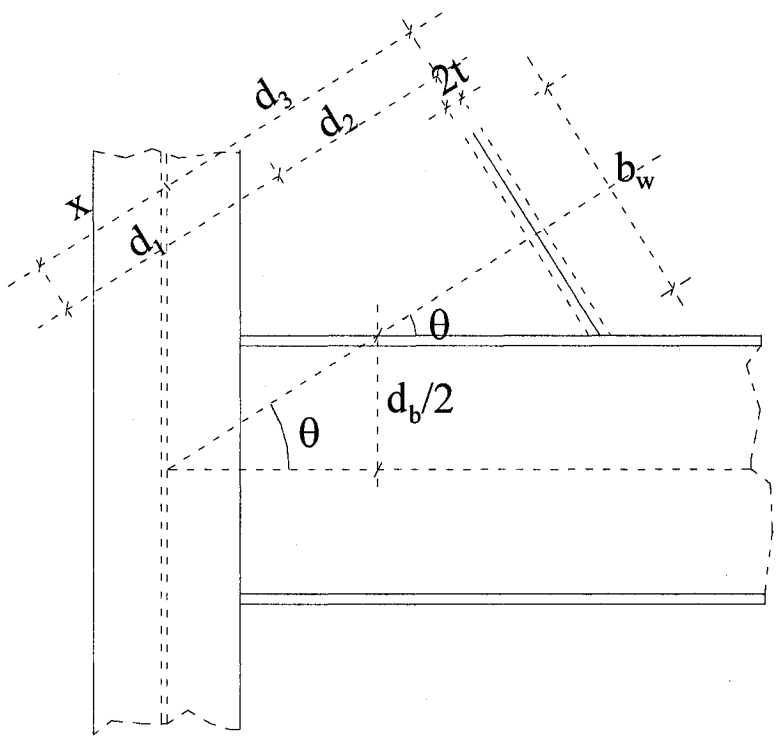

b)

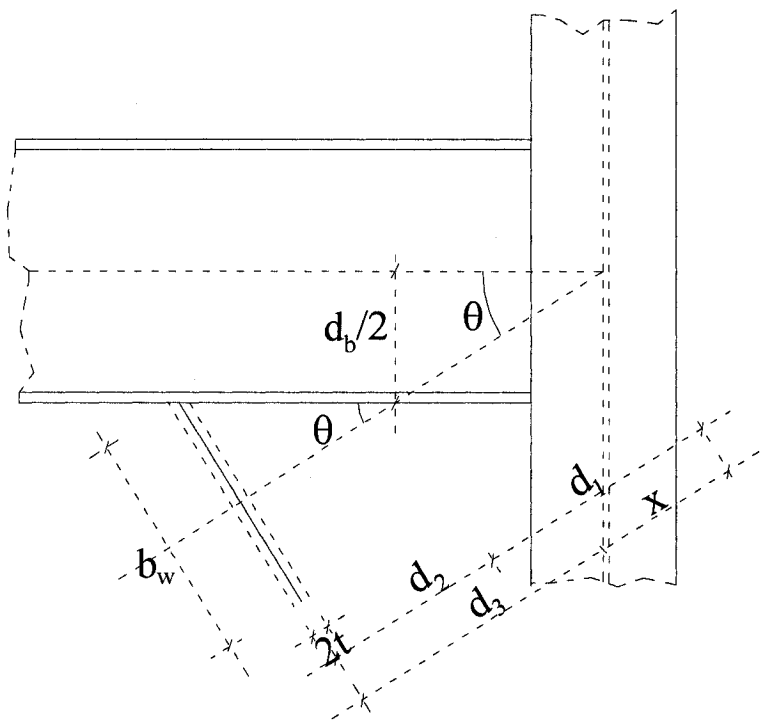

Fig. III.1 Geometry of the brace connections: a) Lower end; b) Upper end.

For the brace connection details of Fig.III.1:

$$\tan\theta = \frac{x}{b_w/2} \rightarrow x = \tan\theta * \frac{b_w}{2}$$

$$\tan\theta = \frac{b_w/2}{d_2} \rightarrow d_2 = \frac{b_w/2}{\tan\theta}$$

$$\text{Assume } b_w = 2 * b_{brace} \rightarrow L_{rigid-zone} = \frac{d_b/2}{\sin\theta} + \frac{b_{brace}}{\tan\theta}$$

$$L_{rigid-zone} = d_1 + d_2$$

$$\sin\theta = \frac{d_b/2}{d_1} \rightarrow d_1 = \frac{d_b/2}{\sin\theta}$$

$$d_3 = L_{rigid-zone} - x$$

The detail of the brace end connection at the base of the bracing bent is shown in Fig. III.2:

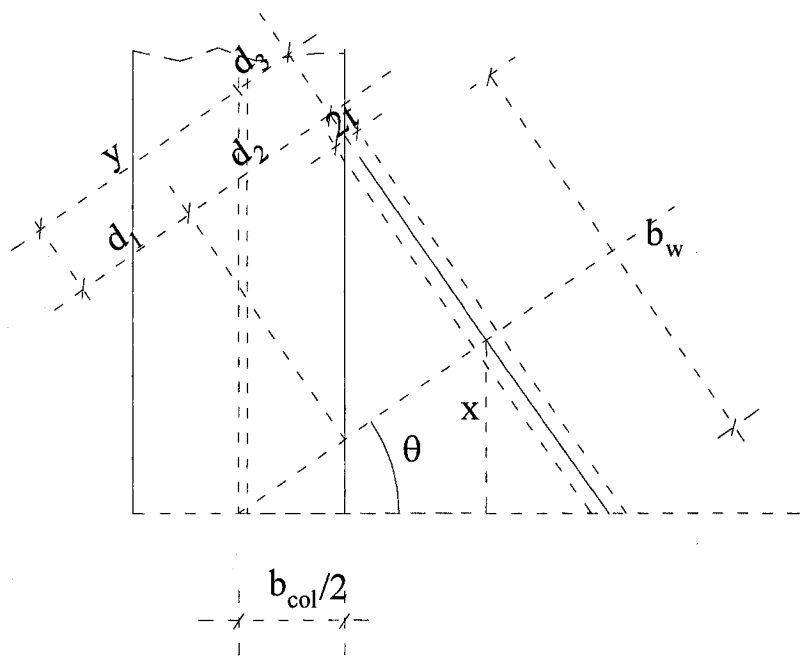

Fig.III.2 Geometry of the brace connection at the base of the bracing bent

For this connection:

$$\cos\theta = \frac{b_{col}/2}{d_1} \rightarrow d_1 = \frac{b_{col}/2}{\cos\theta}$$

$$\sin\theta = \frac{x}{d_1 + d_2} \quad , \quad \cos\theta = \frac{x}{b_w / 2} \quad \rightarrow \quad x = (b_w / 2)\cos\theta$$

$$L_{rigid-zone} = d_1 + d_2 = \frac{x}{\sin\theta} = \frac{b_w}{2} * \frac{\cos\theta}{\sin\theta}$$

$$\tan\theta = \frac{y}{b_w / 2} \quad \rightarrow \quad y = (b_w / 2) * \tan\theta$$

$$d_3 = \frac{b_w / 2}{\tan\theta} - (b_w / 2) * \tan\theta$$

APPENDIX IV.

Gusset plate orientation

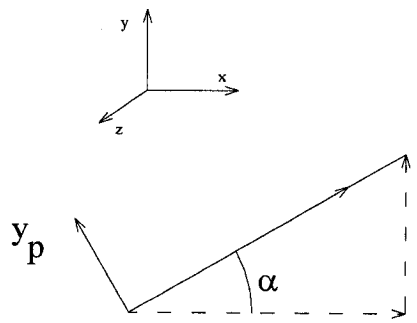

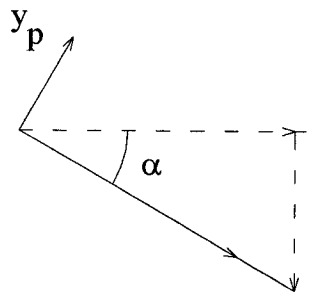

$x1A = \cos\alpha$ (dir. x)

$x2A = \sin\alpha$ (dir. y)

$x3A = 0$ (dir. z)

For y_p the angle is $\left(\frac{\pi}{2}+\alpha\right)$

$y_p1A = \cos\left(\frac{\pi}{2}+\alpha\right) = -\sin\alpha$

$y_p2A = \sin\left(\frac{\pi}{2}+\alpha\right) = \cos\alpha$

$y_p3A = 0$

$x1B = \cos\alpha$ (dir. x)

$x2B = -\sin\alpha$ (dir. y)

$x3B = 0$ (dir. z)

For y_p the angle is $\left(\frac{\pi}{2}-\alpha\right)$

$y_p1B = \cos\left(\frac{\pi}{2}-\alpha\right) = \sin\alpha$

$y_p2B = \sin\left(\frac{\pi}{2}-\alpha\right) = \cos\alpha$

$y_p3B = 0$

APPENDIX V.

Geometries and stiffness of the gusset plates

The factored resistance of the gusset plate in tension $T_r = \phi F_y b_w t$ should exceed the capacity in tension of the brace $P_{y\ brace} = AR_yF_y \rightarrow$ The gusset plate thickness from tension $t = \frac{P_{y\_brace}}{\phi b_w F_y}$. In this expression b_w is the Whitmore length and F_y = 345 Mpa.

The factored resistance in compression of the gusset plate $C_r = \phi A F_y (1 + \lambda^{2n})^{-1/n}$ must exceed the expected capacity in compression of the brace $P_{max} = 1.2C_u$ (see Tables 5.2.1 to 5.2.5), where $\lambda = \frac{KL_c}{r}\sqrt{\frac{F_y}{\pi^2 E}}$, K = 1.2, L_c is the length of the gusset plate equivalent columns $L_c = \frac{L_1 + L_2 + L_3}{3}$, $A = b_w t$; $I = \frac{b_w t^3}{12}$ and $r = \frac{I}{A} = \frac{t}{\sqrt{12}}$

Therefore, the gusset plate resistance in compression is given by the formula:

$$C_r = \phi b_w t F_y \left[1 + \left(\frac{KL_c}{t}\sqrt{\frac{F_y * 12}{\pi^2 E}}\right)^{2*1.34}\right]^{-1/1.34}$$

The gusset plate thickness for compression resistance was obtained by equalizing the capacities in compression of the brace and of the gusset plate. The largest value of t from the tension and compression was taken as the final gusset plate thickness.

Numerical values for the length of the rigid end connections, the gusset plate dimensions and stiffness for all the studied buildings are given in the Tables V.1 to V.15.

In the tables:

alpha is a parameter equal to

B is half of the bracing bent width

H is the storey height

d beam is the beam cross-section height

b brace is the width of the brace cross-section

b column is the column flange width

bwhitmore is the Whitmore effective width presented in Fig. 5.2.3

d2 and d3 are the dimensions mentioned in Appendix III, Fig. III.1 to III.3

t is the gusset plate thickness

Lnonsupmoy is the length of the gusset plate equivalent columns

B1c_up is the length of the rigid extension at the upper end of the brace

B1c_low is the length of the rigid extension at the lower end of the brace

LBrace is the theoretical length of the brace (o/c)

Effec length is the brace length between the hinge lines in the gusset plates

Cf and Ct are the out-of-plane bending stiffness and torsional stiffness of the gusset plates

Mp is the flexural capacity of the gusset plates

Table V.1. The length of the rigid connections at the brace ends 2-storey building

alpha 2

	2nd-up	2nd-down	1st-up	1st-down
B	6000	6000	6000	6000
H	3800	3800	4200	4200
theta	0.56	0.56	0.61	0.61
sin theta	0.54	0.54	0.57	0.57
cos theta				0.82
tg theta	0.63	0.63	0.70	0.70
d beam	306.00	357.00	357.00	
b brace	254.00	254.00	372.00	372.00
b column				308.00
bwhitmore	**508.00**	**508.00**	**744.00**	**744.00**
d2	**401.05**	**401.05**	**531.43**	**343.45**
d3	**526.14**	**573.80**	**582.30**	**271.03**
t	**33.00**	**33.00**	**42.00**	**42.00**
Lnonsupmoy	**320.06**	**335.95**	**385.24**	**218.83**
B1c_up	**687.01**		**842.70**	
B1c_low		**734.67**		**531.43**

LBrace		7102.11	7323.93
Effec length		5680.44	5949.81

E (N/mm2)	200000
Fy (N/mm2)	345
G N/mm2)	76923.0769
Φ	0.9
K	1.2

Table V.2. The gusset plates dimensions 2-storey building

	2nd	1st	1stdown
1.2Cu (N)	4004000	7083000	7083000
bw (mm)	508.00	744.00	744.00
Lnonsupmoy	335.95	385.24	218.83
Cr(form)	4004000	7083000	7083000
t (mm)	**30.27**	**36.02**	**32.27**
Cr(form)-Cr	0.00	0.00	0.00
RyAFy (N)	5161000	9488000	
t (mm)	**32.72**	**41.07**	
Max(t)	**32.72**	**41.07**	
t (mm)	**33.00**	**42.00**	

Table V.3. The gusset plates rigidities 2-storey building

	2nd	1st
2*t	66	84
5*t	165	210
I (mm^4)	1521333	4593456
Cf (kNm)	**6915.15**	**16405.2**
6*t	198	252
J (mm^4)	6085332	18373824
Ct(kNm)	**7092.46154**	**16825.846**

Mp (kNm)	**52.4859885**	**124.51547**

Table V.4. The length of the rigid connections at the brace ends 4-storey building

alpha 2

	4th-up	4th-down	3rd-up	3rd-down	2nd-up	2nd-down	1st-up	1st-down
B	6000	6000	6000	6000	6000	6000	6000	6000
H	3800	3800	3800	3800	3800	3800	4200	4200
theta	0.56	0.56	0.56	0.56	0.56	0.56	0.61	0.61
sin theta	0.54	0.54	0.54	0.54	0.54	0.54	0.57	0.57
cos theta								0.82
tg theta	0.63	0.63	0.63	0.63	0.63	0.63	0.70	0.70
d beam	313.00	318.00	318.00	463.00	463.00	313.00	313.00	
b brace	178.00	178.00	203.00	203.00	254.00	254.00	254.00	254.00
b column								394.00
bwhitmore	**356.00**	**356.00**	**406.00**	**406.00**	**508.00**	**508.00**	**508.00**	**508.00**
d2	**281.05**	**281.05**	**320.53**	**320.53**	**401.05**	**401.05**	**362.86**	**122.39**
d3	**460.81**	**465.49**	**489.13**	**304.10**	**672.85**	**131.63**	**457.96**	**185.06**
t	**26.00**	**26.00**	**32.00**	**32.00**	**28.00**	**28.00**	**34.00**	**34.00**
Lnonsupmoy	**255.96**	**257.51**	**280.55**	**218.88**	**367.30**	**186.89**	**284.94**	**113.82**
B1c_up	**573.55**		**617.69**		**833.72**		**635.76**	
B1c_low		**578.22**		**432.67**		**292.49**		**362.86**

LBrace		7102.1124	7102.1124	7102.112	7323.93337
Effec length		5950.3449	6051.7506	5975.897	6325.31538

E (N/mm2)	200000
Fy (N/mm2)	345
G N/mm2)	76923.077
Φ	0.9
K	1.2

Table V.5. The gusset plates dimensions 4-storey building

	4th	3rd	2nd	1st	1stdown
1.2 Cu (N)	1107000	2425000	3313000	3894000	3894000
bw (mm)	356.00	406.00	508.00	508.00	381.00
Lnonsupmoy	257.51	280.55	367.30	284.94	113.82
Cr(form)	1107000	2425000	3313000	3894000	3894000
t (mm)	**15.46**	**23.64**	**27.52**	**28.35**	**33.20**
Cr(form)-Cr	0.00	0.00	0.00	0.00	0.00
λRyAFy (N)	2869000	4023000	4212000	5161000	
t (mm)	**25.95**	**31.91**	**26.70**	**32.72**	
Max(t)	**25.95**	**31.91**	**27.52**	**33.20**	
t (mm)	**26.00**	**32.00**	**28.00**	**34.00**	

Table V.6. The gusset plates rigidities 4-storey building

	4th	3rd	2nd	1st
2*t	52	64	56	68
5*t	130	160	140	170
I (mm^4)	521421.33	1108650.7	929301.33	1663869.3
Cf (kNm)	**3008.2**	**5196.8**	**4978.4**	**7340.6**
6*t	156	192	168	204
J (mm^4)	2085685.3	4434602.7	3717205.3	6655477.3
Ct(kNm)	**3085.3333**	**5330.0513**	**5106.0513**	**7528.8205**

Mp (kNm)	**22.832238**	**39.443712**	**37.786056**	**55.715154**

Table V.7. The length of the rigid connections at the brace ends 8-storey building

alpha 2

	8th-up	8th-down	7th-up	7th-down	6th-up	6th-down	5th-up	5th-down	4th-up	4th-down
B	6000	6000	6000	6000	6000	6000	6000	6000	6000	6000
H	3800	3800	3800	3800	3800	3800	3800	3800	3800	3800
theta	0.56	0.56	0.56	0.56	0.56	0.56	0.56	0.56	0.56	0.56
sin theta	0.54	0.54	0.54	0.54	0.54	0.54	0.54	0.54	0.54	0.54
cos theta										
tg theta	0.63	0.63	0.63	0.63	0.63	0.63	0.63	0.63	0.63	0.63
d beam	313.00	313.00	313.00	413.00	413.00	205.00	205.00	463.00	463.00	205.00
b brace	178.00	178.00	203.00	203.00	203.00	203.00	203.00	203.00	203.00	203.00
b column										
bwhitmore	**356.00**	**356.00**	**406.00**	**406.00**	**406.00**	**406.00**	**406.00**	**406.00**	**406.00**	**406.00**
d2	**281.05**	**281.05**	**320.53**	**320.53**	**320.53**	**320.53**	**320.53**	**320.53**	**320.53**	**320.53**
d3	**460.81**	**460.81**	**484.45**	**577.90**	**577.90**	**383.53**	**383.53**	**624.63**	**624.63**	**383.53**
t	**26.00**	**26.00**	**28.00**	**28.00**	**27.00**	**27.00**	**32.00**	**32.00**	**32.00**	**32.00**
Lnonsupmoy	**255.96**	**255.96**	**277.66**	**308.81**	**308.48**	**243.69**	**245.35**	**325.72**	**325.72**	**245.35**
B1c_up	**573.55**		**613.02**		**706.47**		**512.10**		**753.19**	
B1c_low		**573.55**		**706.47**		**512.10**		**753.19**		**512.10**

LBrace	7102.11	7102.11	7102.11	7102.11	7102.11
Effec length	5955.02	5782.62	5883.55	5836.82	5836.82

E (N/mm2)	200000
Fy (N/mm2)	345
G N/mm2)	76923.1
Φ	0.9
K	1.2

Table V.7.(cont'd) **The length of the rigid connections at the brace ends 8-storey building**

	3rd-up	3rd-down	2nd-up	2nd-down	1st-up	1st-down
B	6000	6000	6000	6000	6000	6000
H	3800	3800	3800	3800	4200	4200
theta	0.56	0.56	0.56	0.56	0.61	0.61
sin theta	0.54	0.54	0.54	0.54	0.57	0.57
cos theta						0.82
tg theta	0.63	0.63	0.63	0.63	0.70	0.70
d beam	205.00	466.00	466.00	257.00	257.00	
b brace	254.00	254.00	254.00	254.00	254.00	254.00
b column						416.00
bwhitmore	**508.00**	**508.00**	**508.00**	**508.00**	**508.00**	**508.00**
d2	**401.05**	**401.05**	**401.05**	**401.05**	**362.86**	**108.96**
d3	**431.76**	**675.66**	**675.66**	**480.35**	**409.13**	**185.06**
t	**28.00**	**28.00**	**28.00**	**28.00**	**27.00**	**27.00**
Lnonsupmoy	**286.94**	**368.24**	**368.24**	**303.13**	**266.33**	**107.01**
B1c_up	**592.62**		**836.52**		**586.93**	
B1c_low		**836.52**		**641.22**		**362.86**

LBrace	7102.11	7102.11	7323.93
Effec length	5672.97	5624.37	6374.14

Table V.8. **The gusset plates dimensions 8-storey building**

	8th	7th	6th	5th	4th	3rd	2nd	1st	1stdown
1.2 Cu (N)	1107000	1713000	2030000	2425000	2425000	3313000	3E+06	3224000	3224000
bwhitmore (mm)	356.00	406.00	406.00	406.00	406.00	508.00	508.00	508.00	508.00
Lnonsupmoy	**255.96**	**308.81**	**308.48**	**325.72**	**325.72**	**368.24**	**368.24**	**266.33**	**107.01**
Cr(form)	1107000	1713000	2030000	2425000	2425000	3313000	3E+06	3224000	3224000
t (mm)	**15.42**	**19.83**	**21.86**	**24.90**	**24.90**	**27.54**	**27.54**	**24.26**	**20.94**
Cr(form)-Cr	0.00	0.00	0.00	0.00	0.00	0.00	0.00	0.00	0.00
λRyAFy (N)	2869000	3438000	3294000	4023000	4023000	4212000	4E+06	4212000	
t (mm)	**25.95**	**27.27**	**26.13**	**31.91**	**31.91**	**26.70**	**26.70**	**26.70**	
Max(t)	25.95	27.27	26.13	31.91	31.91	27.54	27.54	26.70	
t (mm)	**26.00**	**28.00**	**27.00**	**32.00**	**32.00**	**28.00**	**28.00**	**27.00**	

Table V.9. **The gusset plates rigidities 8-storey building**

	8th	7th	6th	5th	4th	3rd	2nd	1st
2*t	52.00	56.00	54.00	64.00	64.00	56.00	56.00	54.00
5*t	130.00	140.00	135.00	160.00	160.00	140.00	140.00	135.00
I (mm^4)	521421	742709	665942	1108651	1108651	929301	929301	833247
Cf (kNm)	**3008.20**	**3978.80**	**3699.68**	**5196.80**	**5196.80**	**4978.40**	**4978.40**	**4629.15**
6*t	156.00	168.00	162.00	192.00	192.00	168.00	168.00	162.00
J (mm^4)	2085685	2970837	2663766	4434603	4434603	3717205	4E+06	3332988
Ct(kNm)	**3085.33**	**4080.82**	**3794.54**	**5330.05**	**5330.05**	**5106.05**	**5106.05**	**4747.85**

Mp (kNm)	**22.8322**	**30.1991**	**28.0805**	**39.4437**	**39.4437**	**37.7861**	**37.786**	**35.1352**

Table V.10. **The length of the rigid connections at the brace ends 12-storey building**

alpha **2**

	12th-up	12th-down	11th-up	11th-down	10th-up	10th-down	9th-up	9th-down	8th-up	8th-down	7th-up	7th-down
B	6000	6000	6000	6000	6000	6000	6000	6000	6000	6000	6000	6000
H	3800	3800	3800	3800	3800	3800	3800	3800	3800	3800	3800	3800
theta	0.56	0.56	0.56	0.56	0.56	0.56	0.56	0.56	0.56	0.56	0.56	0.56
sin theta	0.54	0.54	0.54	0.54	0.54	0.54	0.54	0.54	0.54	0.54	0.54	0.54
cos theta												
tg theta	0.63	0.63	0.63	0.63	0.63	0.63	0.63	0.63	0.63	0.63	0.63	0.63
d beam	313.00	313.00	313.00	463.00	463.00	257.00	257.00	466.00	466.00	266.00	266.00	466.00
b brace	178.00	178.00	203.00	203.00	254.00	254.00	254.00	254.00	254.00	254.00	254.00	254.00
b column												
bwhitmore	**356.00**	**356.00**	**406.00**	**406.00**	**508.00**	**508.00**	**508.00**	**508.00**	**508.00**	**508.00**	**508.00**	**508.00**
d2	**281.05**	**281.05**	**320.53**	**320.53**	**401.05**	**401.05**	**401.05**	**401.05**	**401.05**	**401.05**	**401.05**	**401.05**
d3	**460.81**	**460.81**	**484.45**	**624.63**	**672.85**	**480.35**	**480.35**	**675.66**	**675.66**	**488.76**	**488.76**	**675.66**
t	**26.00**	**26.00**	**32.00**	**32.00**	**28.00**	**28.00**	**28.00**	**28.00**	**28.00**	**28.00**	**33.00**	**33.00**
Lnonsupmoy	**255.96**	**255.96**	**278.99**	**325.72**	**367.30**	**303.13**	**303.13**	**368.24**	**368.24**	**305.94**	**307.60**	**369.90**
B1c_up	**573.55**		**613.02**		**833.72**		**641.22**		**836.52**		**649.63**	
B1c_low		**573.55**		**753.19**		**641.22**		**836.52**		**649.63**		**836.52**

LBrace	7102.11	7102.11	7102.11	7102.11	7102.11	7102.11	
Effec length	5955.02	5735.90	5627.18	5624.37	5615.96	5615.96	

E (N/mm2)	200000
Fy (N/mm2)	345
G N/mm2)	76923.1
Φ	0.9
K	1.2

Table V.10. (cont'd) **The length of the rigid connections at the brace ends 12-storey building**

alpha **2**

	6th-up	6th-down	5th-up	5th-down	4th-up	4th-down	3rd-up	3rd-down	2nd-up	2nd-down	1st-up	1st-down
B	6000	6000	6000	6000	6000	6000	6000	6000	6000	6000	6000	6000
H	3800	3800	3800	3800	3800	3800	3800	3800	3800	3800	4200	4200
theta	0.56	0.56	0.56	0.56	0.56	0.56	0.56	0.56	0.56	0.56	0.61	0.61
sin theta	0.54	0.54	0.54	0.54	0.54	0.54	0.54	0.54	0.54	0.54	0.57	0.57
cos theta												0.82
tg theta	0.63	0.63	0.63	0.63	0.63	0.63	0.63	0.63	0.63	0.63	0.70	0.70
d beam	466.00	350.00	350.00	544.00	544.00	257.00	257.00	544.00	544.00	257.00	257.00	
b brace	254.00	254.00	305.00	305.00	305.00	305.00	305.00	305.00	305.00	305.00	305.00	305.00
b column												448.00
bwhitmore	**508.00**	**508.00**	**610.00**	**610.00**	**610.00**	**610.00**	**610.00**	**610.00**	**610.00**	**610.00**	**610.00**	**610.00**
b2	**401.05**	**401.05**	**481.58**	**481.58**	**481.58**	**481.58**	**481.58**	**481.58**	**481.58**	**481.58**	**435.71**	**162.29**
b3	**675.66**	**567.26**	**615.48**	**796.77**	**796.77**	**528.58**	**528.58**	**796.77**	**796.77**	**528.58**	**446.29**	**222.21**
t	**28.00**	**28.00**	**37.00**	**37.00**	**37.00**	**37.00**	**37.00**	**37.00**	**37.00**	**37.00**	**34.00**	**34.00**
Lnonsupmoy	**368.24**	**332.10**	**378.02**	**438.45**	**438.45**	**349.05**	**349.05**	**438.45**	**438.45**	**349.05**	**305.34**	**139.50**
B1c_up	**836.52**		**808.65**		**989.94**		**721.74**		**989.94**		**659.79**	
B1c_low		**728.12**		**989.94**		**721.74**		**989.94**		**721.74**		**435.71**

LBrace	7102.11	7102.11	7102.11	7102.11	7102.11	7323.93
Effec length	5537.46	5303.52	5390.43	5390.43	5390.43	6228.43

Table V.11. The gusset plates dimensions 12-storey building

	12th	11th	10th	9th	8th	7th	6th	5th	4th
1.2 Cu (N)	1455000	2425000	3313000	3313000	3313000	4004000	3313000	5656000	5656000
bwhitm (mm)	356.00	406.00	508.00	508.00	508.00	508.00	508.00	610.00	610.00
Lnonsupm	**255.96**	**325.72**	**367.30**	**368.24**	**368.24**	**369.90**	**368.24**	**438.45**	**438.45**
Cr(form)	1455000	2425000	3313000	3313000	3313000	4004000	3313000	5656000	5656000
t (mm)	**17.98**	**24.90**	**27.52**	**27.54**	**27.54**	**31.19**	**27.54**	**36.78**	**36.78**
Cr(form)-Cr	0.00	0.00	0.00	0.00	0.00	0.00	0.00	0.00	0.00
RyAFy (N)	2839000	4023000	4212000	4212000	4212000	5161000	4212000	6300000	6300000
t (mm)	**25.68**	**31.91**	**26.70**	**26.70**	**26.70**	**32.72**	**26.70**	**33.26**	**33.26**
Max(t)	25.68	31.91	27.52	27.54	27.54	32.72	27.54	36.78	36.78
t (mm)	**26.00**	**32.00**	**28.00**	**28.00**	**28.00**	**33.00**	**28.00**	**37.00**	**37.00**

Table V.12. The gusset plates rigidities 12-storey building

	12th	11th	10th	9th	8th	7th	6th	5th	4th
2*t	52.00	64.00	56.00	56.00	56.00	66.00	56.00	74.00	74.00
5*t	130.00	160.00	140.00	140.00	140.00	165.00	140.00	185.00	185.00
I (mm^4)	521421	1108651	929301	929301	929301.3	1521333	929301	2574861	2574861
Cf (kNm)	**3008.20**	**5196.80**	**4978.40**	**4978.40**	**4978.40**	**6915.15**	**4978.40**	**10438.63**	**10438.63**
6*t	156.00	192.00	168.00	168.00	168.00	198.00	168.00	222.00	222.00
J (mm^4)	2085685	4434603	3717205	3717205	3717205	6085332	3717205	10299443	10299443
Ct(kNm)	**3085.33**	**5330.05**	**5106.05**	**5106.05**	**5106.05**	**7092.46**	**5106.05**	**10706.28**	**10706.28**
Mp (kNm)	**22.83**	**39.44**	**37.79**	**37.79**	**37.79**	**52.49**	**37.79**	**79.23**	**79.23**

Table V.11.(cont'd) **The gusset plates dimensions 12-storey building**

	3rd	2nd	1st	1stdown
1.2 Cu (N)	5656000	5656000	5542000	5542000
bwhitm (mm)	610.00	610.00	610.00	610.00
Lnonsupm	**438.45**	**438.45**	**305.34**	**139.50**
Cr(form)	5656000	5656000	5542000	5542000
t (mm)	**36.78**	**36.78**	**32.81**	**29.83**
Cr(form)-Cr	0.00	0.00	0.00	0.00
RyAFy (N)	6300000	6300000	6300000	
t (mm)	**33.26**	**33.26**	**33.26**	
Max(t)	36.78	36.78	33.26	
t (mm)	**37.00**	**37.00**	**34.00**	

Table V.12.(cont'd) **The gusset plates rigidities 12-storey building**

	3rd	2nd	1st
2*t	74.00	74.00	68.00
5*t	185.00	185.00	170.00
I (mm^4)	2574860.8	2574860.8	1997953.3
Cf (kNm)	**10438.63**	**10438.63**	**8814.50**
6*t	222.00	222.00	204.00
J (mm^4)	10299443	10299443	7991813.3
Ct(kNm)	**10706.28**	**10706.28**	**9040.51**

Mp (kNm)	**79.23**	**79.23**	**66.90**

Table V.13. The length of the rigid connections at the brace ends 16-storey building

alpha **2**

	16th-up	16th-down	15th-up	15th-down	14th-up	14th-down	13th-up	13th-down	12th-up	12th-down
B	6000	6000	6000	6000	6000	6000	6000	6000	6000	6000
H	3800	3800	3800	3800	3800	3800	3800	3800	3800	3800
theta	0.56	0.56	0.56	0.56	0.56	0.56	0.56	0.56	0.56	0.56
sin theta	0.54	0.54	0.54	0.54	0.54	0.54	0.54	0.54	0.54	0.54
cos theta										
tg theta	0.63	0.63	0.63	0.63	0.63	0.63	0.63	0.63	0.63	0.63
d beam	313.00	358.00	358.00	466.00	466.00	350.00	350.00	544.00	544.00	305.00
b brace	178.00	178.00	254.00	254.00	254.00	254.00	305.00	305.00	305.00	305.00
b column										
bwhitmore	**356.00**	**356.00**	**508.00**	**508.00**	**508.00**	**508.00**	**610.00**	**610.00**	**610.00**	**610.00**
d2	**281.05**	**281.05**	**401.05**	**401.05**	**401.05**	**401.05**	**481.58**	**481.58**	**481.58**	**481.58**
d3	**460.81**	**502.87**	**574.73**	**675.66**	**675.66**	**567.26**	**615.48**	**796.77**	**796.77**	**573.43**
t	**18.30**	**18.30**	**27.54**	**27.54**	**27.54**	**27.54**	**36.78**	**36.78**	**37.00**	**37.00**
Lnonsupmoy	**253.39**	**267.41**	**334.44**	**368.08**	**368.08**	**331.95**	**377.95**	**438.38**	**438.45**	**364.00**
B1c_up	**573.55**		**735.60**		**836.52**		**808.65**		**989.94**	
B1c_low		**615.60**		**836.52**		**728.12**		**989.94**		**766.60**

LBrace	7102.11	7102.11	7102.11	7102.11	7102.11
Effec length	5912.97	5529.99	5537.46	5303.52	5345.57

E (N/mm2)	200000
Fy (N/mm2)	345
G N/mm2)	76923.077
Φ	0.9
K	1.2

Table V.13.(cont'd) **The length of the rigid connections at the brace ends 16-storey building**

alpha **2**

	11th-up	11th-down	10th-up	10th-down	9th-up	9th-down	8th-up	8th-down	7th-up	7th-down	6th-up	6th-down
B	6000	6000	6000	6000	6000	6000	6000	6000	6000	6000	6000	6000
H	3800	3800	3800	3800	3800	3800	3800	3800	3800	3800	3800	3800
theta	0.56	0.56	0.56	0.56	0.56	0.56	0.56	0.56	0.56	0.56	0.56	0.56
sin theta	0.54	0.54	0.54	0.54	0.54	0.54	0.54	0.54	0.54	0.54	0.54	0.54
cos theta												
tg theta	0.63	0.63	0.63	0.63	0.63	0.63	0.63	0.63	0.63	0.63	0.63	0.63
d beam	305.00	544.00	544.00	358.00	358.00	472.00	472.00	358.00	358.00	546.00	546.00	305.00
b brace	305.00	305.00	305.00	305.00	373.00	373.00	305.00	305.00	373.00	373.00	373.00	373.00
b column												
bwhitmore	**610.00**	**610.00**	**610.00**	**610.00**	**746.00**	**746.00**	**610.00**	**610.00**	**746.00**	**746.00**	**746.00**	**746.00**
d2	**481.58**	**481.58**	**481.58**	**481.58**	**588.95**	**588.95**	**481.58**	**481.58**	**588.95**	**588.95**	**588.95**	**588.95**
d3	**573.43**	**796.77**	**796.77**	**622.96**	**687.26**	**793.79**	**729.49**	**622.96**	**687.26**	**862.94**	**862.94**	**637.73**
t	**37.00**	**37.00**	**37.00**	**37.00**	**38.00**	**38.00**	**37.00**	**37.00**	**38.00**	**38.00**	**38.00**	**38.00**
Lnonsupmoy	**364.00**	**438.45**	**438.45**	**380.51**	**438.07**	**473.58**	**416.02**	**380.51**	**438.07**	**496.63**	**496.63**	**421.56**
B1c_up	**766.60**		**989.94**		**923.49**		**922.66**		**923.49**		**1099.18**	
B1c_low		**989.94**		**816.13**		**1030.03**		**816.13**		**1099.18**		**873.97**

LBrace	7102.11	7102.11	7102.11	7102.11	7102.11	7102.11
Effec length	5345.57	5296.05	5148.59	5363.33	5079.44	5128.97

Table V.13.(cont'd) **The length of the rigid connections at the brace ends 16-storey building**

alpha **2**

	5th-up	5th-down	4th-up	4th-down	3rd-up	3rd-down	2nd-up	2nd-down	1st-up	1st-down
B	6000	6000	6000	6000	6000	6000	6000	6000	6000	6000
H	3800	3800	3800	3800	3800	3800	3800	3800	4200	4200
theta	0.56	0.56	0.56	0.56	0.56	0.56	0.56	0.56	0.61	0.61
sin theta	0.54	0.54	0.54	0.54	0.54	0.54	0.54	0.54	0.57	0.57
cos theta										0.82
tg theta	0.63	0.63	0.63	0.63	0.63	0.63	0.63	0.63	0.70	0.70
d beam	305.00	482.00	482.00	262.00	262.00	489.00	489.00	305.00	305.00	
b brace	374.00	374.00	374.00	374.00	394.00	394.00	394.00	394.00	394.00	394.00
b column										500.00
bwhitmore	**748.00**	**748.00**	**748.00**	**748.00**	**788.00**	**788.00**	**788.00**	**788.00**	**788.00**	**788.00**
d2	**590.53**	**590.53**	**590.53**	**590.53**	**622.11**	**622.11**	**622.11**	**622.11**	**562.86**	**257.69**
d3	**638.68**	**804.08**	**804.08**	**598.50**	**617.41**	**829.54**	**829.54**	**657.59**	**552.99**	**287.06**
t	**41.00**	**41.00**	**41.00**	**41.00**	**43.00**	**43.00**	**43.00**	**43.00**	**43.00**	**43.00**
Lnonsupmoy	**423.40**	**478.54**	**478.54**	**410.01**	**427.50**	**498.21**	**498.21**	**440.90**	**386.28**	**195.92**
B1c_up	**875.55**		**1040.95**		**866.94**		**1079.07**		**828.79**	
B1c_low		**1040.95**		**835.36**		**1079.07**		**907.12**		**562.86**

LBrace	7102.11	7102.11	7102.11	7102.11	7323.93
Effec length	5185.62	5225.80	5156.10	5115.92	5932.29

Table V.14. The gusset plates dimensions 16-storey building

	16th	15th	14th	13th	12th	11th	10th	9th
1.2 Cu (N)	1455000	3313000	3313000	5656000	5656000	5656000	5656000	6620000
bwhitmore (mm)	356.00	508.00	508.00	610.00	610.00	610.00	610.00	746.00
Lnonsupmoy	**267.41**	**368.08**	**368.08**	**438.38**	**438.45**	**438.45**	**438.45**	**473.58**
Cr(form)	1455000	3313000	3313000	5656000	5656000	5656000	5656000	6620000
t (mm)	**18.30**	**27.54**	**27.54**	**36.78**	**36.78**	**36.78**	**36.78**	**36.70**
Cr(form)-Cr	0.00	0.00	0.00	0.00	0.00	0.00	0.00	0.00
RyAFy (N)	2839000	4212000	4212000	6300000	6300000	6300000	6300000	8653000
t (mm)	**25.68**	**26.70**	**26.70**	**33.26**	**33.26**	**33.26**	**33.26**	**37.36**
Max(t)	25.68	27.54	27.54	36.78	36.78	36.78	36.78	37.36
t (mm)	**26.00**	**28.00**	**28.00**	**37.00**	**37.00**	**37.00**	**37.00**	**38.00**

Table V.15. The gusset plates rigidities 16-storey building

	16th	15th	14th	13th	12th	11th	10th	9th
2*t	52.00	56.00	56.00	74.00	74.00	74.00	74.00	76.00
5*t	130.00	140.00	140.00	185.00	185.00	185.00	185.00	190.00
I (mm^4)	521421	929301	929301	2574861	2574861	2574861	2574860.8	3411209
Cf (kNm)	**3008.20**	**4978.40**	**4978.40**	**10438.63**	**10438.63**	**10438.63**	**10438.63**	**13465.30**
6*t	156.00	168.00	168.00	222.00	222.00	222.00	222.00	228.00
J (mm^4)	2085685	3717205	3717205	10299443	10299443	10299443	10299443	13644837
Ct(kNm)	**3085.33**	**5106.05**	**5106.05**	**10706.28**	**10706.28**	**10706.28**	**10706.28**	**13810.56**

Mp (kNm)	**22.83**	**37.79**	**37.79**	**79.23**	**79.23**	**79.23**	**79.23**	**102.20**

Table V.14.(cont'd) **The gusset plates dimensions 16-storey building**

	8th	7th	6th	5th	4th	3rd	2nd	1st	1stdown
1.2 Cu (N)	5656000	6620000	6620000	7286000	7286000	8412000	8412000	8412000	
bwhitmore (mm)	610.00	746.00	746.00	748.00	748.00	788.00	788.00	788.00	788.00
Lnonsupmoy	**416.02**	**496.63**	**496.63**	**478.54**	**478.54**	**498.21**	**498.21**	**386.28**	**195.92**
Cr(form)	5656000	6620000	6620000	7286000	7286000	8412000	8412000	8412000	0.000996
t (mm)	**36.17**	**37.35**	**37.35**	**39.13**	**39.13**	**42.16**	**42.16**	**39.22**	**0.01**
Cr(form)-Cr	0.00	0.00	0.00	0.00	0.00	0.00	0.00	0.00	0.00
RyAFy (N)	6300000	8653000	8653000	9488000	9488000	10436000	10436000	10436000	
t (mm)	**33.26**	**37.36**	**37.36**	**40.85**	**40.85**	**42.65**	**42.65**	**42.65**	
Max(t)	36.17	37.36	37.36	40.85	40.85	42.65	42.65	42.65	
t (mm)	**37.00**	**38.00**	**38.00**	**41.00**	**41.00**	**43.00**	**43.00**	**43.00**	

Table V.15.(cont'd) **The gusset plates rigidities 16-storey building**

	8th	7th	6th	5th	4th	3rd	2nd	1st
2*t	74.00	76.00	76.00	82.00	82.00	86.00	86.00	86.00
5*t	185.00	190.00	190.00	205.00	205.00	215.00	215.00	215.00
I (mm^4)	2574861	3411209.3	3411209.3	4296075.7	4296075.7	5220959.7	5220960	5220959.7
Cf (kNm)	**10438.63**	**13465.30**	**13465.30**	**15717.35**	**15717.35**	**18212.65**	**18212.65**	**18212.65**
6*t	222.00	228.00	228.00	246.00	246.00	258.00	258.00	258.00
J (mm^4)	10299443	13644837	13644837	17184303	17184303	20883839	20883839	20883839
Ct(kNm)	**10706.28**	**13810.56**	**13810.56**	**16120.36**	**16120.36**	**18679.64**	**18679.64**	**18679.64**

Mp (kNm)	**79.23**	**102.20**	**102.20**	**119.29**	**119.29**	**138.23**	**138.23**	**138.23**

APPENDIX VI.

Flexural stiffness of the gravity column splice connection

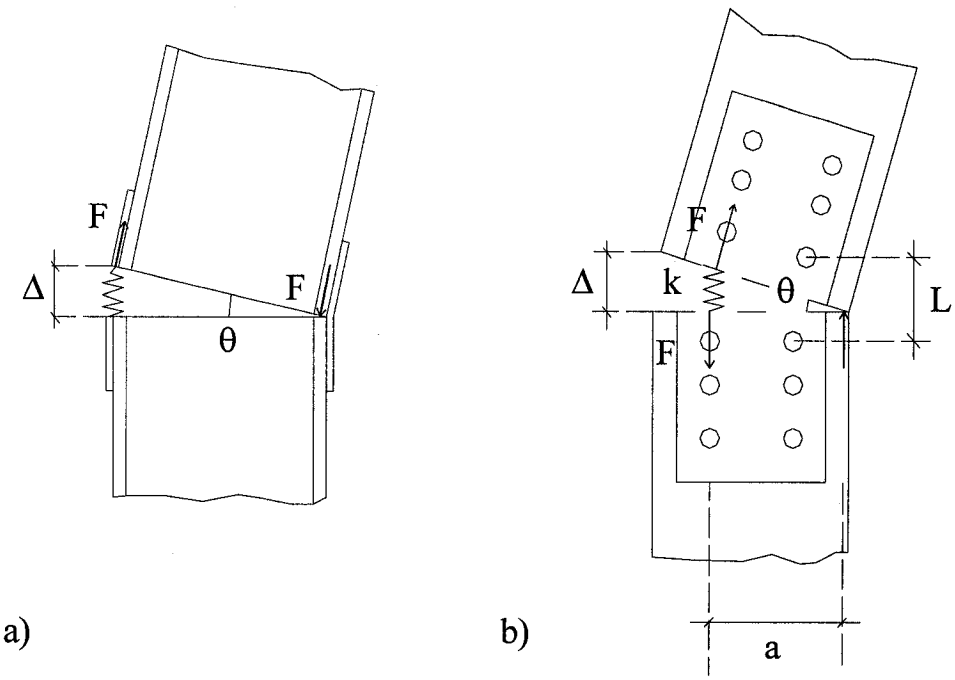

Fig.VI.1 Kinematics assumed for the column splice connection in bending: a) Bending about the column strong axis; b) Bending about the column weak axis

Column splice connections for the gravity columns were assumed to be built with plates connecting the two column flanges. For bending about the strong column axis, it was assumed that the rotation would develop about the flange in compression (Fig.VI.1a). The flexural stiffness is therefore equal to:

$$F = k\Delta = \frac{EA}{L}\Delta;\ M = Fd;$$

$$\theta = \frac{\Delta}{d};\ C_{x-x} = \frac{M}{\theta} \quad \rightarrow \quad C_{x-x} = \frac{EAd^2}{L},$$

where $A = b_f t_{splice}$, t_{splice} is the thickness of the splice, b_f is the width of the column flange and d is the depth of the column section. The length is taken equal to 90 mm.

For the weak axis orientation, the axis of rotation is taken as the tip of the column flanges (Fig. VI.1b). The flexural stiffness can be taken equal to:

$$F = k\Delta = \frac{EA}{L}\Delta;\ M = Fa \text{ and } \theta = \frac{\Delta}{a} = \frac{4}{3}\frac{\Delta}{b_f};$$

The length a is assumed equal to: $a = \frac{3}{4}b_f$ and the stiffness can then be obtained from: $C_{y-y} = \frac{M}{\theta} \rightarrow C_{y-y} = \frac{9}{16}\frac{EAb_f^2}{L}$, where $A = \frac{b_f}{2}t_{splice}$.

APPENDIX VII.

Calculation of the Rayleigh damping parameters

The proportional damping (Rayleigh damping) is given by the relation below (Cook et al, 2002):

$$[C] = \alpha[M] + \beta[K]$$

where C is the damping matrix, M is the mass matrix and K is the stiffness matrix. In this project, the damping was specified as a fraction, ξ, of the critical damping in the first two modes of vibration of the structures in the direction of the earthquake ground motion, ξ_1 and ξ_2. The parameters α and β can be obtained from:

$$\alpha = 2\omega_1\omega_2(\xi_1\omega_2 - \xi_2\omega_1)/(\omega_2^2 - \omega_1^2)$$
$$\beta = 2(\xi_2\omega_2 - \xi_1\omega_1)/(\omega_2^2 - \omega_1^2)$$

where ω_1 and ω_2 are the frequencies associated to the first and second modes of the structures, respectively. The frequencies ca be obtained from the first two periods T_1 and T_2 of the buildings given in Table 5.1.1 (direction X): $\omega_1 = \frac{2\pi}{T_1}$ and $\omega_2 = \frac{2\pi}{T_2}$, and the same fraction of critical damping was assigned in the first two modes: $\xi = \xi_1 = \xi_2 = 3\%$. Therefore :

$$\alpha = 2\omega_1\omega_2\xi(\omega_2 - \omega_1)/(\omega_2^2 - \omega_1^2) = 2\omega_1\omega_2\xi/(\omega_2 + \omega_1) \quad ; \quad \alpha = \xi\frac{4\pi}{T_1 + T_2}$$

and $$\beta = 2\xi(\omega_2 - \omega_1)/(\omega_2^2 - \omega_1^2) = 2\xi/(\omega_2 + \omega_1) \quad ; \quad \beta = \xi\frac{T_1T_2}{\pi(T_1 + T_2)}$$

APPENDIX VIII.

Effective length factor calculation

The effective length factor of the braces was determined by examining the stability of the prismatic member with end rotational springs with flexural stiffness shown in Fig. VIII.1.

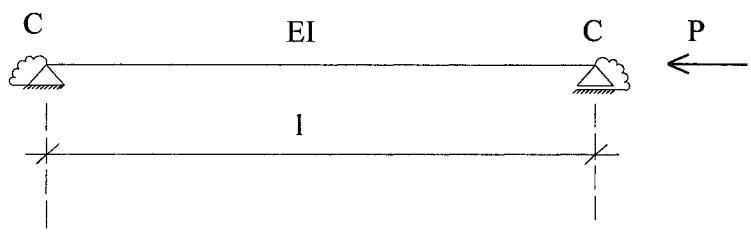

Fig.VIII.1 Prismatic bar with elastic rotational end restraints

The elastic buckling load, P_{cr}, for the member in Fig.VIII.1 can be determined by solving the characteristic equation (Tremblay, 2006):

$$\frac{\tan(kl/2)}{kl/2} = -\frac{2EI}{Cl} \quad \rightarrow k$$

where I is the moment of inertia of the brace cross-section

C is the flexural stiffness of the gusset plate

l is the length of the member.

This equation can be solved for the parameter k, from which the critical load can be found:

$$k = \sqrt{\frac{P_{cr}}{EI}} \rightarrow P_{cr} = k^2 EI$$

Once the critical load is obtained, one can determine the effective length factor K:

$$K = \sqrt{\frac{P_{cr}}{P_{Euler}}}, \text{ where } P_{Euler} = \frac{\pi^2 EI}{l^2}.$$

The calculation were performed for the 8-storey building and the results are given in the Table VIII.1. As shown, the average effective length factor of the braces for this building is equal to 0.77.

Table VIII.1 Effective length factor of braces of the 8-storey building

8 floors	1	2	3	4	5	6	7	8
E (MPa)	200000	200000	200000	200000	200000	200000	200000	200000
I (mm^4)	104000000	104000000	104000000	59500000	59500000	50600000	50600000	26300000
L (mm)	6374.14	5624.37	5672.97	5836.82	5836.82	5883.54	5782.62	5955.02
C (Nmm)	4.63E+09	4.98E+09	4.98E+09	5.20E+09	5.20E+09	3.70E+09	3.98E+09	3.01E+09
k	0.0006	0.0007	0.0007	0.0007	0.0007	0.0007	0.0007	0.0007
tg(kl/2)/(kl/2)	-1.4097	-1.4856	-1.4729	-0.7847	-0.7849	-0.9298	-0.8803	-0.5876
2EI/CL	-1.4098	-1.4857	-1.4730	-0.7846	-0.7846	-0.9298	-0.8797	-0.5873
Diff	0.0001	0.0001	0.0000	-0.0001	-0.0003	0.0001	-0.0006	-0.0003
P_{cr} (N)	7580490	9591744	9450907	6240452	6239925	4930236	5198374	2934537
P_{Euler} (N)	5052658	6489561	6378846	3447416	3447419	2885376	2986971	1463926
K	**0.82**	**0.82**	**0.82**	**0.74**	**0.74**	**0.77**	**0.76**	**0.71**